Studies on Electronic Properties of Aromatic Amines with Unique Structures

Daisuke Sakamaki

2013

Preface

The developments of modern chemistry have enabled us to create various molecules that no one has ever made before. Hence, in this connection, it should be more important to predict the properties of molecules before their syntheses. In essence, the physical and electronic properties of a molecule are considered to be determined by the following two factors: which chemical elements it is made of and how the atoms of these elements are arranged. And hence, there are countless examples of compounds with identical elemental composition but different structures that show completely different physical and electronic properties. For instance, it is well known that carbon has a number of allotropes and each of these exhibits characteristic physical and electronic properties that reflect its structure. This is a remarkable example to show that both of the molecular structures and their electronic properties are closely related to each other, and this also tells us importance of the molecular designing in materials science. This has a lot in common with the concept of rapidly developing organic electronics, because one of the main purposes of organic electronics is to replace the rare, expensive and/or toxic chemical elements composing electronic devices with the properly designed organic materials that are composed of abundant elements and are easily handled.

Today, aromatic amines belong to an important class of compounds in organic electronics because of their charge-transfer properties, and moreover, aromatic amines are considered to be hopeful constituents of organic magnetic materials that have not been in practical use yet. The purpose of this thesis is to clarify the structure-property relationships of aromatic amine molecules, especially with unusual structures so as to propose guidelines for creating new functional materials with the desired properties. The author hopes that the studies in this thesis will contribute to fundamental physical organic chemistry and further development of materials science.

Acknowledgments

The present thesis is the summary of the author's studies from 2008 to 2013 at the Department of Molecular Engineering, Graduate School of Engineering, Kyoto University under the supervision of Professor Kazuyoshi Tanaka.

The author would like to express his deepest gratitude to Professor Kazuyoshi Tanaka for his valuable suggestions, helpful discussions and continuous encouragement through the course of his studies. He is also sincerely grateful to Associate Professor Akihiro Ito for his stimulating suggestions, informative discussions and his kind encouragement.

The author wishes to express his sincere gratitude to Professor Tatsuhisa Kato (Kyoto University) and Dr. Ko Furukawa (Institute for Molecular Science) for their kind help in the pulsed ESR measurements. He would like to thank Dr. Motoo Shiro (RIGAKU Corporation) for his kind help in the X-ray crystallographic analyses.

He wishes to thank Associate Professor Tohru Sato for his valuable comments and discussions. Acknowledgment is also made to Dr. Hiroyuki Fueno for his helpful advice on the computational methods. He also wishes to thank Associate Professor Yoshihiro Matano for his collaborations. He would like to acknowledge Dr. Keiko Kuwata for the mass spectrometry analyses. He is indebted to Mr. Yusuke Ichikawa and Mr. Yuichiro Yokoyama for their collaborations. The author heartily thanks Dr. Yasukazu Hirao, Dr. Katsuyuki Shizu, Mr. Shuji Inoue, Dr. Naoya Iwahara, and Mr. Motoyuki Uejima for their continuous encouragement and kind advice. He is also grateful to Mr. Yusuke Noma, Mr. Kazuaki Kamiya, Mr. Kazuhira Hata, Ms. Yuko Yamagishi, Mr. Ryosuke Aihara, Mr. Kensuke Kawamoto, Mr. Yoshiteru Kira, Mr. Yoshiaki Saito, Mr. Koji Fukui, Mr. Hajime Tsuetaki, Ms. Shoko Eguchi, Mr. Ryosuke Arai, Mr. Sho Kohigashi, Ms. Mariko Kinoshita, Ms. Yoshimi Motonari, Mr. Hiroshi Ishikawa, Mr. Yasuyuki Masuda, Mr. Shin Omae, Mr. Ryohei Kurata, Mr. Masashi Uebe, and Mr. Soichiro Yano

<div align="right">
Daisuke Sakamaki

Kyoto, January 2013
</div>

Contents

$$*\quad*\quad*\quad*\quad*$$

*   *   *   *   *

General Introduction

1. Electronic aspects of aromatic amine derivatives

For the past decade or so, remarkable progress has been made in the field of organic electronics. In this field, aromatic amines are highly important substances as hole-transporting materials.[1] In addition, aromatic amines have been regarded also to make variable class of compounds from the view points of fundamental physical organic chemistry. This is greatly due to the redox activities of aromatic amines and the feasible generations of the positively charged radical cations by chemical or electrochemical oxidations. Additionally, considering the generated radical spins as spin sources, aromatic amines are expected to be hopeful components of the organic spintronic devices.[2] Until the 90's, copper-catalyzed Ullmann coupling reaction[3] had been the most effective method to prepare triarylamines. However, the Ullmann reaction generally requires harsh reaction conditions and results in unsatisfactory yields because of by-products. However, the recent progress of research on the palladium-catalyzed amination reactions[4] has enabled us to readily synthesize various kinds of aromatic amine derivatives. It is well known that aromatic amine derivatives show various electronic properties depending on their molecular structures. In other words, we become able to control the electronic properties of aromatic amines by designing their

structures properly. In this sense, it is highly important to understand the fundamental relationship between the structures and the electronic properties of this class of compounds so as to design the molecules with the desired properties. The following sections describe the basic knowledge about the relationships between molecular structures and two remarkable electronic properties of aromatic amines: the charge-transport properties (Section 2) and magnetic properties (Section 3).

2. Intramolecular electron-transfer (ET) processes in aromatic amines

### 2.1 Intramolecular ET processes in aromatic amines with two redox sites

Radical cations of aromatic amines are one of the most comprehensively studied organic mixed-valence (MV) compounds.[5] One reason for this comes from that most of triarylamine radical cations show characteristic absorption in visible and/or near-infrared region[6] to arise from intramolecular ET processes. Furthermore, these radical species often show the electron spin resonance (ESR) spectra with well-resolved hyperfine splitting from the nuclear spins of the ^{14}N nuclei, and we can obtain the information about the spin distribution in the molecule. As mentioned in the previous Section, triarylamine derivatives are widely used as hole-transport materials in photoconductors and organic light-emitting devices.[1] Thus, it is highly important to clarify the intramolecular ET processes from the view point of not only the physical organic chemistry but also the materials science.

The aromatic amines which have two redox-active units could be considered as convenient models for investigating the intramolecular ET processes. Wherein, this section describes the intramolecular ET phenomena in various aromatic amines containing two redox centers. When an electron is removed from these amines, one of the two triarylamine redox centers becomes a radical cationic state and the other remains a neutral state. Robin and Day classified the redox systems into three classes (I, II, and III) according to the degree of the distribution of charge (or radical spin).[7] In

class I systems, the redox-active centers do not interact with each other, and the charge (or spin) is completely localized on one redox center. In Class II compounds, the two redox centers weakly interact with each other, and therefore, the charge (or spin) can transfer between the two redox sites by the thermal or optical excitation. In class III, the interaction between two redox sites is so strong that the charge (or spin) is completely delocalized, and the two redox sites are considered to have the same charge and spin density. As mentioned above, the optical absorption properties of triarylamine MV compounds are considered to be beneficial because their cationic states show characteristic bands reflecting the condition of the charge distribution.

2.2 The substitution pattern effects on the intramolecular ET properties

Phenylenediamine is considered to be the simplest system of the aromatic amine with the two redox-active units. There exist three structural isomers for phenylenediamine derivatives: *ortho-*, *meta-*, and *para*-isomers. The substitution pattern is the crucial factor determining the electronic interaction between the two redox-active amino groups, along with the distance between the redox sites.[5d] As can be understood from Figure 1, the numbers of covalent bonds between the amino groups in the each structural isomer are 3 (for *ortho*-), 4 (for *meta*-) and 5 (for *para*-isomer). However, the electronic coupling[8] becomes the strongest in the *para*-isomer with the longest separation and the *ortho*-isomer the second strongest, and the *meta*-isomer the weakest.
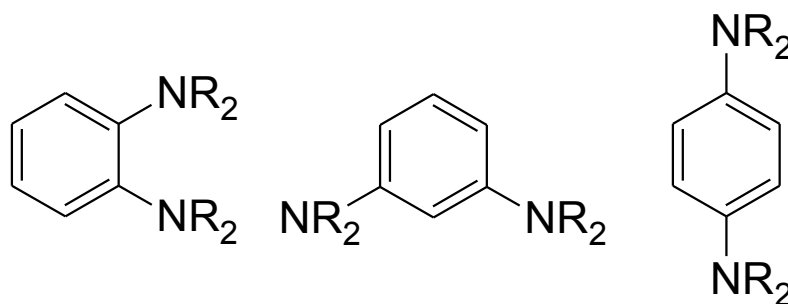

Figure 1. Three structural isomers of phenylenediamines.

Generally speaking, a non-Kekulé-type aromatic unit like a *meta*-linked phenylene unit is by far a less effective coupling linker than Kekulé-type spacers (the definitions of the words "Kekulé" and "non-Kekulé" are explained in Section 3.1). The intramolecular electron-transfer behaviors of the radical cations of these three structural isomers of phenylenediamine have already been studied in detail.[5d] The electronic coupling in tetraanisyl *para*-phenylenediamine (**p1**) was determined by means of optical analysis, and it was concluded that the monocationic state of **p1** is class III system.[9] The large redox potential splitting of **p1** ($\Delta E \simeq 495$ mV) also reflects the strong electronic interaction between two amino groups. For the *meta*-isomers of phenylenediamines, although the values of the electronic coupling in the radical cationic state have not been obtained by optical measurements; however, the electrochemical measurements or the valuable-temperature ESR measurements suggest that there exists a much weaker electronic communication. For example, *meta*-phenylenediamine **m1** has the smaller redox potential splitting, $\Delta E \simeq 190$ mV,[10] compared with $\Delta E = 495$ mV for *para*–phenylenediamine **p1**. For *ortho*-phenylenediamine derivatives **o1-4**, the values of the redox potential splitting are very large ($\Delta E \simeq 500$ mV), which is even greater than that of the *para*–phenylenediamine **p1**.[11] However, these results were considered to be due to the strong Coulomb repulsions resulting from the proximity of the redox active amino groups that make the second oxidation potential higher. The absorption spectral studies of *ortho*-phenylenediamine **o2** were conducted by Nöll and Avola, and they observed a moderately intense and asymmetric charge-transfer (CT) absorption at about 4250 cm^{-1} in dichloromethane.[12] Because this CT band showed negligibly small solvatochromic behavior, they concluded this radical cation is a typical class III system. By the fitting of the observed spectrum, the electronic coupling element *V* was estimated to be nearly half of the value of the *para*-phenylenediamine **p1** probably because of an unfavorable twisted conformation which restricts an effective conjugation between the *p*-orbitals of the nitrogen atoms and the benzene unit as a spacer. The effect

4

of the torsion angle between the redox unit and the bridge unit on the electronic coupling is more thoroughly described in the next section. Since the radical cation of **o2** was regarded as a class III system despite having the unfavorable twisted structure, Nöll and Avola suggested that the through-space interaction between the two nitrogen lone-pair orbitals may play an important role.

R = OMe
p1

m1

R = Me, H
o1-4

o5

5
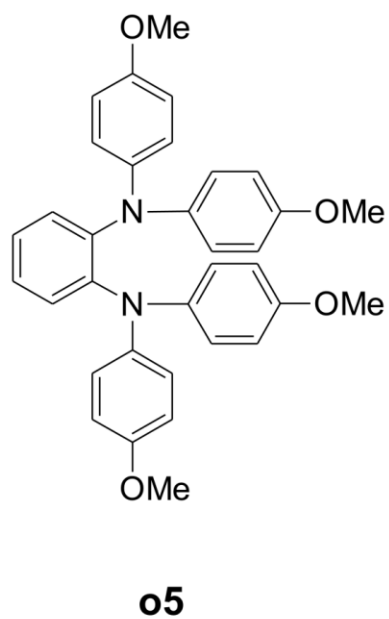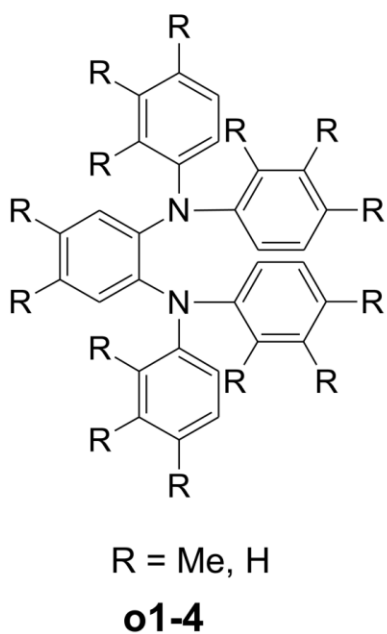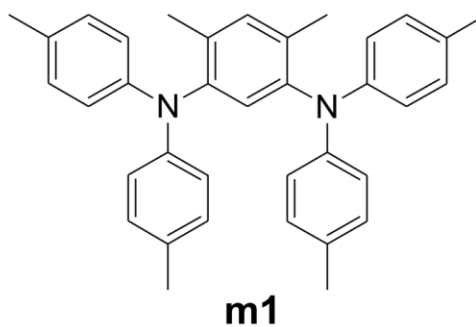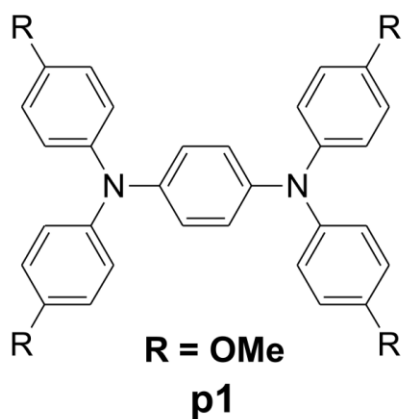
2.3 Steric effects on intramolecular electron-transfer processes

In this section, we will discuss how steric effects, especially torsional angles between the redox-active units and the bridging unit, will influence the intramolecular electron transfer processes. Lambert *et al*. have investigated the electronic structure of a series of bis [*N,N*-di-(4-methoxyphenyl)amino]arenes, where the arene varies from benzene to naphthalene and anthracene to vary the angles between the amino units and the arene bridge (Figure 2a).[9] They studied the electronic properties of the radical cations of these compounds by a series of quantum-chemical calculation, gas-phase photoelectron spectroscopy, visible and near-infrared (vis-NIR) spectroscopy, and cyclic voltammetry. The results of all the measurement clearly showed that the electronic coupling decreases in the order of benzene > naphthalene > anthracene. This result is strikingly different from the case of systems in which the phenylethynyl groups are inserted between the redox active groups and the bridging aryl unit (Figure 2b)[13,14] and contradicts the usual expectation that anthracene is superior to benzene as a bridging unit in electron-(or hole-)transport processes.[15] The reverse tendency in the electronic coupling can be explained by the increasing steric interactions between the dianisyl amino groups as the redox units and the bridging unit resulting in an increase twist angle between these units. The density functional theory (DFT) calculations at the unrestricted B3LYP (UB3LYP)/6-31G** level estimated the torsion angles represent the dihedral angles between the plane defined by the arylene bridge and that defined by the three carbon-nitrogen bonds around the nitrogen atom for these compounds. The dihedral angles were calculated to be 27° for the phenyl-bridged molecule and 62° for the anthracene-bridged molecule. Hence, the smallest twist angles in the phenylene-linked isomer allow a stronger interaction; on the other hand, the large twist angles in the anthracene-linked isomer weaken the electronic coupling and result in a weaker interaction.[9] In contrast to these systems, for the molecules with acetylene spacers, there exists no steric interaction between the bridging aryl unit and the redox-active

groups because of the acetylene spacers,[13] and therefore, the extended aromatic bridges (anthracene and naphthalene) showed the intrinsic properties as the good electronic-coupling units than the phenyl unit.
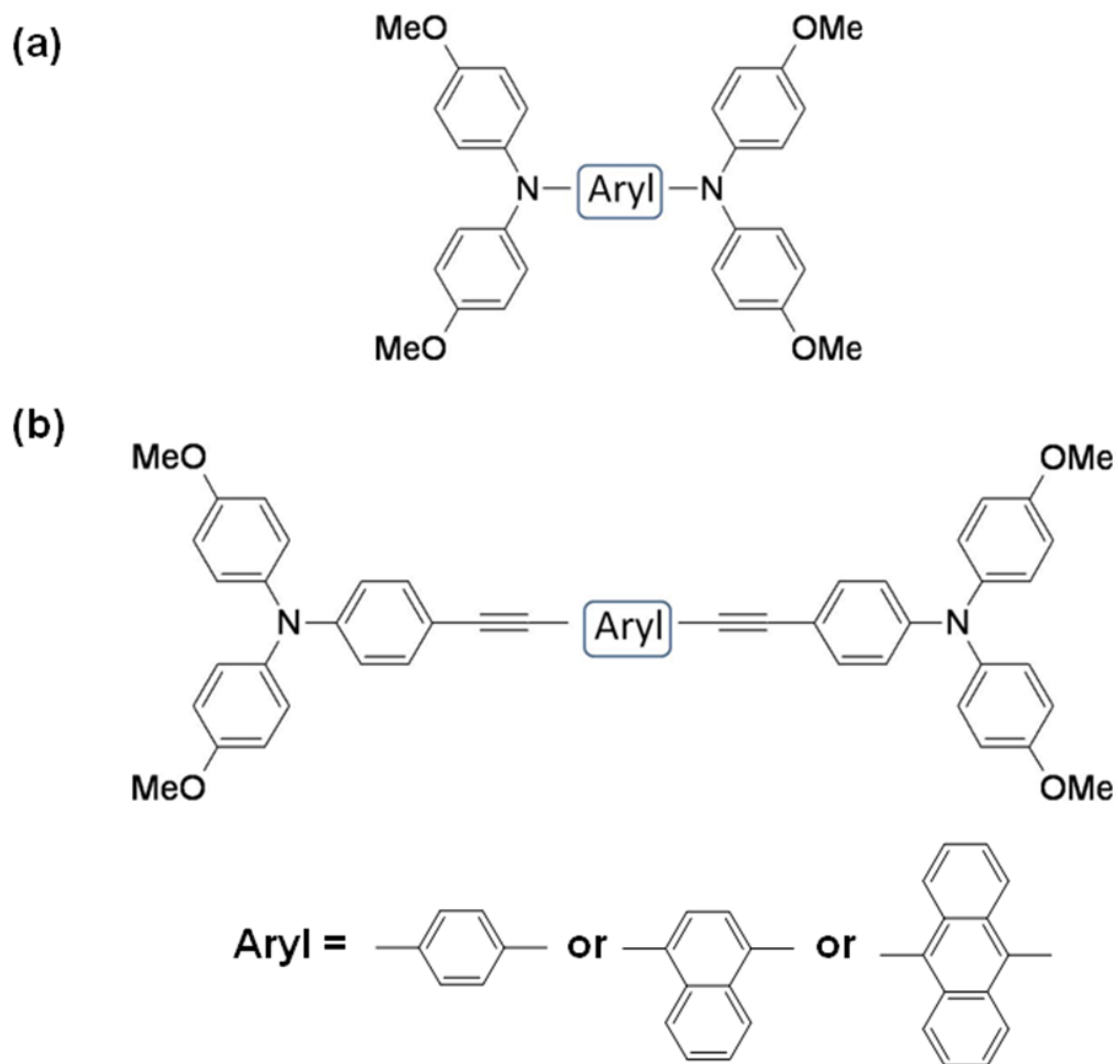
**Figure 2.** Bis(triarylamine) molecules with the different conjugated bridge.

3. Organic multispin systems

3.1 Effects of molecular topology on spin-spin interaction in organic radicals

A multi-electron oxidation property is one of the remarkable properties of oligoarylamine compounds. When more than two electrons are removed from a

molecule, we need to consider the relative alignment of the generated radical spins. In most cases the generated spins tend to be aligned antiferromagnetically so as to eventually form a new covalent bond. Therefore, the achievement of the ferromagnetic alignment of radical spins in organic multispin systems has been an important subject because this will lead to the realization of organic magnetic materials.[16] In 1950, Longuet-Higgins presented a theory which offers a useful suggestion in the designing of high-spin molecules.[17] This theory claims that the alternant hydrocarbon[18] has at least (N-$2T$) non-bonding molecular orbitals (NBMOs), where N is the number of the carbon atoms and T the maximum number of double bonds in possible resonance structures. According to the Longuet-Higgins theory, alternant hydrocarbons could be categorized into the following two groups: Kekulé molecules and non-Kekulé molecules. The alternant hydrocarbons with (N-$2T$) = 0 are called as Kekulé molecules, while the others non-Kekulé molecules with non-zero value of (N-$2T$). Following this theory, o- and p-benzoquinodimethanes are classified as the Kekulé molecules, whereas m-benzoquinodimethane is the non-Kekulé molecule (Figure 3). Therefore, applying the analogy of the Hund's rule[19] on the molecular systems, it is predicted that o- and p-isomers with no degenerate NBMO have the singlet ground state with the closed shell electronic structure, and m-isomer the triplet ground state in which each of the two degenerate NBMOs are occupied with one electron. This is called topological rule, since the topological symmetry of the molecule decides the MO degeneracy and the spin alignment therein. Although this simple principle has been valid for a number of organic systems, in some cases, there are some non-Kekulé type multispin systems that do not have a high-spin ground state. A well-known exception to the Longuet-Higgins theory is tetramethyleneethane (TME) which is a hydrocarbon with two unpaired electrons (Figure 4a).[20] From the comparison of the ground states of TME and trimethylenemethane (TMM) which also is a hydrocarbon with two unpaired electrons (Figure 4b),[21] we can understand the limitation of the predictions of the spin

multiplicity by using the Longuet-Higgins theory alone. Although both two molecules have non-Kekulé structures, however, only TMM has a triplet ground state and TME has a singlet ground state. This result is explained by a concept of "disjoint" and "non-disjoint" which was introduced by Borden and Davidson.[22] The main point of this concept is that the spatial overlaps of the degenerate singly occupied MOs (SOMOs) are important to realize strong exchange interactions between the unpaired electrons. As shown in Figure 4, the two SOMOs of TMM have spatial overlap with each other, and TMM is regarded as a non-disjoint system. In this case, the effective exchange interaction will occur between these SOMOs and therefore, TMM has the triplet ground state. On the other hand, the two SOMOs of TME have no spatial overlap (disjoint), which resulted in the singlet ground state in this case. The two degenerate SOMOs of m-benzoquinodimethane are spatially overlapped (non-disjoint), and this agrees with the fact that this molecule has the spin triplet state.
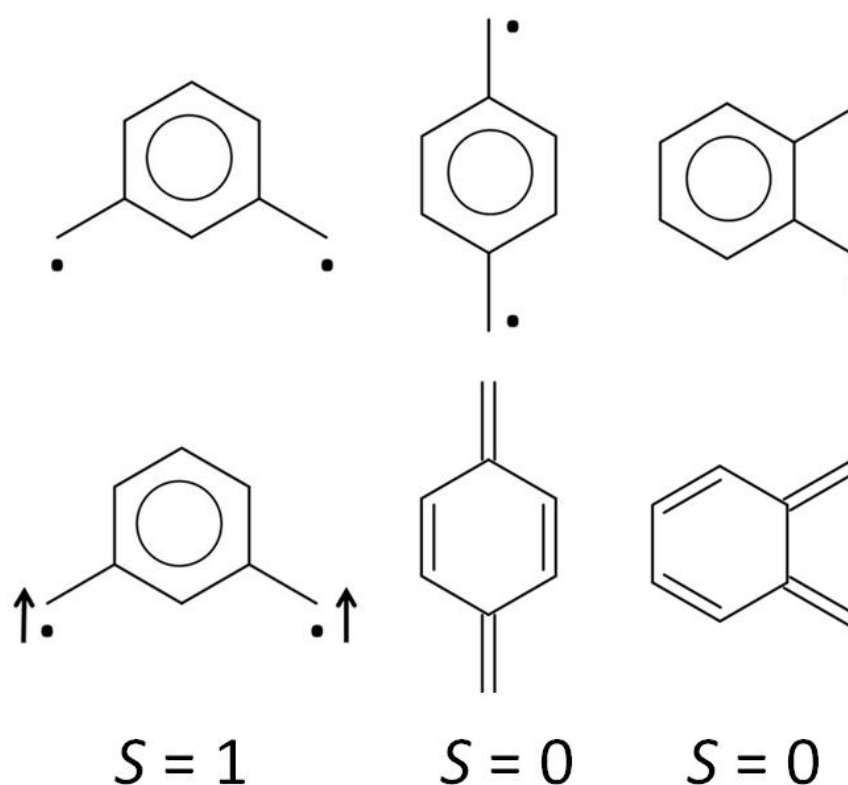
Figure 3. The three isomers of benzoquinodimethane with their predicted ground states.

9
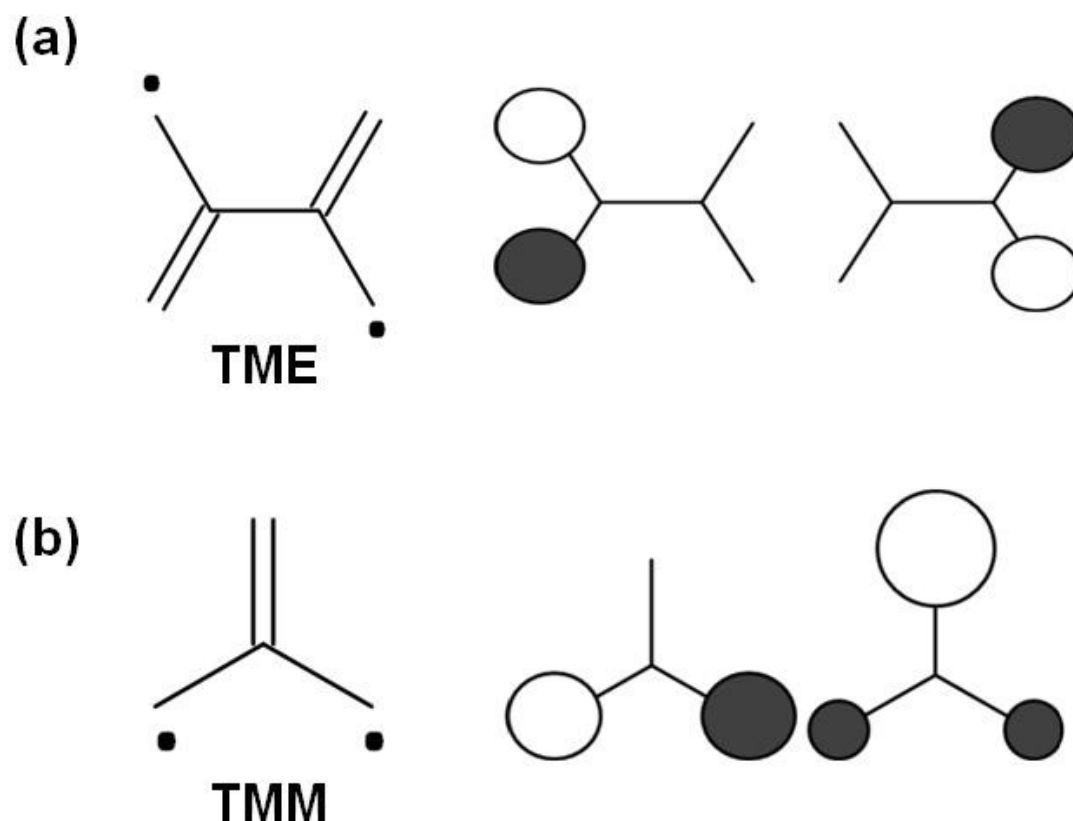
Figure 4. SOMOs of a) TME and b) TMM.

3.2 Through-space spin-spin interactions

The previous section explained the basic rules of the spin-spin interactions through covalent bond in organic radicals. However, when two radicals are placed in proximity, the through-space spin-spin interactions can also occur. In 1963, McConnell presented a basic theory for predicting the interaction between π-radicals that are arranged to stack in close proximity, which is called McConnell Type 1 mechanism.[23] This theory states that: in two aromatic radicals which are stacked cofacially, the relative alignment of the two spins of each radical is determined so as that the products of spin densities at interacting sites between different molecules are all negative. The concept of this theory can be applied to both of the inter- and intramolecular interactions between two π-radicals as long as they are in proximity and stacked cofacially. A

10

[2,2]paracyclophane consisting of two benzene rings connected by two ethylene units at *para*-positions is considered to be a convenient model of the stacked π-systems. When the two substituents with radical spins (*e.g.* carben, nitroxide, etc.) are attached to each of the upper and lower benzene rings with different orientations, these isomers can be regarded as the partial models to investigate the intermolecular magnetic interaction in the crystals of organic free radicals. According to the McConnell's theory, as shown in Figure 5, the ground-state spin-multiplicities of *pseudo-ortho*, *pseudo-meta*, and *pseudo-para* isomers of [2,2]paracyclophane with two monoradical groups are predicted to be triplet, singlet, and triplet, respectively. To confirm this theory, Iwamura and co-workers actually synthesized the three isomers of bis(diphenylmethylenyl)[2,2]paracyclophane with two carben units by irradiation of their diazo precursors.[24] They investigated the ground spin multiplicity by the low-temperature ESR measurements, and clarified that the *pseudo-ortho* and *pseudo-para* isomers had a ground quintet state, and the *pseudo-meta* isomer had a ground singlet state in agreement with the prediction of the McConnell's theory.
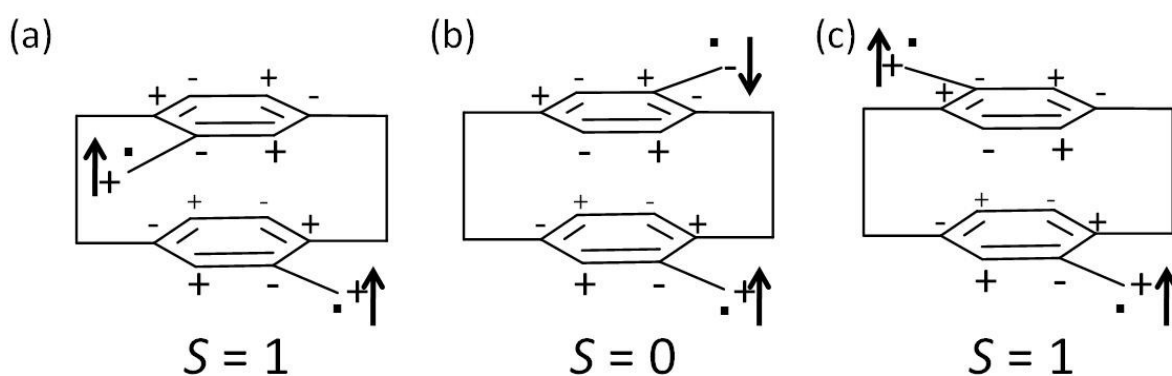

Figure 5. Biradical-substituted [2,2]paracyclophanes: a) *pseudo-ortho*, b) *pseudo-meta*, and c) *pseudo-para* isomers.

3.3 Origoarylamine-based high-spin molecules

So far, there have been various studies to create high-spin molecules from oligoarylamines using the radical spins generated by oxidations as the spin sources. In such studies, the *meta*-phenylenediamine and 1,3,5-benzenetriamine units are the key compounds as the ferromagnetic coupling units. It is seemingly possible to constitute high-spin oligomers and/or polymers by simply connecting the amino groups through these ferromagnetic couplers. However, it was found difficult to realize such high-spin aromatic amine systems from only the *meta*-phenylene linkages because of the instability of their polycationic states.[25] One effective remedy to increase the stability of the polycationic states is to incorporate the *para*-phenylene units into a molecular framework and to connect the amino groups by the *meta*- and *para*-phenylene units alternatively.[26] In this Section, we will introduce such oligoarylamine derivatives which have been prepared and investigated their electronic and magnetic properties. The linear *meta-para*-polyanilines are the simplest examples of such compounds, and these linear amines have been prepared and studied by some groups (Figure 6a).[27] However, in the simple linear polymers, it was found that the observed spin states after the multi-electron oxidations were at most the triplet states, and the higher spin states have not been detected.[27d,e,f] This was probably because of the inherent flexibility of the linear structures and/or the effect of the spin defects.[30d] The dendritic oligoarylamine derivatives are also well-studied compounds as the possible high-spin molecules. Most of the compounds of this group have 1,3,5-benzenetriamine unit in the center (Figure 6b).[26a,b,c,28] In these molecules, the stable spin-quartet species were generated after the three-electron oxidation reflecting the property of central 1,3,5-benzenetriamine unit as the ferromagnetic coupler. However, even in the high weight polymers made of 1,3,5-benzenetriamine units, no remarkable increase of the spin multiplicity has been accomplished probably because of the flexibility and/or the effect of the spin defects similarly in the cases of the linear oligoarylamines.

12
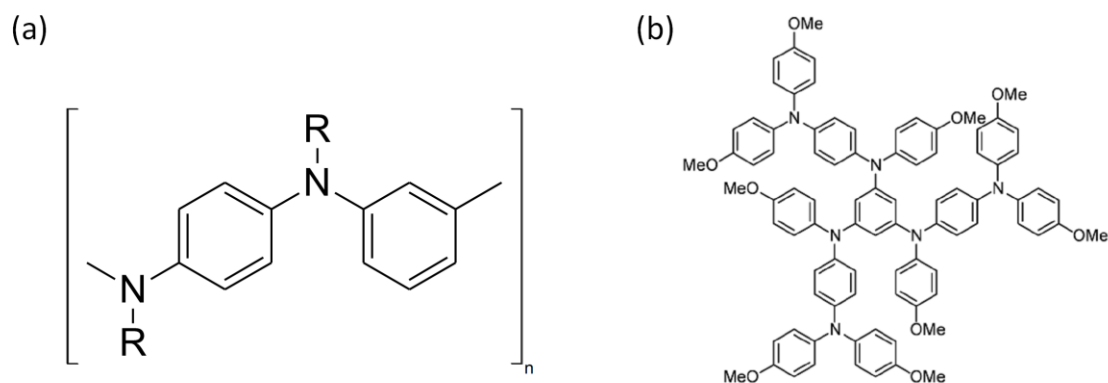
Figure 6. a) The linear *meta-para*-polyaniline; b) an example of the dendritic oligoarylamine.[26c]

On the other hand, recent research of our and other groups revealed the availability of macrocyclic aromatic amines in fabricating the high-spin molecules.[29] For example, tetraaza[1₄]*m,p,m,p*-cyclophane can be feasibly derived to give pure spin triplet species by two-electron oxidation (Figure 7a).[30] This is considered to come from that the rigidness of the macrocyclic structure suppresses the molecular distortions which disturb the spin alignment and guarantees the ferromagnetic interaction in the molecule. Afterword, Hartwig and co-workers extended this cyclic structure to the ladder-like molecular system (Figure 7b).[31] However, the ground spin multiplicity of the dication of this molecule was determined to be a spin-singlet state. We have succeeded in synthesizing the star-shaped trimacrocyclic molecule (Figure 7c) by fusing the three tetraaza[1₄]*m,p,m,p*-cyclophanes.[32] This trimacrocycle can be oxidized up to a stable hexacation, and the tricationic state shows the spin quartet state, whereas the tetracation the triplet state probably because of the partial antiferromagnetic coupling among the four radical spins. we have also reported the synthesis of the [1₄]*m,m,m,m*-cyclophane with the four dianisylamino groups stabilizing the cationic states at the terminals of the molecule, and the tetracation of this maclocyclic amine is in the spin quintet state by the pulsed ESR measurements at low temperature (Figure 7d). As shown here, the

13

macrocyclic aromatic amines have been extended mainly toward planar systems with two-dimensional structure, and on the other hand, there have been few studies aimed at the extension of macrocyclic aromatic amines toward the three-dimensional systems.[33]
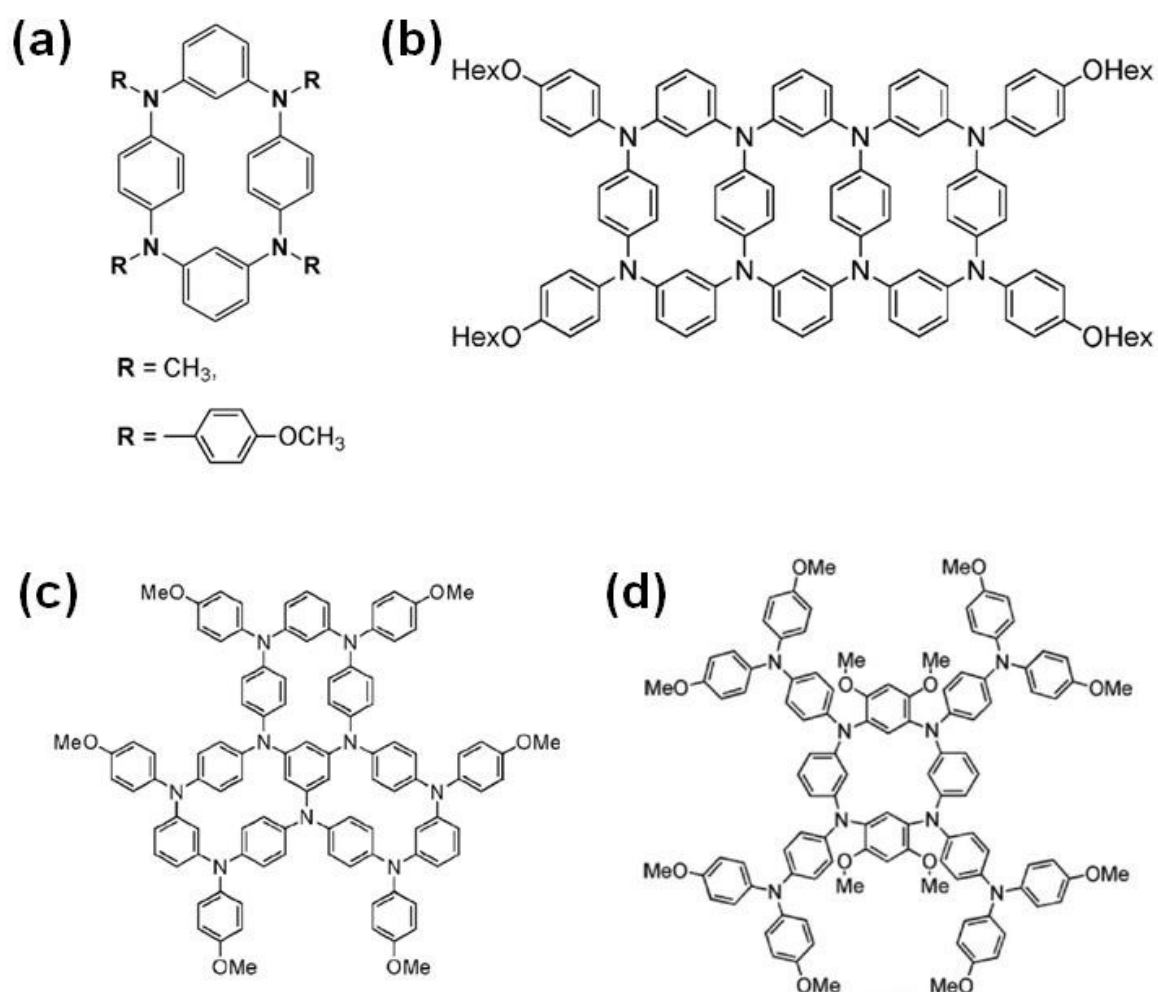
Figure 7. The macrocyclic aromatic amines reported previously.

Survey of this thesis

In this thesis, the author presents the syntheses, the structures, and the electronic properties of several oligoarylamines that have a unique steric structure toward the further understanding of the structure-property relationships of organic compounds. Especially, the author focused on the extension of aromatic amines with two dimensional structures such as macrocyclic molecules to three-dimensional structures such as cage-like molecules and multilayered molecules which have not been studied in detail before.

In Chapter 1, the charge distribution of the cationic states of two kinds of dendritic (or starburst) all–*para*–phenylene–linked oligotriarylamines were investigated by the electrochemical and spectroscopic methods. From the ESR and spectroelectrochemistry measurement, it was suggested that the charge distribution of the cationic states gradually change so as to reduce the electrostatic repulsion between the generated radical spins.

In Chapter 2, the syntheses and the electronic properties of two novel octaazacyclophanes, octaaza[1_8]*m,p,m,p,m,p,m,p*-cyclophane and octaaza[1_8]*m,p,p,p,m,p,p,p*-cyclophane have been investigated. The electrochemical measurement demonstrated that these two macrocycles can be reversibly oxidized up to octacations. The electrochemical UV-Vis-NIR measurement revealed the existence of intramolecular charge transfer in the oxidized states of the both molecules and confirmed that the radical spins in the latter were more widely delocalized than in the former reflecting the expanded PD moieties. The pulsed ESR spectroscopy detected the signals corresponding to the spin-quintet state in the tetracation of octaaza[1_8]*m,p,m,p,m,p,m,p*-cyclophane, and almost pure spin-triplet signal for the dication of octaaza[1_8]*m,p,p,p,m,p,p,p*-cyclophane.

In Chapter 3, the syntheses and the electronic properties of the novel aromatic amine consisting of two tetraazacyclophanes linked by the ferromagnetic coupling unit. This

molecule has been prepared from the palladium-catalyzed coupling reaction between two easily-available triamine and diamine in a one-pot manner. It was confirmed by the electrochemical measurement that this molecule was oxidizable up to dodecacation. The two-dimensional electron spin transient nutation (2D-ESTN) measurement succeeded to determine the spin-multiplicities of the di-, tri-, tetra-, and hexacation of this molecule, and revealed that the hexacation showed the signals suggesting the existence of the spin-septet states, which is the highest spin-multiplicity expected from its structure.

In Chapter 4, a novel macrocyclic compound incorporating two tetraazacyclophanes in the cyclic moiety was synthesized, and its structure and electronic properties were investigated. This compound was prepared by the facile one-pot reaction using 1,4-dibromobenzene and the readily available 1,3,5-benzenetriamine derivative. The electrochemical studies revealed that this compound was able to be oxidized to dodecacation reversibly due to the six PD units incorporated into the molecular structure. The spin-multiplicities of the polycationic states of this compound were investigated by using the 2D-ESTN measurements and the high-spin species up to $S = 2$ state were observed.

In Chapter 5, the syntheses and characterization of the 1,3,5-benzenetriamine double- and triple-decker, which are the first examples of layered oligoarylamines stacked cofacially through multiple arene linkers were described. The molecular structures were clarified by the X-ray analysis for the first time. The methoxy-group-substituted double- and triple-deckers carried out the electrochemical polymerization owing to the instability of the oxidized species. On the other hand, the dianisylaminophenyl-group-substituted double-decker revealed reversible multi-redox activity, and the polycationic states, which are generated by treatment of 2 and 6 equiv. of oxidant, were found to be in high-spin state.

In Chapter 6, the preparation and electronic structures of a double-layered TPA linked by three *meta*-phenylenediamine pillars, that is, TPA double-decker were investigated. It

was clarified that the generated spin in the monocationic state of this molecule is delocalized over the whole molecular skeleton, probably due to through-bond interaction through three-dimensional connectivity. From the ESR measurement, the dication of this molecule showed the distinct spin-triplet signal at 123 K. The variable-temperature ESR studies clarified that the ground state of the dication was spin singlet state.

In Chapter 7, a novel cyclophane consisting of two *para*-phenylenesiamine moieties connected by *ortho*-phenylene linkers was synthesized and investigated its structure and electronic properties. This molecule is the first example of an *o,p,o,p*-tetraazacyclophane. The variable-temperature NMR measurements revealed that this molecule had two conformational isomers and the rate of the isomerization was slower than the NMR time-scale at room temperature, indicating the further rigidness of the *o,p,o,p*-tetraazacyclophane structure. The fluorescence measurements and the ESR measurements demonstrated that the electronic communication between the two PD moieties was significantly enhanced in the *o,p,o,p*-tetraazacyclophane compared to that in the PD cyclophanes with alkyl linkers and in the *m,p,m,p*-tetraazacyclophane.

References and Notes

[1] a) Y. Shirota, *J. Mater. Chem*. **2000**, *10*, 1; b) M. Thelakkat, *Macromol. Mater. Eng.* **2002**, *287*, 442. c) Y. Shirota, H. Kageyama, *Chem. Rev*. **2007**, *107*, 953.

[2] S. A. Wolf, D. D. Awschalom, R. A. Buhrman, J. M. Daughton, S. von Molnár, M. L. Roukes, A. Y. Chtchelkanova, D. M. Treger, *Science* **2001**, *294*, 1488, and references therin.

[3] a) F. Ullmann, *Chem. Ber*. **1903**, *36*, 2389; b) I. P. Beletskaya, A. V. Cheprakov, *Coord. Chem. Rev*. **2004**, *248*, 2337.

[4] a) J. P. Wolfe, S. Wagaw, S. L. Buchwald, *J. Am. Chem. Soc*. **1996**, *118*, 7215; b) M.

S. Driver, J. F. Hartwig, *J. Am. Chem. Soc.* **1996**, *118*, 7217.

[5] a) V. Coropceanu, M. Malagoli, J. M. Andre, J. L. Brédas, *J. Am. Chem. Soc*. **2002**, *124*, 10519; b) A. V. Szeghalmi, M. Erdmann, V. Engel, M. Schmitt, S. Amthor, V. Kriegisch, G. Nüll, R. Stahl, C. Lambert, D. Leusser, D. Stalke, M. Zabel, J. Popp, *J. Am. Chem. Soc*. **2004**, *126*, 7834; c) S. F. Nelsen, *Chem. Eur. J.* **2006**, 6, 581; d) A. Heckmann, C. Lambert, *Angew. Chem. Int. Ed*. **2012**, *51*, 326.

[6] S. Amthor, B. Noller, C. Lambert, *Chemical Physics* **2005**, *316*, 141.

[7] M. Robin, P. Day, *Adv. Inorg. Chem. Radiochem*. **1967**, *10*, 247.

[8] a) N. S. Hush, *Prog. Inorg. Chem.* **1967**, *8*, 391; b) N. S.Hush, *Electrochim. Acta* **1968**, *13*, 1005; c) N. S. Hush, *Coord. Chem. Rev*. **1985**, *64*, 135.

[9] C. Lambert, C. Risko, V. Coropceanu, J. Schelter, S. Amthor,N. E. Gruhn, J. C. Durivage, J.-L. Brédas, *J. Am. Chem. Soc*. **2005**, *127*, 8508.

[10] M. Yano, K. Sato, D. Shiomi, A. Ichimura, K. Abe, T. Takui, K.Itoh, *Tetrahedron Lett.* **1996**, *37*, 9207.

[11] M. J. Plater, T. Jackson, *J. Chem. Soc. Perkin Tra*ns. 1 **2001**, 2548.

[12] G. Nöll, M. Avola, *J. Phys. Org. Chem*. **2006**, 19, 238.

[13] C. Lambert, G. Nöll, J. Schelter, *Nat. Mater.* **2002**, *1*, 69.

[14] C. Lambert, S. Amthor, J. Schelter, *J. Phys. Chem. A* **2004**, *108*, 6474.

[15] a) P. Karafiloglou, J. P. Launay, *Chem. Phys.* **2003**, *289*, 231; b) S. Fraysse, C. Coudret, J. P. Launay, *J. Am. Chem. Soc.* **2003**, *125*, 5880; c) C. Lambert, G. Nöll, J. Schelter, *Nat. Mater*. **2002**, *1*, 69; d) C. Lambert, S. Amthor, J. Schelter, *J. Phys. Chem. A* **2004**, *108*, 6474; e) S. F. Nelsen, R. F. Ismagilov, D. R. Powell, *J. Am. Chem. Soc*. **1996**, *118*, 6313; f) S. F. Nelsen, R. F. Ismagilov, D. R. Powell, *J. Am. Chem. Soc*. **1997**, *119*, 10213; g) S. F. Nelsen, R. F. Ismagilov, D. R. Powell, *J. Am. Chem. Soc*. **1998**, *120*, 1924; h) S. F. Nelsen, R. F. Ismagilov, K. E. Gentile, D. R. Powell, *J. Am. Chem. Soc*. **1999**, *121*, 7108; i) P. N. Taylor, A. P. Wylie, J. Huuskonen, H. L. Anderson, *Angew. Chem.Int. Ed*. **1998**, *37*, 986; j) J. J. Piet, P. N. Taylor, H. L. Anderson, A. Osuka, J. M.

Warman, *J. Am. Chem. Soc.* **2000**, *122*, 1749.

[16] a) N. Mataga, *Theor. Chim. Acta* **1968**, *10*, 372; b) A. Rajca, *Chem. Rev.* **1994**, *94*, 871, and references therin; c) J. A. Crayston, J. N. Devine, J. C. Walton, Tetrahedron **2000**, *56*, 7829, and references therin.

[17] H.C. Longuet-Higgins, *J. Chem. Phys.* **1950**, *19*, 265.

[18] C. A. Coulson, H.C. Longuet-Higgins, *Proc. Roy. Soc.* **1947**, A*192*, 16.

[19] F. Hund, *Z. Phys.* **1928**, *51*, 759.

[20] a) P. Du, W.T. Borden, *J. Am. Chem. Soc.* **1987**, *109*, 930; (b) P. Nachtigall, K.D. Jordan, *J. Am. Chem. Soc.* **1992**, *114*, 4743; c) P. Nachtigall, K.D. Jordan, *J. Am. Chem. Soc.* **1993**, *115*, 270; d) J.J. Nash, P. Dowd, K.D. Jordan, *J. Am. Chem. Soc.* **1992**, *114*, 10071.

[21] a) W. T. Borden, *J. Am. Chem. Soc.* **1976**, *98*, 2695; b) E. R. Davidson, W. T. Borden, *J. Chem. Phys.* **1976**, *64*, 633; c) E. R. Davidson, W. T. Borden, *J. Am. Chem. Soc.* **1977**, *99*, 2053.

[22] a) W. T. Borden, E.R. Davidson, *J. Am. Chem. Soc.* **1977**, *99*, 4587; b) W. T. Borden, E. R. Davidson, *Acc. Chem. Res.* **1981**, *14*, 69; c) D. A. Dougherty, *Acc. Chem. Res.* **1991**, *24*, 88; d) W. T. Borden, H. Iwamura, J. A. Berson, *Acc. Chem. Res.* **1994**, *27*, 109.

[23] H. M. McConnell, *J. Chem. Phys.* **1963**, *39*, 1910.

[24] A. Izuoka, S. Murata, T. Sugawara, H. Iwamura, *J. Am. Chem. Soc.* **1987**, *109*, 2631.

[25] K. R. Stickly, S. C. Blackstock, *Tetrahedron Lett.* **1995**, *36*, 1585.

[26] a) M. M. Wienk, R. A. J. Janssen, *Synth. Met.* **1997**, *85*, 1725; b) M. M. Wienk, R. A. J. Janssen, *J. Am. Chem. Soc.* **1997**, *119*, 4492; c) K. R. Stickley, T. D. Selby, S. C. Blackstock, *J. Org. Chem.* **1997**, *62*, 448. d) A. Ito, H. Ino, Y. Matsui, Y. Hirao, K. Tanaka, *J. Phys. Chem. A* **2004**, *108*, 5715.

[27] a) M. M. Wienk, R. A. J. Janssen, *J. Am. Chem. Soc.* **1996**, *118*, 10626; b) M. M.

Wien, R. A. J. Janssen, *J. Am. Chem. Soc.* **1997**, *119*, 4492; c)M. P. Struijk, R. A. J. Janssen, *Synth. Met.* **1999**, *103*, 2287; d) A. Ito, A. Taniguchi, T. Yamabe, K. Tanaka, *Org. Lett.* **1999**, *1*, 741; e) I. Kulszewicz-Bajer, M. Zagorska, I. Wielgus, M. Pawłowski, J. Gosk, A. Twardowski, *J. Phys. Chem. B* **2007**, *111*, 34; f) I. Kulszewicz-Bajer, J. Gosk, M. Pawłowski, S. Gambarelli,D. Djurado and A. Twardowski, *J. Phys. Chem. B* **2007**, *111*, 9421; g) M. Gałecka, I. Wielgus, M. Zagorska, M. Pawłowski, I. Kulszewicz-Bajer, *Macromolecules* **2007**, *40*, 4924; h) A. Ito, D. Sakamaki, H. Ino, A. Taniguchi, Y. Hirao, K. Tanaka, K. Kanemoto, T. Kato. *Eur. J. Org. Chem.* **2009**, 4441.

[28] a) K. Yoshizawa, A. Chano, A. Ito, K. Tanaka, T. Yamabe, H. Fujita, J. Yamauchi, M. Shiro, *J. Am. Chem. Soc.* **1992**, *114*, 5994; b) K. Yoshizawa, M. Hatanaka, H. Ago, K. Tanaka, T. Yamabe, *Bull. Chem. Soc. Jpn.* **1996**, *69*, 1417; c) K. Sato, M. Yano, M. Furuichi, D. Shiomi, T. Takui, K. Abe, K. Itoh, A. Higuchi, K. Katsuma, Y. Shirota, *J. Am. Chem. Soc.* **1997**, *119*, 6607; d) T. Michinobu, J. Inui, H. Nishide, *Org. Lett.* **2003**, *5*, 2165; e) Y. Hirao, A. Ito, K. Tanaka, *J. Phys. Chem. A* **2007**, *111*, 2951.

[29] A. Ito, K. Tanaka, *Pure. Appl. Chem.* **2010**, *82*, 979.

[30] a) A. Ito, Y. Ono, K. Tanaka, *Angew. Chem, Int. Ed.* **2000**, *39*, 1072; b) T. D. Selby, S. C. Blackstock, *Org. Lett.* **1999**, *1*, 2053; c) S. I. Hauck, K. V. Lakshmi, J. F. Hartwig, *Org. Lett.* **1999**, *1*, 2057; I. Kulszewicz-Bajer, V. Maurel, S. Gambarelli, I. Wielgus, D. Djurado, *Phys. Chem. Chem. Phys.* **2009**, *11*, 1362.

[31] X. Z. Yan, J. Pawlas, T. Goodson, III, J. F. Hartwig, *J. Am. Chem. Soc.* **2005**, *127*, 9105.

[32] A. Ito, Y. Yamagishi, K. Fukui, S. Inoue, Y. Hirao, K. Furukawa, T. Kato, K Tanaka, *Chem. Commun.* **2008**, 6573.

[33] F. A. Neugebauer, S. Kuhnhäuser, *Angew. Chem. Int. Ed.* **1985**, *24*, 596.

Chapter 1

Spin–Delocalization in Charged States of
para–Phenylene–Linked Dendritic Oligoarylamines

## 1.1 Introduction

Since the first report of the multilayered organic light–emitting diodes (OLEDs) made from a bistriarylamine and Alq$_3$ by Tang and VanSlyke,[1] triarylamine derivatives are becoming one of the main components in OLED devices.[2] Owing to their electron–rich property, the positively charged (or hole) states of aromatic amines are generally so stable that they act as good hole–transport materials in various applications such as xerography, solar cells, photorefractive systems, and so forth, in addition to the use of hole–transport layer for OLED devices.[2] Hence, the efforts in the synthesis of many kinds of oligotriarylamines and their polymers are being continued to clarify their characterization in device performance. In particular, "star–shaped" oligoarylamines are considered to be useful for the wide variety of electro–optical applications due to their

ability to form grassy amorphous phases.[2] In addition, the intervalence (IV) compounds bearing two redox-active amino groups have been exhausively examined so far, and it has been clarified that the *para*-phenylene-linked bistriarylamines has the delocalized and/or almost delocalized IV states.[3-6]

In this chapter, we focused on two kinds of dendritic (or starburst) all–*para*–phenylene–linked oligotriarylamines **1** and **2**, which are generated from *para*–phenylenedimine and triphenylamine as core units, respectively (Chart 1). Although the dendritic compound possessing the same[7] and/or similar[8-12] molecular backbone as **2** has been extensively studied, we revisited to elucidate the spin electronic structure of the charged species in more detail. To enhance both of the electron–donating property and the stability of the generated charged species, the dendritic oligotriarylamines **1** and **2** contain the methoxy groups at all the *para*–positions of the peripheral phenyl rings. Herein, we report the synthesis and electrochemical properties of **1** and **2**, and in particular, the electronic structures including intramolecular spin distribution in the charged states for **1** and **2**, based on the absorption and ESR spectroscopic studies.

Chart 1. Dendritic Oligoarylamines **1** and **2**.
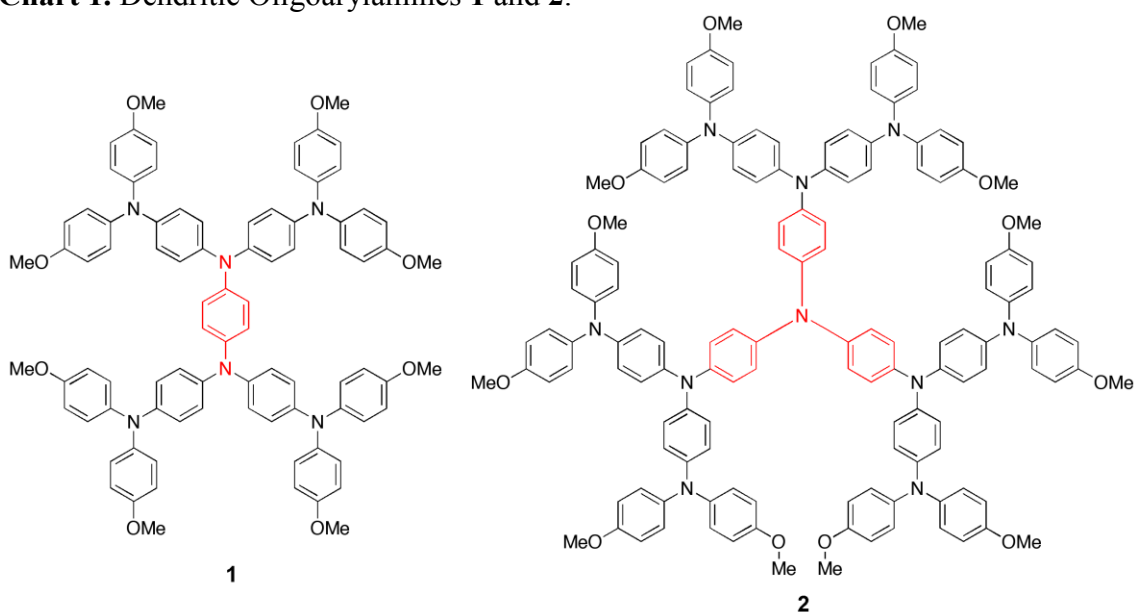
1.2 Experimental Section

General Methods: Commercial grade regents were used without further purification. Solvents were purified, dried, and degassed following standard procedures. Elemental analyses were performed by Center for Organic Elemental Microanalysis, Kyoto University. ^{1}H and ^{13}C NMR spectra were measured by a JEOL JNM-EX400 FT-NMR spectrometer. Chemical shifts of NMR spectra are determined relative to tetramethylsilane (TMS) internal standard.

Theoretical Calculations. Quantum chemical calculations were carried out by using a hybrid Hartree–Fock/density functional theory (HF/DFT) method (B3LYP).[13] Full geometrical optimization of **1**, **2**, **5**, and their radical cations were conducted under D_2 and D_3 symmetrical constraints for **1** and **2**, respectively. Excitation energies for the radical cations of **1** and **2** were examined on the basis of the time–dependent density functional method (TD–DFT).[14] All the computations employed the 3–21G basis set.[15] All these quantum chemical approaches are implemented in Gaussian 03 package of ab initio MO calculation.[16]

Electrochemical and Spectroelectrochemical Measurements. Cyclic voltammogarms were recorded using an ALS/chi Electrochemical Analyzer model 612A with a three–electrode cell using a Pt disk (2 mm^2) as the working electrode, a Pt wire as the counter electrode, and an Ag/0.01 M AgNO$_3$ (MeCN) as the reference electrode calibrated against a ferrocene/ferrocenium (Fc$^{0/+}$) redox couple in a solution of 0.1 M tetra–*n*–butylammonium tetrafluoroborate as a supporting electrolyte (298 K, csan rate 100 mV s^{-1}). The absorption spectra were measured with a Perkin–Elmer Lambda 19 spectrometer. Spectroelectrochemical measurements were carried out with a custom-made optically transparent thin-layer electrochemical (OTTLE) cell (light pass length = 1mm) equipped with a platinum mesh, a platinum coil, and a silver wire as the working, the counter, and the pseudo-reference electrodes, respectively. The potential was applied with an ALS/chi Electrochemical Analyzer Model 612A.

23

ESR measurements. ESR spectra were measured using a JEOL JES–TE200 X–band spectrometer in which temperatures were controlled by a JEOL ES–DVT3 variable–temperature unit.

Synthetic Details. Dendritic oligoarylamine (1): Triamine **3** (0.62 g, 0.99 mmol), 1,4–dibromobenzene (0.078 g, 0.33 mmol), Pd(OAc)$_2$ (0.0046 g, 0.020 mmol), DPPF (0.0022 g, 0.040 mmol) and NaOt-Bu (0.11 g, 1.2 mmol) was charged into a clean dry flask under an argon atmosphere, and then anhydrous toluene (20 mL) was added. The resulting solution was refluxed under an argon atmosphere for 4 days. The reaction mixture was washed with aqueous solution of NaHCO$_3$, and then the organic layer was dried over Na$_2$SO$_4$. After evaporation of the solvent, column chromatography on silica gel with toluene afforded **1** (0.33 g, 76.2 %) as a yellow powder: ^{1}H NMR (400 MHz, THF–d_8); δ (ppm) = 6.97 (m, 18H), 6.88 (m, 12H), 6.79 (m, 24H), 3.72 (s, 24H). ^{13}C NMR (100 MHz, C$_6$D$_6$) δ (ppm) = 156.0, 144.3, 143.2, 142.3, 142.0, 126.2, 125.3, 124.7, 123.3, 115.1, 55.1; FABMS (NBS): m/z calcd for C$_{86}$H$_{77}$N$_6$O$_8$, m/z = 1321.5590; found m/z =1321.5803[M]$^+$; Anal. Calcd for C$_{86}$H$_{76}$N$_6$O$_8$: C, 78.16; H, 5.80; N, 6.36; O, 9.69; Found: C, 78.35; H, 6.11; N, 6.06; O, 9.94.

Dendritic oligoarylamine (2): Triamine **3** (1.25 g, 2.0 mmol), tris(4-bromophenyl)amine (0.24 g, 0.50 mmol), Pd(OAc)$_2$ (0.0067 g, 0.030 mmol), DPPF (0.0033 g, 0.060 mmol) and NaOt-Bu (0.17 g, 1.8 mmol) was charged into a clean dry flask under an argon atmosphere, and then anhydrous toluene (20 mL) was added. The resulting solution was refluxed under an argon atmosphere for 4 days. The reaction mixture was washed with aqueous solution of NaHCO$_3$, and then the organic layer was dried over Na$_2$SO$_4$. After evaporation of the solvent, column chromatography on silica gel with toluene afforded **2** (0.32 g, 30.3 %) as a greenish powder: ^{1}H NMR (400 MHz, THF–d_8) δ (ppm) = 6.96 (m, 24H), 6.89 (m, 24H), 6.79 (m, 36H), 3.72 (s, 36H). ^{13}C NMR (100 MHz, THF–d_8) δ (ppm) = 155.8, 143.9, 141.4, 141.3, 125.7, 125.6, 124.8, 124.6, 124.2, 123.4, 122.2, 114.4, 54.7. Anal. Calcd for C$_{138}$H$_{120}$N$_{10}$O$_{12}$: C,

78.54; H, 5.73; N, 6.64; O, 9.10; Found: C, 77.83; H, 5.73; N, 6.45; O, 8.96.

4-methoxydiphenylamine (6):   A mixture of bromobenzene (0.250 g, 2.03 mmol), *p*-anisidine (0.314 g, 2.00 mmol), Pd(dba)$_2$ (0.057 g, 0.10 mmol), P(*t*-Bu)$_3$ (0.040g, 0.20 mmol) and NaO*t*-Bu (0.311 g, 3.24 mmol) in toluene (22 ml) was refluxed under an argon atmosphere for 23 h. The resulting mixture was washed with brine, and then the organic layer was dried over MgSO$_4$. After evaporation of the solvent, the crude product was chromatographed on silica gel with toluene as eluent to afford **6** (0.180 g, 45%) as faint yellow powder: ^{1}H NMR (400 MHz, acetone-d_6) δ (ppm) = 7.16 (m, 2H), 7.09 (d, 2H, J = 9.0 Hz), 7.04 (br s, 1H), 6.95 (m, 2H), 6.87 (d, 2H, J = 9.0 Hz), 6.73 (t, 1H, J = 7.3 Hz), 3.76 (s, 3H). ^{13}C NMR (100 MHz, C$_6$D$_6$) δ (ppm) = 145.72, 136.10, 129.51, 128.56, 122.62, 119.71, 115.99, 114.93, 55.13.

4-methoxy-4',4''-bis[N-(4-methoxyphenyl)-N-phenylamino]triphenylamine   (5): A mixture of **6** (0.166 g, 0.83 mmol), 4-methoxy-*N*,*N*-bis(4-bromophenyl)aniline (0.132 g, 0.30 mmol), Pd(OAc)$_2$ (0.009 g, 0.04 mmol), 1,1'-bis(diphenylphosphanyl)ferrocene (0.047 g 0.08 mmol), and NaO*t*-Bu (0.119 g, 1.24 mmol) in toluene (8 ml) was refluxed under an argon atmosphere for 19 h. The resulting mixture was washed with brine, and then the organic layer was dried over MgSO$_4$. After evaporation of the solvent, the crude product was chromatographed on silica gel with toluene as eluent to afford **5** (0.096 g, 47%) as white powder: ^{1}H NMR (400 MHz, acetone-d_6) δ (ppm) = 7.20 (dd, 4H, J = 8.8, 7.3 Hz), 7.08 (d, 2H, J = 9.0 Hz), 7.05 (d, 4H, J = 9.0 Hz), 6.92 (m, 20H), 3.79 (s, 6H), 3.78 (s, 3H). ^{13}C NMR (100 MHz, C$_6$D$_6$) δ (ppm) = 156.59, 156.49, 152.03, 149.06, 143.72, 142.87, 141.33, 129.39, 128.57, 127.40, 127.12, 125.24, 124.21, 122.32, 121.52, 115.20, 55.05, 55.05.

1.3 Results and Discussion

1.3.1 Synthesis

The syntheses of the dendritic oligoarylamines **1** and **2** were carried out in 76 and 30 % yield, respectively, by using a palladium–catalyzed Buchwald-Hartwig amination reaction between triamine **3** and the corresponding benzene halides (Scheme 1).[17]

**Scheme 1.** Syntheses of **1**, **2**, and **5**.
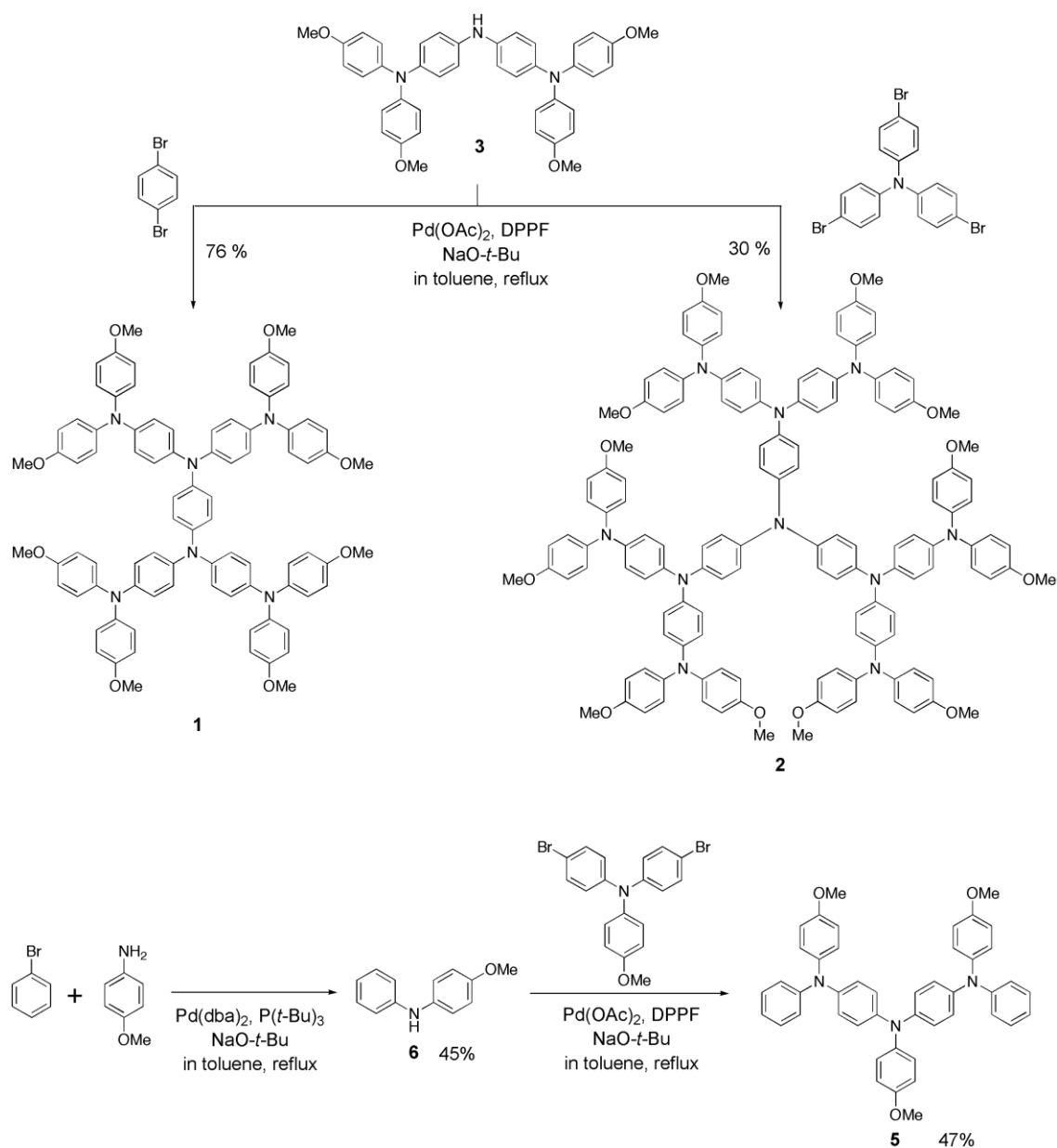
1.3.2 Electrochemistry

The redox properties of **1** and **2** were evaluated by cyclic voltammetry (CV) in CH_2Cl_2 solution at 298 K with 0.1 M tetra-*n*-butylammonium tetrafluoroborate as supporting electrolyte. Both **1** and **2** exhibited five redox couples as shown in Figure 1, and the first three reversible oxidation processes are chemically stable after repeated potential cycling in CH_2Cl_2. The oxidation potentials [E_{ox} vs. $Fc^{0/+}$ (*n*e)] of **1** were determined to be –0.28 (1e), –0.03 (1e), +0.28 (2e) by digital simulations (Figure 2a), and therefore, **1** is stably oxidizable up to tetracation. The first and third oxidation potentials [E_{ox} vs. $Fc^{0/+}$ (*n*e)] of **2** were determined to be –0.30 (1e), +0.18 (3e), and the second oxidation process was demonstrated to be two separate one-electron-oxidation processes [–0.12 (1e) and –0.06 (1e)] by digital simulations (Figure 2b). Hence, **2** is stably oxidizable up to hexacation. The lower first oxidation potentials of **1** and **2** indicate that the present dendritic oligoarylamines are promising as hole transport materials because of strong electron–donating properties. The results are summarized in Table 1, together with those of the related compounds [**3**, **4**,[11f], **5**, *N,N,N',N'*–tetraanisyl–1,4–benzenediamine (**TAPD**)[18] (Chart 2)] under the same conditions. It should be noted that the potential differences between first and second oxidation potentials ($\Delta E_{1\text{-}2}$) of **1** and **2** are smaller than that of **TAPD**, in which the radical cation is stabilized by charge delocalization via π–conjugation. This strongly suggests that planarity (or π–conjugation) of **1** and **2** decreases to some extent as compared to that of **TAPD**, due to hyperbranched structures in **1** and **2**.
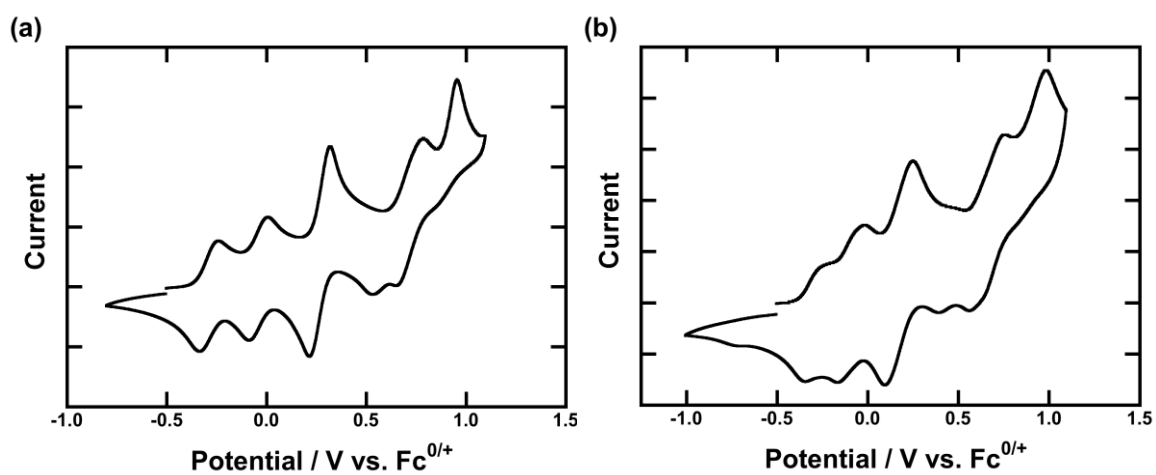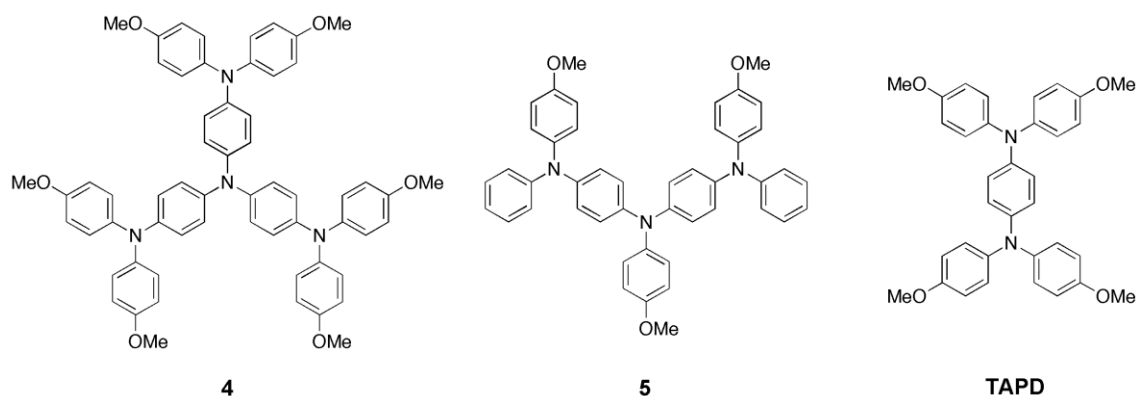
Figure 1. Cyclic voltammograms of **1** and **2** in CH_2Cl_2 / 0.1 M n–Bu_4NBF_4 at 298 K (scan rate 100 mV s^{-1})
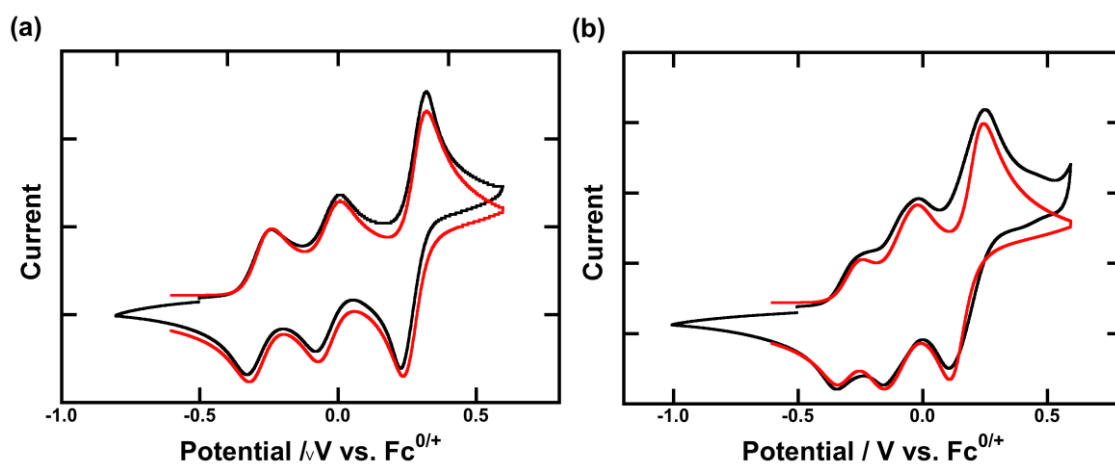
Figure 2. Simulated cyclic voltammograms (red lines) for reversible redox regions (black lines) of (a) **1** and (b) **2**.

Chart 2. Related Compounds **4**, **5**, and TAPD.

Table 1: Redox Potentials (V vs. $Fc^{0/+}$) and Potential Differences of **1–5** and TAPD in CH_2Cl_2 at 298 K.

	E_1	E_2	E_3	E_4E_5	E_5	$\Delta E_{1\text{-}2}$
1[a]	−0.28	−0.03	+0.28[b]	0.79	0.96	——	0.25
2[a]	−0.30	−0.12	−0.06	0.18[c]	0.76	0.99	0.18
3[a]	−0.19	+0.11	+0.71[d]	0.90	——	——	0.30
4[e]	−0.16	+0.17	+0.56	——	——	——	0.33
5[a]	−0.11	+0.25	+0.83[d]	——	——	——	0.36
TAPD[f]	−0.13	+0.35	——	——	——	——	0.48

[a] Reversible oxidation potentials were digitally simulated. [b] Quasi-two-electron oxidation. [c] Quasi-three-electron oxidation. [d] Oxidation peak potential (irreversible).
[e] Ref. 11(f). The reported oxidation potentials vs. $Fc^{0/+}$ were corrected by the redox potential of $Fc^{0/+}$ vs. SCE (+0.48 V in CH_2Cl_2).[19] [f] Ref. 18.

1.3.3 Spectroelectrochemical Studies

In order to investigate the charge distribution in the charged states of **1** and **2**, we measured the optical absorption spectral changes of **1** and **2** in CH_2Cl_2 during the course of the oxidation going from neutral to $\mathbf{1}^{4+}$ or $\mathbf{2}^{6+}$ by using an optically transparent thin–layer electrochemical cell. First of all, we started to check the spectral change from $\mathbf{5}^{\bullet+}$ to $\mathbf{5}^{2+}$, because **5** can be considered to be a good reference compound for the dendron groups in **1** and **2**. Moreover, the previous studies have already established that the radical cation of the unsubstituted compound of **5** is in a charge resonance (CR) intervalence (IV) state. It should be noted that the CR states in IV compounds containing three redox-active centers like **5** differ from those in IV compounds with two redox-active centers. CR IV compounds with multiple redox-centers have inevitably unsymmetrical charge distribution, originating from the unsymmetrical molecular structures, while CR IV compounds with two redox-active centers have usually symmetrical charge distribution. In addition, the electronic structure for the CR IV compounds can be explained by the quantum chemical calculations such as MO and/or DFT calculations. As shown in Figure 3, the lowest energy bands at 0.99 eV (1250 nm) in $\mathbf{5}^{\bullet+}$ was changed into more intense band at 1.13 eV (1100 nm) in $\mathbf{5}^{2+}$ with an isosbestic point at 1.01 eV (1225 nm). Judging from the DFT calculations of $\mathbf{5}^{\bullet+}$ and $\mathbf{5}^{2+}$, the charge distribution can be predicted to be completely changed; the generated charge is distributed mainly on the inner triarylamine moiety, whereas the charge is distributed mainly on the outer triarylamine moieties to avoid the electrostatic repulsion between two charges (Figure 3). Herein note that the delocalized electronic state in CR IV compounds with multiple redox-active centers do not necessarily have the symmetrical charge distribution among the redox-active centers. As is the same as the radical cation of the unsubstituted compound of **5**,[9e] the lowest energy band of both $\mathbf{5}^{\bullet+}$ can be assigned to the transition from β (HOMO) to β (LUMO) on the basis of the time–dependent density functional theory (TD–DFT) calculations. In addition, the

30

TD-DFT calculations showed that the lowest energy band of 5^{2+} is also due to the transition from HOMO to LUMO. The calculated results are summarized in Table 2 together with those for the next lowest band of $5^{\bullet+}$ and 5^{2+}. Note that the difference in relative intensity of the lowest energy band between $5^{\bullet+}$ and 5^{2+} is well-reproduced by the calculated oscillator strengths. The fact that the TD–DFT calculations can explain the observed absorption spectral change strongly suggests that both $5^{\bullet+}$ and 5^{2+} are in the CR IV states: the charge distribution for the CR state of 5^{2+} is determined by the electrostatic repulsion between the charged centers.

In view of change in charge distribution between $5^{\bullet+}$ and 5^{2+}, let us then turn to the spectral change observed during the stepwise electrochemical oxidations of **1** and **2**. During the electrochemical oxidation of **1**, a lowest energy band appeared at 1650 nm (0.75 eV) with a shoulder at 1050 nm (1.18 eV). This lowest energy band for $1^{\bullet+}$ continued to grow up until the oxidation to 1^{2+} has been completed with an isosbestic point at 390 nm (3.18 eV) (Figure 4a). This observation suggests that 1^{2+} dislikes the quinoid structure, as is often the case with the dicationic state of **TAPD** and its derivatives, probably due to the bulky dendron groups. By increasing the electrode potential to the value of the third oxidation process (1^{2+} to 1^{4+}), both of the blue shift (1300 nm (0.95 eV)) and increase in the intensity of the lowest energy band were observed together with several isosbestic points (Figure 4b). This spectral change in the lowest energy band from $1^{\bullet+}$ to 1^{4+} showed the same behavior as that from $5^{\bullet+}$ to 5^{2+}. Hence, it is suggested that the charge distribution changes on going from $1^{\bullet+}$ to 1^{4+}, as shown in Figure 6a.

Similar spectral change was also observed for the electrochemical oxidation of **2**, in which the conjugated π–system is extended by the core triphenylamine and the number of dendron groups. During the electrochemical oxidation of **2**, a lowest energy band appeared at 1850 nm (0.67 eV) with a shoulder at 1250 nm (0.99 eV) (Figure 5a). By increasing the electrode potential to the value of the second oxidation process ($2^{\bullet+}$ to

31

2^{3+}), both of the blue shift (1300 nm (0.95 eV)) and increase in the intensity of the lowest energy band were observed together with some isosbestic points (Figure 5b). This spectral change in the lowest energy band from **$2^{•+}$** to **2^{3+}** showed the same behavior as that from **$5^{•+}$** to **5^{2+}**. Hence, it is suggested that the charge distribution changes on going from **$2^{•+}$** to **2^{3+}**, as shown in Figure 6b. Moreover, at the electrode potential of the third oxidation process (**2^{3+}** to **2^{6+}**), further blue shift (1300 nm (0.95 eV)) and increase in the intensity of the lowest energy band were observed together with several isosbestic points (Figure 5b). This process corresponds to further charge up on each of the charged dendron groups.

It should be noted that the typical localized triarylamine radical cation bands (~ 750 nm)[4a,21] are not observed in all the absorption spectra for the charged states of **1**, **2**, and **5**. This strongly suggests that the observed charged states are not in localized IV states but in CR IV states. Furthermore, as will be clarified in the next section, the observed lowest energy bands can be considered as the charge resonance (CR) bands originating from the delocalized electronic states. This means that the usual quantum chemical calculations allow us to assign the lowest energy absorption bands of the charged states of **1** and **2** to specific electronic transitions. Hence, we carried out the TD–DFT calculations[14] on **$1^{•+}$** and **$2^{•+}$**. As is shown in Table 2, it was found that the TD–DFT–calculated results qualitatively elucidated the characteristics of the observed lowest energy bands including relative intensity. The lowest energy band of **$1^{•+}$** can be regarded as an overlap of three transitions: the peak at 0.75 eV can be assigned to the transition from β (HOMO) to β (LUMO), while the shoulder at 1.18 eV can be assigned to a mixture of two transitions; (i) from β ((HO–1)MO) to β (LUMO) , and (ii) from β ((HO–2)MO) to β (LUMO). Similarly, The lowest energy band of **$2^{•+}$** can be regarded as an overlap of two transitions: the peak at 0.67 eV can be assigned to a transition from doubly degenerate β (HOMOs) to β (LUMO), while the shoulder at 0.99 eV can be assigned to a transition from β ((HO–1)MO) to β (LUMO). As is apparent from the MO

energy diagrams in Figure 7, these transitions are explainable to be charge resonance between the peripheral dendron groups and the core amine moieties.
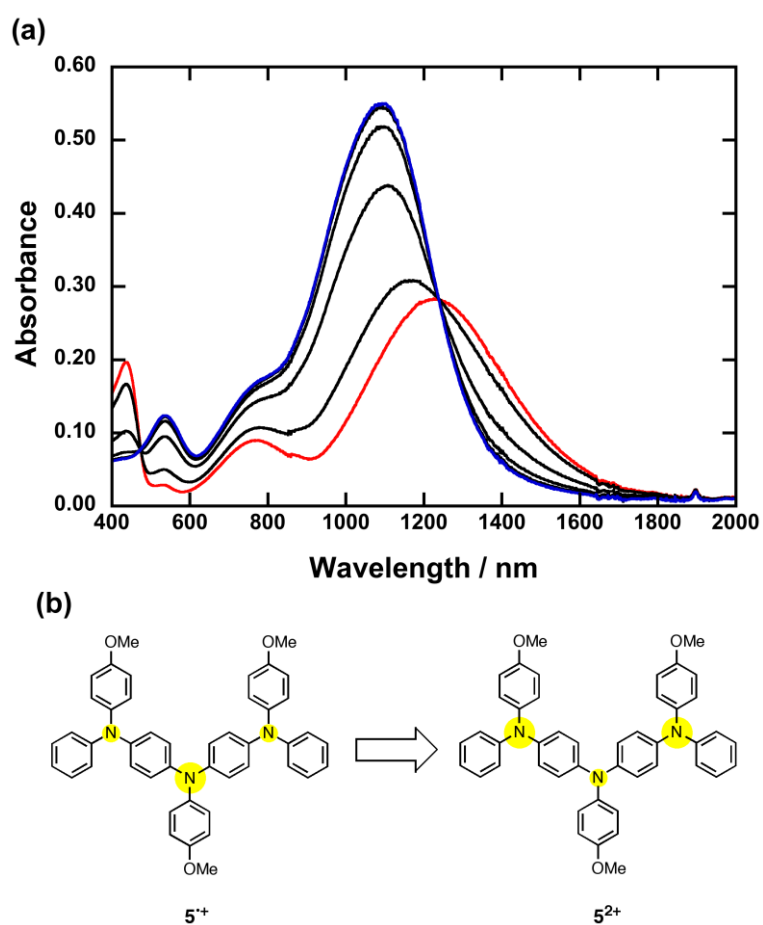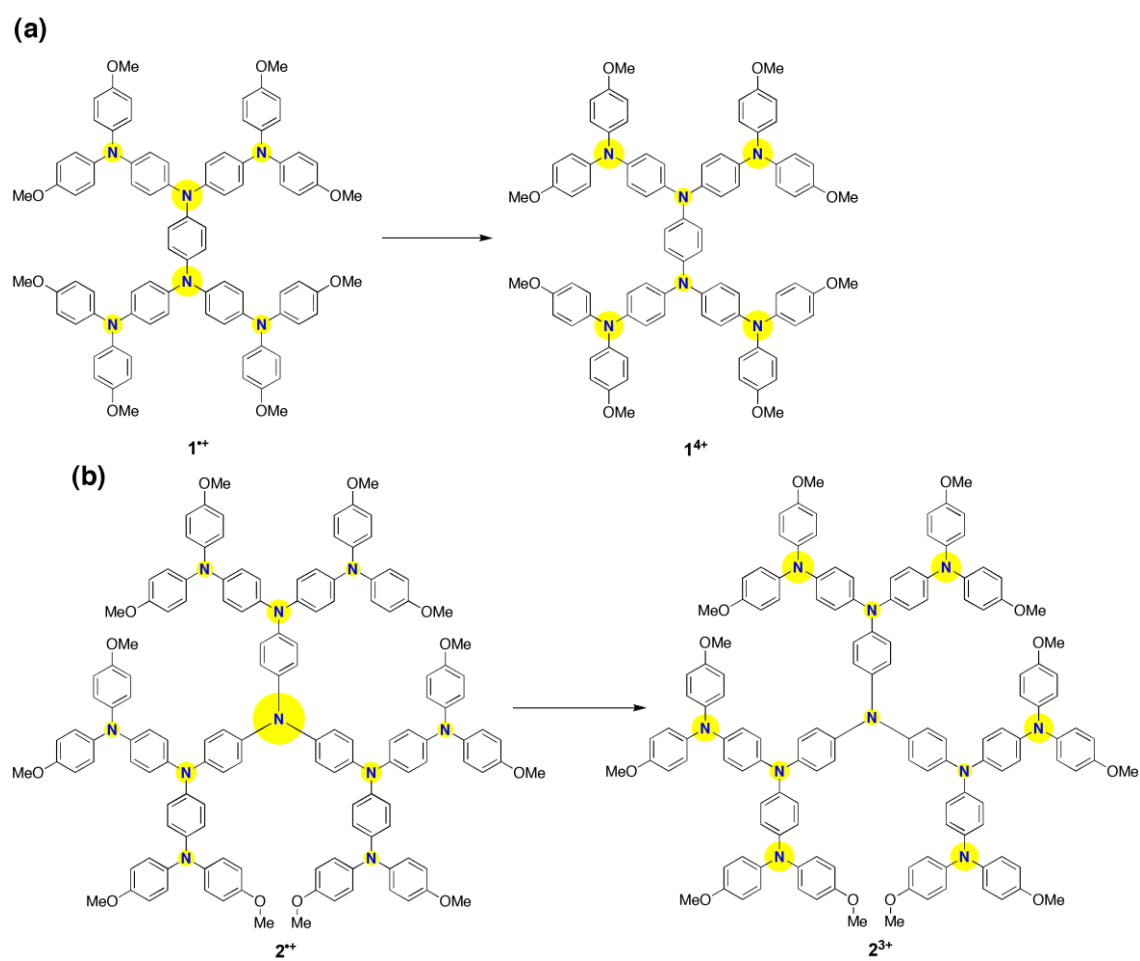

Figure 3. (a) UV/vis/NIR spectra of the stepwise electrochemical oxidation of $5^{\bullet+}$ (in red) to 5^{2+} (in blue) in CH_2Cl_2/0.1 M n–Bu_4NBF_4 at room temperature. It was confirmed by global analysis with HypSpec[20] that no other species than $5^{\bullet+}$ and 5^{2+} contain in this spectral change. (b) the schematic Mulliken charge distributions (in yellow) of $5^{\bullet+}$ and 5^{2+} at the B3LYP/3–21G calculations.
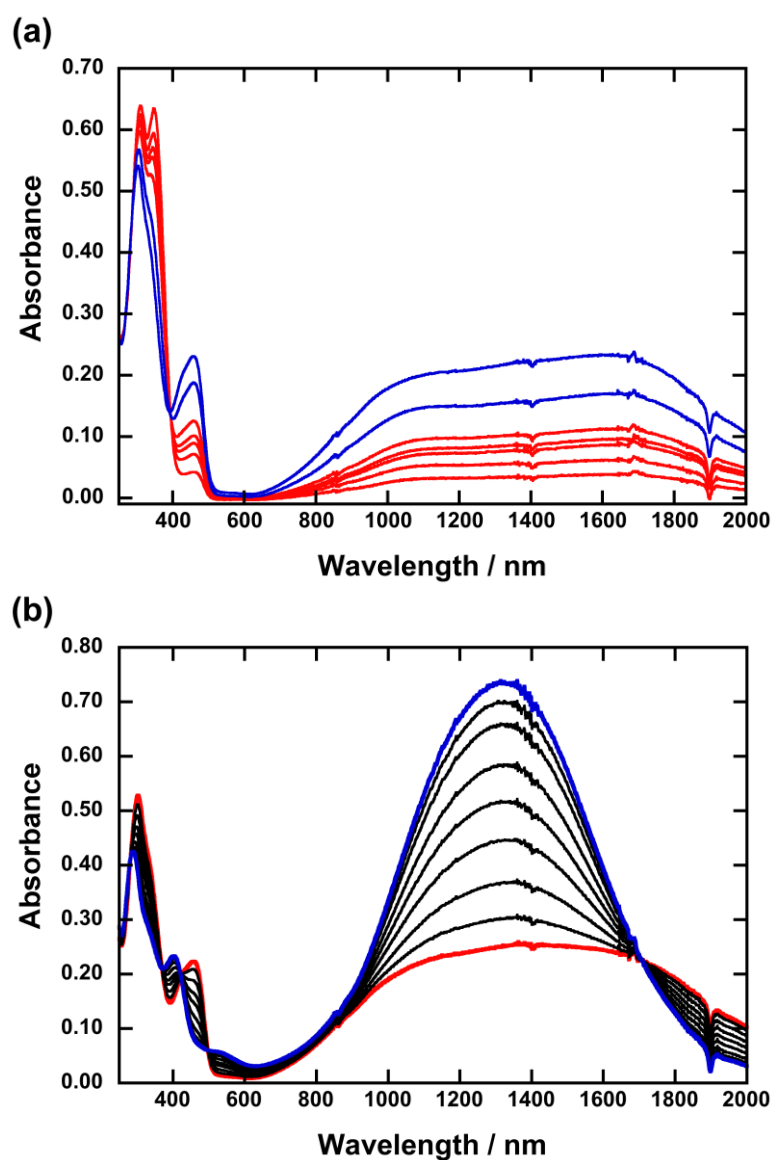
Figure 4. UV/vis/NIR spectra of the stepwise electrochemical oxidation of (a) **1** to **1$^{\bullet+}$** (in red) and **1$^{\bullet+}$** to **1^{2+}** (in blue) and (b) **1^{2+}** (in red) to **1^{4+}** (in blue) in CH$_2$Cl$_2$/0.1 M *n*–Bu$_4$NBF$_4$ at room temperature. It was confirmed by the global analysis with HypSpec[20] that no other species than **1**, **1$^{\bullet+}$**, **1^{2+}**, and **1^{4+}** contain in these spectral changes.
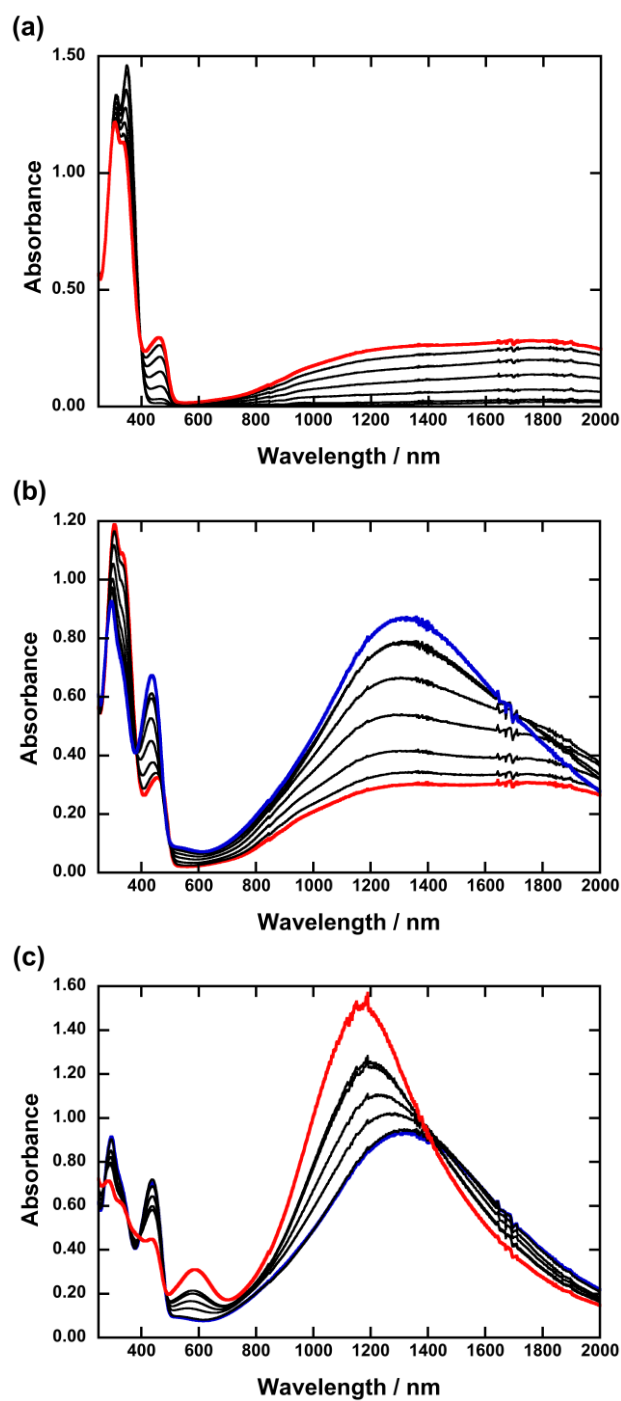
Figure 5. UV-vis-NIR spectra of the stepwise electrochemical oxidation of (a) **2** to **2**$^{•+}$ (in red), (b) **2**$^{•+}$ (in red) to **2**$^{3+}$ (in blue), and (c) **2**$^{3+}$ (in blue) to **2**$^{6+}$ (in red) in CH$_2$Cl$_2$ / 0.1 M n–Bu$_4$NBF$_4$ at room temperature. It was confirmed by global analysis with HypSpec[20] that no other species than **2**, **2**$^{•+}$, **2**$^{2+}$, **2**$^{3+}$, and **2**$^{6+}$ contain in these spectral changes.

Figure 6. Hypothetical charge distributions (in yellow) of (a) $1^{\bullet+}$ to 1^{4+} and (b) $2^{\bullet+}$ to 2^{3+}.

(a)

349 (b₂) 348 (b₃) β–LUMO β–HOMO 347 (b₁) β–(HO–1)MO β–(HO–2)MO 346 (a) α β

(b)

557 (a₂) 556 (e) 555 (e) β–LUMO β–HOMOs β–(HO–1)MO β–(HO–2)MOs 554 (a₁) α β
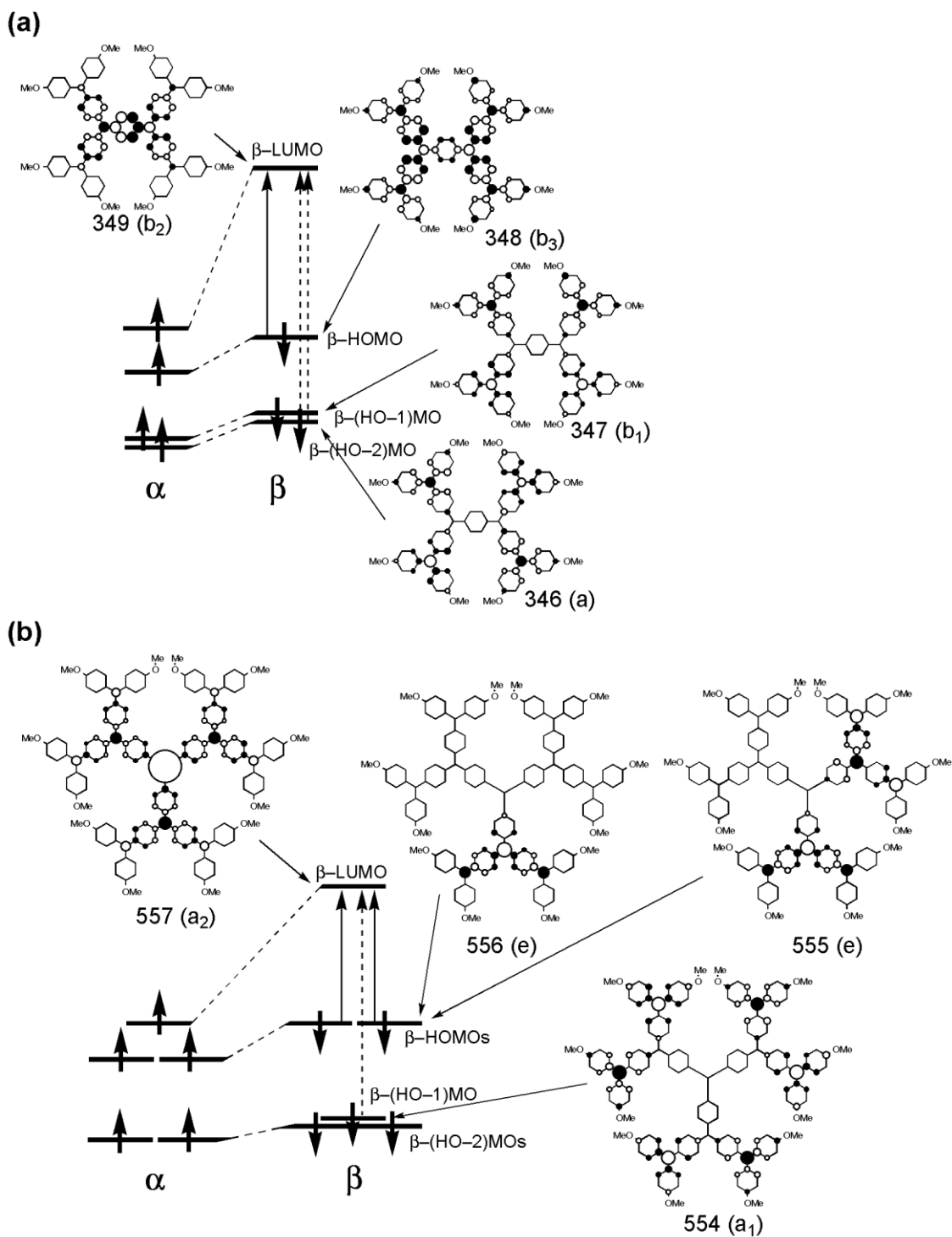
Figure 7. Relative energy levels of the frontier MOs for (a) $\mathbf{1}^{\bullet+}$ and (b) $\mathbf{2}^{\bullet+}$ based on the UB3LYP/3–21G calculations. The arrows with solid and dashed lines represent the major contributions to the lowest and next–lowest energy transitions, respectively.

37

Table 2: TD-DFT (UB3LYP/3-21G) Calculations of the Low Energy Excitation Energies for $1^{\bullet+}$, $2^{\bullet+}$, $5^{\bullet+}$ and 5^{2+}.

		TD-DFT calcn	
species	$h\nu$ (obs) (eV)	$h\nu$ (eV) (f)	assignment
$1^{\bullet+}$	0.75	0.52 (0.52)	348β (HOMO) → 349β (LUMO)
	1.18	0.90 (0.36)	347β ((HO–1)MO) → 349β (LUMO)
		0.92 (0.16)	346β ((HO–2)MO) → 349β (LUMO)
$2^{\bullet+}$	0.67	0.50 (0.41)	555β, 556β (HOMOs) → 557β (LUMO)
	0.99	0.86 (0.28)	554β ((HO–1)MO) → 557β (LUMO)
$5^{\bullet+}$	0.99	0.94 (0.49)	176β (HOMO) → 177β (LUMO)
	1.62	1.38 (0.18)	175β ((HO–1)MO) → 177β (LUMO)
5^{2+}	1.13	1.16 (0.99)	176 (HOMOs) → 177 (LUMO)
	~1.65(sh)	1.52 (0.44)	175 ((HO–1)MO) → 177 (LUMO)
	2.34	2.03 (0.18)	173 ((HO–3)MO) → 177 (LUMO)

1.3.4 ESR Studies

To further evaluate the electronic structure of the charged states of **1** and **2**, the ESR spectra of the chemically oxidized samples in CH_2Cl_2 were recorded. In addition, we also checked the ESR spectral change from $5^{•+}$ to 5^{2+}. The radical cation and dication of **5** were generated by treating with 1 and 2 equiv. of tris(4-bromophenyl)aminium hexachloroantimonate in CH_2Cl_2 at 195 K. As shown in Figure 8a, the ESR spectrum of $5^{•+}$ showed the similar spectral shape to that of the radical cation for the unsubstituted compound of **5**.[9e] On the basis of the spectrum simulation, the hyperfine coupling constants were determined: a_N = 0.660 mT (1N), a_N = 0.275 mT (2N), a_H = 0.100 mT (2H), a_H = 0.050 mT (4H), a_H = 0.030 mT (8H), and the contributions from the negligible hydrogen nuclei were incorporated in the line width of the spectral simulation (0.20 mT) (Figure 8b). On the other hand, the dication 5^{2+} was ESR-silent, and therefore, we could not obtain any information on the charge distribution (Figure 9).
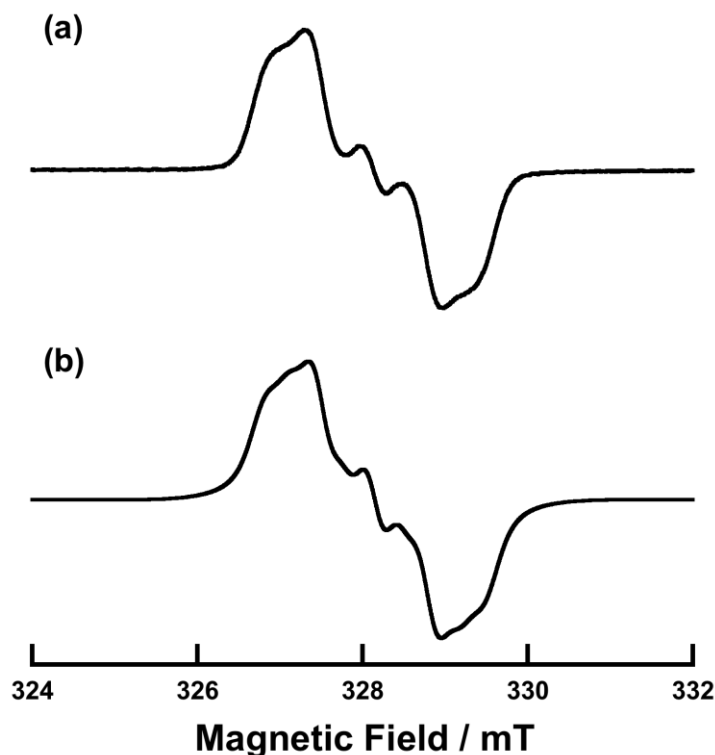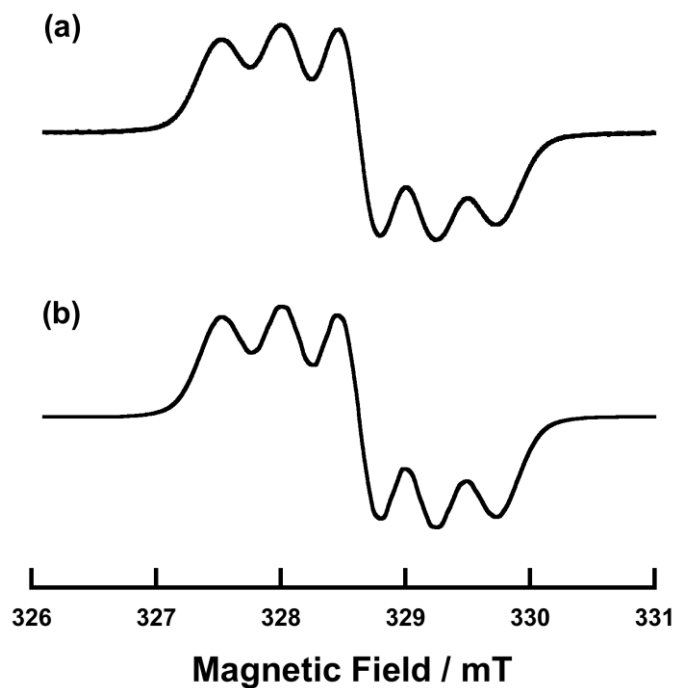

Figure 8. ESR spectrum of $5^{•+}$: a) in CH_2Cl_2 at 290 K; b) simulated.
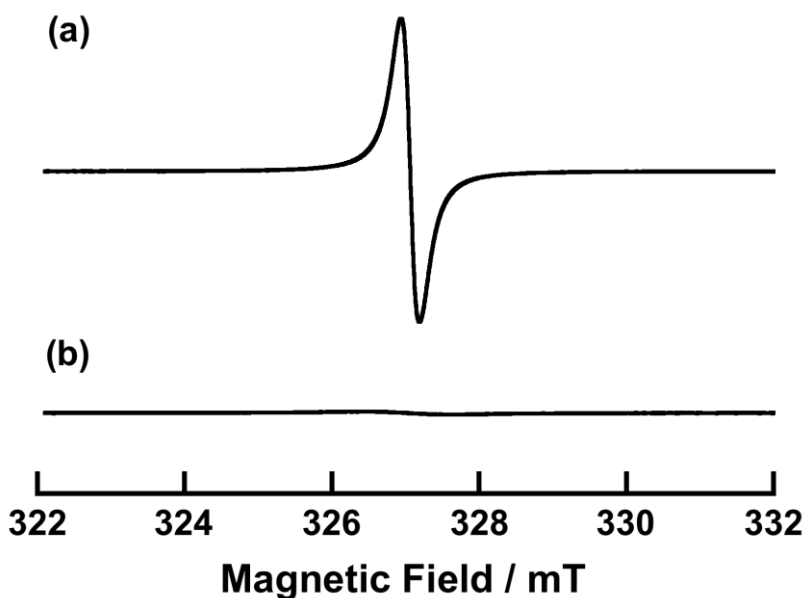
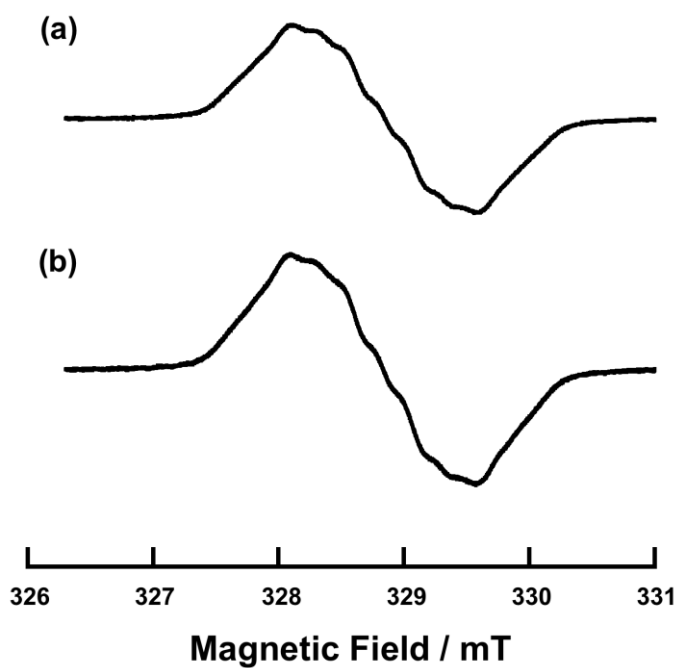**Figure 9.** ESR spectra of (a) $5^{\bullet+}$ and (b) 5^{2+} in CH_2Cl_2 at 123 K.

The ESR spectra of $1^{\bullet+}$ and $2^{\bullet+}$ generated by chemical oxidation of **1** by 1 equiv. of tris(4-bromophenyl)aminium hexachloroantimonate in CH_2Cl_2 at 195 K showed a multiplet hyperfine structures (Figures 10 and 11). Note that $1^{\bullet+}$ and $2^{\bullet+}$ were found to be stable under anaerobic conditions at room temperature for a few months, as indicated by there being no loss in the ESR signal intensity. The splitting pattern of $1^{\bullet+}$ can be explained by the presence of two and four equivalent nitrogen nuclei and 4 equivalent hydrogen nuclei originating from the central *para*-phenylene moiety, although the broadness of the signals suggests additional small hyperfine coupling constants due to the other hydrogen nuclei (Figure 10a). The optimum simulation of the observed spectrum gave the following hyperfine coupling constants: $a_N = 0.455$ mT (2N), $a_N = 0.100$ mT (4N) and $a_H = 0.060$ mT (4H), and the contributions from the negligible hydrogen nuclei were incorporated in the line width of the spectral simulation (0.10 mT) (Figure 10b). On the other hand, the generated 1^{2+} gave an ESR spectrum with no hyperfine nor fine structures, and therefore, we could not extract any information on the charge distribution from the spectrum (Figures 12a and 13a).

40

On the one hand, the hyperfine structure of $2^{\bullet+}$ was clarified by the presence of one, three and six equivalent nitrogen nuclei and 12 equivalent hydrogen nuclei originating from the central triphenylamine moiety, although the broadness of the signals suggests additional small hyperfine coupling constants due to the other hydrogen nuclei (Figure 11a). The best fit simulated spectrum was obtained by the following hyperfine coupling constants: a_N = 0.455 mT (1N), a_N = 0.218 mT (3N), a_N = 0.047 mT (6N) and a_H = 0.033 mT (12H), and the contributions from the negligible hydrogen nuclei were incorporated in the line width of the spectral simulation (0.10 mT) (Figure 11b). Like 1^{2+}, the generated 2^{2+} also gave an ESR spectrum with no hyperfine nor fine structures, and therefore, we could not extract any information on the charge distribution from the spectrum (Figures 12b and 13b).
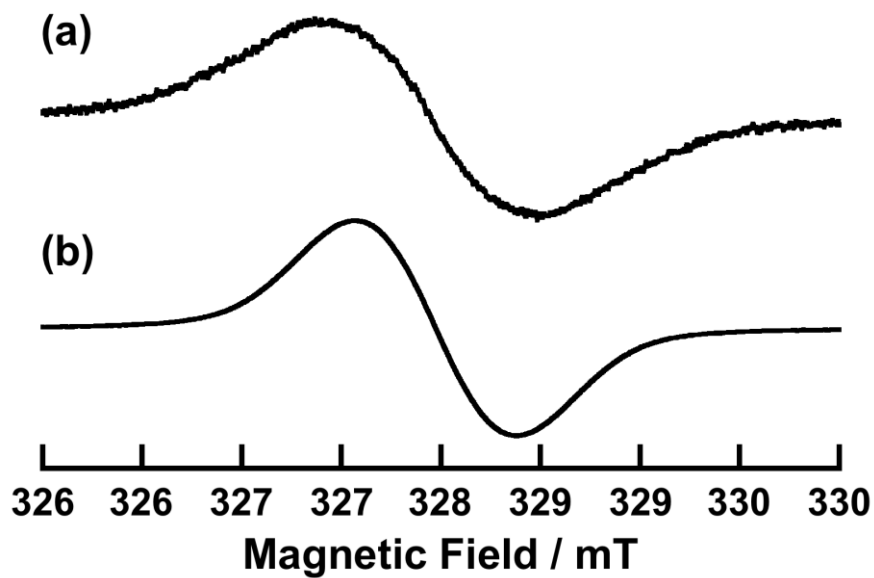
Figure 10. ESR spectrum of $\mathbf{1}^{\bullet+}$: a) in CH_2Cl_2 at 290 K; b) simulated.

Figure 11. ESR spectrum of $\mathbf{2}^{\bullet+}$: a) in CH_2Cl_2 at 290 K; b) simulated.

**Figure 12.** ESR spectra of (a) $\mathbf{1}^{2+}$ and (b) $\mathbf{2}^{2+}$ in CH_2Cl_2 at 290 K.
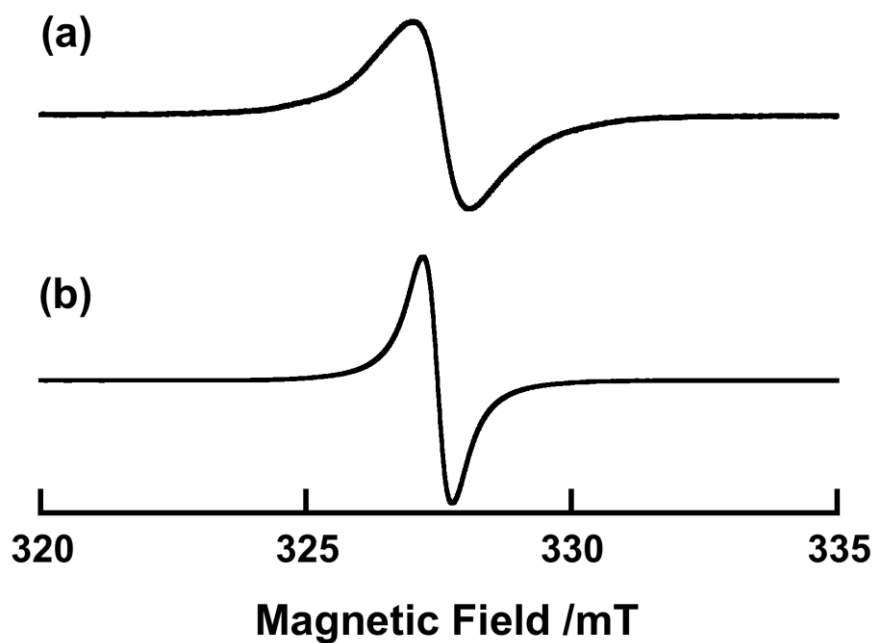
Figure 13. ESR spectra of (a) $\mathbf{1}^{2+}$ and (b) $\mathbf{2}^{2+}$ in CH_2Cl_2 at 123 K.

43

It is interesting to note that the ESR spectral shape for both $1^{\cdot+}$ and $2^{\cdot+}$ did not change in the temperature range from -60 to 20 ˚C (Figure 14), and hence, the observed temperature independency clearly demonstrated that the both $1^{\cdot+}$ and $2^{\cdot+}$ are in CR IV states. As a consequence, it was found that the generated spins in $1^{\cdot+}$, $2^{\cdot+}$, and $5^{\cdot+}$ are distributed over the dendritic molecular backbones, judging from the hyperfine coupling constants. These spin distributions are in good accordance with the DFT–calculated spin densities on $1^{\cdot+}$, $2^{\cdot+}$, and $5^{\cdot+}$, as shown in Figure 15. Again note that the delocalized electronic state in CR IV compounds with multiple redox-active centers like $1^{\cdot+}$, $2^{\cdot+}$, and $5^{\cdot+}$ do not necessarily have the symmetrical charge distribution among the redox-active centers.
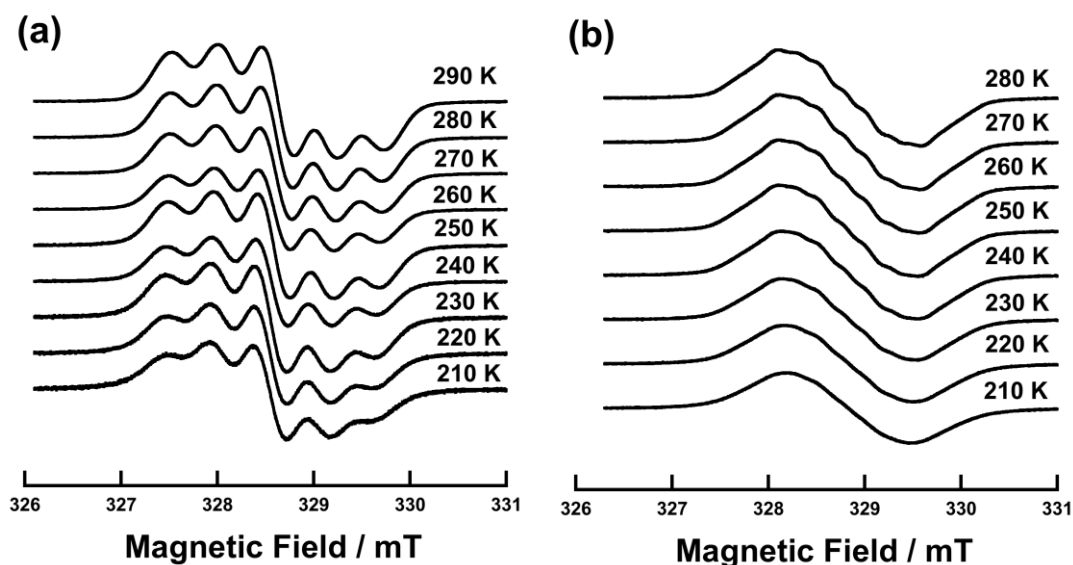
Figure 14. Temperature-dependence of the ESR spectrum for (a) $1^{\cdot+}$ and (b) $2^{\cdot+}$ in CH_2Cl_2.
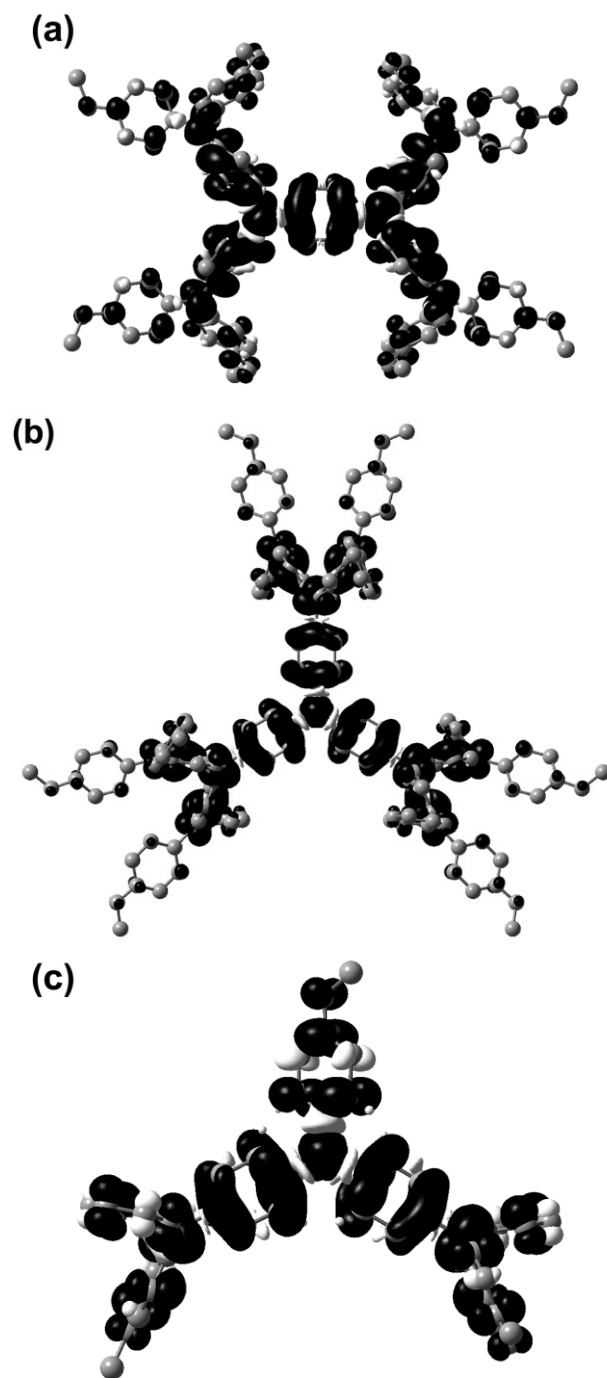
Figure 15. DFT-computed spin density distributions (black: positive spin, white: negative spin; spin isosurface value = 0.0003 electron/au^3; UB3LYP/3–21G) of (a) **1**$^{\bullet+}$, (b) **2**$^{\bullet+}$, and (c) **5**$^{\bullet+}$.

1. 4 Conclusion

In this chapter, the synthesis and electrochemical, spectroelectrochemical, ESR spectroscopic results of two kinds of basic dendritic (or starburst) all–*para*–phenylene–linked oligotriarylamines **1** and **2** were investigated. We have demonstrated that **1** and **2** are oxidizable up to tetra– and hexacations, respectively, and, according to the degree of oxidation, the charge distribution of the charged states of **1** and **2** gradually changed so as to reduce the electrostatic repulsion between increased charges. Moreover, spin distribution in the CR state for the radical cations of **1** and **2** was confirmed by the ESR measurements. These findings are of great interest in connection with the intermolecular hole hopping transfer in the solid state of the oligoarylamines utilized in hole transport layer in OLEDs.[22]

References and Notes

[1] C. W. Tang, S. A. Van Slyke, *Appl. Phys. Lett*. **1987**, *51*, 913.

[2] a) Y. Shirota, *J. Mater. Chem*. **2000**, *10*, 1; b) M. Thelakkat, *Macromol. Mater. Eng*. **2002**, *287*, 442. c) Y. Shirota, H. Kageyama, *Chem. Rev*. **2007**, *107*, 953.

[3] a) S. F. Nelsen, H. Q. Tran, M. A. Nagy, *J. Am. Chem. Soc*. **1998**, *120*, 298; b) S. F. Nelsen, R. F. Ismagilov, D. R. Powell, *J. Am. Chem. Soc*. **1998**, *120*, 1924; c) S. F. Nelsen, R. F. Ismagilov, Y. Teki, *J. Am. Chem. Soc*. **1998**, *120*, 2200; d) S . E. Bailey, J. I. Zink, S. F. Nelsen, *J. Am. Chem. Soc*. **2003**, *125*, 5939; e) J. V. Lockard, J. .I Zink, A. E. Konradsson, M. N. Weaver, S. F. Nelsen, *J. Am. Chem. Soc*. **2003**, *125*, 13471.

[4] a) C. Lambert, G. Nöll, *J. Am. Chem. Soc.* **1999**, *121*, 8434; b) A. V. Szeghalmi, M. Erdmann, V. Engel, M. Schmitt, S. Amthor, V. Kriegisch, G. Nöll, R. Stahl, C. Lambert, D. Leusser, D. Stalke, M. Zabel, J. Popp, *J. Am. Chem. Soc*. **2004**, *126*, 7834.

[5] a) V. Coropceanu, C. Lambert, G. Nöll, J. L. Brédas, *Chem. Phys. Lett*. **2003**, 373,

153; b) V. Coropceanu, N. E. Gruhn, S. Barlow, C. Lambert, J. C. Durivage, T. G. Bill, G. Nöll, S. R. Marder, J. L. Brédas, *J. Am. Chem. Soc.* **2004**, *126*, 2727.

[6] T. Nishiumi, Y. Nomura, Y. Chimoto, M. Higuchi, K. Yamamoto, *J. Phys. Chem. B* **2004**, *108*, 7992.

[7] a) J. Louie, J. F. Hartwig, *J. Am. Chem. Soc.* **1997**, *119*, 11695; b) M. I. Ranasinghe, O. P. Varnavski, J. Pawlas, S. I. Hauck, J. Louie, J. F. Hartwig, T. III. Goodson, *J. Am. Chem. Soc.* **2002**, *124*, 6520.

[8] K. V. Hagedorn, O. Varnavski, J. F. Hartwig, T. III. Goodson, *J. Phys. Chem. C* **2008**, *112*, 2235.

[9] a) K. Yoshizawa, A. Chano, A. Ito, K. Tanaka, T. Yamabe, H. Fujita, J. Yamauchi, M. Shiro, *J. Am. Chem. Soc.* **1992**, *114*, 5994; b) A. Ito, H. Ino, Y. Matsui, Y. Hirao, K. Tanaka, K. Kanemoto, T. Kato, *J. Phys. Chem. A* **2004**, 108, 5715; c) Y. Hirao, H. Ino, A. Ito, K. Tanaka, T. Kato, *J. Phys. Chem. A* **2006**, 110, 4866; d) Y. Hirao, H. Ishizaki, A. Ito, T. Kato, K. Tanaka, *Eur. J. Org. Chem.* **2007**, 186; e) Y. Hirao, A. Ito, K. Tanaka, *J. Phys. Chem. A* **2007**, *111*, 2951; f) A. Ito, D. Sakamaki, H. Ino, A. Taniguchi, Y. Hirao, K. Tanaka, K. Kanemoto, T. Kato, *Eur. J. Org. Chem.* **2009**, 4441.

[10] C. Lambert, G. Nöll, *Angew. Chem. Int. Ed.* **1998**, *37*, 2107. b) C. Lambert, G. Nöll, *Chem. Eur. J.* **2002**, *8*, 3467.

[11] a) K. R. Stickley, T. D. Selby, S. C. Blackstock, *J. Am. Chem. Soc.* **1994**, *116*, 11576; b) K. R. Stickley, T. D. Selby, S. C. Blackstock, *J. Org. Chem.* **1997**, *62*, 448; c) T. D. Selby, S. C. Blackstock, *J. Am. Chem. Soc.* **1998**, *120*, 12155; d) T. D. Selby, K. Y. Kim, S. C. Blackstock, *Chem. Mater.* **2004**, *14*, 1685; e) K. Y. Kim, J. D. Hassenzahl, T. D. Selby, G. J. Szulczewski, S. C. Blackstock, *Chem. Mater.* **2004**, *14*, 1691; f) J. C. Li, K. Y. Kim, S. C. Blackstock, G. J. Szulczewski, *Chem. Mater.* **2004**, *16*, 4711; g) J. C. Li, S. C. Blackstock, G. J. Szulczewski, *J. Phys. Chem. B* **2006**, *110*, 17493; h) C. Chotsuwan, S. C. Blackstock, *J. Am. Chem. Soc.* **2008**, *130*, 12556.

[12] M. M. Wienk, R. A. J. Janssen, *J. Am. Chem. Soc.* **1997**, *119*, 4492.

[13] K. Ragavachari, *Theor. Chem. Acc*. **2000**, *103*, 361 and references cited therein.

[14] a) R. Bauernschmitt, R. Ahlrichs, *Chem. Phys. Lett*. **1996**, *256*, 454; b) M. E. Casida, C. Jamorski, K. C. Casida, D. R. Salahub, *J. Chem. Phys*. **1998**, *108*, 4439; c) R.E. Stratmann, G. E. Scuseria, M. J. Frisch, *J. Chem. Phys*. **1998**, *109*, 8218.

[15] W. J. Hehre, L. Radom, P. v. R. Schleyer, J. A. Pople, *Ab Initio Molecular Orbital Theory*, Wiley: New York, 1986.

[16] J. A. Pople et al. *Gaussian 03*, Gaussian, Inc.: Pittsburgh, PA, **2003**.

[17] a) J. P. Wolfe, S. Wagaw, S. L. Buchwald, *J. Am. Chem. Soc.* **1996**, *118*, 7215; b) M. S. Driver, J. F. Hartwig, *J. Am. Chem. Soc.* **1996**, *118*, 7217.

[18] A. Ito, S. Inoue, Y. Hirao, K. Furukawa, T. Kato, K. Tanaka, *Chem. Commun.* **2008**, 3242.

[19] S. L. Kelly, K. M. Kadish, *Inorg. Chem*. **1984**, *23*, 679.

[20] a) P. Gans, A. Sabatini, A. Vacca, *Talanta* **1996**, *43*, 1739; b) P. Gans, A. Sabatini, A. Vacca, *Annali di Chimica* **1999**, *89*, 45.

[21] a) F. A. Neugebauer, S. Bamberger, W. R. Groh, *Chem. Ber*. **1975**, *108*, 2406; b) W. Schmidt, E. Steckhan, *Chem. Ber*. **1980**, *113*, 577; c) S. Dapperheld, E. Steckhan, K. H. Grosse Brinkhaus, T. Ecsh, *Chem. Ber*. **1991**, *124*, 2557.

[22] a) P. M. Borsenberger, L. Pantmeier, H. Bässler, *J. Chem. Phys*. **1991**, *94*, 5447; b) P. M. Borsenberger, D. S. Weiss, *Organic Photoreceptors for Imaging Systems*, Marcel Dekker: New York, **1993**; c) S. Heun, P. M. Borsenberger, *Chem. Phys*. **1995**, *200*, 245.

Chapter 2

*Meta–Para–*Linked Octaaza[1$_8$]cyclophanes and Their Polycationic States

2.1 Introduction

Hetera[1$_n$]cyclophanes, in which the methylene linkages between the arene rings are replaced by heteroatoms, have recently gained considerable interest in conjunction with applications to supramolecular and material chemistry.[1–3] Of large number of heteroatom-bridged [1$_n$]cyclophanes, aza[1$_n$]cyclophanes[3–11] are considered as attractive scaffolds for realization of multi-spin systems,[12] mainly due to their multi-redox activity, their stability of generated polycationic species, and their synthetic availability by the recent exploitation of palladium-catalyzed aryl amination reactions ("Buchwald–Hartwig reactions"[13]). However, it has been confirmed that strong Coulombic interactions between charged centers generated in aza[1$_n$]metacyclophanes prevent the formation of higher oxidation states with high-spin multiplicity (Coulombic penalty).[7,8,14] As we have shown recently, the insertion of *para*-phenylendiamine (PD) units into macrocyclic molecular backbones can lead to alleviation of the Coulombic penalty between charged triarylaminium radical centers in aza[1$_n$]metacyclophanes and

to lower their oxidation potentials.[15]

On the other hand, tetraaza[1$_4$]m,p,m,p-cyclophane (**1**), the smallest macrocyclic oligoarylamine bearing the alternating *meta-para*-linkage, are known to create an almost pure spin-triplet diradical dication by two-electron oxidation.[16,17] In addition, we have shown that incorporation of the tetraazacyclophane moieties into a oligoarylamine backbone with one-dimensional connectivity can overcome the inherent fragility in spin-coupling pathway of one-dimensional multi-spin systems, and that the robust high-spin alignment in a one-dimensional multi-spin is recovered.[18] In this chapter, as extensions of **1**, we prepared two kinds of octaazacyclophanes with different linkage patterns: octaaza[1$_8$]m,p,m,p,m,p,m,p-cyclophane (**2**), which doubles the ring size of **1**, and octaaza[1$_8$]m,p,p,p,m,p,p,p-cyclophane (**3**), in which two extended *para*-phenylene-linked oligotriarylamines as spin-bearing units are linked by two *meta*-phenylenes. Apparently, in the octaazacyclophane **2**, the structural rigidity can be weakened due to the extension of ring size, and therefore, it is interesting to examine how such a flexible structure influence the spin-coupling pathway in the polycationic species of **2**, as compared to that of **1**$^{2+}$. In addition, the octaazacyclophane **3** enables us to judge whether the extended *para*-phenylene-linked oligotriarylamine moieties can serve as spin-containing units.[19]
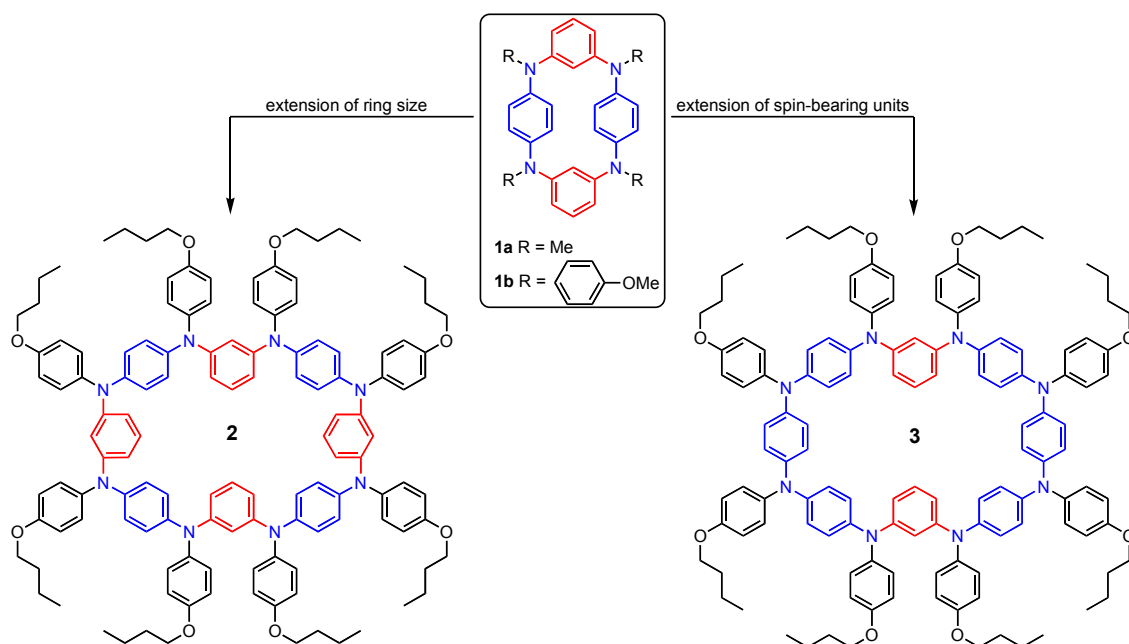
Figure 1. Two kinds of extension of tetraaza[1₄]*m,p,m,p*-cyclophane **1** and their target macrocycles **2** and **3**.

2.2 Experimental Section

General Experimental methods: Commercial grade regents were used without further purification. Solvents were purified, dried, and degassed following standard procedures. Compounds **4** and **5** were synthesized according to literature procedures, and were checked by ^{1}H NMR, ^{13}C NMR, and FAB LRMS spectroscopy. Elemental analyses were performed by Center for Organic Elemental Microanalysis, Kyoto University. ^{1}H and ^{13}C NMR spectra were measured by a JEOL JNM-EX400 FT-NMR spectrometer. Chemical shifts of NMR spectra are determined relative to internal tetramethylsilane (TMS) standard (δ), are given in parts per million (ppm). Low resolution (LR) fast-atom-bombardment (FAB) mass spectra (MS) were recorded on a JEOL JMS-HX110A mass spectrometer with *m*-nitrobenzyl alcohol as a matrix. High

resolution electrospray ionization (ESI) mass spectrum was acquired using a mass spectrometer (Thermo Fisher EXACTIVE).

Synthetic Details. **(6):** A mixture of **5** (0.59 g, 0.67 mmol), *p*-dibromobenzene (1.91 g, 8.10 mmol), Pd(OAc)$_2$ (0.076 g, 0.03 mmol), 1,1'-bis(diphenylphosphanyl)ferrocene (DPPF) (0.039 g, 0.07 mmol) and NaO*t*-Bu (0.268 g, 2.79 mmol) in toluene (3.4 ml) was refluxed under an argon atmosphere for 36 h. After evaporation of the solvent, the residue was dissolved in CH$_2$Cl$_2$ and washed with brine. The organic layer was separated and dried over Na$_2$SO$_4$. After evaporation of the solvent, the crude product was chromatographed on silica gel (toluene/ hexane = 1:1 as eluent) to afford **6** (0.66 2g, 82.8%) as a pale yellow solid. ^{1}H NMR (400MHz, acetone-*d$_6$*): δ = 0.939-0.986 (m, 12H), 1.432-1.543 (m, 8H), 1.693-1.780 (m, 8H), 3.929-3.981 (m, 8H), 6.432 (dd, *J* = 2.20, 8.05 Hz, 2H), 6.682 (t, *J* = 2.20 Hz, 1H), 6.802-7.046 (m, 29H), 7.307 (d, *J* = 9.03 Hz, 4H); ^{13}C NMR (100 MHz, acetone-*d$_6$*): δ = 14.22, 20.02, 32.24, 68.59, 103.17, 115.32, 115.68, 116.26, 116.49, 123.26, 125.26, 125.89, 128.09, 128.30, 130.49, 132.80, 140.75, 141.01, 142.93, 144.23, 148.84, 149.94, 156.97, 157.31. HR-ESI-MS: *m/z* calcd for C$_{70}$H$_{72}$N$_4$O$_4$Br$_2$: 1190.3915, found 1190.3933 [M]$^+$.

Octaaza[1$_8$]*m,p,m,p,m,p,m,p*-cyclophane (2): Anhydrous toluene (100 ml) was added to Pd(dba)$_2$ (0.016 g, 0.027 mmol), Ph$_5$FcP(*t*-Bu)$_3$ (Q-Phos) (0.037 g, 0.052 mmol), and NaO*t*-Bu (0.196 g, 2.036 mmol) in a flask equipped with a dropping funnel which was charged with a toluene solution (50 ml) of **4** (0.443 g, 0.501 mmol) and **5** (0.599 g, 0.502 mmol), and the toluene solution was stirred under an argon atmosphere at 110 ˚C for a while. The solution in the dropping funnel was gradually added to the solution containing the palladium catalyst for 1 h, and then, the reaction mixture was refluxed for 21 h with stirring. The reaction mixture was cooled down to room temperature, washed with brine, and dried over Na$_2$SO$_4$. After evaporation of the

solvent, the crude product was chromatographed on silica gel (toluene/ hexane = 2:1 as eluent) to afford **2** (0.259 g, 26.9%) as a white powder. ^{1}H NMR (400MHz, tetrahydrofuran-d_8): δ = 0.964 (t, J = 7.32 Hz, 24H), 1.485 (m, 16H), ~1.7 (m,16H; the corresponding signals are masked by the solvent signal (due to the β-protons)), 3.882 (t, J = 6.34 Hz, 16H), 6.360 (dd, J = 2.20, 8.29 Hz, 8H), 6.757 (d, J = 9.03 Hz, 16H), 6.846 (m, 24H), 6.964 (d, J = 9.03 Hz, 16H); ^{13}C NMR (100 MHz, tetrahydrofuran-d_8): δ = 14.21, 20.15, 32.43, 68.33, 115.23, 115.80, 124.64, 127.67, 141.02, 143.09, 149.46, 156.56. Anal. Calcd for $C_{128}H_{136}N_8O_8$: C, 80.30; H, 7.16; N, 5.85; O, 6.69, found: C, 80.50; H, 7.27; N, 5.87; O, 6.92. HR-ESI-MS: m/z calcd for $C_{128}H_{136}N_8O_8$: 1913.0476, found 1913.0539 [M]$^+$.

Octaaza[1$_8$]m,p,p,p,m,p,p,p-cyclophane (3): Anhydrous toluene (100 ml) was added to Pd(dba)$_2$ (0.013 g, 0.023 mmol), Ph$_5$FcP(t-Bu)^3 (Q-Phos) (0.0029 g, 0.040 mmol), and NaOt-Bu (0.155 g, 1.610 mmol) in a flask equipped with a dropping funnel, which was charged with a toluene solution (50 ml) of **5** (0.351 g, 0.397 mmol) and **6** (0.471 g, 0.394 mmol), and the toluene solution was stirred under an argon atmosphere at 110 ˚C for a while. The solution in the dropping funnel was gradually added to the solution containing the palladium catalyst, and then, the reaction mixture continued stirring. After 16 h, the reaction mixture was refluxed for 20 h. The reaction mixture was cooled down to room temperature, washed with brine, and dried over Na$_2$SO$_4$. After evaporation of the solvent, the crude product was chromatographed on silica gel (toluene as eluent) to afford **3** (0.197 g, 26.0%) as a pale yellow powder. ^{1}H NMR (400MHz, tetrahydrofuran-d_8): δ = 0.963 (t, J = 7.56 Hz, 24H), 1.487 (m, 16H), ~1.7 (m, 16H; the corresponding signals are masked by the solvent signal (due to the β-protons)), 3.834 (m, 16H), 6.295 (dd, J = 1.95, 8.05 Hz, 4H), 6.734 (d, J = 8.78 Hz, 8H), 6.785-6.880 (m, 36H), 6.941 (d, J = 9.03 Hz, 8H), 7.018 (d, J = 8.78 Hz, 8H); ^{13}C NMR (100 MHz, tetrahydrofuran-d_8): δ= 14.18, 14.20, 20.14, 20.17, 32.42, 32.47, 68.39, 68.40, 114.30, 115.92, 115.94, 124.05, 124.86, 125.47, 126.93, 128.03, 128.88, 129.64,

141.07, 141.70, 142.82, 143.52, 144.20, 149.69, 156.33, 156.89; Anal. Calcd for $C_{128}H_{136}N_8O_8$: C, 80.30; H, 7.16; N, 5.85; O, 6.69, found: C, 80.42; H, 7.15; N, 5.70; O, 6.82. HR-ESI-MS: m/z calcd for $C_{128}H_{136}N_8O_8$: 1913.0476, found 1913.0544 $[M]^+$.

Electrochemical measurements. The redox properties were evaluated by cyclic voltammetry in CH_2Cl_2 solution at 298 K with 0.1 M tetra-n-butylammonium tetrafluoroborate as supporting electrolyte (scan rate 100 mV s^{-1}) using an ALS/chi Electrochemical Analyzer model 612A. A three-electrode assembly was used, which was equipped with platinum disk (2 mm^2), a platinum wire, and Ag/0.01 M $AgNO_3$ (acetonitrile) as the working electrode, the counter electrode, and the reference electrode, respectively. The redox potential were referenced against a ferrocene/ferrocenium ($Fc^{0/+}$) redox potential measured in the same electrolytic solution.

UV-Vis-NIR spectrum measurements. UV-Vis-NIR absorption spectra were obtained with a Perkin-Elmer Lambda 19 spectrometer. Spectroelectrochemical measurements were carried out with a custom-made optically transparent thin-layer electrochemical (OTTLE) cell (light pass length = 1 mm) equipped with a platinum mesh, a platinum coil, and a silver wire as the working electrode, the counter electrode, and the pseudo-reference electrode, respectively. The potential was applied with an ALS/chi Electrochemical Analyzer model 612A.

ESR measurements. ESR spectra were recorded on a JEOL JES-SRE2X or a JEOL JES-TE200 X-band spectrometer, in which the temperature was controlled by a JEOL DVT2 variable-temperature unit or an Oxford ITC503 temperature controller combined with an ESR 910 continuous flow cryostat, respectively. A Mn^{2+}/MnO solid solution was used as a reference for the determination of g-values and hyperfine coupling constants. Pulsed ESR measurements were carried out on a Bruker ELEXSYS E580 X-band FT ESR spectrometer.

2.3 Results and Discussion

2.3.1 Synthesis

As shown in Scheme 1, *meta-para*-linked octaazacyclophanes **2** and **3** were prepared by the convergent fragment double-coupling between tetraamine **5**[20] and the corresponding dihalides **4**[20] and **6** utilizing palladium-catalyzed aryl amination reaction (Buchwald-Hartwig reaction) as a key reaction. Although the generation of **2** by the same cross-coupling reaction of **5** with 1,3-dibromobenzene was also attempted, the main product was found to be tetraazacyclophane **1**, and we were unable to detect the desired product **2** in the reaction mixture.
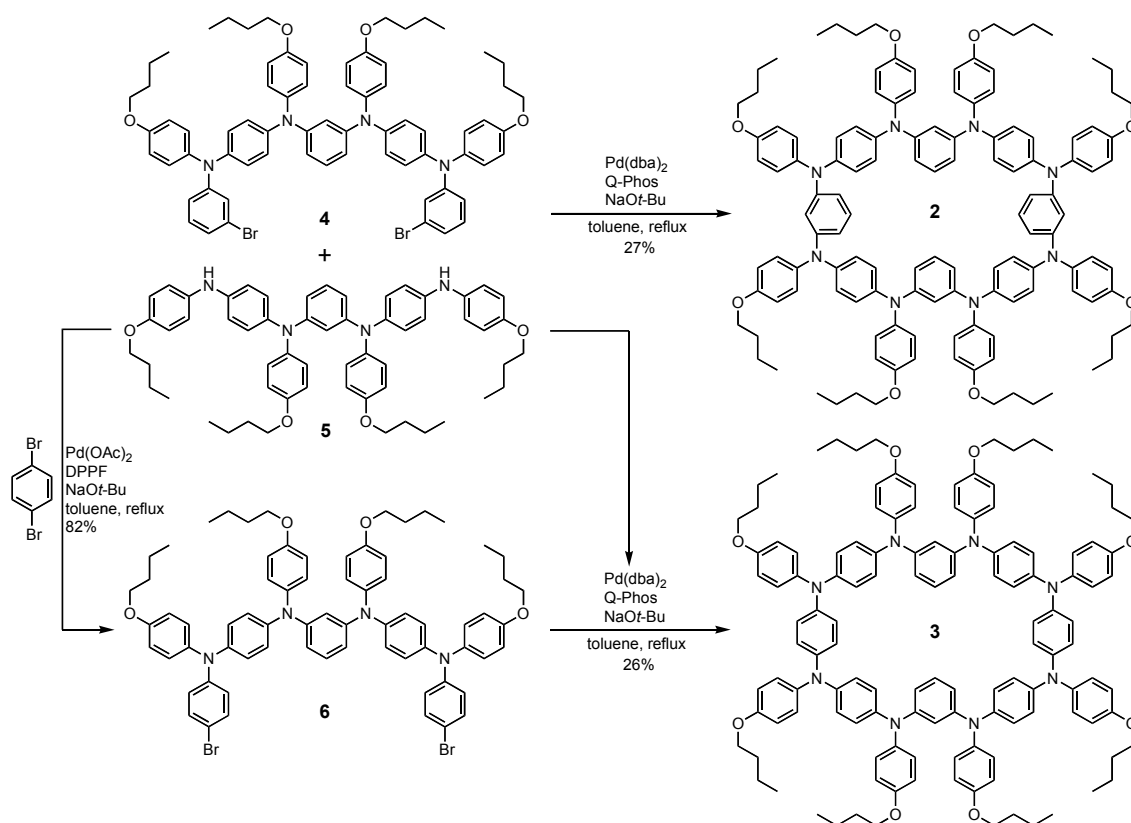

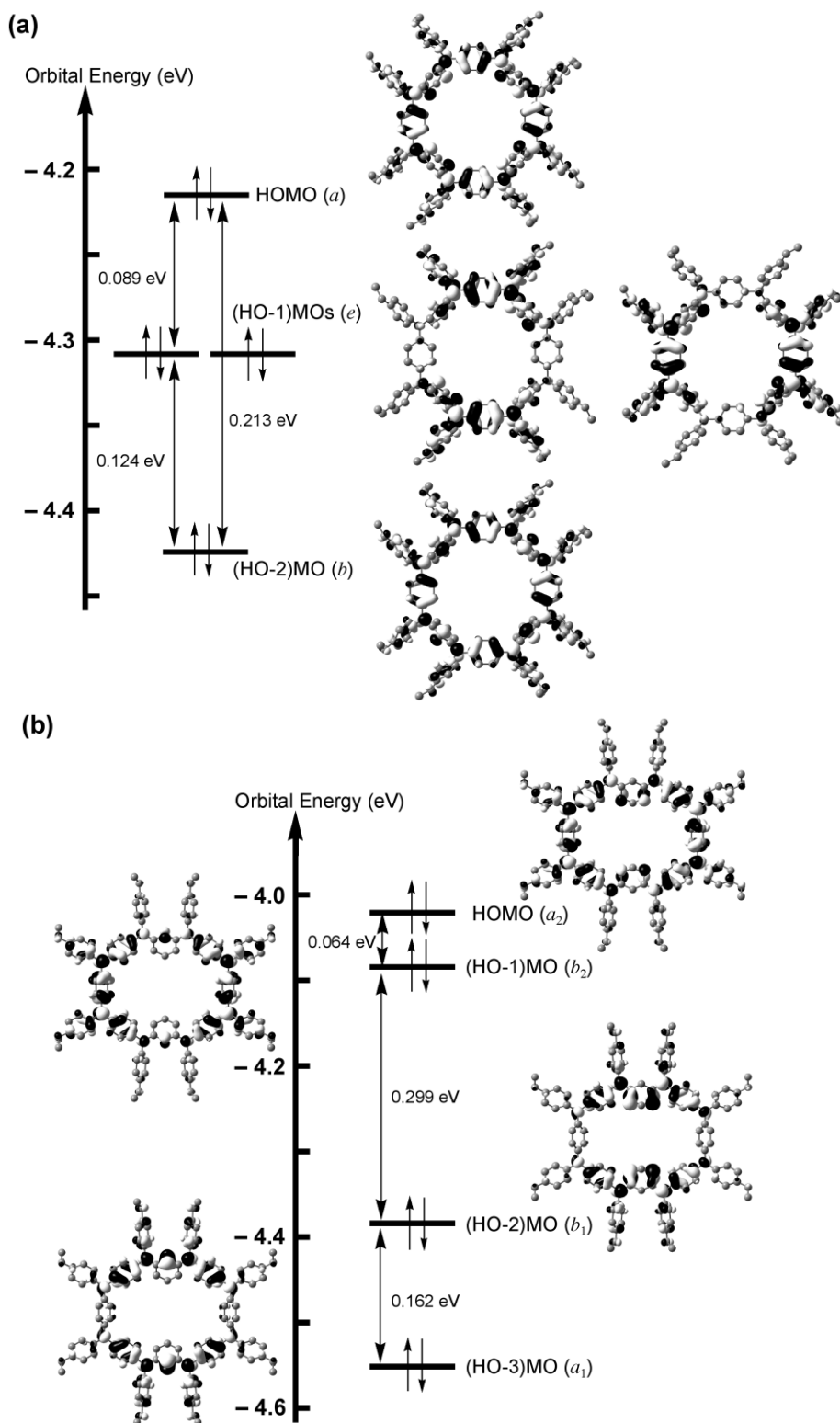**Scheme 1**. Synthetic routes for **2** and **3**.

2.3.2 DFT Calculations

To address the electronic structures of **2** and **3**, we carried out the DFT calculations (B3LYP/6-31G*) on the model compounds **2'** and **3'**, in which all *n*-butoxy groups of **2** and **3** were replaced by methoxy groups to reduce the computational cost. The global energy minimum of **2'** was predicted to be a pseudo-cone conformation (all the *meta*-phenylene rings are oriented in the same direction) with C_4 symmetry, while a pseudo-1,3-alternate conformer (all the adjacent *meta*-phenylene rings are oriented in the opposite directions) with D_{2d} symmetry was estimated to be 0.89 kcal/mol less stable than the pseudo-cone conformer (Figure 2a and 2c). Thus, all the *meta*-phenylene rings of **2** are anticipated to be inclined to the molecular plane defined by eight nitrogen atoms. On the other hand, a C_{2v}-symmetric conformer with a globally planer structure as compared to **2'** was placed at the global energy minimum for **3**, whereas the next lowest energy conformer (one of the *meta*-phenylene rings is almost perpendicular to the slightly warped molecular plane) with C_s symmetry was slightly above the C_{2v} conformer by only 0.03 kcal/mol (Figure 2b and 2d). The presence of the energetically low-lying conformers predicts the flexible structures of **2** and **3**. This point is reflected in the observed simplified ^{1}H and ^{13}C NMR spectra of **2** and **3**.

The calculated frontier Kohn–Sham MOs of **2'** (HOMO, doubly degenerate (HO-1)MOs, and (HO-2)MO) are shown in Figure 3a. The energy gap between HOMO and (HO-2)MO were evaluated to be small (0.21 eV), and moreover, judging from their MO patterns, they can be classified as non-disjoint or coexistensive MOs.[7,21] Accordingly, when four electrons are removed from **2**, the resulting tetracation is predicted to be in spin-quintet state. In the case of model compound **3'**, however, the energy gap between the (HO-1)MO and (HO-2)MO were considerably large, whereas the HOMO and (HO-1)MO were quasi-degenerate. As a consequence, it is anticipated that the higher oxidized states, **3**$^{3+}$ and **3**$^{4+}$, are in spin-doublet and closed-shell electronic structures, respectively, while dication **3**$^{2+}$ is predicted to be in spin-triplet

state.
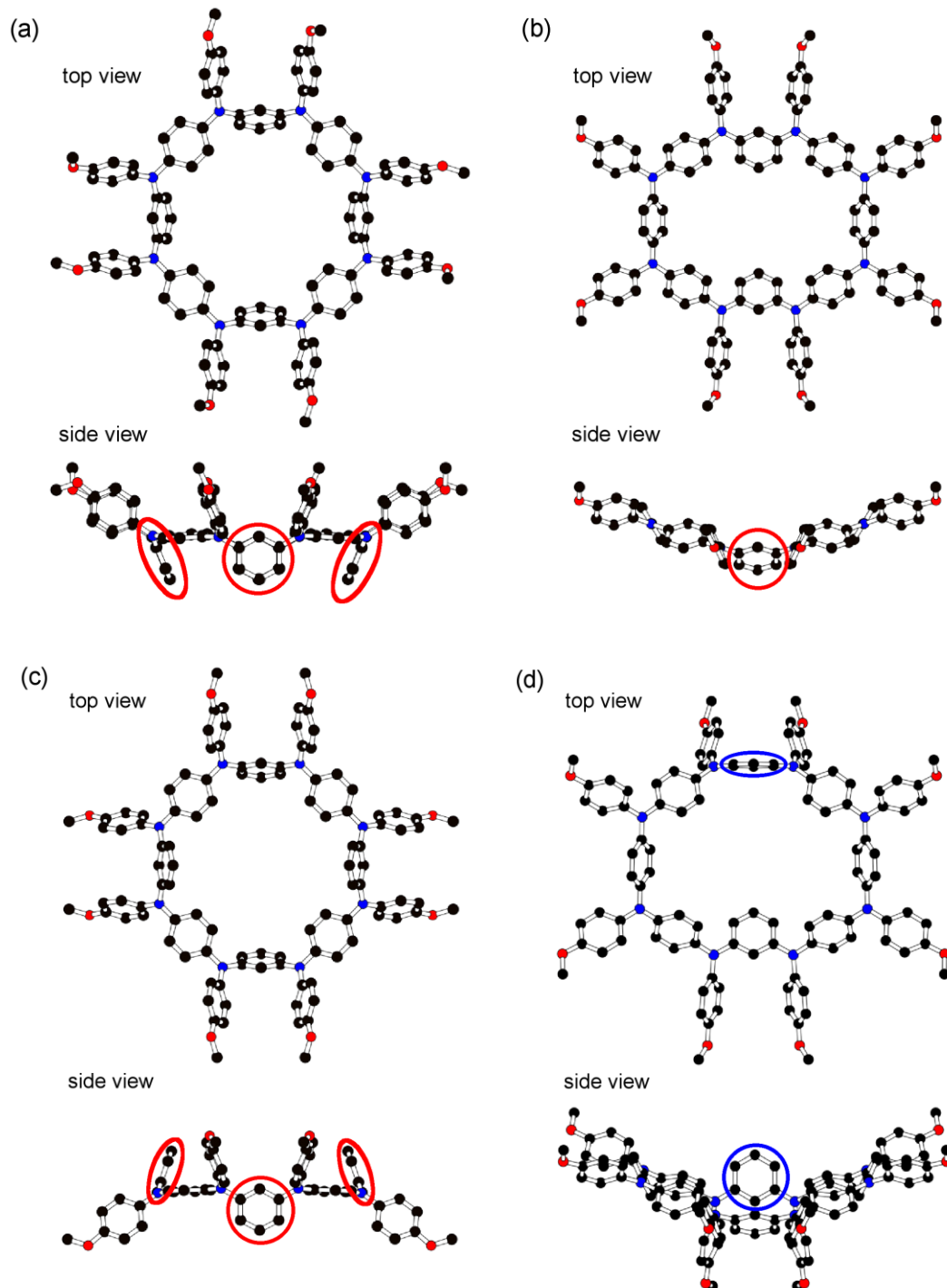
Figure 2. Optimized structures of the model compounds **2**' and **3**': the lowest energy conformers for (a) **2**' (C_4) and (b) **3**' (C_{2v}), and the next lowest energy conformers for (c) **2**' (D_{2d}) and (d) **3**' (C_s).

(a)

Orbital Energy (eV)

− 4.2 — HOMO (*a*)

0.089 eV

− 4.3 — (HO-1)MOs (*e*)

0.213 eV

0.124 eV

− 4.4 — (HO-2)MO (*b*)

(b)

Orbital Energy (eV)

− 4.0 — HOMO (*a*₂)

0.064 eV

(HO-1)MO (*b*₂)

− 4.2

0.299 eV

− 4.4 — (HO-2)MO (*b*₁)

0.162 eV

− 4.6 — (HO-3)MO (*a*₁)

Figure 3. Relative energy levels of the frontier Kohn–Sham molecular orbitals for the model compounds (a) **2'** and (b) **3'** based on calculations at the B3LYP/6-31G* level.

58

2.3.3 Electrochemistry

In order to estimate the multi-electron redox activity originating from four *para*-phenylenediamine (PD) units in **2** and two *para*-phenylene-linked oligotriarylamine units in **3**, we measured the cyclic voltammograms of **2** and **3** in CH_2Cl_2 containing 0.1 M *n*-Bu_4NBF_4 as the supporting electrolyte at 298 K. As shown in Figure 4, the redox behaviors of **2** and **3** are roughly viewed as four reversible oxidation steps (1e, 1e, 2e, and 4e for **2** and 2e, 2e, 1e, and 3e for **3**; *n*e = number of electrons). Differential pulse voltammetry (DPV) and the digital simulation[22] of the observed DPV curves afforded the oxidation potential at each oxidation process for **2** and **3**. The oxidation potentials of **2**, **3**, and the reference compounds [*N,N,N',N'*-tetraanisyl-*para*-phenylenediamine (**TAPD**) and tetraaza- cyclophane **1b**] are summarized in Table 1. This result indicates that both of the present octaazacyclophanes are oxidizable up to octacation, corresponding to the number of nitrogen atoms as redox-active centers. As compared to the large E_3–E_2 separation (0.32 V) for **1b**, the first four one-electron oxidation processes of **2** correspond to the formation of four semi-quinoidal PD radical cations, while the remaining one two-electron oxidation and two one-electron oxidation processes give rise to the formation of six quinoidal PD dications, leading to a spinless state. On the other hand, the large E_3–E_2 separation (0.23 V) for **3** can be interpreted by the generation of the delocalized radical cation on each *para*-phenylene-linked oligotriarylamine units. More noteworthy is that the first oxidation potential (E_1 = –0.24 V) of **3** was considerably lower than those of **1b** (E_1 = –0.01 V) and **2** (E_1 = –0.09 V). This result indicates that the generated radical cation is stabilized by spin- and/or charge delocalization due to elongation of π-conjugation in *para*-phenylene-linked oligotriarylamine unit. In addition, since the third and forth oxidations of **3** also take place at the lower oxidation potentials (E_3 = +0.05 V; E_4 = +0.12 V), the formation of tetracation for **3** is strongly facilitated as compared with tetraazacyclophane **1b** (E_3 = +0.54 V; E_4 = +0.67 V).
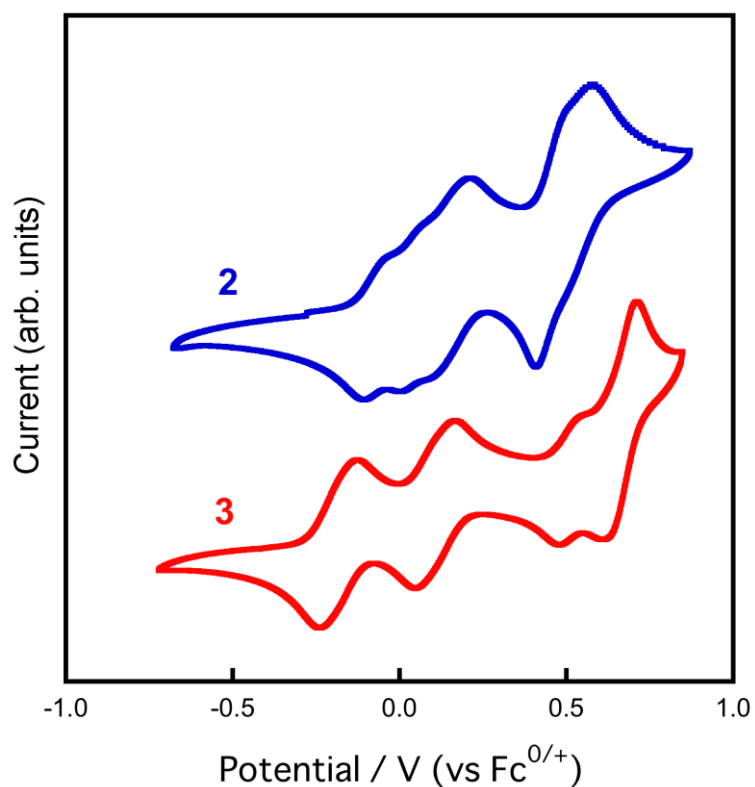
Figure 4. Cyclic voltammograms (CV) of **2** (blue curve) and **3** (red curve), measured in CH$_2$Cl$_2$ containing 0.1 M *n*-Bu$_4$NBF$_4$ at 298 K (scan rate 100 mV s^{-1}).
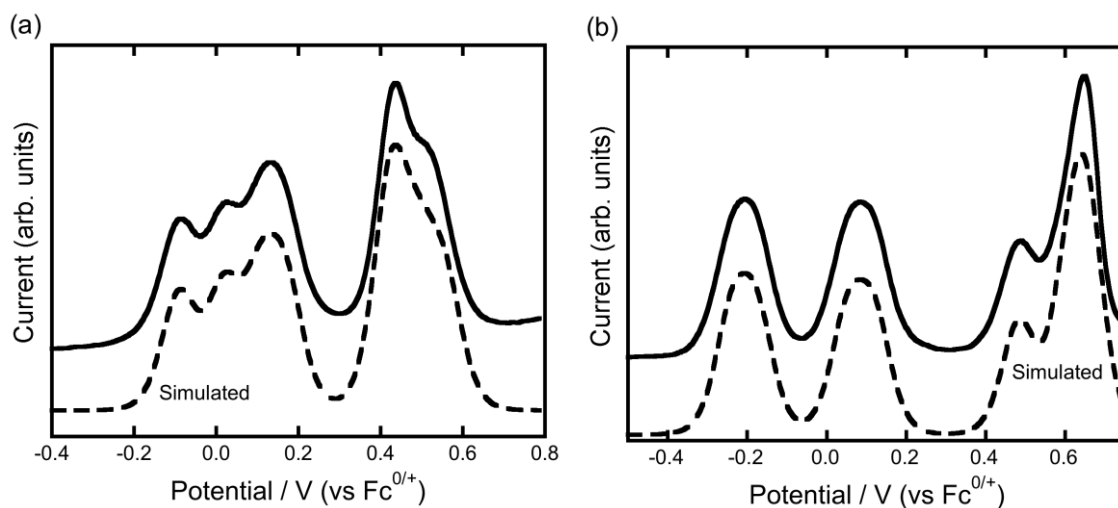
Figure 5. Differential pulse voltammograms (DPV) of (a) **2** and (b) **3**, measured in CH$_2$Cl$_2$ containing 0.1 M *n*-Bu$_4$NBF$_4$ at 298 K (scan rate 100 mV s^{-1}). The simulated DPVs are drawn with a broken line and the oxidation potentials listed in Table 1 were estimated by the digital simulation of the observed DPVs.

Table 1: Oxidation Potentials (V versus $Fc^{0/+}$) by Cyclic Voltammetry and Differential Pulse Voltammetry (Scan Rate: 0.1 V s^{-1}) of **2**, **3**, and the Related Compounds in CH_2Cl_2 (0.1 M n-Bu_4BF_4) at 298 K.

Compd	E_1	E_2	E_3	E_4	E_5	E_6	E_7
TAPD [a]	−0.13	+0.35	——	——	——	——	——
1b [b]	−0.01	+0.22	+0.54	+0.67	——	——	——
2 [c]	−0.09	+0.02	+0.11	+0.17	+0.43 [d]	+0.50	+0.56
3 [c]	−0.24	−0.18	+0.05	+0.12	+0.48	+0.60	+0.65 [d]

[a] Taken from ref 15. [b] Taken from ref 26. [c] Determined from the digital simulation of the observed DPV. [d] Quasi-two-electron transfer.

2.3.4 Spectroelectrochemistry

To provide information on the electronic structure at each oxidation step of **2** and **3**, we have measured the UV-Vis-NIR absorption spectral change during the course of the oxidation of **2** and **3** by using an optically transparent thin-layer electrochemical cell. The spectral changes during the oxidation process of **2** to **2**$^{2+}$ are shown in Figure 6a. As the oxidation proceeds, a π-π* band at 3.90 eV (318 nm) for **2** was changed into three new bands corresponding to the oxidized states from **2**$^+$ to **2**$^{2+}$ [1.29 eV (960 nm), 2.16 eV (575 nm), and 3.01 eV (412 nm)] with an isosbestic point at 3.50 eV (354 nm). The observed lowest energy band can be regarded as the so-called charge-resonance (CR) intervalence band (IV) band owing to the formation of semi-quinone radical cation of the *para*-phenylenediamine (PD) moiety,[23-25] and showed a slight blue shift (1.25 (**2**$^+$) to 1.29 eV (**2**$^{2+}$)) with increasing oxidation number, as is often observed for oligoarylamines containing several PD moieties.[11a,18,25-27] On going from **2**$^{2+}$ to **2**$^{4+}$, the

newly appeared three bands exhibited continuous increase in absorbance with an isosbestic point at 3.37 eV (368 nm), and finally the absorbance reached up to twice that of 2^{2+} (Figure 6b). As is shown in Figure 6c, it should be noted that the absorbance in lower-energy region of the CR IV band of 2^{2+} decreased during the course of the oxidation from 2^{2+} to 2^{4+} with an isosbestic point at 0.94 eV (1325 nm), clearly demonstrating the decrease of absorbance in the weak Class II intervalence charge-transfer (IVCT) band (which is often masked by the intense CR IV and/or other bands)[18,28] between the neutral and one-electron oxidized PD moieties through *meta*-phenylene linkers, accompanied by the disappearance of the charge-transferable neutral PD moieties. This indicates the coexistence of two types of the IV states, that is, the localized Class II and delocalized Class III states, in the single molecule, as is observed in organic IV compounds with multiple redox-active centers linked by both *meta*-phenylene and *para*-phenylene linkers.[26] When 2^{4+} was further oxidized, the intense CR IV band began to decreased, and a new band at 1.58 eV (786 nm) emerged with an isosbestic point at 1.45 eV (855 nm). This new band is attributable to the formation of diamagnetic dicationic quinoidal PD structures (Figure 6d).
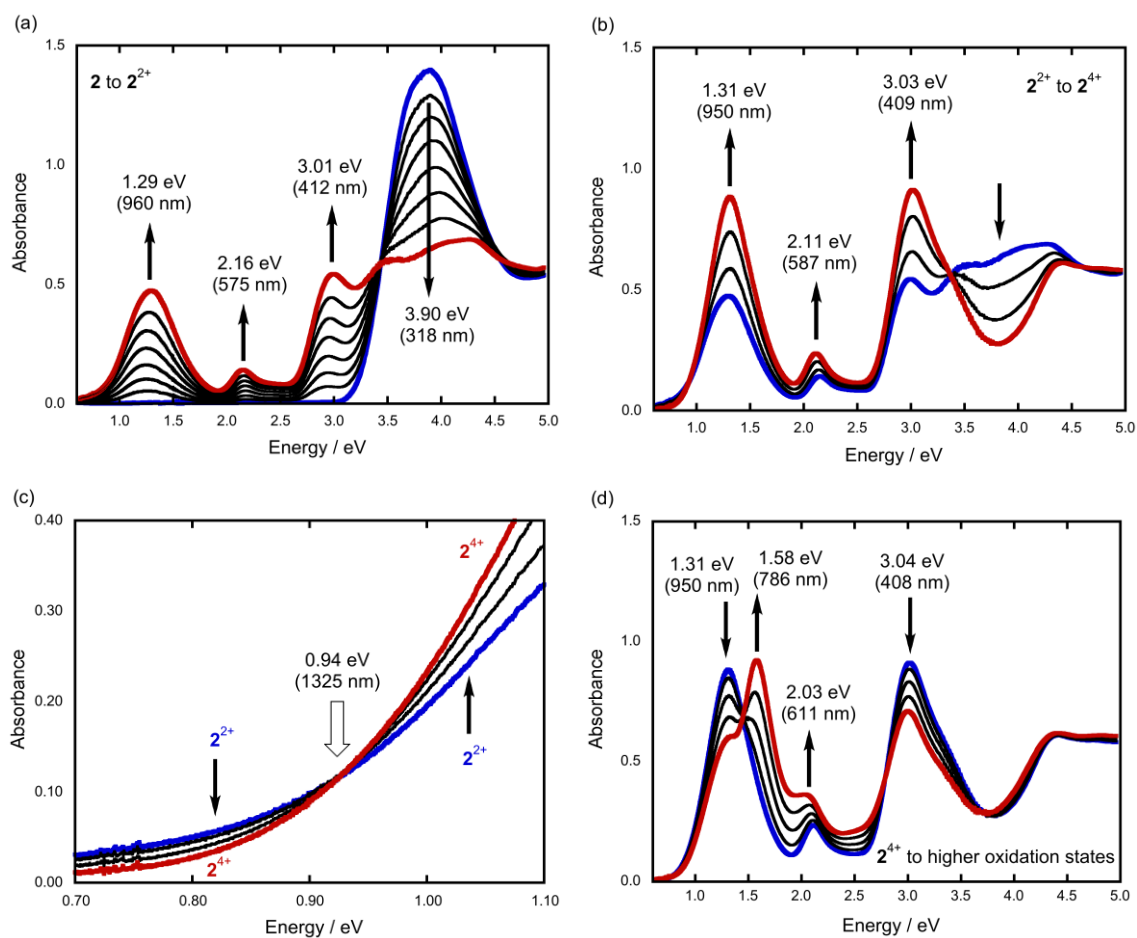
Figure 6. UV-Vis-NIR absorption spectra of the stepwise electrochemical oxidation of **2** in CH$_2$Cl$_2$ with 0.1 M n-Bu$_4$NBF$_4$ at 298 K: a) **2** (in blue) to **2**$^{2+}$ (in red); b) **2**$^{2+}$ (in blue) to **2**$^{4+}$ (in red); c) Enlargement of the NIR region for the oxidation process from **2**$^{2+}$ (in blue) to **2**$^{4+}$ (in red); d) further oxidation process from **2**$^{4+}$ (in blue).

Turning now to the spectral change during the oxidation of neutral to dication for **3**, similar with that for **2**, three low energy bands at 0.97 eV (1272 nm), 2.34 eV (530 nm), and 2.79 eV (444 nm) continued to grow up with a small blue shift (ca 0.85 (**3**$^+$) to 0.97 eV (**3**$^{2+}$)) of the lowest energy band (Figure 7a). The lowest energy band accompanied by two shoulders at 1.31 eV (950 nm) and 1.80 eV (690 nm), which are probably ascribed to partially resolved vibrational fine structure, as is typically observed in delocalized Class III IV compounds,[29,30] and therefore, it is strongly suggested that the generated charge and/or spin is delocalized over the *para*-phenylene-linked oligotriarylamine unit of **3**. Upon further oxidation from **3**$^{2+}$ to **3**$^{4+}$, both of the blue shift (1.03 eV (1200 nm)) and the increase in the intensity of the lowest energy band were observed together with an isosbestic point around 0.90 eV (1385 nm) (Figure 7b). When the electrode potential exceeded the oxidation potential of **3**$^{4+}$, this trend toward the blue shift and increase in intensity of the lowest energy band remained unchanged with appearance of a new isosbestic point around 0.99 eV (1250 nm) (Figure 7c). Accordingly, we could not observe no definite spectral change corresponding to the structural change from the semi-quinoidal structure to the quinoidal one, which was observed in the spectral change for **2** (Figure 6d). This is probably due to the constraint by macrocyclic molecular structure, which hinders the planarization of molecular structure accompanied by the quinoidal deformation. Similar spectral changes are also seen in those for the dendritic all-*para*-phenylene-linked origoarylamines, in which possible cause is probably due to overcrowding by bulky dendron groups.[25]
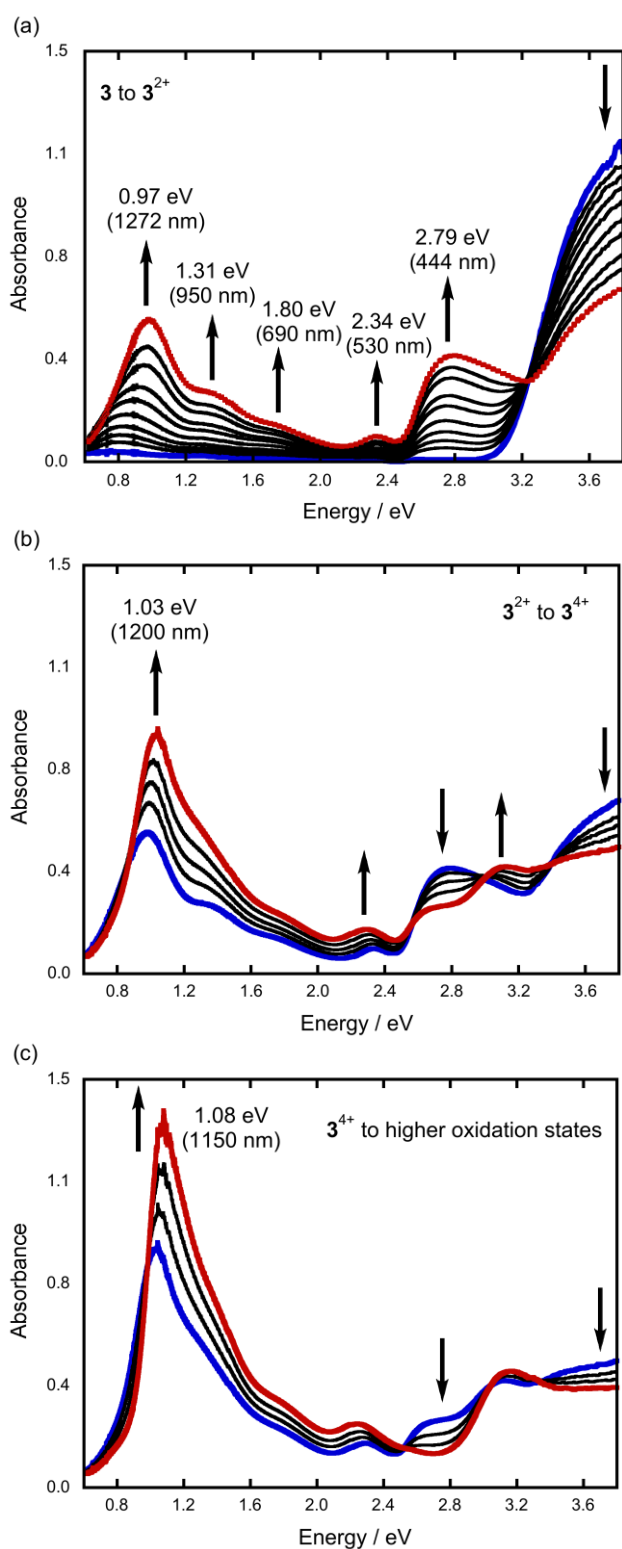
Figure 7. UV-Vis-NIR absorption spectra of the stepwise electrochemical oxidation of **3** in CH$_2$Cl$_2$ with 0.1 M *n*-Bu$_4$NBF$_4$ at 298 K: a) **3** (in blue) to **3**$^{2+}$ (in red); b) **3**$^{2+}$ (in blue) to **3**$^{4+}$ (in red); c) further oxidation process from **3**$^{4+}$ (in blue).

2.3.4 ESR Spectroscopy

In order to estimate the effect by the extension of macrocyclic ring size from tetraazacyclophane **1** to octaazacyclophanes **2** and **3**, we examined the spin-multiplicities for the polycationic specices of **2** and **3**. The present quantum chemical, electrochemical, and spectroelectrochemical studies on **2** and **3** open the possibility that the dicationic and tetracationic species for **2** and the dicationic species for **3** are accessible by appropriate chemical oxidations. The oxidized samples of **2** and **3** were generated at 195 K by adding 2 and/or 4 equivalents of tris(4-bromophenyl)aminium hexachloroantimonate (Magic Blue).[31] To determine the spin multiplicity of the high-spin components of each oxidation state for **2** and **3**, we carried out the electron spin transient nutation (ESTN) measurements based on the pulsed ESR method.[32] The observed nutation frequency ω_{nut} for an allowed spin-state transition from $|S, M_S\rangle$ to $|S, M_S + 1\rangle$ can be approximately represented by the following relationship:

$$\omega_{\text{nut}} = \sqrt{S(S+1) - M_S(M_S+1)} \ \omega_0 \qquad (1)$$

This equation indicates that ω_{nut} can be scaled with the total spin quantum number S and the spin magnetic quantum number M_S in a unit of ω_0, which corresponds to the nutation frequency for the spin–doublet species (ω_{doublet}). The field-swept ESTN spectra observed for each oxidation state for **2** and **3** are shown in Figure 8. The projection along the magnetic field axis approximately corresponds to the usual continuous wave ESR (CW-ESR) spectrum, while the projection along the frequency axis corresponds to the transient nutation spectrum. The nutation frequencies observed for each oxidation state of **2** and **3** are summarized in Table 2. As shown in Figure 8a, the ESTN spectrum showed two signals corresponding to the spin-doublet and spin-triplet states, when **2** was treated with 2 molar equivalents of oxidant. Apparently,

the signal intensity of the spin-doublet state was larger than that of the spin-triplet state. The generated two unpaired spins are probably localized on opposite sides of the macrocyclic structure so as to reduce the Coulombic repulsion interactions. As a consequence, the magnetic interaction between two unpaired spins was strongly attenuated due to the resulting long spin-coupling pathway. When oxidized with 4 molar equivalents of oxidant, the oxidized species exhibited four nutation signals corresponding to different spin states (S = 1/2, 1, 3/2, and 2) (Figure 8b). The spin-quintet signals (26.0 and 31.0 MHz) indicate that four unpaired spins localized on four PD units are ferromagnetically coupled through m-phenylene ferromagnetic coupler in the macrocyclic structure, as is also predicted from quasi-degenerate non-disjoint MOs (Figure 3a). However, the definite competing spin-triplet signal (19.4 MHz) reveals that the spin triplet-quintet energy splitting is considerably small, probably due to attenuation of spin-coupling pathway by facile conformational change. In addition, the spin-quartet species originating from partially oxidized 2^{3+} were not negligible. This finding suggests that the present ring extension to alternating *meta-para*-linked octaazacyclophane **2** attenuates the spin-coupling pathway, and, in this regard, octaazacyclophane **2** is similar to linear oligoarylamines.[33]

In contrast, the ESTN spectrum for dication 3^{2+} generated by treatment with 2 molar equivalents of oxidant clearly displayed the formation of an almost pure spin-triplet state (Figure 8c). On the other hand, when **3** was treated by 4 molar equivalents of oxidant, the ESTN signal almost disappeared and only a very weak spin-doublet signal was observed, thus indicating the generated 3^{4+} is diamagnetic, although the corresponding absorption spectrum showed no bands ascribed to the quinoidal structure of *para*-phenylene-linked oligotriarylamine unit of **3** (Figure 7). This result is also supported by comparison of the CW-ESR spectra between 3^{2+} and 3^{4+} (Figure 9).
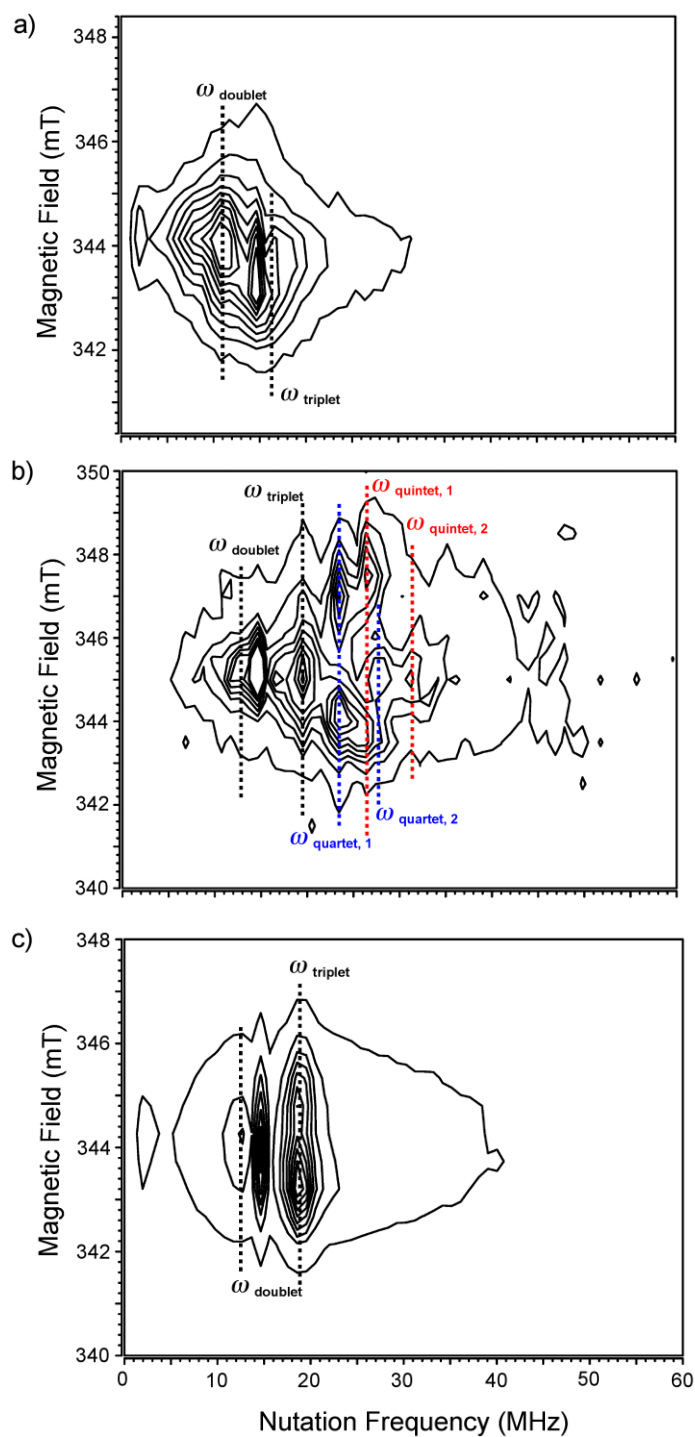
Figure 8. Magnetic Field-swept electron-spin transient nutation (ESTN) spectra of **2** (after the addition of a) 2 and b) 4 molar equiv of Magic Blue) and **3** (after the addition of c) 2 molar equiv of Magic Blue) in CH_2Cl_2 at 5K.

Table 2: Spectroscopic Data of the ESTN Spectroscopy for Poly(radical cation)s of **2** and **3**.

Species	Observed nutation frequency (MHz)	Transition assignment
2^{2+}	16.8 ($\omega_{triplet} = \sqrt{2}\ \omega_{doublet}$)	$\|1, \pm1\rangle \Leftrightarrow \|1, 0\rangle$
(doublet impurity	11.5 ($\omega_{doublet}$)	$\|1/2, +1/2\rangle \Leftrightarrow \|1/2, -1/2\rangle$)
2^{4+}	26.0 ($\omega_{quintet,\ 1} = 2\omega_{doublet}$)	$\|2, \pm2\rangle \Leftrightarrow \|2, \pm1\rangle$
	31.0 ($\omega_{quintet,\ 2} = \sqrt{6}\omega_{doublet}$)	$\|2, \pm1\rangle \Leftrightarrow \|2, 0\rangle$
(quartet impurity	23.4 ($\omega_{quartet,\ 1} = \sqrt{3}\ \omega_{doublet}$)	$\|3/2, \pm3/2\rangle \Leftrightarrow \|3/2, \pm1/2\rangle$
	27.4 ($\omega_{quartet,\ 2} = 2\omega_{doublet}$)	$\|3/2, +1/2\rangle \Leftrightarrow \|3/2, -1/2\rangle$)
(competing triplet	19.4 ($\omega_{triplet} = \sqrt{2}\ \omega_{doublet}$)	$\|1, \pm1\rangle \Leftrightarrow \|1, 0\rangle$)
(doublet impurity	13.0 ($\omega_{doublet}$)	$\|1/2, +1/2\rangle \Leftrightarrow \|1/2, -1/2\rangle$)
3^{2+}	18.3 ($\omega_{triplet} = \sqrt{2}\ \omega_{doublet}$)	$\|1, \pm1\rangle \Leftrightarrow \|1, 0\rangle$
(doublet impurity	13.0 ($\omega_{doublet}$)	$\|1/2, +1/2\rangle \Leftrightarrow \|1/2, -1/2\rangle$)
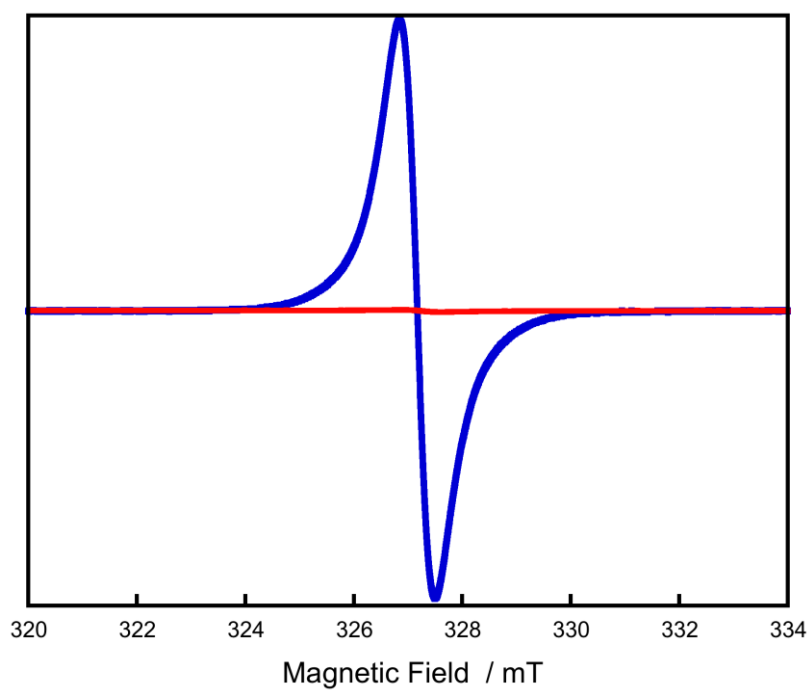
Figure 9. ESR spectra of **3** treated by 2 molar equiv of Magic Blue (blue line) and 4 molar equiv of Magic Blue (red line) in the same volume of CH_2Cl_2 at 123 K. The comparison between these two spectra supports the closed-shell diamagnetic state of **3**$^{4+}$ in CH_2Cl_2 solution.

2.4 Conclusion

The alternate *meta-para*-linked octaazacyclophane **2** and the macrocycle **3** containing extended *para*-phenylene-linked oligoarylamine moieties as spin-bearing units were prepared as simple extensions of tetraaza[1_4]*m,p,m,p*-cyclophane **1**. The DFT calculations on the model compounds suggested that such an expansion of the macrocyclic ring-size leads to facile conformational changes, and that both macrocycles are categorized into non-disjoint or coextensive molecules, which serve as promising candidates for high-spin molecules. From the electrochemical measurements, both exhibited multi-redox activity, and thus they are oxidizable up to the octacation. Owing to the different linkage patterns, however, there are clear differences in the electronic structures of both macrocycles: (i) the UV-vis-NIR spectroelectrochemical measurements revealed that the generated charges and/or unpaired spins are mainly confined into *para*-phenylenediamine (PD) moieties in **2**, thus allowing the deformation from the semi-quinoidal structure to quinoidal one with increasing oxidation number, whereas higher oxidation states for **3** did not show definite quinoidal deformation of PD moieties, (ii) Pulsed ESR measurements demonstrated that almost pure spin-triplet state was realized for **3**$^{2+}$, whereas unpaired spins in **2**$^{2+}$ and **2**$^{4+}$ were virtually uncoupled even at low temperatures, probably due to fragility of spin-coupling pathway caused by facile conformational changes. In addition, **3**$^{4+}$ was found to be a closed-shell electronic structure. Overall, as has been already pointed out for linear oligoarylamines, conformational flexibility resulted in the fragility in spin-coupling pathway for multi-spin systems, even in octaaza[1_8]*m,p,m,p,m,p,m,p*-cyclophane **2**. On the other hand, it was suggested that the extension of spin-bearing units does not affect the high-spin correlation of macrocyclic multi-spin systems, as has been exemplified by the diradical dications of octaaza[1_8]*m,p,p,p,m,p,p,p*-cyclophane **3**.

References and Notes

[1] a) B. König, M. H. Fonseca, *Eur. J. Inorg. Chem*. **2000**, 2303; b) M. X. Wang, *Chem. Commun*. **2008**, 4541; c) W. Maes, W. Dehaen, *Chem. Soc. Rev*. **2008**, *37*, 2393; d) H. Takemura, *Curr. Org. Chem*. **2009**, *13*, 1633; e) M. X. Wang, *Acc. Chem. Res*. **2012**, *45*, 182; f) P. J. Cragg, K. Sharma, *Chem. Soc. Rev*. **2012**, *41*, 597.

[2] a) P. Chen, F. Jäkle, *J. Am. Chem. Soc*. **2011**, *133*, 20142; b) P. Chen, R. A. Lalancette, F. Jäkle, *Angew. Chem. Int. Ed*. **2012**, *51*, 7994.

[3] H. Tsue, K. Ishibashi, R. Tamura, *Top. Heterocycl. Chem*. **2008**, *17*, 73.

[4] a) A. Ito, Y. Ono, K. Tanaka, *New J. Chem*. **1998**, 779; b) A. Ito, Y. Ono, K. Tanaka, *J. Org. Chem*. **1999**, *64*, 8236.

[7] R. J. Bushby, C. A. Kilner, N. Taylor, M. E. Vale, *Tetrahedron* **2007**, *63*, 11458.

[8] K. Ishibashi, H. Tsue, N. Sakai, S. Tokita, K. Matsui, J. Yamauchi, R. Tamura, *Chem. Commun*. **2008**, 2812.

[9] M. Vale, M. Pink, S. Rajca, A. Rajca, *J. Org. Chem*. **2008**, *73*, 27.

[10] A. M. Panagopoulos, M. Zeller, D. P. Becker, *J. Org. Chem*. **2010**, *75*, 7887.

[11] a) A. Ito, Y. Yokoyama, R. Aihara, K. Fukui, S. Eguchi, K. Shizu, T. Sato, K. Tanaka, *Angew. Chem. Int. Ed*. **2010**, *49*, 8205; b) K. Tsuchiya, H. Miyaishi, K. Ogino, *Chem. Lett. 2011*, **40**, 931.

[12] A. Ito, K. Tanaka, *Pure Appl. Chem*. **2010**, *82*, 979.

[13] a) J. P. Wolfe, S. Wagaw, J. F. Marcoux, S. L. Buchwald, *Acc. Chem. Res*. **1998**, *31*, 805; b) J. F. Hartwig, *Acc. Chem. Res*. **1998**, *31*, 852; c) J. F. Hartwig, *Angew. Chem. Int. Ed*. **1998**, *37*, 2046; d) A. R. Muci, S. L. Buchwald, *Top. Curr. Chem*. **2002**, *219*, 133.

[14] a) R. J. Bushby, D. R. McGill, K. M. Ng, N. Taylor, *Chem. Commun*. **1996**, 2641; b) R. J. Bushby, D. R. McGill, K. M. Ng, N. Taylor, *J. Chem. Soc., Perkin Trans. 2*, **1997**, 1405.

[15] A. Ito, S. Inoue, Y. Hirao, K. Furukawa, T. Kato, K. Tanaka, *Chem. Commun*. **2008**,

3242.

[16] a) A. Ito, Y. Ono, K. Tanaka, *Angew. Chem. Int. Ed.* **2000**, *39*, 1072; b) T. D. Selby, S. C. Blackstock, *Org. Lett.* **1999**, *1*, 2053; c) S. I. Hauck, K. V. Lakshmi, J. F. Hartwig, *Org. Lett.* **1999**, *1*, 2057.

[17] I. Kulszewicz-Bajer, V. Maurel, S. Gambarelli, I. Wielgus, D. Djurado, *Phys. Chem. Chem. Phys.* **2009**, *11*, 1362.

[18] D. Sakamaki, A. Ito, K. Furukawa, T. Kato, K. Tanaka, *Chem. Commun.* **2009**, 4524.

[19] Hexaaza[1$_6$]*m,p,p,m,p,p*-cyclophane with similar linkage pattern to macrocycle **3** has been already reported in Ref. 17.

[20] F. E. Goodson, S. I. Hauck, J. F. Hartwig, *J. Am. Chem. Soc.* **1999**, *121*, 7527.

[21] a) W. T. Borden, E. R. Davidson, *J. Am. Chem. Soc.* **1977**, *99*, 4587; b) D. A. Dougherty, *Acc. Chem. Res.* **1991**, *24*, 88.

[22] W. Huang, T. L. E. Henderson, A. M. Bond, K. B. Oldham, *Anal. Chim. Acta* **1995**, *304*, 1.

[23] a) A. Ishitani, S. Nagakura, *Mol. Phys.* **1967**, *12*,1; b) B. Badger, B. Brocklehurst, R. D. Russell, *Chem. Phys. Lett.* **1967**, *1*, 122; c) A. V. Szeghalmi, M. Erdmann, V. Engel, M. Schmitt, S. Amthor, V. Kriegisch, G. Nöll, R. Stahl, C. Lambert, D. Leusser, D. Stalke, M. Zabel, J. Popp, *J. Am. Chem. Soc.* **2004**, *126*, 7834.

[24] Y. Hirao, A. Ito, K. Tanaka, *J. Phys. Chem. A* **2007**, *111*, 2951.

[25] A. Ito, D. Sakamaki, Y. Ichikawa, K. Tanaka, *Chem. Mater.* **2011**, *23*, 841.

[26] A. Ito, Y. Yamagishi, K. Fukui, S. Inoue, Y. Hirao, K. Furukawa, T. Kato, K. Tanaka, *Chem. Commun.* **2008**, 6573.

[27] D. Sakamaki, A. Ito, K. Furukawa, T. Kato, M. Shiro, K. Tanaka, *Angew. Chem. Int. Ed.* **2012**, *51*, 12776.

[28] a) J. Bonvoisin, J. P. Launay, M. Van der Auweraer, F. C. De Schryver, *J. Phys. Chem.* **1994**, *98*, 5052 (see also correction: J. Bonvoisin, J. P. Launay, M. Van der

Auweraer, F. C. D. Schryver, *J. Phys. Chem*. **1996**, *100*, 18006.); b) J. Bonvoisin, J. P. Launay, W. Verbouwe, M. Van der Auweraer, F. C. D. Schryver, *J. Phys. Chem*. **1996**, *100*, 17079; c) J. Sedó, D. Ruiz, J. Vidal-Gancedo, C. Rovira, J. Bonvoisin, J. P. Launay, J. Veciana, *Adv. Mater*. **1996**, *8*, 748; d) M. M. Wienk, R. A. J. Janssen, *J. Am. Chem. Soc*. **1997**, *119*, 4492; e) C. Rovira, D. Ruiz-Molina, O. Elsner, J. Vidal-Gancedo, J. Bonvoisin, J. P. Launay, J. Veciana, *Chem. Eur. J*. **2001**, *7*, 240.

[29] S. F. Nelsen, A. E. Konradsson, M. N. Weaver, J. P. Telo, *J. Am. Chem. Soc*. **2003**, *125*, 12493.

[30] A. Ito, Y. Nakano, M. Urabe, T. Kato, K. Tanaka, *J. Am. Chem. Soc*. **2006**, *128*, 2948.

[31] a) F. A. Bell, A. Ledwith, D. C. Sherrington, *J. Chem. Soc*. **1969**, 2719; b) N. G. Connell, W. E. Geiger, *Chem. Rev*. **1996**, *96*, 877.

[32] a) J. Isoya, H. Kanda, J. R. Norris, J. Tang, M. K. Brown, *Phys. Rev. B*. **1990**, *41*, 3905; b) A. V. Astashkin, A. Schweiger, *Chem. Phys. Lett*. **1990**, *174*, 595.

[33] A. Ito, D. Sakamaki, H. Ino, A. Taniguchi, Y. Hirao, K. Tanaka, K. Kanemoto, T. Kato, *Eur. J. Org. Chem*. **2009**, 4441.

Chapter 3

High-Spin Polycationic States of an Alternate *meta–para*–Linked Oligoarylamine Incorporating Two Macrocycles

3.1 Introduction

Poly(radical cation) form of poly(*m*-aniline) (Figure 1a), the position isomer of polyaniline as the well-known conductive polymer, is anticipated to be a candidate of the ferromagnetic polymers from the viewpoint of superdegeneracy among the half-filled bands,[1] and has been investigated so far through the direct polymerization study[2-4] and the oligomer model study.[5–7] Afterwards, it has been widely accepted that the semi-quinone radical cation of *para*-phenylenediamine (PD) moiety is far more stable than the aminium radical cation as the spin-containing unit in poly(*m*-aniline), and therefore, the main forcus has been shifted to the alternating *meta-para*-isomers of polyaniline and/or oligoaniline.[8–10] Recently, Kulszewicz-Bajer and co-workers have conducted elaborative work on the oxidized form of poly(*m-p*-aniline) (Figure 1b), and as a consequence, the generated spins in the polymer were shown to be mainly

uncoupled (S = 1/2) except for the existence of minor triplet (S = 1) spin clusters.[10] Furthermore, their unfortunate results are also supported from our oligomer model study.[11]

(a)

(b)

(c)
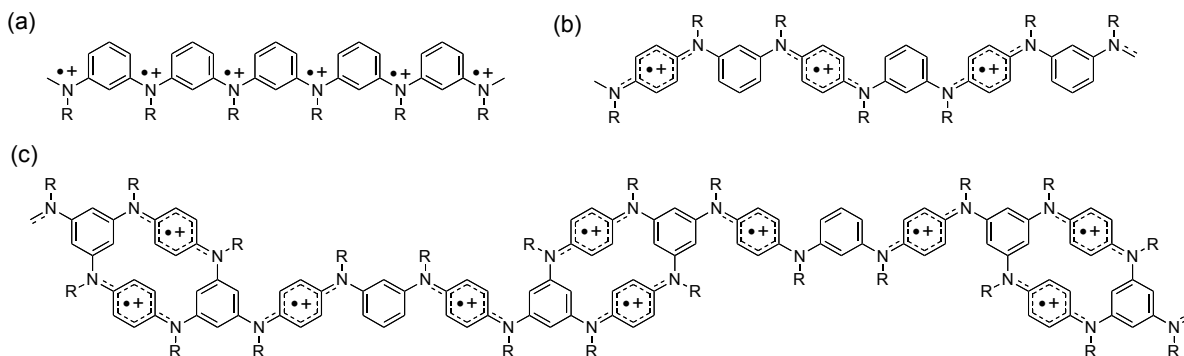
Figure 1. Poly(radical cation)s of a) poly(*m*-aniline), b) poly(*m-p*-aniline), and c) cyclophane-containing poly(*m-p*-aniline).

On the other hand, we have demonstrated that the high-spin alignment has been fulfilled for the macrocyclic oligomers of poly(*m*-aniline) and/or poly(*m-p*-aniline), and hence, the macrocyclic oligoanilines can be effectively utilized as the promising high-spin building blocks to construct the two- and three-dimensional multi-spin system.[12] In particular, tetraaza[1$_4$]*m,p,m,p*-cyclophane has a definite molecular structure, and moreover, can be feasibly derived to pure spin triplet species by two-electron-oxidation.[12a,13] In this context, the introduction of the cyclophane moieties into the polymer backbone may bring in good results to obviate the uncoupled spin difficulty in the one-dimensional poly(*m-p*-aniline). As a first step to verify the validity of the cyclophane-containing poly(*m-p*-aniline) (Figure 1c), we prepared a *meta-para*-linked oligoarylamine **1** incorporating two cyclophane moieties, which is comprised of a central linearly-linked moiety and two peripheral cyclophane moieties.

As shown in Figure 2, the frontier molecular orbitals (MO) are predicted to be virtually six-fold quasi-degenerate non-disjoint π-MOs,[14] judging from the simple Hückel MO calculation of a model compound. Therefore, this molecule could be

considered as a hopeful organic high-spin system. In this chapter, we report the electronic and magnetic properties of the polycationic states of this molecule.
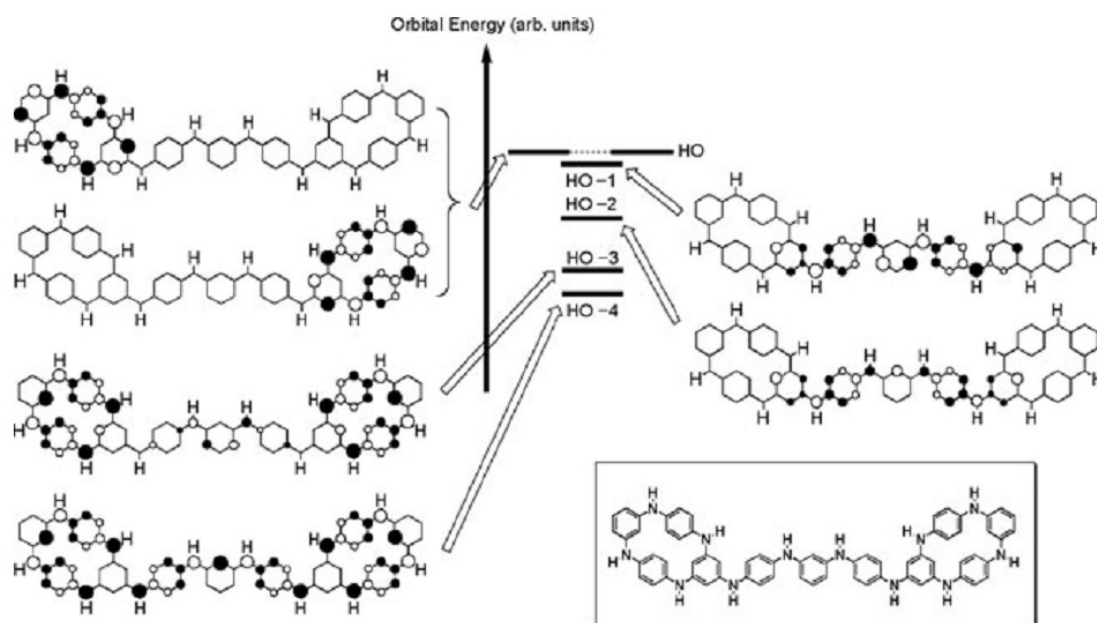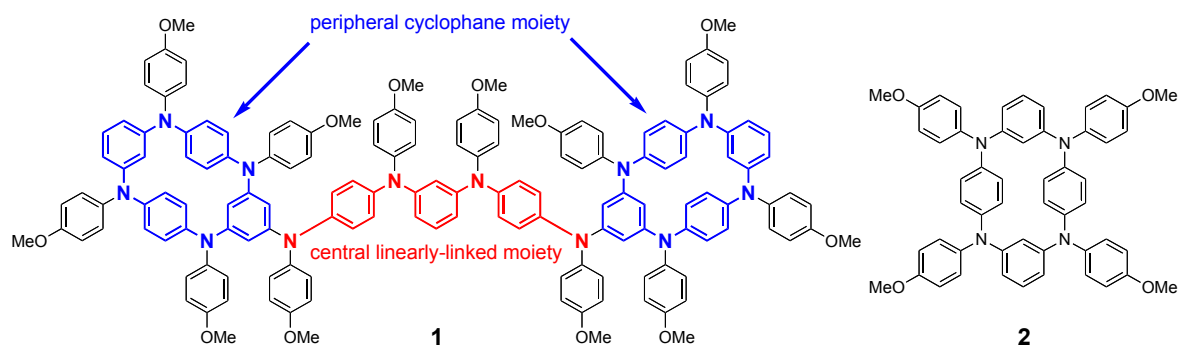
Figure 2. Schematic drawing of the frontier MOs for a model compound of **1**.

3.2 Experimental Section

General Methods: Commercial grade regents were used without further purification. Solvents were purified, dried, and degassed following standard procedures. Elemental analyses were performed by Center for Organic Elemental Microanalysis, Kyoto

University. ^{1}H and ^{13}C NMR spectra were measured by a JEOL JNM-EX400 FT-NMR spectrometer. Chemical shifts of NMR spectra are determined relative to tetramethylsilane (TMS) internal standard.

Electrochemical Measurements. Cyclic voltammograms were recorded using an ALS/chi Electrochemical Analyzer Model 612A with a three-electrode cell using a Pt disk (2 mm^2) as the working electrode, a Pt wire as the counter electrode, and an Ag/0.01 M AgNO$_3$ (MeCN) as the reference electrode calibrated against ferrocene/ferrocenium (Fc/Fc$^+$) redox couple in a solution of 0.1 M tetrabutylammonium tetrafluoroborate as a supporting electrolyte (298 K, scan rate 100 mVs^{-1}).

ESR Measurements. The cw-ESR spectra were measured using a JEOL JES-SRE2X or a JEOL JES-TE200 X-band spectrometer in which temperatures were controlled by a JEOL ES-DVT2 variable-temperature unit or a JEOL ES-DVT3 variable-temperature unit, respectively.

Spectroelectrochemical Measurements. The UV-Vis-NIR spectra were measured with a Perkin Elmer Lambda 19 spectrometer. Spectroelectrochemical measurements were performed using an optically transparent thin-layer electrode quartz cell (light path length = 1 mm). The working and the counter electrodes were a Pt mesh and a Pt coil, respectively. The reference electrode was an Ag wire. The potential was applied with an ALS/chi Electrochemical Analyzer Model 612A.

Pulsed ESR Measurements. Pulsed ESR measurements were carried out on a Bruker ELEXSYS E580 X-band FT ESR spectrometer. The microwave pulse power of 10 mW provided by the microwave bridge was boosted to level of 1 kW using a traveling wave tube (TWT) amplifier. The ESTN measurements were performed by the three-pulse sequence shown below. The two-pulse ($\pi/2 - \pi$ pulses) electron spin-echo signal $S(t_1)$ was detected by increasing the width (t_1) of the nutation pulse. We employed appropriate phase cycles in order to suppress undesirable signals and artifacts which

arise from an inaccurate pulse length [15,16]. The observed signal $S(t_1, B)$ as a function of external magnetic field B is converted into a nutation frequency $S(\omega_{nut}, B)$ spectrum. The parameters used for the measurements were $t_2 = 400$ ns, $t_3 = 8$ ns.

**1**: $C_{150}H_{126}N_{12}O_{12}$
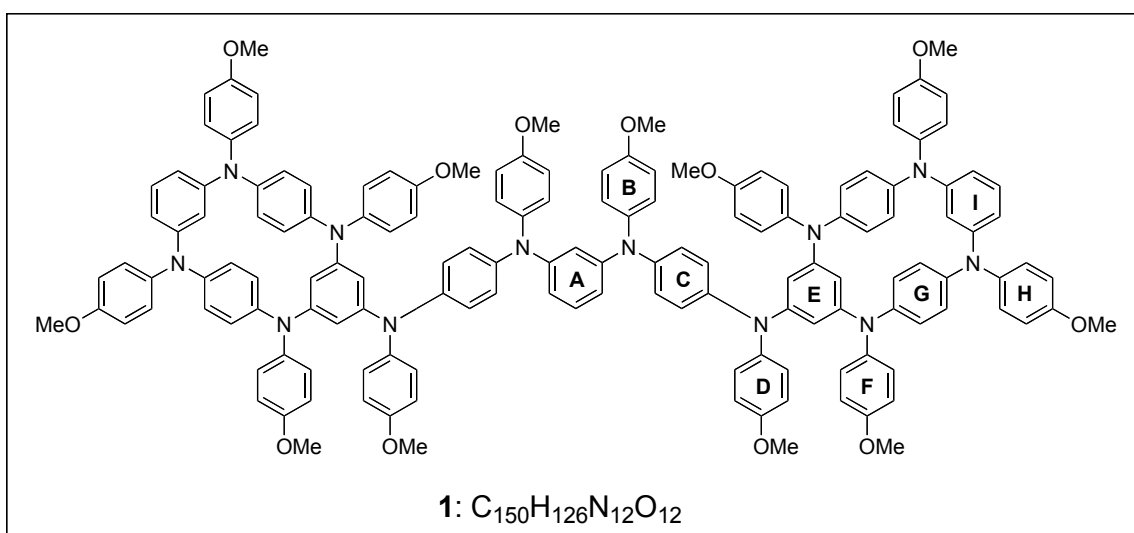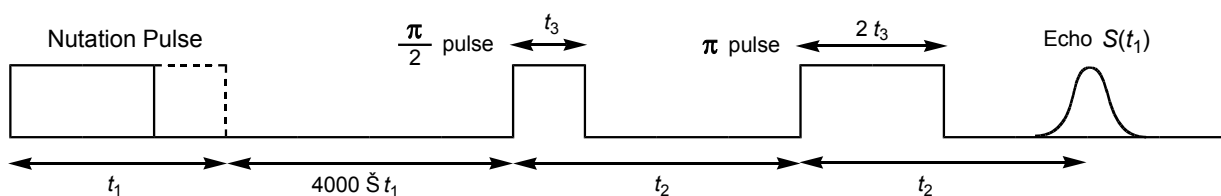
Synthetic Details.

***Meta-para*-linked oligoarylamine incorporating two tetraazacyclophane (1):** Anhydrous toluene (100 mL) was added to Pd(dba)$_2$ (6.4 mg, 0.01 mmol), Ph$_5$FcP(t-Bu)$_2$ [17] (15.1 mg, 0.02 mmol), and NaOt-Bu (0.2054 g, 2.13 mmol) in a flask equipped with a dropping funnel which was charged with a toluene solution (100 mL) of *N,N',N''*-tris(4-anisyl)-1,3,5-benzenetriamine **3** [18] (88.6 mg 0.20 mmol) and *N,N'*-di(4-bromophenyl)-*N,N'*-di(4-anisyl)-1,3-benzenediamine **4** [13b] (189.9 mg 0.30 mmol), and the toluene solution was stirred under an argon atmosphere at 110 ˚C for a while. A half portion of the solution in the dropping funnel was gradually added into the solution containing the toluene solution of the palladium catalyst in the flask for 15 h.

The reaction mixture was refluxed for 20 h with stirring, and furthermore the remaining solution in the dropping funnel was added into the reaction mixture for 7 h. The refluxing was continued for 6 h with stirring. The reaction mixture was cooled down to room temperature, washed with brine, and dried over Na_2SO_4. After removal of the solvent in vacuo, the crude product was purified by column chromatography on silica gel (toluene : ethyl acetate = 19:1 as eluent). Finally, the product was washed with *n*-hexane to afford **1** (16.0 mg 7.0 %) as a beige powder: mp 217–220 ˚C; ^{1}H NMR (400 MHz, tetrahydrofuran-d_8) δ = 3.662 (s, 12H, Ar_F–OCH_3 or Ar_H–OCH_3), 3.675 (s, 6H, Ar_B–OCH_3 or Ar_D–OCH_3), 3.704 (s, 6H, Ar_B–OCH_3 or Ar_D–OCH_3), 3.725 (s, 12H, Ar_F–OCH_3 or Ar_H–OCH_3), 5.886 (t, J=1.95 Hz, 2H, H_E–4), 6.122 (d, J = 1.95 Hz, 4H, H_E–2), 6.320 (t, J = 2.20 Hz, 2H, H_I–2), 6.350 (dd, J = 2.20, 8.05 Hz, 4H, H_I–4), 6.370 (dd, J = 2.20, 8.29 Hz, 2H, H_A–4), 6.562 (t, J = 2.20 Hz, 1H, H_A–2), 6.718 (d, J = 9.03 Hz, 4H, H_B–2 or H_D–2), 6.723 (d, J = 9.03 Hz, 8H, H_F–2 or H_H–2), 6.763-6.861 (m, 39H, H_A–5, H_B–2 or H_D–2, H_C–2, H_C–3, H_F–2 or H_H–3, H_G–2, H_G–3, H_I–5), 6.891 (d, J = 9.03 Hz, 4H, H_B–3 or H_D–3), 6.943(d, J = 9.03 Hz, 4H, H_B–3 or H_D–3), 7.000 (d, J = 9.03 Hz, 8H, H_F–3 or H_H–3), 7.060 (d, J = 9.03 Hz, 8H, H_F–3 or H_H–3); ^{13}C NMR (100 MHz, tetrahydrofuran-d_8) δ = 54.60 (Ar_B–OCH_3 or Ar_D–OCH_3), 54.65 (Ar_F–OCH_3 or Ar_H–OCH_3), 54.68 (Ar_B–OCH_3 or Ar_D–OCH_3, Ar_F–OCH_3 or Ar_H–OCH_3), 107.56 (C_E–4), 108.16 (C_E–2), 112.9 (C_I–4), 113.26, 113.29, 113.35 (C_I–2, C_A–2, C_A–4), 114.25 (C_H–3 or C_F–3), 114.26, 114.39 (C_B–3, C_D–3), 114.41 (C_H–3 or C_F–3), 123.91, 124.58 (C_C–2, C_C–3), 125.21, 125.53 (C_G–2, C_G–3), 126.10, 126.17 (C_B–2, C_D–2), 126.37, 126.88 (C_F–2, C_H–2), 127.92, 128.93 (C_A–5, C_I–5), 139.78, 139.99 (C_F–1, C_H–1), 140.42, 140.59 (C_B–1, C_D–1), 142.05 (C_C–1 or C_C–4), 142.73, 142.82 (C_G–1, C_G–4), 142.98 (C_C–1 or C_C–4), 148.97, 149.33 (C_A–1 or C_E–1), 149.42, 149.56 (C_E–3 or C_I–1), 155.87, 155.94 (C_B–4 or C_D–4), 156.02, 156.35 (C_F–4 or C_H–4); FAB HRMS (*m*-nitrobenzyl alcohol) *m/z* (relative intensity %) calcd for $C_{150}H_{126}N_{12}O_{12}$ [M]$^+$ 2286.9618, found 2286.9661 (65.3).

3.3 Results and Discussion

3.3.1 Synthesis

The target molecule **1** has been prepared from *N,N',N''*-tris(4-anisyl)-1,3,5-benzenetriamine (**3**)[18] and *N,N'*-di(4-bromophenyl)-*N,N'*-di(4-anisyl)-1,3-benzenediamine (**4**)[13b] using a 2:3 ratio of substrates by performing the palladium-catalyzed aryl amination reaction (Buchwald-Hartwig reaction)[19] in a one-pot manner (Scheme 1).
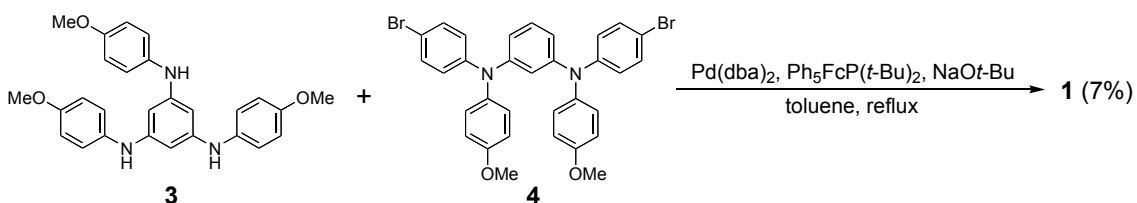

Scheme 1. Synthesis of *meta-para*-linked oligoarylamine incorporating two tetraazacyclophane **1**.

3.3.2 Electrochemistry

As shown in Figure 3, the cyclic voltammogarm of **1** in CH_2Cl_2 showed six redox couples at −0.04, +0.08, +0.16, +0.26, +0.59, and +0.68 V (*vs*. Fc/Fc$^+$), which tentatively correspond to oxidation processes, 1^0 to 1^{2+}, 1^{2+} to 1^{3+}, 1^{3+} to 1^{4+}, 1^{4+} to 1^{6+}, 1^{6+} to 1^{10+}, and 1^{10+} to 1^{12+}, respectively, judging from the differential pulse voltammogram (Figure 4). This indicates that **1** is oxidizable up to dodecacation: as compared to the first and second oxidation potentials (−0.01 and +0.02 V) and the third and forth oxidation potentials (+0.54 and 0.67 V) of tetraazacyclophane **2**,[12c] the first 4 redox couples correspond to the generation of 6 semi-quinoidal PD radical cations, while the remaining 2 redox couples to the generation of 6 quinoidal PD dications to produce diamagnetic (*i.e.* spinless) species; in the first oxidation process, two electrons are removed simultaneously from the two peripheral tetraazacyclophane moieties, so as

81

to reduce the electrostatic repulsions between the charged semi-quinoidal PD units; the subsequent two one-electron-oxidation processes take place from the central two PD units; finally, two electrons are removed furthermore simultaneously from the two peripheral tetraazacyclophane moieties to generate the hexa(radical cation) of **1**. This conjecture is in good accordance with the Hückel MO pictures having the six-fold quasi-degenerate frontier MOs including the doubly degenerate HOMOs (Figure 2).
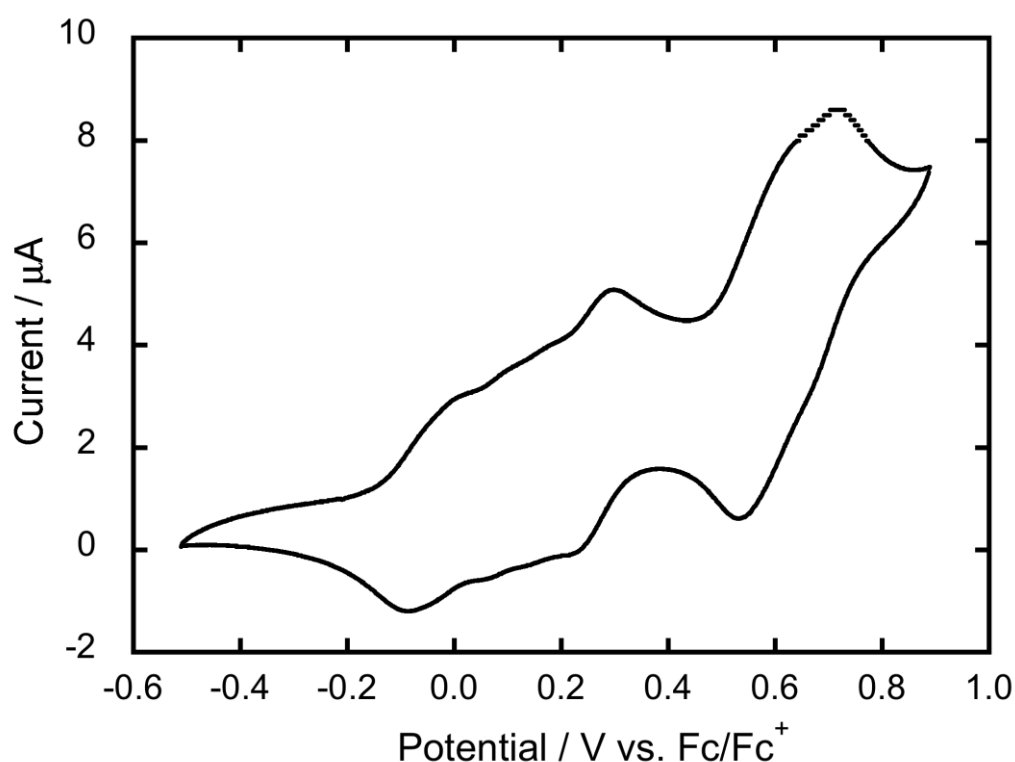
Figure 3. Cyclic voltammogram of **1** measured in CH_2Cl_2 containing 0.1 M n-Bu$_4$NBF$_4$ at 298 K (scan rate 0.1 V s^{-1}).
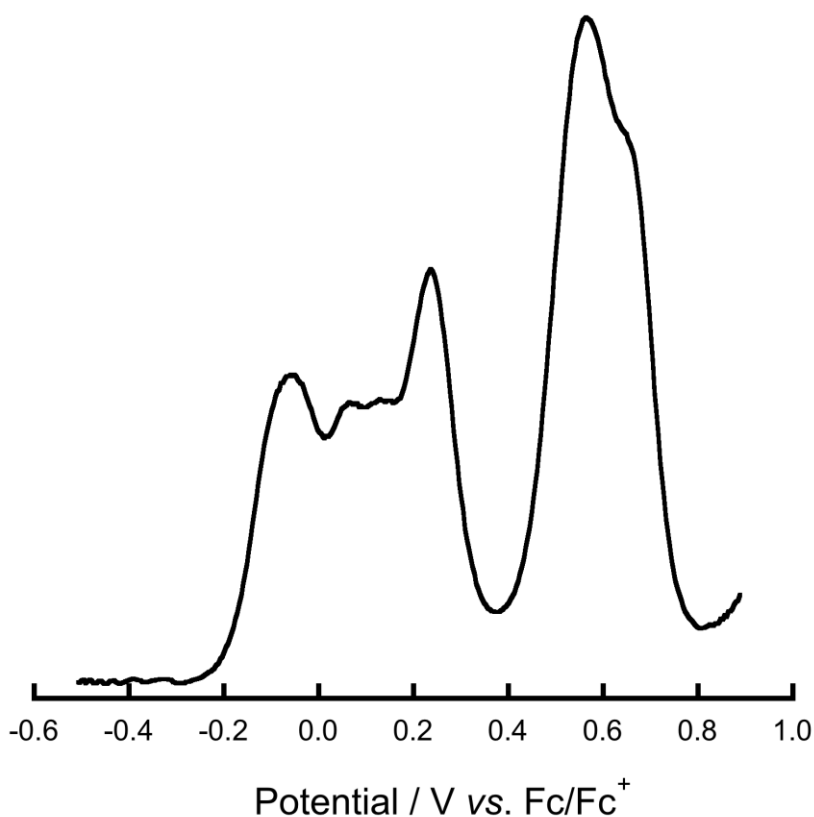
Figure 4. Differential pulse voltammogram of **1** measured in CH_2Cl_2 containing 0.1 M n-Bu$_4$NBF$_4$ at 298 K (scan rate 0.1 V s^{-1}).

3.3.3 UV-Vis-NIR Spectroscopy

The UV-Vis-NIR spectral change during the course of the electrochemical oxidation of **1** was monitored by using an optically-transparent thin-layer electrochemical cell (Figure 5). As the oxidation proceeds, three new bands appeared at 426, 605, and ~1100 nm. The broad band (~1100 nm) in the NIR region is considered to be the intervalence band between the aminium radical cation center and the neutral amine center, and is composed of two bands at ~1000 and ~1200 nm. On going from **1**$^{2+}$ to **1**$^{6+}$, it was found that the intensity of the higher energy band (~1000 nm) was gradually strengthened as compared to that of the lower energy band (~1200 nm), suggesting the charge-localization in the higher oxidation states of **1**. When **1**$^{6+}$ is further oxidized, a

new intense band at 810 nm grew with an isosbestic point at 892 nm, corresponding to the conversion of the semi-quinoidal PD radical cation moieties to the diamagnetic quinoidal PD dication ones.
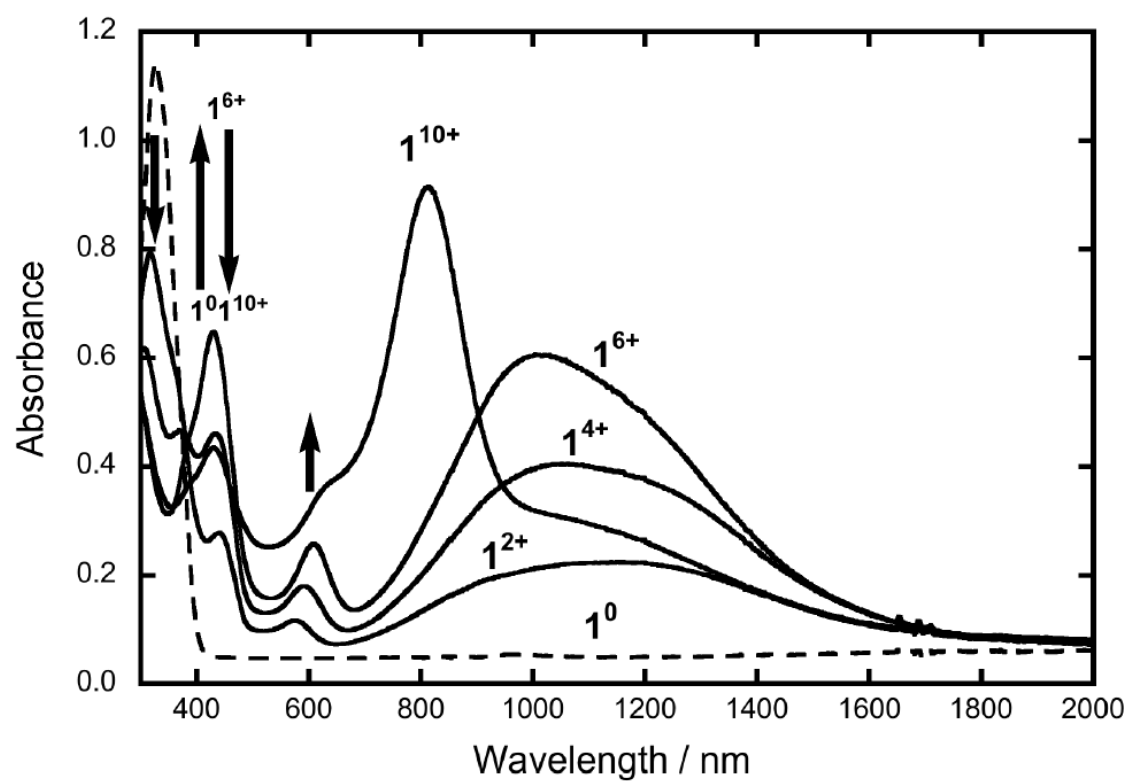
Figure 5. UV–Vis–NIR spectra of the stepwise electrochemical oxidation of **1** to decacation 1^{10+} in CH_2Cl_2/0.1 M n-Bu_4NBF_4 at 298 K.

3.3.4 CW-ESR measurements

Encouraged by the observed electrochemical multi-stage oxidation processes, we have measured the continuous wave ESR (cw-ESR) spectra of 1^+, 1^{2+}, 1^{3+}, 1^{4+}, and 1^{6+} in a rigid-glass of CH_2Cl_2 at 123K. Each oxidized species were generated by adding 1 to 6 molar equivalents of tris(4-bromophenyl)aminium hexachroloantimonate[20] at 195 K. The present poly(radical cation)s were found to be far more stable than the oxidized oligo(*m*-aniline)s, which immediately decompose at room temperature or lower temperatures. For instance, about 80 % of the hexacation of **1** survive in solution after 1 hr at room temperature, judging from the ESR intensity. As is often the case with the high-spin molecules possessing delocalized spin centers, however, neither the definitive fine-structure in the allowed resonance ($\Delta M_S = \pm 1$) nor the forbidden resonance ($\Delta M_S = \pm 2$) were detected (Figure 6).[21] These results prompted us to measure the electron spin transient nutation (ESTN) measurements based on the pulsed ESR method .[22]
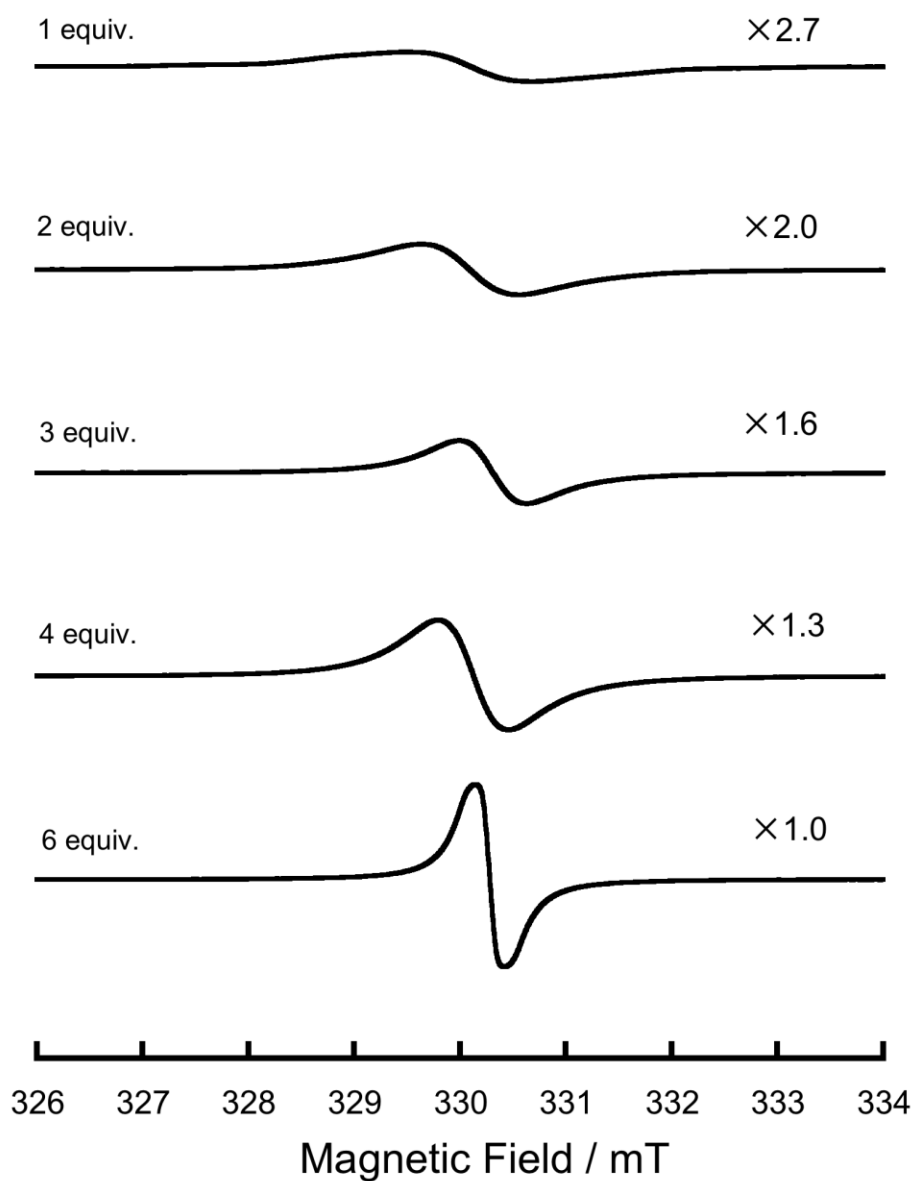
Figure 6. CW-ESR spectra of **1** in CH_2Cl_2 at 123 K after addition of 1 equiv., 2 equiv., 3 equiv., 4 equiv. and 6 equiv. of oxidant.

### 3.3.5 pulsed-ESR measurements

As shown in Figure 7, the observed 2-dimensional ESTN (2D-ESTN) spectra clearly displayed the change of spin-multiplicity corresponding to the stepwise-oxidized species of **1**. The nutation frequency components observed at 5 K for each oxidation

state of **1** are summarized in Table 1. Besides the unknown doublet impurity, the triplet and quartet signals were seen in $\mathbf{1}^{2+}$ and $\mathbf{1}^{3+}$, strongly indicating the high-spin alignment among the semi-quinoidal PD radical cations generated from the peripheral cyclophane moieties and the central linearly-linked moiety. In the higher oxidation states, $\mathbf{1}^{4+}$ and $\mathbf{1}^{6+}$, the competing intermediate spin states (*i.e.* triplet and/or quintet states) were also detected in addition to the predicted quintet and septet states, suggesting that the high-spin state is nearly degenerate with thermally accessible intermediate spin states.

Table 1: Spectral data of the 2D-ESTN spectroscopy for poly(radical cation)s of **1**.

Species	Obs. nutation freq./MHz	Transition assignment
$\mathbf{1}^{2+}$	$24.8\ (\cong \sqrt{2}\omega_{\text{doublet}})$	$\lvert 1, \pm1 \rangle \Leftrightarrow \lvert 1, 0 \rangle$
(doublet impurity	$18.0\ (= \omega_{\text{doublet}})$	$\lvert 1/2, +1/2 \rangle \Leftrightarrow \lvert 3/2, -1/2 \rangle)$
$\mathbf{1}^{3+}$	$34.3\ (\cong \sqrt{3}\omega_{\text{doublet}})$	$\lvert 3/2, \pm3/2 \rangle \Leftrightarrow \lvert 3/2, \pm1/2 \rangle$
	$39.0\ (\cong 2\omega_{\text{doublet}})$	$\lvert 3/2, +1/2 \rangle \Leftrightarrow \lvert 3/2, -1/2 \rangle$
(doublet impurity	$20.0\ (= \omega_{\text{doublet}})$	$\lvert 1/2, +1/2 \rangle \Leftrightarrow \lvert 3/2, -1/2 \rangle)$
$\mathbf{1}^{4+}$	$36.4\ (\cong \sqrt{2}\omega_{\text{triplet}})$	$\lvert 2, \pm2 \rangle \Leftrightarrow \lvert 2, \pm1 \rangle$
	$44.5\ (\cong \sqrt{3}\omega_{\text{triplet}})$	$\lvert 2, \pm1 \rangle \Leftrightarrow \lvert 2, 0 \rangle$
(competing triplet	$26.0\ (= \omega_{\text{triplet}})$	$\lvert 1, \pm1 \rangle \Leftrightarrow \lvert 1, 0 \rangle)$
$\mathbf{1}^{6+}$	$44.4\ (\cong \sqrt{3}\omega_{\text{triplet}})$	$\lvert 3, \pm3 \rangle \Leftrightarrow \lvert 3, \pm2 \rangle$
	$56.8\ (\cong \sqrt{5}\omega_{\text{triplet}})$	$\lvert 3, \pm2 \rangle \Leftrightarrow \lvert 3, \pm1 \rangle$
	$62.9\ (\cong \sqrt{6}\omega_{\text{triplet}})$	$\lvert 3, \pm1 \rangle \Leftrightarrow \lvert 3, 0 \rangle$
(competing quintet	$34.0\ (= \sqrt{2}\omega_{\text{triplet}})$	$\lvert 2, \pm2 \rangle \Leftrightarrow \lvert 2, \pm1 \rangle$
	$44.0\ (= \sqrt{3}\omega_{\text{triplet}})$	$\lvert 2, \pm1 \rangle \Leftrightarrow \lvert 2, 0 \rangle)$
(competing triplet	$25.0\ (= \omega_{\text{triplet}})$	$\lvert 1, \pm1 \rangle \Leftrightarrow \lvert 1, 0 \rangle)$
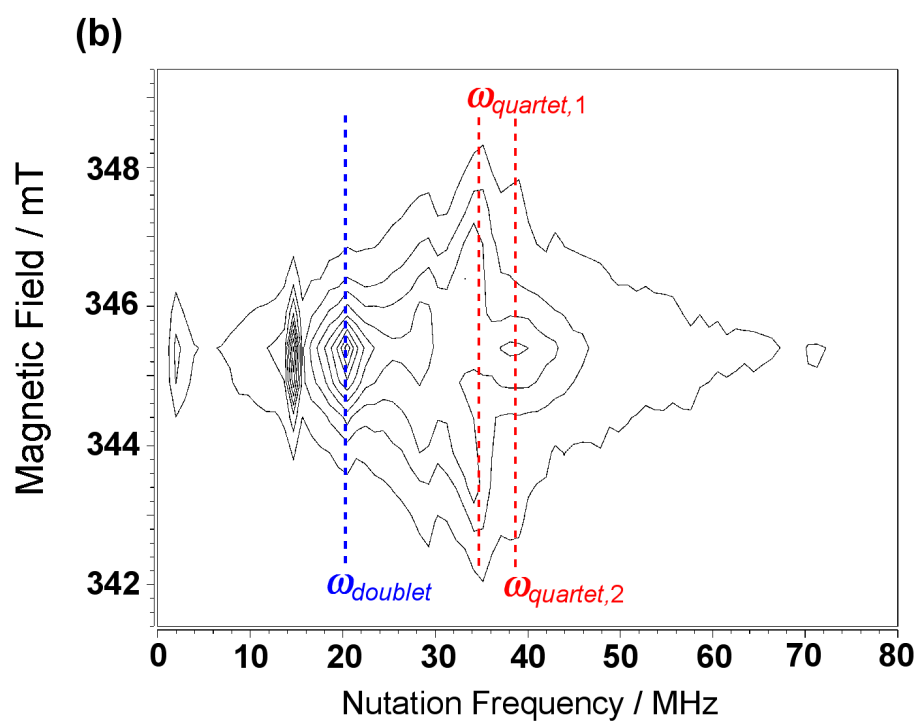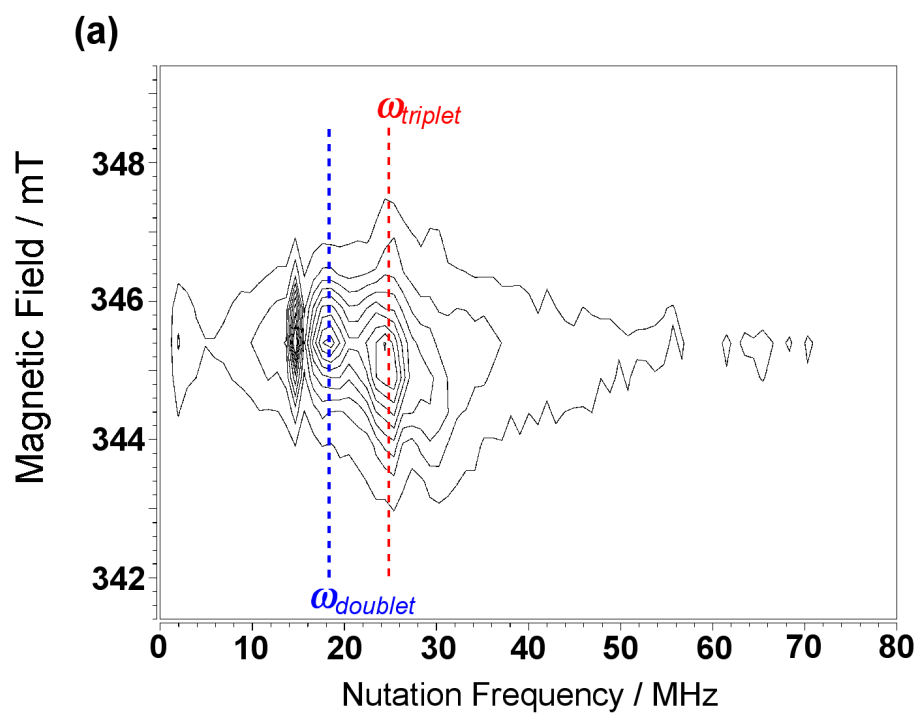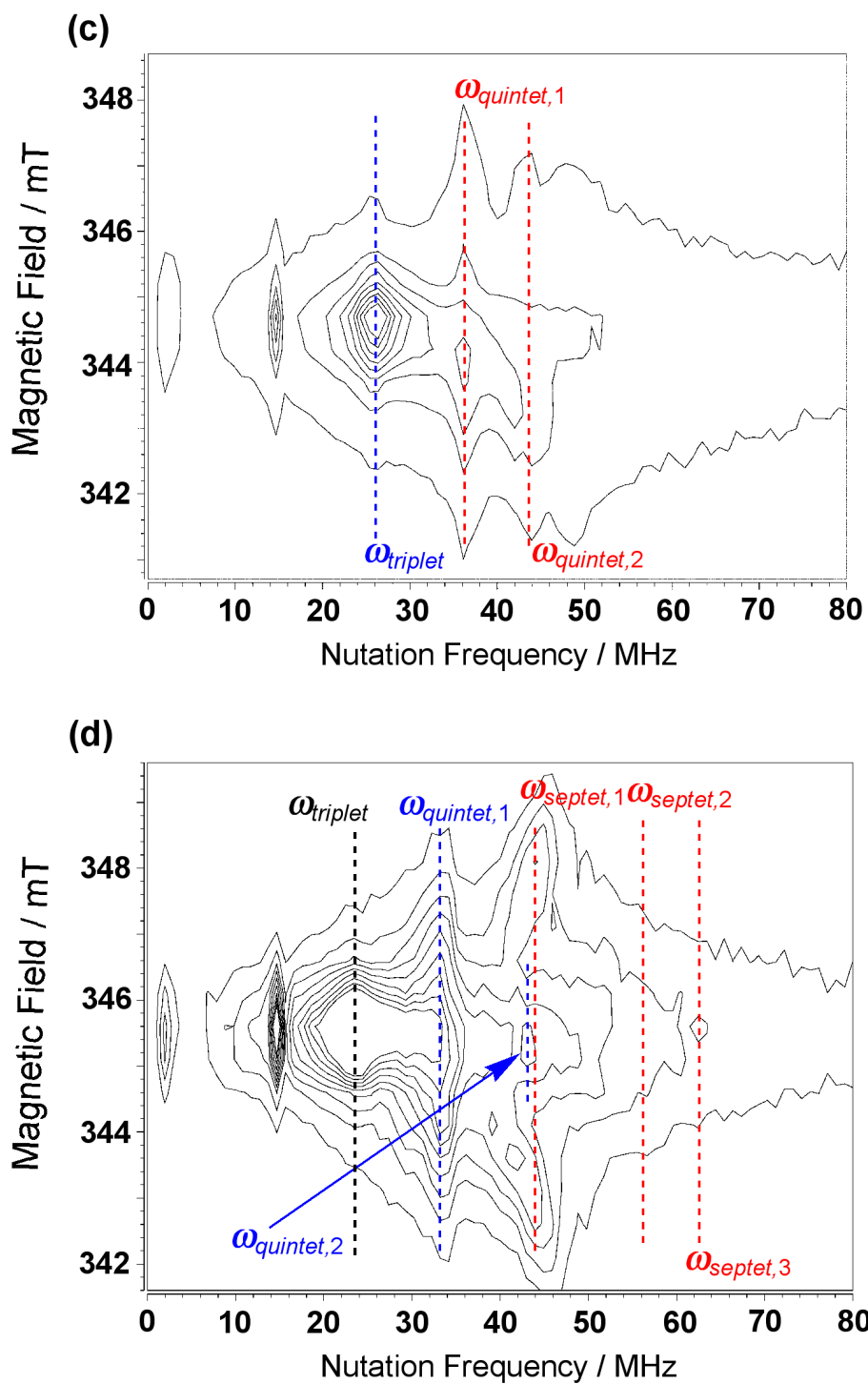
Figure 7. 2D-ESTN spectra of **1** in CH_2Cl_2 at 5K after the addition of a) 2 equiv., b) 3 equiv., c) 4 equiv., and d) 6 equiv. of oxidant.

3.4 Conclusion

In summary, we have succeeded in preparation and characterization of a *meta-para*-linked oligoarylamine incorporating two tetraazacyclophanes. The pulsed ESR measurements revealed that the spins on the two macrocycles and the linker unit were ferromagnetically coupled in the higher oxidation states. These results demonstrated the validity of the strategy proposed in this chapter, and the hope of the high-spin organic polymers can be pinned on the *meta-para*-linked polyarylamines.

References and Notes

[1] a) N. Mataga, *Theor. Chim. Acta* **1968**, *10*, 372; b) T. Hughbanks, M. Kertesz, *Mol. Cryst. Liq. Cryst*. **1989**, *176*, 115; K. Yoshizawa, R. Hoffmann, *Chem. Eur. J*. **1995**, *1*, 403.

[2] a) K. Yoshizawa, K. Tanaka, T. Yamabe, *Chem. Lett*. **1990**, 1331; b) T. Ishida, H. Iwamura, *Chem. Lett*. **1991**, 317; *c*) K. Yoshizawa, K. Tanaka, T. Yamabe, J. Yamauchi, *J. Chem. Phys*. **1992**, *96*, 5516; d) K. Yoshizawa, A. Takata, K. Tanaka, T. Yamabe, *Polym. J*. **1992**, *24*, 857; e) K. Yoshizawa, A. Ito, K. Tanaka, T. Yamabe, *Solid State Commun*. **1993**, *87*, 935; f) A. Ito, K. Ota, K. Tanaka, T. Yamabe, K. Yoshizawa, *Macromolecules* **1995**, *28*, 5618.

[3] a) M. Baumgarten, K. Müllen, N. Tyutyulkov, G. Madjarova, *Chem. Phys*. **1993**, *169*, 81; b) G. Madjarova, M. Baumgarten, K. Müllen, N. Tyutyulkov, *Macromol. Theory Simul*. **1994**, *3*, 803.

[4] a) J. Louie, J. F. Hartwig, *Macromolecules* **1998**, *31*, 6737; b) F. E. Goodson, S. I. Hauck, J. F. Hartwig, *J. Am. Chem. Soc*. **1999**, *121*, 7527.

[5] a) A. Ito, T. Saito, K. Tanaka, T. Yamabe, *Tetrahedron Lett*. **1995**, *36*, 8809; b) A. Ito, T. Saito, K. Ota, T. Miura, Y. Misaki, K. Tanaka, T. Yamabe, *J. Mater. Chem*. **1998**,

8, 1799; c) A. Ito, H. Ino, K. Tanaka, K. Kanemoto, T. Kato, *J. Org. Chem*. **2002**, *67*, 491.

[6] a) K. Sato, M. Yano, M. Furuichi, D. Shiomi, T. Takui, K. Abe, K. Itoh, A. Higuchi, K. Katsuma, Y. Shirota, *J. Am. Chem. Soc*. **1997**, *119*, 6607; b) M. Yano, A. Fujiwara, M. Tatsumi, M. Oyama, K. Sato, T. Takui, *Polyhedron* **2007**, *26*, 2008.

[7] R. J. Bushby, C. A. Kilner, N. Taylor, M. E. Vale, *Tetrahedron*, **2007**, *63*, 11458.

[8] a) M. M. Wienk, R. A. J. Janssen, *J. Am. Chem. Soc*. **1996**, *118*.10626; b) M. M. Wienk, R. A. J. Janssen, *J. Am. Chem. Soc*. **1997**, *119*, 4492; c) M. P. Struijk, R. A. J. Janssen, *Synth. Met*. **1999**, *103*, 2287.

[9] A. Ito, A. Taniguchi, T. Yamabe, K. Tanaka, *Org. Lett*. **1999**, *1*, 741.

[10] a) I. Kulszewicz-Bajer, M. Zagórska, I. Wielgus, M. Pawłowski, J. Gosk, A. Twardowski, *J. Phys. Chem. B* **2007**, *111*, 34; b) I. Kulszewicz-Bajer, J. Gosk, M. Pawłowski, S. Gambarelli, D. Djurado, A. Twardowski, *J. Phys. Chem. B* **2007**, *111*, 9421; c) M. Gałecka, I. Wielgus, M. Zagórska, M. Pawłowski, I. Kulszewicz-Bajer, *Macromolecules* **2007**, *40*, 4924.

[11] A. Ito, D. Sakamaki, H. Ino, Y. Hirao, A. Taniguchi, K. Kanemoto, T. Kato, K. Tanaka, *Eur. J. Org. Chem*. **2009**, 4441.

[12] a) A. Ito, Y. Ono, K. Tanaka, *Angew. Chem. Int. Ed*. **2000**, *39*, 1072; b) A. Ito, S. Inoue, Y. Hirao, K. Furukawa, T. Kato, K. Tanaka, *Chem. Commun*. **2008**, 3242; c) A. Ito, Y. Yamagishi, K. Fukui, S. Inoue, Y. Hirao, K. Furukawa, T. Kato, K. Tanaka, *Chem. Commun*. **2008**, 6573.

[13] a) T. D. Selby, S. C. Blackstock, *Org. Lett*. **1999**, *1*, 2053; b) S. I. Hauck, K. V. Lakshmi, J. F. Hartwig, *Org. Lett*. **1999**, *1*, 2057; c) I. Kulszewicz-Bajer, V. Maurel, S. Gambarelli, I. Wielgus, D. Djurado, *Phys. Chem. Chem. Phys*. **2009**, *11*, 1362.

[14] W. T. Borden, E. R. Davidson, *J. Am. Chem. Soc*. **1977**, *99*, 4587.

[15] J. M. Fauth, A. Schweiger, L. Braunschweiger, J. Forrer, R. R. Ernst, *J. Magn. Res*. **1986**, *66*, 74.

[16] C. Gemperle, G. Aebli, A. Schweiger, R. R. Ernst, *J. Magn. Res.* **1990**, *88*, 241.

[17] a) Q. Shelby, N. Kataoka, G. Mann, J. F. Hartwig, *J. Am. Chem. Soc.* **2000**, *122*, 10718; b) N. Kataoka, Q. Shelby, J. P. Stambuli, J. F. Hartwig, *J. Org. Chem.* **2002**, *67*, 5553.

[18] Ng. Ph. Buu-Hoï, *J. Chem. Soc.* **1952**, 4346.

[19] a) J. P. Wolfe, S. Wagaw, J. F. Marcoux, S. L. Buchwald, *Acc. Chem. Res.* **1998**, *31*, 805; b) J. F. Hartwig, *Acc. Chem. Res.* **1998**, *31*, 852; c) J. F. Hartwig, *Angew. Chem. Int. Ed.* **1998**, *37*, 2046; d) A. R. Muci, S. L. Buchwald, *Top. Curr. Chem.* **2002**, *219*, 133.

[20] F. A. Bell, A. Ledwith, D. C. Sherrington, *J. Chem. Soc.* **1969**, 2719.

[21] W. Weltner, Jr. *Magnetic Atoms and Molecules*, Dover, New York, **1989**.

[22] a) J. Isoya, H. Kanda, J. R. Norris, J. Tang, M. K. Brown, *Phys. Rev. B* **1990**, 41, 3905; b) A. V. Astashkin, A. Schweiger, *Chem . Phys. Lett.* **1990**, *174*, 595.

Chapter 4

A Polymacrocyclic Oligoarylamine with Pseudobeltane

Motif: Towards a Cylindrical Multi-Spin System

4.1 Introduction

Although several types of belt-shaped compounds with novel structures have been reported over the past 30 years,[1] they are currently receiving increasing attention in conjunction with the synthesis of shortest possible segments of single-walled carbon nanotube segments.[2] Nanoscaled belt-like molecules are considered to be "cycle of cycles", and thus they have well-defined shapes with rigid cavities and can conceivably be used to construct solid-state materials with nanoporous networks. In addition, polymacrocycles with electron- (or hole-) delocalized (or localized) scaffolds are fascinating for potential applications towards electron- (or hole-) transport and/or magnetic materials. In this context, oligoarylamine-based macrocyclic spin systems are being pursued to take advantage of the multi-electron redox property of oligoarylamines and the relative stability of their poly(radical cation)s to advantage.[3-5] It is well-known that strong Coulombic interactions between charged centers in oligoarylamine-based macrocycles hinders generation of higher oxidation states with maximum spin

multiplicity (Coulombic penalty).[6] As we have shown recently, however, the insertion of *para*-phenylendiamine (PD) units into the molecular backbone can alleviate the Coulombic penalty between the charged triarylaminium radical centers in oligoarylamines and to lower their oxidation potentials.[5]

Tetraaza[1_4]*m,p,m,p*-cyclophane, the smallest macrocyclic oligoarylamine bearing the alternating *meta-para*-linkage, is transformed into an almost pure spin-triplet diradical dication by two-electron oxidation.[7] Moreover, it has been demonstrated that the introduction of the macrocycles into oligoarylamine backbones with one-dimensional connectivity can convert the one-dimensional multi-spin system with a fragile spin-coupling pathway into a robust, aligned high-spin system.[8] Thus the polymacrocycles provided by the tetraazacyclophanes may be an indication for the further development of cylindrical multi-spin systems, which could culminate in nanotube-like surfaces with multi-electron redox activity. These findings led to the idea of utilizing the tetraazacyclophane unit as a building component for a belt-shaped polymacrocyclic oligoarylamine. Polymacrocycle **1** (Scheme 1), which is classified as a pseudobeltane according to Vögtle's nomenclature,[1f, 9] can be viewed as a kind of molecular belt containing six PD units connected by four 1,3,5-benzenetriyl ferromagnetic couplers,[10] and thereby the higher oxidation states of **1** can lead to multispin systems. We succeeded to synthesize this molecule with an intriguing structure for the first time. In this chapter, we describe the details of the synthesis and the properties of **1** and its cationic states.
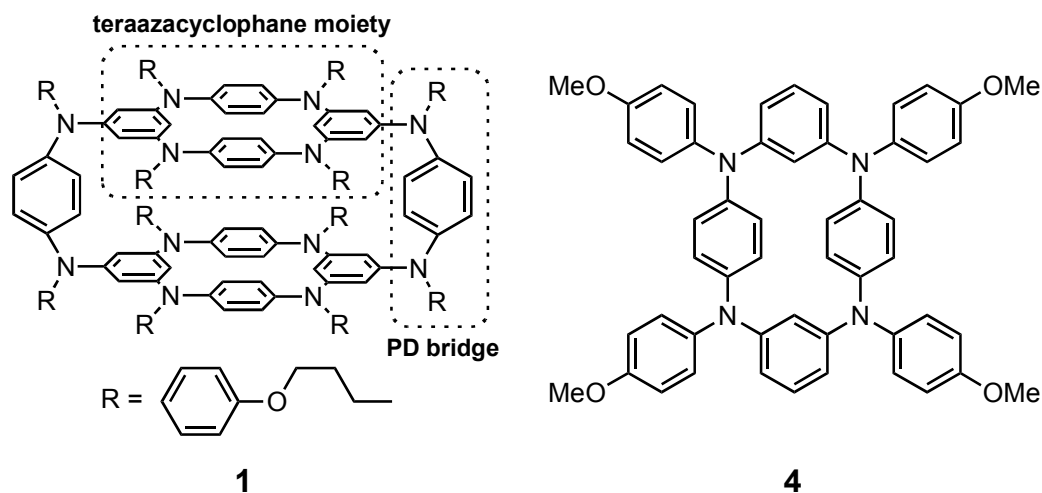
Scheme 1. Polymacrocyclic oligoarylamine **1** with pseudobeltane structure and tetraza[1₄]*m,p,m,p*-cyclophane **4** as a reference compound.

4.2 Experimental Section

General Methods: All the purchased reagents were of standard quality, and used without further purification. All the purchased solvents were purified, dried, and degassed by standard procedures. Column chromatography was performed with silica gel (Kanto Chemical Co., Inc., silica gel 60N, spherical neutral). Elemental analyses were performed by Center for Organic Elemental Microanalysis, Kyoto University. 1H and 13C NMR spectra were measured by a JEOL JNM-AL400 FT-NMR spectrometer. Chemical shifts of NMR spectra are determined relative to internal tetramethylsilane (TMS) standard (δ), and are given in parts per million (ppm). Low resolution (LR) fast-atom-bombardment (FAB) mass spectra (MS) were recorded on a JEOL JMS-HX110A mass spectrometer with m-nitrobenzyl alcohol as a matrix. UV-Vis-NIR absorption spectra were obtained with a Perkin-Elmer Lambda 19 spectrometer. High resolution matrix assisted-laser-deposition/ionization (MALDI) mass spectrum was acquired using a MALDI linear ion trap - orbitrap hybrid mass spectrometer (Thermo Fischer MALDI-LTQ-Orbitrap) with 1,8-dihydroxy-9,10-dihydroanthracen-9-one (dithranol) as a matrix.

1
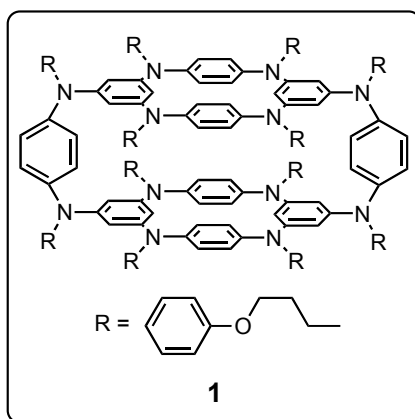
Synthetic Details. *Psuedobeltane* **(1):** Anhydrous toluene (150 mL) was added to a mixture of *N,N',N''*-tris(4-*n*-butoxyphenyl)-1,3,5-benzenetriamine **2**[11] (1.1964 g, 2.11 mmol), Pd(dba)$_2$ (0.1408 g, 0.25 mmol), P(*t*-Bu)$_3$ (0.20 mmol), and NaO*t*-Bu (0.8643 g, 8.99 mmol) in a flask equipped with a dropping funnel which was charged with a toluene solution (50 mL) of *p*-dibromobenzene (0.4801 g, 2.04 mmol), and the resulting toluene solution was stirred under an argon atmosphere at 85˚C. The charged solution in the dropping funnel was gradually added into the toluene solution containing palladium catalysts for 2 h, and then, the resulting reaction mixture was stirred for 5h at 85˚C. A toluene solution (20 ml) of *p*-dibromobenzene (0.2431 g, 1.03 mmol) was again charged to the dropping funnel, and the charged solution was gradually dropped into the reaction mixture for 2 h. The reaction mixture was stirred for 12 h at 85˚C. The reaction mixture was cooled down to room temperature, filtered through Celite, and washed with brine. The organic layer was separated and dried over Na$_2$SO$_4$. After evaporation of the solvent, the crude product was chromatographed on silica gel (toluene as eluent) to afford **1** (47.1 mg, 3.5%) as a white powder: ^{1}H NMR (400MHz, tetrahydrofuran-*d*$_8$); δ = 0.937-0.985 (m, 36H), 1.426-1.529 (m, 24H), ~1.7 (m, 24H; the corresponding signals are masked by the solvent signal (due to the *β*-protons)), 3.850-3.881 (m, 24H), 6.051 (t, *J* = 1.95 Hz, 4H), 6.390 (d, *J* = 1.95 Hz, 8H), 6.671-6.718 (m, 32H), 6.817 (s, 8H), 6.886 (d, *J* = 9.03 Hz, 16H), 6.959 (d, *J* = 9.03 Hz, 16H); ^{1}H NMR (400MHz, CDCl$_3$); δ = 0.943-0.987 (m, 36H), 1.422-1.522 (m, 24H), 1.689-1.759 (m, 24H), 3.884

(t, J = 6.34 Hz, 24H), 6.698-6.998 (br-m, 84H); ^{13}C NMR (100 MHz,

tetrahydrofuran-d_8); δ = 14.19, 14.23, 20.16, 20.16 (the two signals are accidentally

overlapped.), 32.45, 32.47, 68.36, 68.41, 115.60, 115.67, 116.04, 116.64, 121.99, 124.50,

125.26, 125.94, 127.14, 140.62, 141.72, 142.87, 143.84, 150.85, 151.35, 155.93,

156.08; MALDI HRMS (dithranol): m/z calcd for $C_{180}H_{192}N_{12}O_{12}$: 2713.47772 $[M]^+$;

found 2713.47603.

X-ray Crystallography for 1. Data collections were performed on a Rigaku

RAXIS-RAPID diffractometer equipped with Rigaku VariMax RAPID imaging plate

area detector with Cu-Kα radiation at -180°C. The data were corrected for Lorentz and

polarization effects. The structure was solved by using direct methods (SIR-2004[12]),

and expanded by using Fourier techniques (DIRDIF-99[13]), and refined by full-matrix

least-squares of F^2 on the basis of 10024 observed reflections and 846 variable

parameters (SHELXL-97[14]). The non-hydrogen atoms were refined anisotropically,

except for several disordered non-hydrogen atoms, which were refined isotropically.

Hydrogen atoms were included in the refinement but restrained to ride on the atom to

which they are bonded. The crystal contains benzene and n-hexane molecules, which

were used as mixed solvents. Two benzene molecules and one and half n-hexane

molecules per one polymacrocycle **1** were contained in the crystal. One n-hexane

molecule has a crystallographic centrosymmetric point, and another n-hexane molecule

is overlapped with the n-hexane molecule, and thus n-hexane molecules were disordered

on two positions (1:1). In addition, two n-butyloxy groups in **1** were also disordered on

two positions (0.454:0.546). Moreover, benzene molecules were also disordered, and

therefore, the resultant structures were refined as rigid groups. All the calculations were

performed by using CrystalStructure crystallographic software package,[15] except for

refinement, which was performed by using SHELXL-97.

DFT Calculations of 1' and 1'$^+$. Quantum chemical calculations were performed

with using a hybrid Hartree–Fock/density functional theory (HF/DFT) method

((U)B3LYP).[16] Full geometrical optimization of **1'** and **1'+** were carried out under C_{2h} symmetrical constraint and furthermore, their local minimum structures were confirmed by performing subsequent frequency analyses. All the computations employed the 6-31G* basis set.[17] All these computational approaches are implemented in Gaussian 09 package of ab initio MO calculation.[18]

Electrochemical Measurements.   The redox properties were evaluated by cyclic voltammetry (CV) and differential pulse voltammetry (DPV) in CH_2Cl_2 solution at 298 K with 0.1 M tetra-*n*-butylammonium tetrafluoroborate (TBABF$_4$) as supporting electrolyte (scan rate 100 mV s^{-1}) using an ALS/chi Electrochemical Analyzer model 612A. A three-electrode assembly was used, which was equipped with platinum disk (2 mm^2), a platinum wire, and Ag/0.01 M AgNO$_3$ (acetonitrile) as the working electrode, the counter electrode, and the reference electrode, respectively. The redox potential were referenced against a ferrocene/ferrocenium (Fc$^{0/+}$) redox potential measured in the same electrolytic solution.

Spectroelectrochemical Measurements.   Spectroelectrochemical measurements were carried out with a custom-made optically transparent thin-layer electrochemical (OTTLE) cell (light pass length = 1 mm) equipped with a platinum mesh, a platinum coil, and a silver wire as the working electrode, the counter electrode, and the pseudo-reference electrode, respectively. The potential was applied with an ALS/chi Electrochemical Analyzer model 612A.

ESR Measurements.   ESR spectra were recorded on a JEOL JES-TE200 X-band ESR spectrometer, in which temperature was controlled by a JEOL ES-DVT3 variable-temperature unit in the range of 120-300 K. A Mn^{2+}/MnO solid solution was used as a reference for the determination of *g*-values and hyperfine coupling constants.

Pulsed ESR Measurements.   The magnetic moments with distinct spin quantum numbers (*S*) precess with their specific nutation frequency (ω_{nut}) in the presence of a microwave irradiation field and a static magnetic field.   The nutation frequency for a

transition from $| S, M_S >$ to $| S, M_S +1>$ can be expressed as $\omega_{nut} = [S(S +1) - M_S(M_S +1)]^{1/2}\omega_0$ under certain conditions.   This indicates that ω_{nut} can be scaled with the total spin quantum number S and the spin magnetic quantum number M_S in the unit of ω_0 ($= \omega_{doublet}$).   For determination of spin-multiplicity for high-spin molecules by using the pulsed ESR technique, see: *a*) J. Isoya, H. Kanda, J. R. Norris, J. Tang, M. K. Brown, *Phys. Rev. B* **1990**, *41*, 3905; *b*) A. V. Astashkin, A. Schweiger, *Chem. Phys. Lett*. **1990**, *174*, 595; *c*) K. Sato, M. Yano, M. Furuichi, D. Shiomi, T. Takui, K. Abe, K. Itoh, A. Higuchi, K. Katsuma, Y. Shirota, *J. Am. Chem. Soc*. **1997**, *119*, 6607; *d*) H. Bock, K. Gharagozloo-Hubmann, M. Sievert, T. Prisner, Z. Havlas, *Nature* **2000**, *404*, 267; *e*) A. Ito, H. Ino, K. Tanaka, K. Kanemoto, T. Kato, *J. Org. Chem*. **2002**, *67*, 491.

Pulsed ESR measurements were carried out on a Bruker ELEXSYS E580 X-band FT ESR spectrometer, in which temperature was controlled by an Oxford ITC503 temperature controller combined with an Oxford ESR900 continuous-flow cryostat. The microwave pulse power of 10 mW provided by the microwave bridge was boosted to level of 1 kW using a traveling wave tube (TWT) amplifier. The ESTN measurements were performed by the three-pulse sequence shown below. The two-pulse ($\pi/2$ - π pulses) electron spin-echo signal $S(t_1)$ was detected by increasing the width (t_1) of the nutation pulse. We employed appropriate phase cycles in order to suppress undesirable signals and artifacts which arise from an inaccurate pulse length.[19,20] The observed signal $S(t_1, B)$ as a function of external magnetic field B is converted into a nutation frequency $S(\omega_{nut}, B)$ spectrum. The parameters used for the measurements were $t_2 = 400$ ns, $t_3 = 8$ ns. The signals observed at ca. 14 MHz in Figure 4 are due to the electron spin echo envelope modulation (ESEEM),[21] which results from weak interaction with proton nuclei ($I = 1/2$) originating from the solvent molecules surrounding the paramagnetic species.
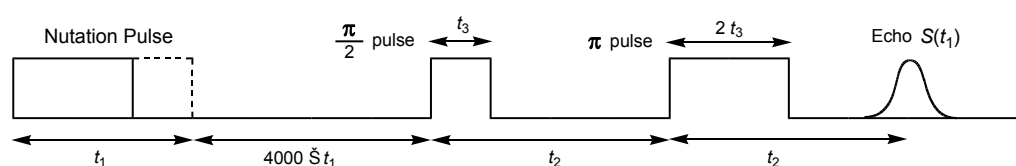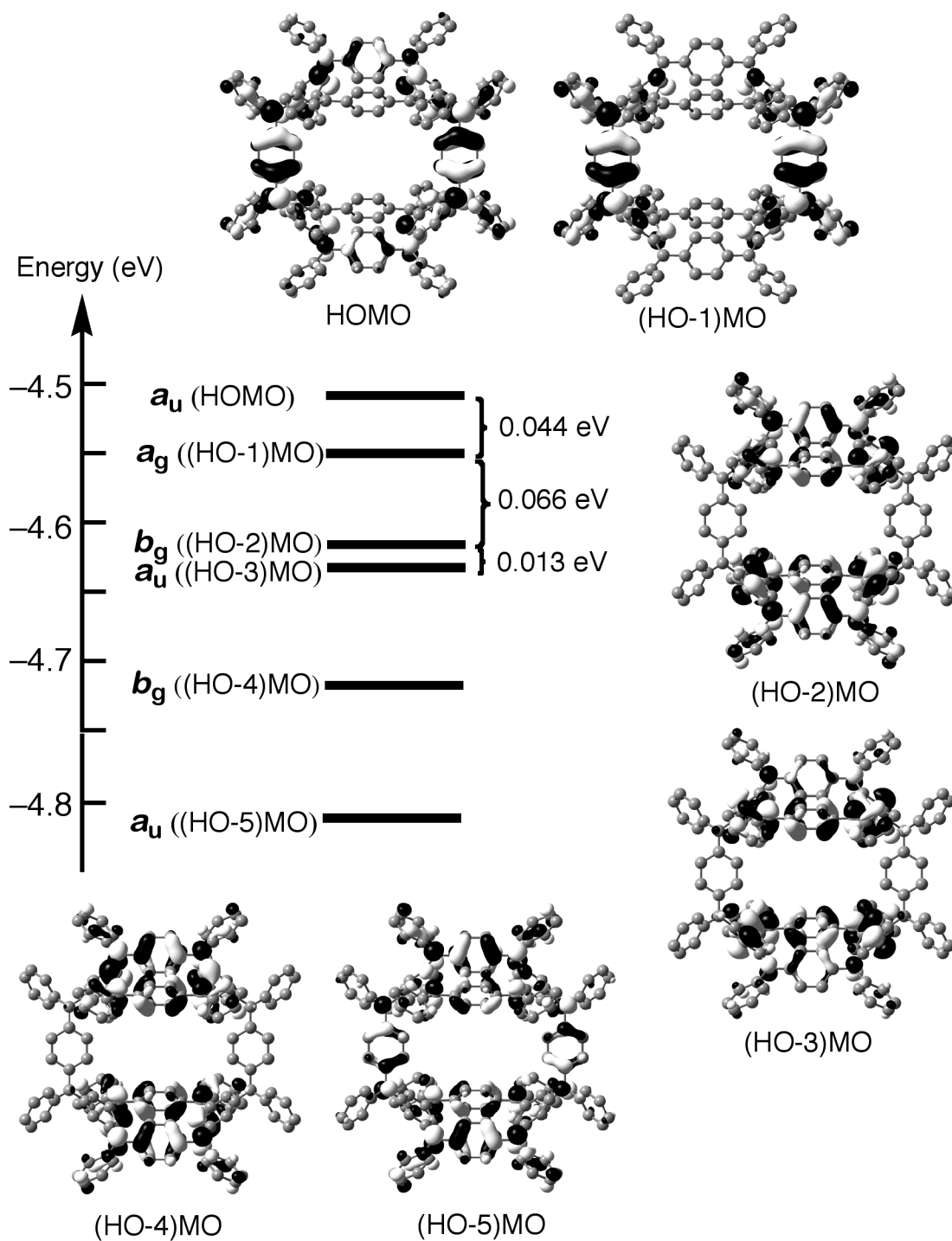
4.3 Results and Discussion

4.3.1 DFT Calculations

According to density functional theory (DFT) calculations for the model compound **1**',
in which the *n*-butoxy groups in **1** are replaced by hydrogen atoms for simplicity, at the
B3LYP/6-31G* level, the optimized structure is a C_{2h}-symmetrical structure that closely
resembles the X-ray structure of **1** (Figure 2).[22] The HOMO and (HO-1)MO are largely
localized on the two PD bridges connecting two tetraazacyclophane moieties, whereas
the (HO-2)MO and (HO-3)MO are mainly localized on the two tetraazacyclophane
moieties (Figure 1). Moreover, as is apparent from the orbital energy diagram, these
frontier MOs from HOMO to (HO-3)MO are quasi-fourfold degenerate, so that a
spin-quintet state can be anticipated in the tetracation of **1**$^{4+}$.

Energy (eV)

−4.5 — a_u (HOMO)

a_g ((HO-1)MO) — 0.044 eV

— 0.066 eV

−4.6 — b_g ((HO-2)MO)
a_u ((HO-3)MO) — 0.013 eV

−4.7 — b_g ((HO-4)MO)

−4.8 — a_u ((HO-5)MO)

HOMO

(HO-1)MO

(HO-2)MO

(HO-3)MO

(HO-4)MO

(HO-5)MO

Figure 1. Frontier MOs for **1**' and their relative energy levels at the B3LYP/6-31G* level of theory.

101

4.3.2 Synthesis

The target molecule **1** was successfully prepared from 1,3,5-benzenetriamine **2**[23] and *p*-dibromobenzene in a one-pot manner by using the Buchwald-Hartwig cross-coupling amination reaction[24] (Scheme 2). A solution of *p*-dibromobenzene in toluene was slowly added to the stirred mixture of **2**, P(*t*-Bu)$_3$, Pd(dba)$_2$, and NaO*t*-Bu in toluene at 85˚C for 2 h, and then the reaction mixture was continued stirring at 85˚C. The reaction was monitored by MALDI-MS; the spectra exhibited an increase of a peak assigned not to **1** (*m/z* = 2715) but to a compound with tetraazacyclophane framework **3** (*m/z* = 1284). After 5 h stirring, an additional solution of *p*-dibromobenzene in toluene was added to the stirred reaction mixture over 2 h, and subsequently the reaction mixture was continued stirring for 12 h at 85˚C. Finally, macrocyclization to **1** was confirmed by the appearance of a peak at *m/z* = 2715, and purification by silica gel column chromatography afforded **1** in 3.5% yield as a white powder. Evidence of rigidity in the molecular structure appears in the ^{1}H and ^{13}C NMR spectra. Whereas only one singlet ^{1}H NMR signal is expected for the freely rotating *para*-phenylenes because of the highly symmetrical structure of **1**, a multiplet signal was observed for the corresponding protons attached to *para*-phenylenes in the tetraazacyclophane moieties. In addition, the ^{13}C NMR spectrum of **1** also exhibits not 16-line but 17-line signals in the aromatic region, thus indicating that the free rotation of *para*-phenylenes in the tetraazacyclophane moieties is prohibited even in solution at room temperature. In contrast, judging from the reported solution NMR spectra, free rotation of *para*-phenylene rings have been confirmed for the tetraazacyclophanes[7a,c] and their two-dimensionally expanded polymacrocycles.[4,5b]
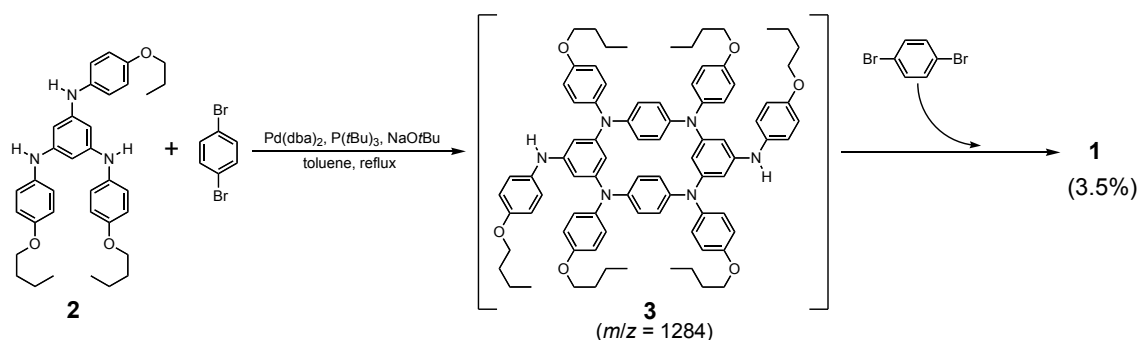
Scheme 2. Synthesis of **1**. dba = *trans,trans*-dibenzylideneacetone.

4.3.3 X-ray Structural Analysis

As shown in Figure 2, direct information about the structure of **1** was clarified by X-ray crystallographic analysis of colorless needlelike single crystals grown from a mixed solution (benzene/*n*-hexane) (Table 1).[25] In the crystal, each molecule of **1** possesses a crystallographic centrosymmetric point, and moreover, is associated with two benzene molecules and 1.5 *n*-hexane molecules, which penetrate the cavity (ca. 5Å×8Å) formed between the two tetraazacyclophane macrocycles (Figures 2b and 2c). In addition, two tetraazacyclophane moieties are sideslipped by 3 Å in parallel with each other in association with an inclination (56˚) of the two PD bridges.
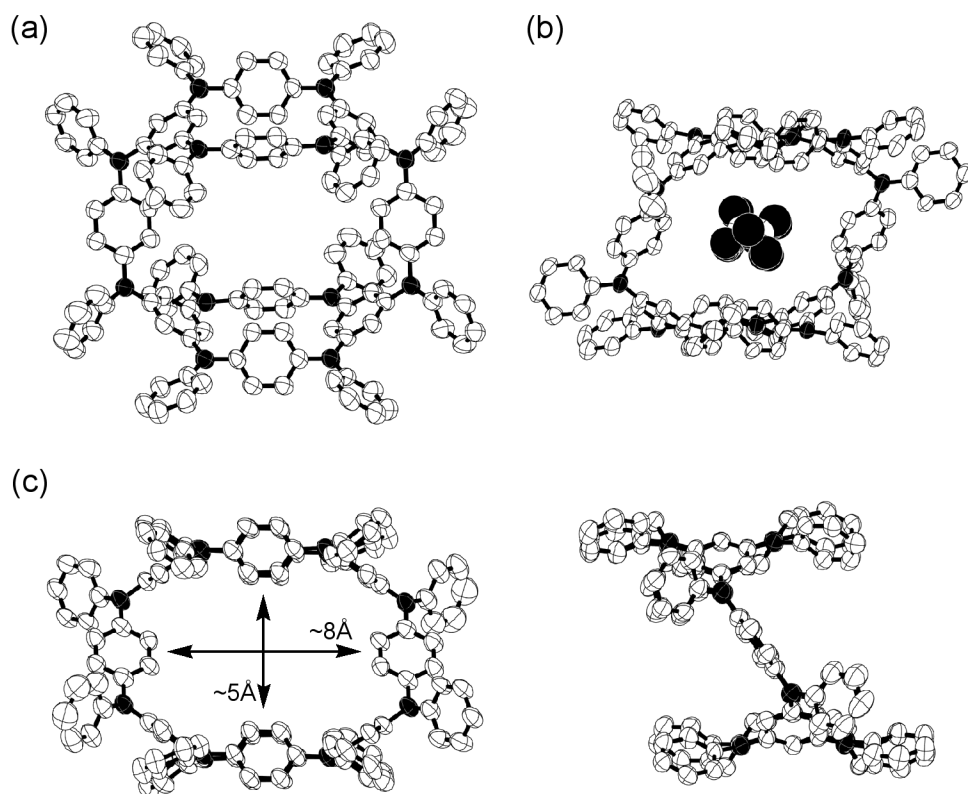
Figure 2. a) ORTEP representations of **1**. Crystallization solvent molecules (benzene and *n*-hexane), *n*-butoxy groups, and hydrogen atoms are omitted for clarity Nitrogen atoms are colored in black. Ellipsoids are set at 50% probability; b) another view including *n*-hexane; c) side views.

Table 1: X-ray crystallographic data for **1**.

empirical formula	$C_{201}H_{225}N_{12}O_{12}$
	$[\mathbf{1} \bullet (C_6H_6)_2 \bullet (C_6H_{14})_{1.5}]$
formula weight	3001.06
$T\,[^\circ C]$	-180 ± 1
$\lambda\,[\text{Å}]$	1.54187
crystal system	triclinic
space group	$P\bar{1}$ (#2)
Z	1
$a\,[\text{Å}]$	13.9732(5)
$b\,[\text{Å}]$	18.8502(6)
$c\,[\text{Å}]$	21.1130(15)
$\alpha\,[^\circ]$	110.456(8)
$\beta\,[^\circ]$	108.875(8)
$\gamma\,[^\circ]$	90.515(6)
$V\,[\text{Å}^3]$	4883.3(4)
$\rho_{\text{calcd}}\,[\text{g cm}^{-3}]$	1.020
$\mu\,(\text{CuK}\alpha)[\text{cm}^{-1}]$	4.908
collected data	41081
unique data / R_{int}	10024/0.065
no. of parameters	846
goodness-of-fit[a]	1.242
$R1\,(I>2\sigma)$, $wR2$ (all reflections)[b]	0.1375, 0.3789
residual density $[\text{e Å}^{-3}]$	0.82/-0.32

[a] GOF $= \left\{ \sum\left[w\left(F_0^2 - F_c^2\right)^2 \right] \Big/ (n-p) \right\}^{1/2}$, where n and p denote the number of data and parameters.

[b] R1 $= \sum\left(\|F_0\| - \|F_c\|\right) / \sum\|F_0\|$ and wR2 $= \left\{ \sum\left[w\left(F_0^2 - F_c^2\right)^2 \right] \Big/ \sum\left[w\left(F_0^2\right)^2 \right] \right\}^{1/2}$ where

$w = 1 \Big/ \left[\sigma^2\left(F_0^2\right) + \left(a \cdot P\right)^2 + b \cdot P \right]$ and $P = \left[\left(\text{Max}; 0, F_0^2\right) + 2 \cdot F_c^2 \right] / 3$.

4.3.4 Electrochemistry

Electrochemical analysis of **1** indicated multi-electron redox activity originating from six PD units: quasi-two-electron transfer (–0.138 (2e) [V vs. $Fc^{0/+}$ (number of electrons)]); two one-electron transfers (+0.046 (1e) and +0.137 (1e)); quasi-two-electron transfer (+0.292 (2e)); quasi-four-electron transfer (+0.511 (2e), +0.560 (1e), and +0.598 (1e)); quasi-two-electron transfer (+0.666 (1e) and +0.702 (1e)). Thus, **1** can be oxidized up to a stable dodecacation on the cyclic and/or differential pulse voltammetric timescale (Figure 3). Under the same conditions, the oxidation potentials for the tetraazacyclophane **4** as a reference compound are –0.01 (1e), +0.22 (1e), +0.54 (1e), and +0.67 (1e).[5b] Therefore, it is deducible that removal of the first six electrons from **1** leads to the generation of six PD-based semiquinone radical cations, while the removal of further six electrons corresponds to the generation of six diamagnetic PD-based quinone dications.
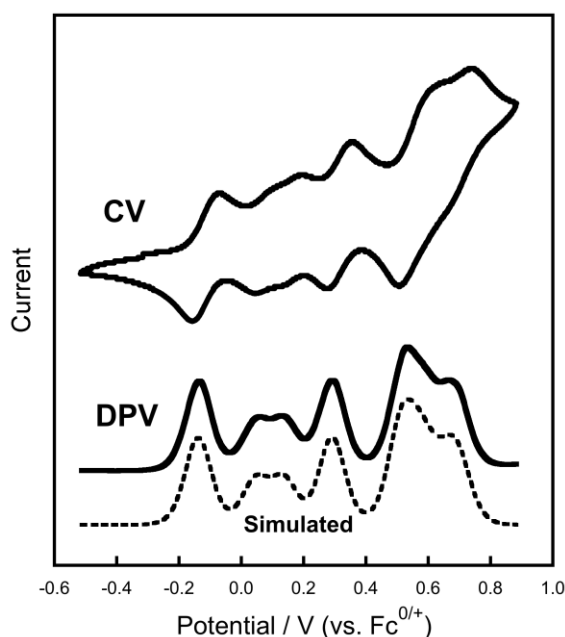
Figure 3. Cyclic voltammogram (CV) and differential pulse voltammogaram (DPV) of **1**, measured in CH_2Cl_2 containing 0.1 M nBu$_4$NBF$_4$ at 298 K (scan rate 100 mV s^{-1}). The simulated DPV[26] is drawn by the dotted line and the oxidation potentials were estimated by the DPV simulation.

4.3.5 UV-Vis-NIR Spectroscopy

To gain more insights into the electronic structure corresponding to each oxidation state indicated in the electrochemical study, we recorded changes in the absorption spectrum upon electrochemical oxidation of **1** to **1**$^{6+}$ by using an optically transparent thin-layer electrochemical cell (Figure 4). As shown in Figure 4a, the growing lower energy bands at 1.37 eV (λ_{max} = 904 nm) and 2.23 eV (λ_{max} = 556 nm) for **1**$^{+}$ were gradually red-shifted to 1.28 eV (λ_{max} = 966 nm) and 2.14 eV (λ_{max} = 579 nm) with an isosbestic point at 3.44 eV (360 nm) upon oxidation to **1**$^{2+}$. This observation strongly suggests that the radical cation **1**$^{+}$ can be generated by treatment with less than one equiv of an oxidant, although the first oxidation process can be considered to be a two-electron transfer process based on the present electrochemical study. Further oxidation into **1**$^{6+}$ was accompanied by the continuous increase in intensity of the lowest energy band which is assignable to the charge-resonance (CR) intervalence (IV) band originating from generation of the semiquinone radical cation in the PD unit.[27] Finally the absorbance intensity reached up to about thrice that of **1**$^{2+}$, thus indicating that all the PD moieties were converted to the corresponding semiquinone radical cations (Figure 4b) . When **1**$^{6+}$ was oxidized further, the intense CR IV band rapidly decreased together with the higher energy band at 3.01 eV (λ_{max} = 412 nm), which had been observed for **1**$^{6+}$ (Figure 4b), and simultaneously, a new band at 1.51 eV (λ_{max} = 823 nm) grew with two isosbestic points [1.44 eV (863 nm) and 2.70 eV (460 nm)]. This new band corresponds to the conversion from the semiquinoidal radical cation into the diamagnetic quinoidal dication in the PD units (Figure 4c).
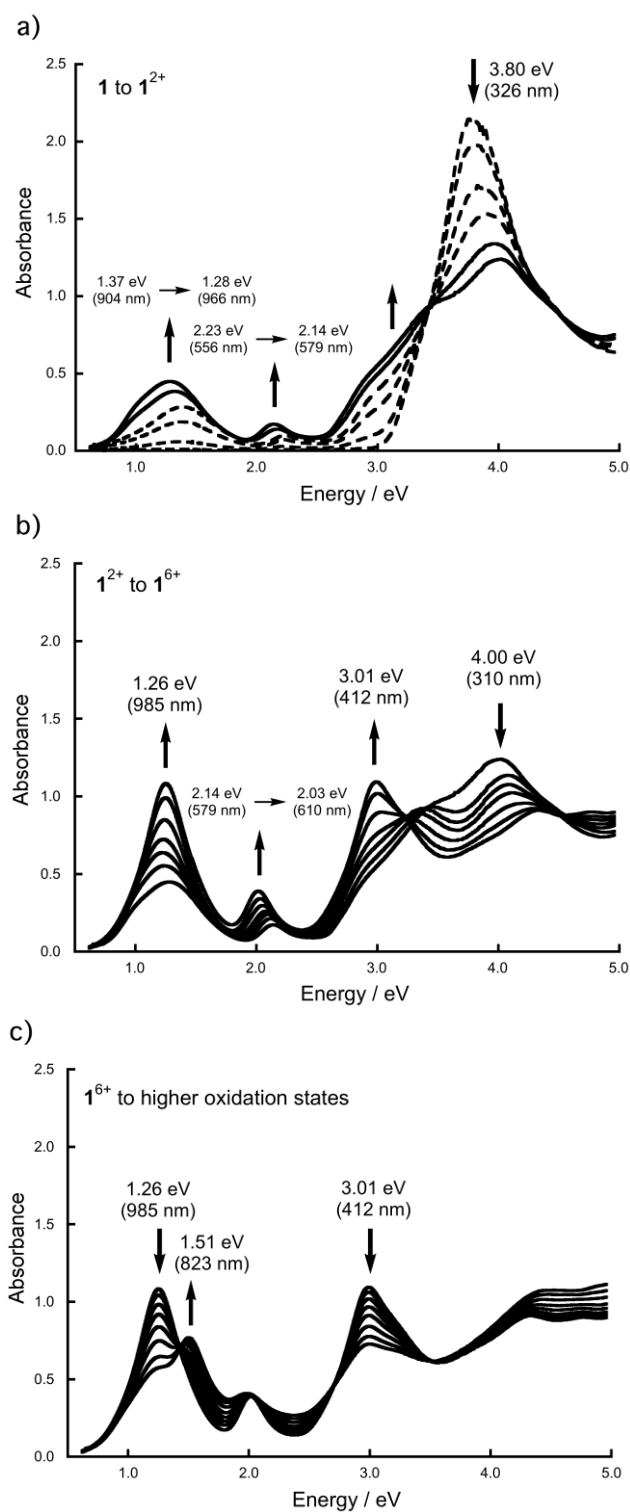
**Figure 4.** UV/Vis-NIR absorption spectra of the stepwise electrochemical oxidation of **1** in CH_2Cl_2 with 0.1 M nBu$_4$NBF$_4$ at 298 K: a) **1** to **1**$^{2+}$; b) **1**$^{2+}$ to **1**$^{6+}$; c) further oxidation process from **1**$^{6+}$.

4.3.6 CW-ESR measurements

The solution ESR spectrum of 1^+ generated by chemical oxidation with 0.5 equivalents of tris(4-bromophenyl)aminium hexachloroantimonate (Magic Blue)[28] in CH_2Cl_2 at 295 K exhibited a multiplet hyperfine structure at $g = 2.0029$ (Figure 5). The observed spectrum was reasonably reproduced by the following hyperfine coupling (hfc) constants: $a_{N1} = 0.250$ mT (4N) and $a_{N2} = 0.035$ mT (8N), and the contribution from unresolved hydrogen nuclei was assumed to be incorporated in the linewidth of the spectrum simulation (0.20 mT) (Figure 5), indicating that the spin density resides mainly on the two PD bridges (Figure 6a). However, on closer inspection of the spin-density distribution over the tetraazacyclophane moieties in $1'^+$ (Figure 6a) we found that no spin density is distributed on the inner PD units, whereas a part of the spin density is on the outer PD units, probably originating from the sideslipped structure of **1** (Figures 2c and 6b).[11] Indeed, these findings were reflected in the temperature dependence of the observed ESR spectrum (Figure 7a). The hyperfine structure for 1^+ became vague with decreasing temperature, and we found that such a spectral change is reproducible only by considering a windshield-wiper-like motion interconverting two sideslipped structures with a rate constant k (Figure 6b). The rate constants at various temperatures were determined by spectral simulations of the observed ESR spectra by using the ESR-EXN program on the basis of the stochastic Liouville method (Figure 7b).[29] In the measured temperature range, plots of $\ln(k)$ versus $1/T$ gave a linear relationship, thus indicating an Arrhenius-type temperature dependence [$k = A\exp(-\Delta G^*/k_B T)$, where k_B is the Boltzmann constant] (Figure 8). Consequently, from the Arrhenius plots, the barrier to thermal interconversion between two sideslipped structures, ΔG^* and the prefactor A were estimated to be 5.0 kcal mol^{-1} and 2.3×10^{11} s^{-1}, respectively.
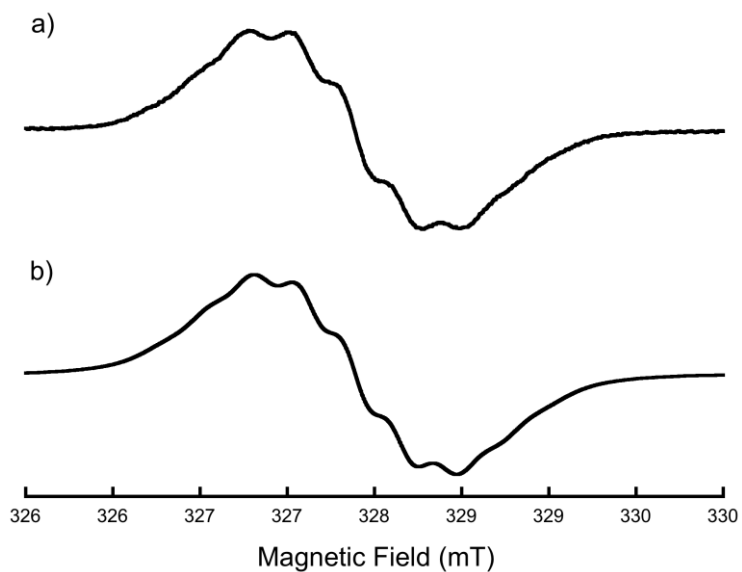
Figure 5. ESR spectrum of $\mathbf{1}^{\bullet+}$: a) in CH_2Cl_2 at 293 K; b) simulated.
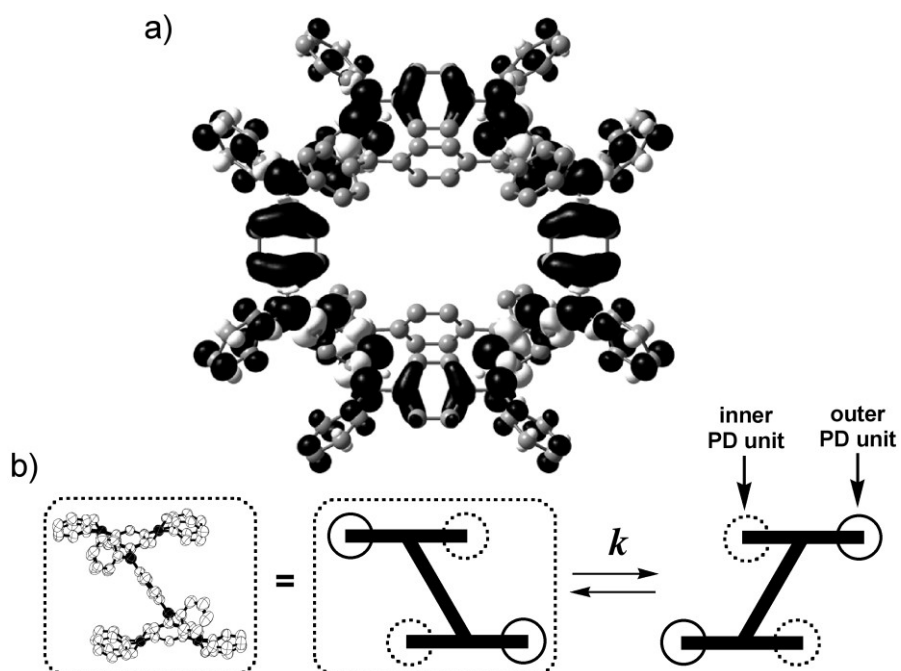
Figure 6. a) Spin density distribution of $\mathbf{1'}^{+}$ (UB3LYP/6-31G*; black: positive spin, white: negative spin; spin isosurface value = 0.0003 electron au^{-3}), and b) a windshield wiper-like interconversion between two sideslip structures at a rate constant k.
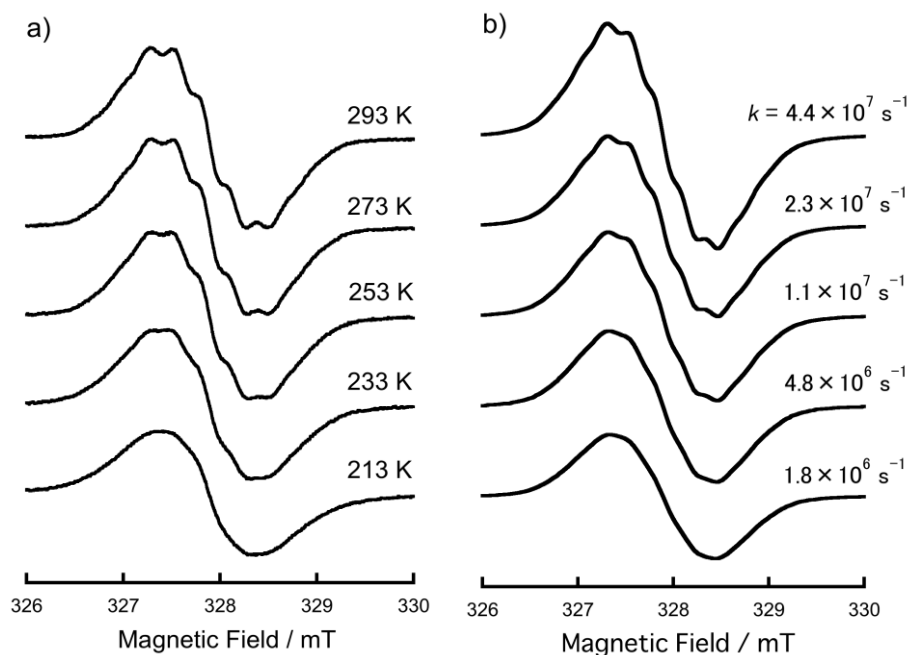
Figure 7. a) Temperature-dependent ESR spectra of 1^+ in CH_2Cl_2, and b) the simulated spectra.
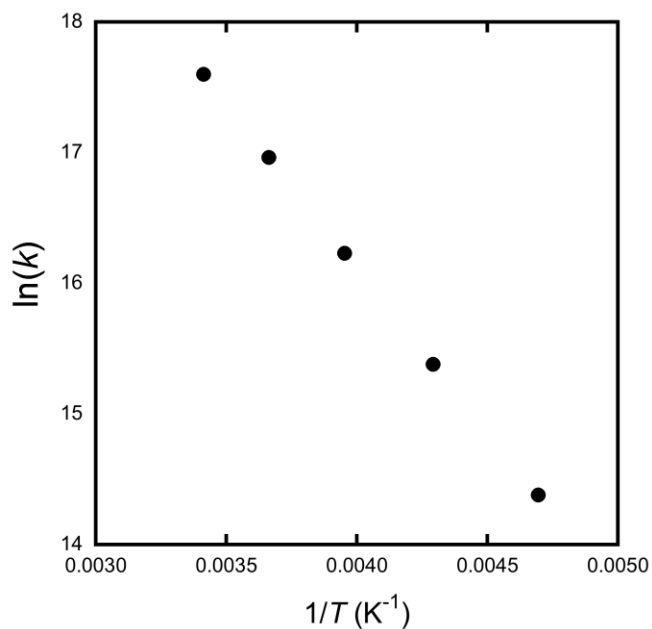
Figure 8. Arrhenius plots of the rate constants (k) for interconversion between two sideslip structures in $1^{\bullet+}$ estimated from the dynamic ESR simulations.

4.3.7 pulsed-ESR measurements

The electrochemical and spectroelectrochemical studies of **1** (Figures 3 and 4) indicate that the dicationic, tetracationic, and hexacationic species are accessible by appropriate chemical oxidation, and therefore, their spin multiplicities at low temperatures are of great interest in view of the realization of cylindrical multispin systems. Polycations $\mathbf{1}^{2+}$ and $\mathbf{1}^{4+}$ were readily generated by adding 2 and 4 molar equivalents of Magic Blue at 195 K in CH_2Cl_2. However, treatment of **1** with 6 or more equivalents of Magic Blue did not generate $\mathbf{1}^{6+}$. At this stage, we did not search for oxidizing agents suitable for the generation of $\mathbf{1}^{6+}$. Information about the spin multiplicities at 5K for $\mathbf{1}^{2+}$ and $\mathbf{1}^{4+}$ were unequivocally obtained by pulsed ESR spectroscopy detecting the electron spin transient nutation (ESTN) signal.[30] As is apparent from Figure 9a and Table 1, the nutation signal of 25.4 MHz can be assigned to the spin-triplet state of $\mathbf{1}^{2+}$, judging from the nutation signal (18.6 MHz) due to the spin-doublet impurity. Note that no noticeable zero-field splitting was observed in the nutation signal for the spin-triplet $\mathbf{1}^{2+}$, indicating the average distance between two unpaired electrons is quite great. In fact, it is anticipated that the quasi-degenerate HOMO and (HO-1)MO of **1'** (Figure 1) can be regarded as two singly occupied MOs in $\mathbf{1'}^{2+}$, and thus, the two unpaired electrons are mainly distributed over two PD linkers, which are separated 12.83 Å according to the X-ray structure (Figure 2). Concomitantly, we observed the nutation signals of 30.6 and 36.2 MHz due to the spin-quartet state of $\mathbf{1}^{3+}$, which is generated simply because of a slight excess of Magic Blue. In contrast, the ESTN spectrum for the polycationic species geberated by treatment with 4 equivalents of Magic Blue clearly demonstrated the existence of an almost pure spin-quintet state of $\mathbf{1}^{4+}$. The two nutation signals of 27.8 and 35.5 MHz indicate $S = 2$ spin multiplicity of $\mathbf{1}^{4+}$, since only a very weak signal corresponding to the excited triplet state of $\mathbf{1}^{4+}$ was detected at 20.0 MHz (Figure 9b and Table 2). This result indicates that $\mathbf{1}^{4+}$ is in a spin-quintet state at 5K and the excited spin-triplet state is readily accessible owing to the very small energy spacing, and thus

112

four unpaired electrons are accommodated separately in the two PD bridges and the two tetraazacyclopahne moieties, as is expected from the HOMO to (HO–3) MOs on **1'** (Figure 1).
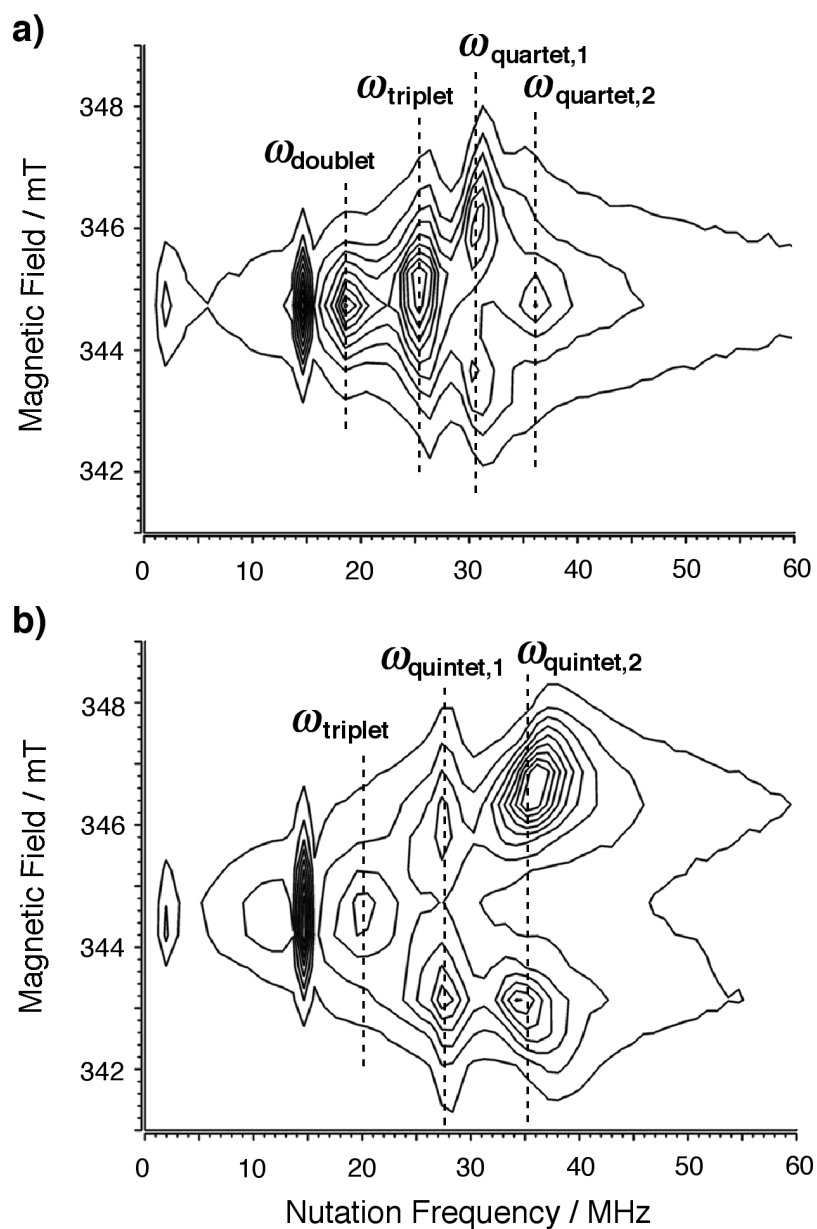
Figure 9. 2D ESTN spectra of **1** in CH_2Cl_2 at 5K after addition of a) 2 equiv and b) 4 equiv of the Magic Blue.

Table 2: Spectroscopic data of the ESTN spectroscopy for $\mathbf{1}^{2+}$ and $\mathbf{1}^{4+}$.

Species	Observed nutation frequency [MHz][a]	Transition assignment
$\mathbf{1}^{2+}$	$25.4\ (\omega_t = \sqrt{2}\ \omega_d)$	$\|1, \pm1\rangle \Leftrightarrow \|1, 0\rangle$
(doublet impurity	$18.6\ (\omega_d)$	$\|1/2, +1/2\rangle \Leftrightarrow \|1/2, -1/2\rangle)$
(quartet impurity	$30.6\ (\omega_{q,1} = \sqrt{3}\ \omega_d)$	$\|3/2, \pm3/2\rangle \Leftrightarrow \|3/2, \pm1/2\rangle$
	$36.2\ (\omega_{q,2} = 2\ \omega_d)$	$\|3/2, +1/2\rangle \Leftrightarrow \|3/2, -1/2\rangle)$
$\mathbf{1}^{4+}$	$27.8\ (\omega_{quintet,1} = \sqrt{2}\ \omega_t)$	$\|2, \pm2\rangle \Leftrightarrow \|2, \pm1\rangle$
	$35.5\ (\omega_{quintet,2} = \sqrt{3}\ \omega_t)$	$\|2, \pm1\rangle \Leftrightarrow \|2, 0\rangle$
(excited triplet	$20.0\ (\omega_t)$	$\|1, \pm1\rangle \Leftrightarrow \|1, 0\rangle)$

[a] d = doublet, t = triplet, q = quartet.

4.4 Conclusion

In summary, the newly prepared pseudobeltane-like polymacrocyclic oligoarylamine **1** displays multi-electron redox activity up to the electrochemical generation of dodecacation, and moreover, the diradical dication $\mathbf{1}^{2+}$ and tetraradical tetracation $\mathbf{1}^{4+}$ generated by chemical oxidatios were found to be in high-spin states at low temperatures. In addition, dynamic ESR spectroscopy revealed the thermally activated interconversion between two sideslipped structures in radical cation $\mathbf{1}^+$. The present toroidal multispin system is thus expected to serve as a useful building block in the extension to cylindrical multispin systems, which we are now actively pursuing.

References and Notes

[1] Deltaphane: a) H. C. Kang, A. W. Hanson, B. Eaton, V. Boekelheide, *J. Am. Chem. Soc.* **1985**, *107*, 1979. Kohnkene: b) F. H. Kohnke, A. M. Z. Slawin, J. F. Stoddart, D. J. Williams, *Angew. Chem. Int. Ed.* **1987**, *26*, 892. Collarene: c) P. R. Ashton, N. S. Isaacs, F. H. Kohnke, A. M. Z. Slawin, C. M. Spencer, J. F. Stoddart, D. J. Williams, *Angew. Chem. Int. Ed.* **1988**, *27*, 966. d) J. Benkhff, R. Boese, F.-G. Klärner, *Liebigs Ann./Recueil* **1997**, 501. Beltane: e) F. Vögtle, A. Schröder, D. Karbach, *Angew. Chem. Int. Ed.* **1991**, *30*, 575. Pseudo-beltane: f) H. Schwierz, F. Vögtle, *Synthesis* **1999**, *2*, 295. Belt cyclophane: g) H. Meier, K. Müller, *Angew. Chem. Int. Ed.* **1995**, *34*, 1437. Picotube: h) S. Kammermeier, P. G. Jones, R. Herges, *Angew. Chem. Int. Ed.* **1996**, *35*, 2669. Cyclic paraphenylacetylene: i) T. Kawase, H. R. Darabi, M. Oda, *Angew. Chem. Int. Ed.* **1996**, *35*, 2664. [8]Cyclacene triquinone: j) R. M. Cory, C. L. McPhail, *Tetrahedron Lett.* **1996**, *37*, 1987. Vögtle belt: k) F. Vögtle, *Top. Curr. Chem.* **1983**, *115*, 157. l) G. J. Bodwell, D. O. Miller, R. J. Vermeij, *Org. Lett.* **2001**, *3*, 2093. m) C. Denekamp, A. Etinger, W. Amrein, A. Stanger, M. Stuparu, A. D. Schlüter, *Chem. Eur. J.* **2008**, *14*, 1628. [6.8]₃Cyclacene: n) B. Esser, F. Rominger, R. Gleiter, *J. Am. Chem. Soc.* **2008**, *130*, 6716.

[2] a) B. D. Steinberg, L. T. Scott, *Angew. Chem. Int. Ed.* **2009**, *48*, 5400; b) R. Jasti, C. R. Bertozzi, *Chem. Phys. Lett.* **2010**, *494*, 1; c) T. Iwamoto, Y. Watanabe, Y. Sakamoto, T. Suzuki, S. Yamago, *J. Am. Chem. Soc.* **2011**, *133*, 8354; d) T. J. Sisto, R. Jasti, *Synlett* **2012**, *23*, 483; e) S. Schrettl, H. Frauenrath, *Angew. Chem. Int. Ed.* **2012**, *51*, 6569; f) U. H. Bunz, S. Menning, N. Martín, *Angew. Chem. Int. Ed.* **2012**, *51*, 7094; g) H. Omachi, Y. Segawa, K. Itami, *Acc. Chem. Res.* **2012**, *45*.

[3] a) A. Ito, Y. Ono, K. Tanaka, *J. Org. Chem.* **1999**, *64*, 8236; b) R. J. Bushby, C. A. Kilner, N. Taylor, M. E. Vale, *Tetrahedron* **2007**, *63*, 11458; c) M. Vale, M. Pink, S. Rajca, A. Rajca, *J. Org. Chem.* **2008**, *73*, 27; d) K. Ishibashi, H. Tsue, N. Sakai, S.

Tokita, K. Matsui, J. Yamauchi, R. Tamura, *Chem. Commun*. **2008**, 2812.

[4] X. Z. Yan, J. Pawlas, T. Goodson, III, J. F. Hartwig, *J. Am. Chem. Soc*. **2005**, *127*, 9105.

[5] a) A. Ito, S. Inoue, Y. Hirao, K. Furukawa, T. Kato, K. Tanaka, *Chem. Commun*. **2008**, 3242; b) A. Ito, Y. Yanagishi, K. Fukui, S. Inoue, Y. Hirao, K. Furukawa, T. Kato, K. Tanaka, *Chem. Commun*. **2008**, 6573.

[6] a) R. J. Bushby, D. R. McGill, K. M. Ng, N. Taylor, *Chem. Commun*. **1996**, 2641; b) R. J. Bushby, D. R. McGill, K. M. Ng, N. Taylor, *J. Chem. Soc*., *Perkin Trans. 2*, **1997**, 1405. On the other hand, macrocyclic high-spin systems containing neutral radical centers are immune to the Coulombic penalty. see, for instance. carbon-centered radicals: a) A. Rajca, S. Rajca, S. R. Desai, *J. Am. Chem. Soc*. **1995**, *117*, 806; b) K. Matsuda, N. Nakamura, K. Takahashi, K. Inoue, N. Koga, H. Iwamura, *J. Am. Chem. Soc*. **1995**, *117*, 5550. nitroxide radicals: a) A. Rajca, S. Mukherjee, M. Pink, S. Rajca, *J. Am. Chem. Soc*. **2006**, *128*, 13497; b) T. Sawai, K. Sato, T. Ise, D. Shiomi, K. Toyota, Y. Morita, T. Takui, *Angew. Chem. Int. Ed*. **2008**, *47*, 3988; c) A. Olankitwanit, V. Kathirvelu, S. Rajca, G. R. Eaton, S. S. Eaton, A. Rajca, *Chem. Commun*. **2011**, *47*, 6443.

[7] a) A. Ito, Y. Ono, K. Tanaka, *Angew. Chem. Int. Ed*. **2000**, *39*, 1072; b) T. D. Selby, S. C. Blackstock, *Org. Lett*. **1999**, *1*, 2053; c) S. I. Hauck, K. V. Lakshmi, J. F. Hartwig, *Org. Lett*. **1999**, *1*, 2057; d) I. Kulszewicz-Bajer, V. Maurel, S. Gambarelli, I. Wielgus, D. Djurado, *Phys. Chem. Chem. Phys*. **2009**, *11*, 1362.

[8] D. Sakamaki, A. Ito, K. Furukawa, T. Kato, K. Tanaka, *Chem. Commun*. **2009**, 4524.

[9] The present compound is structurally akin to Gleiter's π-boat cage compounds: R. Gleiter, K. Hövermann, J. Ritter, B. Nuber, *Angew. Chem. Int. Ed*. **1995**, *34*, 789.

[10] a) K. Yoshizawa, A. Chano, A. Ito, K. Tanaka, T. Yamabe, H. Fujita, J. Yamauchi, M. Shiro, *J. Am. Chem. Soc*. **1992**, *114*, 5994; b) K. R. Stickley, S. C. Blackstock, *J. Am. Chem. Soc*. **1994**, *116*, 11576; c) K. R. Stickley, T. D. Selby, S. C. Blackstock, *J. Org.*

Chem. **1997**, *62*, 448. M. M. Wienk, R. A. J. Janssen, *J. Am. Chem. Soc*. **1997**, *119*, 4492; d) K. Sato, M. Yano, M. Furuichi, D. Shiomi, T. Takui, K. Abe, K. Itoh, A. Higuchi, K. Katsuma, Y. Shirota, *J. Am. Chem. Soc*. **1997**, *119*, 6607.

[11] Ng. Ph. Buu-Hoï, *J. Chem. Soc.* **1952**, 4346.

[12] M. C. Burla, R. Caliandro, M. Camalli, B. Carrozzini, G. L. Cascarano, L. De Caro, C. Giacovazzo, G. Polidori, R. Spagna, *J. Appl. Cryst*. **2005**, *38*, 381.

[13] The DIRDIF-99 Program System, Technical Report of the Crystallography Laboratory, P. T. Beurskens, G. Admiraal, G. Beurskens, W. P. Bosman, R. de Gelder, R. Israel, J. M. M. Smits, University of Nijmegen (The Netherlands), **1999**.

[14] Program for Crystal Structure Solution and Refinement, G. M. Sheldrick, Universität Göttingen, **1997**.

[15] CrystalStructure 3.8, Crystal Structure Analysis Package, Rigaku and Rigaku Americas (2000–2007). 9009 New Trails Dr. The Woodlands TX 77381 USA.

[16] K. Ragavachari, *Theor. Chim. Acc*. **2000**, *103*, 361 and references cited therein.

[17] W. J. Hehre, L. Radom, P.v. R. Schleyer, J. A. Pople, *Ab Initio Molecular Orbital Theory*, Wiley, New York, **1986**.

[18] M. J. Frisch, *et al*., Gaussian 09 (Revision C.01), Gaussian, Inc., Wallingford CT, **2009**.

[19] J.-M. Fauth, A. Schweiger, L. Braunschweiger, J. Forrer, R. R. Ernst, *J. Magn. Res.* **1986**, *66*, 74.

[20] C. Gemperle, G. Aebli, A. Schweiger, R. R. Ernst, *J. Magn. Res.* **1990**, *88*, 241.

[21] W. B. Mims, *Phys. Rev. B* **1972**, *5*, 2409.

[22] The full geometry optimizations of **1'** and **1'$^+$** in C_{2h} symmetry were performed by using Gaussian09 program package: Gaussain09 (Revision C.01), M. J. Frisch et al.

[23] Ng. Ph. Buu-Hoï, *J. Chem. Soc.* **1952**, 4346.

[24] a) J. P. Wolfe, S. Wagaw, J. F. Marcoux, S. L. Buchwald, *Acc. Chem. Res*. **1998**, *31*, 805; b) J. F. Hartwig, *Acc. Chem. Res*. **1998**, *31*, 852; c) J. F. Hartwig, *Angew. Chem. Int.*

Ed. **1998**, *37*, 2046. d) A. R. Muci, S. L. Buchwald, *Top. Curr. Chem*. **2002**, *219*, 133.

[25] CCDC 879828 (**1**) contains the supplementary crystallographic data for this chapter. The data can be obtained free of charge from The Cambridge Crystallographic Data centre via www.ccdc.cam.ac.uk/data_request/cif.

[26] W. Huang, T. L. E. Henderson, A. M. Bond, K. B. Oldham, *Anal. Chim. Acta* **1995**, *304*, 1.

[27] a) A. Ishitani, S. Nagakura, *Mol. Phys*. **1967**, *12*,1; b) B. Badger, B. Brocklehurst, R. D. Russell, *Chem. Phys. Lett*. **1967**, *1*, 122; c) A. V. Szeghalmi, M. Erdmann, V. Engel, M. Schmitt, S. Amthor, V. Kriegisch, G. Nöll, R. Stahl, C. Lambert, D. Leusser, D. Stalke, M. Zabel, J. Popp, *J. Am. Chem. Soc*. **2004**, *126*, 7834; d) Y. Hirao, A. Ito, K. Tanaka, *J. Phys. Chem. A* **2007**, *111*, 2951; e) A. Ito, D. Sakamaki, Y. Ichikawa, K. Tanaka, *Chem. Mater*. **2011**, *23*, 841.

[28] a) F. A. Bell, A. Ledwith, D. C. Sherrington, *J. Chem. Soc*. **1969**, 2719; b) N. G. Connelly, W. E. Geiger, *Chem. Rev*. **1996**, *96*, 877.

[29] a) J. Heinzer, *Mol. Phys*. **1971**, *22*, 167; b) *Quantum Chemistry Program Exchange* **1972**, No. 209. We thank Prof. S. F. Nelsen for a copy of this program (modified by P. A. Petillo, R. F. Ismagilov, and Y. Hirao)

[30] a) J. Isoya, H. Kanda, J. R. Norris, J. Tang, M. K. Brown, *Phys. Rev. B*. **1990**, *41*, 3905; b) A. V. Astashkin, A. Schweiger, *Chem. Phys. Lett*. **1990**, *174*, 595.

Chapter 5

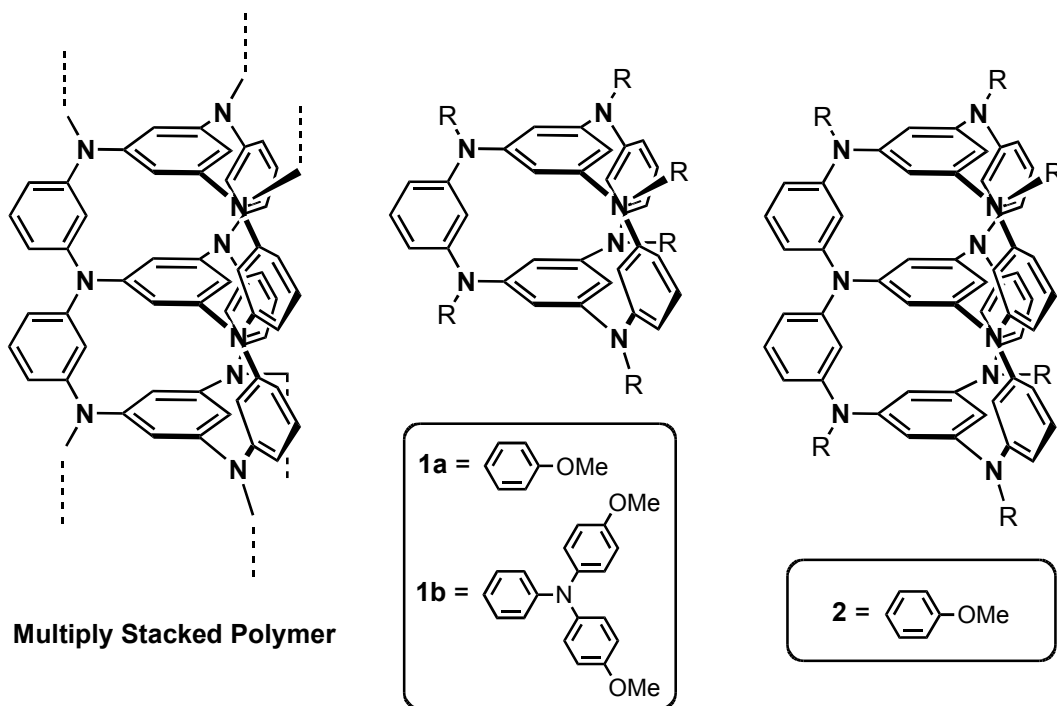# Synthesis and Properties of 1,3,5–Benzenetriamine Double– and Triple–Decker

5.1 Introduction

Triarylamine-based macromolecular system is widely accepted as an appropriate electroactive material for the study of electronic, magnetic, and optical properties, and in fact, oligoarylamines have been utilized as excellent hole-transport materials in photoconductors, light-emitting devices, and so forth.[1] This is mainly due to four factors: (i) low oxidation potentials, (ii) stability of generated radical cations, (iii) relatively small inner reorganization energy,[2] and finally, (iv) advances in palladium-catalyzed amination reactions,[3] which make it possible to synthesize structurally rigid and two-dimensionally expanded polymacrocyclic oligoarylamines.[4,5]

One-dimensional polyarylamines and their oligomers with *meta*-phenylene-linkage and/or alternating *meta-para*-phenylene-linkage in the polymer backbones can be considered as promising candidates for high-spin polymers.[6] However, in spite of various studies on polymers and/or oligomer model compounds, the generated spins in

the oxidized state have been unfortunately shown to be mainly uncoupled except for the existence of minor high-spin components,[7] probably because (i) unexpected defects owing to insufficient oxidation and (ii) interruption of π-conjugation between spin-containing and ferromagnetic coupling units owing to undefined conformations of the one-dimensional polymer chain hamper the robust ferromagnetic exchange coupling pathway through the polymer backbone. Contrary to polyarylamines with one-dimensional connectivity, the retention of high-spin alignment has been accomplished for oligoarylamines incorporating rigid macrocyclic architectures.[5,8]

Inspired by the extensive work on multilayered cyclophanes from Misumi's group,[9] cylindrical cage-structured polyarylamines with increased connectivity among macrocycles (Scheme 1) are potentially intriguing in order to prevent the above-mentioned obstacles.[10] The hypothetical polymer shown in Scheme 1 can be regarded as a 1,3,5-benzenetriamine multiple-decker linked by three *meta*-phenylenes, or in other words, a cofacially stacked benzenes connected by three poly(*m*-aniline) strands. In this chapter, we report the synthesis and characterization of the first double- and triple-decker arylamines **1** and **2** corresponding to dimer and trimer model compounds.[11]

Multiply Stacked Polymer

1a = [phenyl]–OMe

1b = [phenyl]–N with two [phenyl]–OMe groups (OMe at para positions)

2 = [phenyl]–OMe

Scheme 1. A hypothetical multiply stacked poly(arylamine) and 1,3,5-benzenetriamine double- and triple-decker **1a**, **1b**, and **2** as oligomer model compounds.

5.2 Experimental Section

General Methods: Commercial grade regents were used without further purification. Solvents were purified, dried, and degassed following standard procedures. Elemental analyses were performed by Center for Organic Elemental Microanalysis, Kyoto University. ^{1}H and ^{13}C NMR spectra were measured by a JEOL JNM-EX400 FT-NMR spectrometer. Chemical shifts of NMR spectra are determined relative to tetramethylsilane (TMS) internal standard.

   X-ray Crystallography for 1a and 2. Data collections were performed on a Rigaku RAXIS RAPID imaging plate area detector with graphite-monochromated Cu-Kα radiation at -180˚C for **1a** and on a Rigaku R-AXIS RAPID diffractmeter using filtered Cu-Kα radiation at -120˚C for **2**. The data were corrected for Lorentz and polarization effects. The structure was solved by using direct methods (SIR-2004[12] for **1a** and

SHELXL-97[13] for **2**), expanded by using Fourier techniques (DIRDIF-99[14]), and refined by full-matrix least-squares of F^2 on the basis of 10390 observed reflections for **1a** (8980 observed reflections for **2**) and 791 variable parameters (637 variable parameters for **2**) (SHELXL-97[13]). The non-hydrogen atoms were refined anisotropically for **1a**. Some non-hydrogen atoms were refined anisotropically, while the rest (on some of the THF molecules) were refined isotropically for **2**. Hydrogen atoms were refined by using the riding model. All the calculations were performed by using CrystalStructure crystallographic software package,[15] except for refinement, which was performed by using SHELXL-97. CCDC-879818 for **1a** and CCDC-879819 for **2** contain the supplementary crystallographic data for this chapter. These data can be obtained free of charge from the Cambridge Crystallographic Data Centre via www.ccdc.cam.ac.uk/data_request/cif.

Electrochemical Measurements. Cyclic voltammograms were recorded using an ALS/chi Electrochemical Analyzer Model 612A with a three-electrode cell using a Pt disk (2 mm^2) as the working electrode, a Pt wire as the counter electrode, and an Ag/0.01 M AgNO$_3$ (MeCN) as the reference electrode calibrated against ferrocene/ferrocenium (Fc/Fc$^+$) redox couple in a solution of 0.1 M tetrabutylammonium tetrafluoroborate as a supporting electrolyte (298 K, scan rate 100 mVs^{-1}).

ESR Measurements. The cw-ESR spectra were measured using a JEOL JES-SRE2X or a JEOL JES-TE200 X-band spectrometer in which temperatures were controlled by a JEOL ES-DVT2 variable-temperature unit or a JEOL ES-DVT3 variable-temperature unit, respectively.

Spectroelectrochemical Measurements. The UV-Vis-NIR spectra were measured with a Perkin Elmer Lambda 19 spectrometer. Spectroelectrochemical measurements were performed using an optically transparent thin-layer electrode quartz cell (light path length = 1 mm). The working and the counter electrodes were a Pt mesh and a Pt coil,

respectively. The reference electrode was an Ag wire. The potential was applied with an ALS/chi Electrochemical Analyzer Model 612A.

Pulsed ESR Measurements. Pulsed ESR measurements were carried out on a Bruker ELEXSYS E580 X-band FT ESR spectrometer, in which temperature was controlled by an Oxford ITC503 temperature controller combined with an Oxford ESR900 continuous-flow cryostat. The microwave pulse power of 10 mW provided by the microwave bridge was boosted to level of 1 kW using a traveling wave tube (TWT) amplifier. The ESTN measurements were performed by the three-pulse sequence shown below. The two-pulse ($\pi/2$ - π pulses) electron spin-echo signal $S(t_1)$ was detected by increasing the width (t_1) of the nutation pulse. We employed appropriate phase cycles in order to suppress undesirable signals and artifacts which arise from an inaccurate pulse length.[16,17] The observed signal $S(t_1, B)$ as a function of external magnetic field B is converted into a nutation frequency $S(\omega_{nut}, B)$ spectrum. The parameters used for the measurements were t_2 = 400 ns, t_3 = 8 ns. The signals observed at ca. 14 MHz in Figure 4 are due to the electron spin echo envelope modulation (ESEEM),[18] which results from weak interaction with proton nuclei (I = 1/2) originating from the solvent molecules surrounding the paramagnetic species.
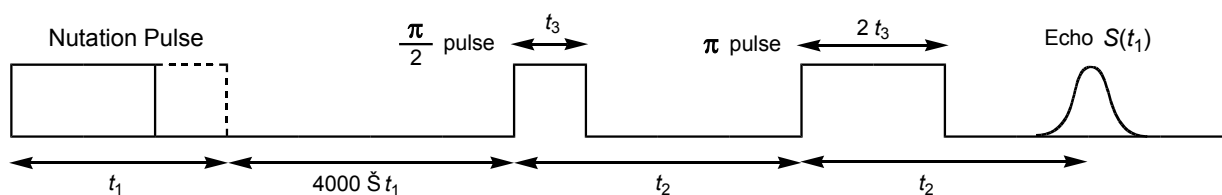
Synthetic Details.

***N,N',N''*-Tris(3-bromophenyl)-*N,N',N''*-tris(4-methoxyphenyl)-1,3,5-benzenetriamine** (**4**): A mixture of *m*-dibromobenzene (8.49 g, 36.0 mmol), *N,N',N''*-tris(4-anisyl)-1,3,5-benzenetriamine **3** (1.32 g, 3.0 mmol), Pd(OAc)$_2$ (0.03 g, 0.15 mmol), DPPF (0.17g, 0.30 mmol) and NaO*t*-Bu (1.14 g, 11.8 mmol) in toluene (30

ml) was refluxed under an argon atmosphere for 38 h. The resulting mixture was cooled down to room temperature and filtered through Celite. The filtrate was washed with brine and the organic layer was separated and dried over Na_2SO_4. After evaporation of the solvent, the crude product was chromatographed on silica gel (toluene as eluent) to afford **4** (1.25 g, 46.1%) as a white solid:^{1}HNMR(400MHz, tetrahydrofuran-d_8); δ = 3.737 (s, 9H), 6.310 (s, 3H), 6.825 (d, J = 9.03 Hz, 6H), 6.848-6.878 (m, 3H), 6.912-6.940 (m, 3H), 6.978-7.035 (m, 12H);^{13}C NMR (100 MHz, tetrahydrofuran-d_8) δ= 55.55, 113.28, 115.75, 121.04, 123.26, 124.84, 125.01, 128.46, 131.06, 140.00, 149.71, 150.15, 158.16; FABMS (*m*-nitrobenzyl alcohol) m/z calcd for $C_{45}H_{36}N_3O_3$ [M]$^+$ 906.50, found 906.

1,3,5-benzenetriamine double-decker (1a): Anhydrous toluene (400 mL) was added to $Pd(dba)_2$ (28.8 mg, 0.05 mmol), $Ph_5FcP(t\text{-}Bu)_2$ (71.8 mg, 0.10 mmol), and NaOt-Bu (0.3912 g, 4.07 mmol) in a flask equipped with a dropping funnel which was charged with a toluene solution (100 mL) of **3** (0.4427g, 1.00 mmol) and **4** (0.9077 g 1.00 mmol), and the toluene solution was stirred under an argon atmosphere at 110°C. The solution in the dropping funnel was gradually added into the solution containing the palladium catalyst for 28 h. The reaction mixture was refluxed for 20 h with stirring. The reaction solution was diluted with CH_2Cl_2 and filtered through Celite and washed with brine. The organic layer was separated and dried over Na_2SO_4. After evaporation of the solvent, the crude product was chromatographed on silica gel (toluene/ethyl acetate = 19:1 as eluent) to afford **1** (0.2556 g, 23.1%) as a white solid: ^{1}HNMR(400MHz, tetrahydrofuran-d_8); δ = 3.716 (s, 18H), 6.107 (t, J = 2.20 Hz, 3H), 6.295 (dd, J = 8.05, 2.20 Hz, 6H), 6.773 (d, J = 8.78 Hz, 12H), 6.812 (t, J = 8.05 Hz, 3H), 6.813 (s, 6H), 7.01 (d, J = 8.78 Hz, 12H); ^{13}C NMR (100 MHz, tetrahydrofuran-d_8) δ= 55.50, 110.67, 111.02, 115.23, 127.37, 127.44, 129.38, 141.05, 150.90, 151.69, 157.41; Anal calcd for $C_{72}H_{60}N_6O_6$ C, 78.24; H, 5.47; N, 7.60; O, 8.69; Found: C, 78.18; H, 5.68; N, 7.44; O, 8.85; FAB HRMS (*m*-nitrobenzyl alcohol) m/z

calcd for C72H60N6O6 [M]+ 1104.45688, found 1104.45703.

N,N',N"-tris(4-chlorophenyl)-1,3,5-benzenetriamine (**5**): A mixture of phloroglucinol (1.2684 g, 10.01 mmol), 4-chloroaniline (5.7677 g, 45.02 mmol), I_2 (0.1582 g, 0.62 mmol) in toluene (5 ml) was refluxed for 16 h. The reaction mixture was cooled down to room temperature and then the crude product was precipitated. The crude product was washed with methanol and collected by filtration to afford **5** (2.9407 g, 64.7%) as a purple solid: ^{1}HNMR (400MHz, acetone-d_6); δ = 6.442 (s, 3H), 7.121 (d, J = 8.78 Hz, 6H), 7.229 (d, J = 8.78, 6H), 7.459 (s, 3H); ^{13}C NMR (100 MHz, acetone-d_6) δ= 99.85, 119.64, 124.63, 129.64, 143.39, 145.78; FAB MS (*m*-nitrobenzyl alcohol) m/z calcd for C24H18N3Cl3 [M]+ 454.78, found 455.

N,N',N"-tris(tert-butoxycarbonyl)-N,N',N"-tris(4-chlorophenyl)-1,3,5-benzenetriamine (**6**): To a solution of di-tert-butyl dicarbonate (1.0 M) in THF (27.0 ml) was added **5** (2.7296 g, 6.0 mmol) and 4-dimethylaminopyridine (0.1454 g, 1.2 mmol), and the mixture was heated to reflux for 4 h with stirring. After cooling, evaporation of the solvent and recrystallization from ethyl acetate/*n*-hexane afforded pure **6** (3.818 g, 84.3 %) as white plates: ^{1}HNMR (400MHz, acetone-d_6); δ = 1.352 (s, 27H), 7.020 (s, 3H), 7.230 (d, J = 8.78, 6H), 7.341 (d, J = 8.78, 6H); ^{13}C NMR (100 MHz, acetone-d_6) δ= 28.56, 82.22, 124.68, 129.33, 129.82, 131.54, 142.94, 144.64, 153.63.

N,N',N"-tris[4-(di-4-anisylamino)phenyl]-1,3,5-benzenetriamine (**7**): A mixture of **6** (3.7552 g, 4.97 mmol), 4,4'-dimethoxydiphenylamine (5.0802 g, 22.16 mmol), Pd(dba)$_2$ (0.2875 g, 0.50 mmol), tri-*tert*-butylphosphine (0.0809g, 0.40 mmol) and NaO*t*-Bu (1.9255 g, 20.00 mmol) in toluene (50 ml) was refluxed under an argon atmosphere for 69 h. The resulting mixture was washed with brine and the organic layer was separated and dried over Na_2SO_4. After evaporation of the solvent, the crude product was chromatographed on silica gel with 19:1 toluene: ethyl acetate to afford **7** as a brown solid. The resulting BOC-protected **7** was dissolved in TFA (15 ml), and the

reaction mixture was stirred at room temperature for 20 min. After evaporation of TFA, dichloromethane was added to the residue, washed with a saturated aqueous solution of NaOH, and dried over Na_2SO_4. Evaporation of the solvent afforded **7** (3.021 g, 58.8%) as a green solid: ^{1}HNMR (400MHz, acetone-d_6); δ = 3.622 (s, 18H), 6.170 (s, 3H), 6.694-6.741 (m, 18H), 6.814 (d, J = 9.03 Hz, 12H), 6.921 (d, J = 9.03, 6H), 6.975 (s, 3H); ^{13}C NMR (100 MHz, acetone-d_8) δ= 55.63, 115.22, 120.42, 124.78, 125.54, 128.41, 139.11, 142.71, 146.86, 155.96; FABMS m/z (*m*-nitrobenzyl alcohol) calcd for $C66H60N6O6$ [M]$^+$ 1033.22, found 1033.

N,N',N''-tris(3-bromophenyl)-N,N',N''-tris[4-(di-4-anisylamino)phenyl]-1,3,5-benzenetriamine (8): A mixture of **7** (1.5530 g, 1.50 mmol), *m*-dibromobenzene (4.2464 g, 18.00 mmol), Pd(OAc)$_2$ (0.0165 g, 0.08 mmol), DPPF (0.0877g, 0.15 mmol) and NaO*t*-Bu (0.5770 g, 6.00 mmol) in toluene (7.5 ml) was refluxed under an argon atmosphere for 37 h. The reaction solution was diluted with CH_2Cl_2 and filtered through Celite and washed with brine. The organic layer was separated and dried over Na_2SO_4. After evaporation of the solvent, the crude product was chromatographed on silica gel with 19:1 toluene: ethyl acetate to afford **8** (1.5010 g, 66.8%) as a brown solid: ^{1}HNMR(400MHz, acetone-d_6); δ = 3.763 (s, 18H), 6.302 (s, 3H), 6.82-7.17 (m, 48H); ^{13}C NMR (100 MHz, acetone-d_6) δ = 55.64, 111.77, 115.48, 122.01, 122.04, 122.95, 125.27, 125.70, 127.17, 127.64, 131.38, 139.56, 141.43, 146.58, 149.43, 149.74, 156.83; FABMS m/z (*m*-nitrobenzyl alcohol) calcd for $C84H69Br3N6O6$ [M]$^+$ 1498.20, found1498.

1,3,5-benzenetriamine double-decker (1b): Anhydrous toluene (200 mL) was added to Pd(dba)$_2$ (20.3 mg, 0.035 mmol), Ph$_5$FcP(*t*-Bu)$_2$ (43.2 mg, 0.061 mmol), and NaO*t*-Bu (0.2348 g, 2.44 mmol) in a flask equipped with a dropping funnel which was charged with a toluene solution (100 mL) of **7** (0.6232 g, 0.60 mmol) and **8** (0.8989 g 0.60 mmol), and the toluene solution was stirred under an argon atmosphere at 110˚C. The solution in the dropping funnel was gradually added

into the solution containing the palladium catalyst for 17 h. The reaction mixture was refluxed for 44 h with stirring. The reaction solution was diluted with CH_2Cl_2 and filtered through Celite and washed with brine. The organic layer was separated and dried over Na_2SO_4. After evaporation of the solvent, the crude product was chromatographed on silica gel (toluene/ethyl acetate = 19:1 as eluent). The clued product was recrystallized from toluene-hexane to afford **1b** (0.1418 g, 10.3%) as a white solid: ^{1}HNMR(400MHz, tetrahydrofuran-d_8); δ = 3.697 (s, 36H), 6.010 (t, J = 2.20 Hz, 3H), 6.488 (dd, J = 2.20, 8.29 Hz, 6H), 6.746 (d, J = 9.03 Hz, 12H), 6.751 (d, J = 9.03 Hz, 24H), 6.865 (s, 6H), 6.886 (d, J = 9.03 Hz, 12H), 6.942 (d, J = 9.03 Hz, 24H); ^{13}C NMR (100 MHz, tetrahydrofuran-d_8) δ = 55.73, 112.27, 112.59, 115.53, 122.60, 125.94, 127.04, 128.57, 129.60, 141.41, 142.21, 145.64, 150.67, 151.72, 157.03; Anal calcd for $C_{152}H_{126}N_{12}O_{12}$ C, 78.72; H, 5.55; N, 7.34; O, 8.39; Found: C, 78.68; H, 5.58; N, 7.21; O, 8.57; MALDI HRMS (*m*-nitrobenzyl alcohol) m/z calcd for C150H126N12O12 [M]+ 2286.96127, found 2286.96143.

N,N',N"-tris(3-chlorophenyl)-1,3,5-benzenetriamine (**9**): A mixture of 1,3,5-trihydroxybenzene (1.2629 g, 10.01 mmol), 3-chloroaniline (5.7 g, 45 mmol), I_2 (0.1565 g, 0.60 mmol) in toluene (5 ml) was refluxed for 16 h. The resulting mixture was diluted with toluene and washed with brine. The organic layer was separated and dried over Na_2SO_4. After evaporation of the solvent, the crude product was chromatographed on silica gel with 19:1 toluene: ethyl acetate to afford **9** (3.2870 g, 72.3%) as dark-red oil: ^{1}HNMR(400MHz, acetone-d_6); δ = 6.544 (s, 3H), 6.815-6.842 (m, 3H), 7.056-7.084 (m, 3H), 7.136 (t, J = 2.20 Hz, 3H), 7.230 (t, J = 8.05 Hz, 3H), 7.589 (s, 3H); ^{13}C NMR (100 MHz, acetone-d_6) δ = 101.48, 116.23, 117.32, 120.21, 131.23, 135.06, 145.33, 146.16; FAB LRMS (*m*-nitrobenzyl alcohol) m/z calcd for C24H18N3Cl3 [M]+ 454.78, found 455.

N,N',N"-tris(3-bromophenyl)-N,N',N"-tris(3-chlorophenyl)-1,3,5-benzenetriamine (**10**): A mixture of **9** (3.1766 g, 6.98 mmol), *m*-dibromobenzene (5.19

g, 83.8 mmol), Pd(OAc)$_2$ (0.0791 g, 0.35 mmol), DPPF (0.4045g, 0.70 mmol) and NaOt-Bu (2.6831 g, 27.92 mmol) in toluene (35 ml) was refluxed under an argon atmosphere for 39 h. After cooling to room temperature, the reaction solution was washed with brine. The organic layer was separated and dried over Na$_2$SO$_4$. After evaporation of the solvent, the crude product was chromatographed on silica gel with 4:1 hexane: toluene to afford **10** (3.8269 g, 59.6%) as a white solid: ^{1}HNMR(400MHz, chloroform-d$_3$); δ = 6.323 (s, 3H), 6.893-6.970 (m, 12H), 7.079-7.182 (m, 12H); ^{13}C NMR (100 MHz, chloroform-d$_3$) δ = 114.35, 122.05, 122.56, 122.82, 123.59, 123.95, 126. 48, 126.84, 130.28, 130.56, 134.80, 147.48, 147.66, 148.37; FAB LRMS (*m*-nitrobenzyl alcohol) m/z calcd for C24H18N3Br3Cl3 [M]+ 919.75, found 919.

N,N,N',N',N",N"-hexakis[3-(4-anisylamino)phenyl]-1,3,5-benzenetriamine (**11**): A mixture of **10** (1.3864 g, 1.51 mmol), *p*-anisidine (1.6961 g, 13.77 mmol), Pd(dba)$_2$ (0.0878 g, 0.15 mmol), tri-*tert*-butylphosphine (0.30 mmol) and NaOt-Bu (1.7386 g, 18.09 mmol) in toluene (15 ml) was refluxed under an argon atmosphere for 19 h. After cooling to room temperature, the reaction solution was washed with brine. The organic layer was separated and dried over Na$_2$SO$_4$. After evaporation of the solvent, the crude product was chromatographed on silica gel with 7:1 toluene: ethyl acetate to afford **11** (1.5686 g, 79.6%) as a brown solid: ^{1}HNMR(400MHz, acetone-d$_6$); δ = 3.684 (s, 18H), 6.458 (dd, J = 8.05, 1.95 Hz, 6H), 6.493 (s, 3H), 6.544 (dd, J = 8.05, 1.95 Hz, 6H), 6.715 (t, J = 2.20 Hz, 6H), 6.780 (d, J = 9.03 Hz, 12H), 7.003 (d, J = 9.03 Hz, 12H), 7.005 (t, J = 8.05 Hz, 6H), 7.032 (s, 6H); ^{13}C NMR (100 MHz, acetone-d$_6$) δ = 55. 58, 110.58, 111.96, 113.95, 115.12, 115.55, 121.52, 130.32, 136.86, 146.79, 148.92, 149.31, 155.32; FAB MS (*m*-nitrobenzyl alcohol) m/z calcd for C84H75N9O6 [M]+ 1306.55, found 1306.

1,3,5-benzenetriamine triple-decker (**3**): A mixture of **11** (0.6553 g, 0.50 mmol), 1,3,5-tribromobenzene (0.3168 g, 1.01 mmol), Pd(dba)$_2$ (44.2 mg, 0.08 mmol),

tri-*tert*-butylphosphine (0.15 mmol) and NaO*t*-Bu (0.4325 g, 4.5 mmol) in toluene (200 ml) was refluxed under an argon atmosphere for 19 h. After cooling to room temperature, the reaction solution was washed with brine. The organic layer was separated and dried over Na_2SO_4. After evaporation of the solvent, the crude product was chromatographed on silica gel with 19:1 toluene: ethyl acetate to afford **3** (47.9 mg, 6.6%) as a white solid; ^{1}HNMR(400MHz, tetrahydrofuran-d_8); δ = 3.691 (s, 18H), 5.872 (t, J = 1.95 Hz, 6H), 6.504-6.530 (m, 6H), 6.727 (d, J = 9.03 Hz, 12H), 6.831 (s, 6H), 6.864 (s, 3H), 6.928 (d, J = 9.03 Hz, 12H), 6.972 (t, J = 7.81 Hz, 6H), 7.010-7.049 (m, 6H); ^{13}C NMR (100 MHz, tetrahydrofuran-d_8) δ = 55.68, 112.20, 114.28, 115.29, 116.50, 125.28, 129.54, 129.56, 132.88, 141.82, 148.32, 150.95, 151.56, 151.97, 156.75; FAB HRMS (*m*-nitrobenzyl alcohol) m/z calcd for $C96H75N9O6$ [M]+ 1449.58403, found 1449.58386.

5.3 Results and Discussion

5.3.1 Synthesis

1,3,5-benzenetriamine double- and triple-decker **1** and **2** were successfully obtained by repeatedly using Buchwald-Hartwig cross-coupling reaction[3] (Scheme 2). In the synthesis of **1a** (and **1b**), the substituted benzenetriamines **3** (or **7**) and the corresponding tribromides **4** (and **8**) were coupled in a one-pot manner to make the cylindrical cage-structure. On the other hand, the triple-decker **2** was prepared by the cross-coupling reaction between a dendritic oligoarylamine with six preorganized reaction points (**11**) and two equivalent of 1,3,5-tribromobenzene.

Compounds **1a** and **2** have anisyl groups at all *N*-positions in order to lower the oxidation potentials, and moreover, in **1b**, dianisylaminophenyl groups are attached at all *N*-positions in order to stabilize the oxidized state.[19]
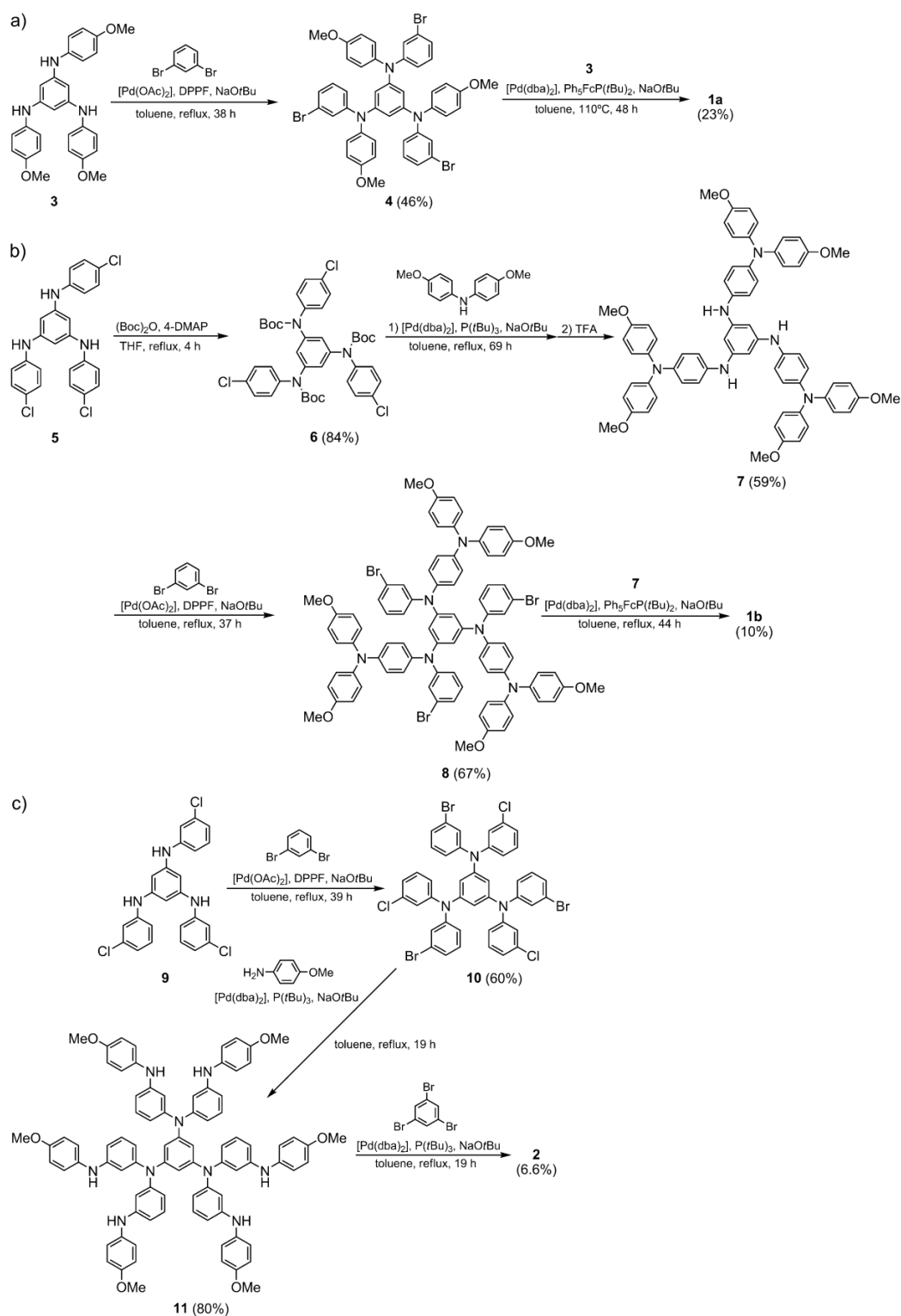
Scheme 2. Synthetic routes for **1a**, **1b**, and **2**. DPPF = 1,1'-bis(diphenylphosphanyl)ferrocene, dba = *trans*, *trans*-debenzylideneacetone, Boc = *tert*-butoxycarbonyl, 4-DMAP = 4-dimethylaminopyridine, TFA = trifluoroacetic acid.

5.3.2 X-ray Structural Analysis of 1a and 2

Colorless blocklike (**1a**) and platelike (**2**) single crystals were grown by slow evaporation of a dilute mixed solution (CH_3OH/CH_2Cl_2 for **1a**; THF/*n*-hexane for **2**) and their molecular structures (CCDC 879818 for **1a** and CCDC 879819 for **2**) were unequivocally determined by X-ray crystallography (Figure 1 and Table 1). As shown in Figure 1a, **1a** adopted a C_3-symmetrical double-decker structure, where the two benzene rings as the decks were cofacially separated by 4.77 Å, and the dihedral angles between the cofacial 1,3,5-benzenetriamine planes and pillar-like three *meta*-phenylene planes were around 76˚~80˚, thus demonstrating that the two cofacial benzene moieties were not totally eclipsed but slightly twisted with each other (ca. 30˚). On the other hand, while **2** also took a C_3-symmetrical triple-decker structure, distances between the cofacial benzene rings were estimated to be slightly longer than that of **1a** (4.84 Å), and moreover, the *meta*-phenylene pillars were nearly perpendicular to the 1,3,5-benzenetriamine planes. As a consequence, the three cofacial benzene moieties were confirmed to be nearly eclipsed with each other (Figure 1b).
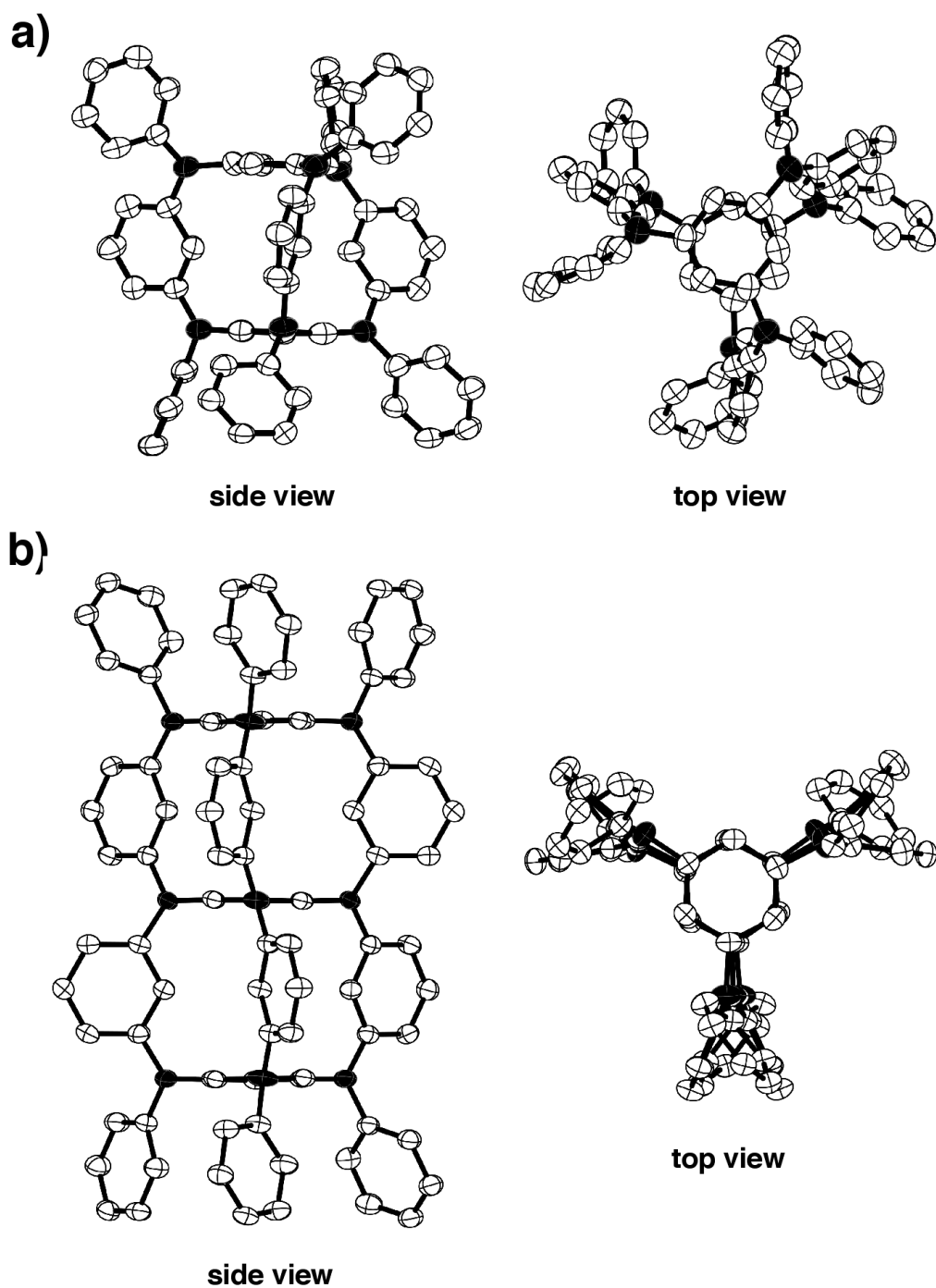
Figure 1. Thermal ellipsoid (50%) plots of a) **1a** and b) **2**. Crystallization solvent molecules, methoxy groups, and hydrogen atoms are omitted for clarity. Nitrogen atoms are colored in black.

**Table 1:** X-ray crystallographic data for **1a** and **2**.

empirical formula	$C_{73}H_{62}Cl_2N_6O_6$	$C_{120}H_{123}N_9O_{12}$
	[**1a**•(CH_2Cl_2)]	[**2**•(THF)$_6$]
formula weight	1190.24	1883.34
T [˚C]	−180±1	−120±1
λ [Å]	1.54187	1.54187
crystal system	triclinic	orthorhombic
space group	$P\bar{1}$ (#2)	Pbcn (#60)
Z	2	4
a [Å]	14.1584(4)	38.205(3)
b [Å]	14.2385(4)	10.0150(1)
c [Å]	18.0545(7)	25.8144(4)
α [˚]	69.4873(14)	——
β [˚]	69.5953(14)	——
γ [˚]	61.6781(12)	——
V [Å^3]	2926.51(15)	9877.0(8)
ρ_{calcd} [g cm^{-3}]	1.351	1.266
μ [cm^{-1}]	15.006	6.519
collected data	54082	174142
unique data / R_{int}	10490/0.094	9030/0.0426
no. of parameters	791	637
goodness-of-fit[a]	1.123	1.092
R1 ($I > 2\sigma$), wR2 (all reflections)[b]	0.1016, 0.3226	0.0696, 0.2176
residual density [e Å^{-3}]	0.59/-0.83	1.17/-0.58

[a] GOF = $\left\{ \sum \left[w \left(F_0^2 - F_c^2 \right)^2 \right] \Big/ (n-p) \right\}^{1/2}$, where n and p denote the number of data and parameters.

[b] R1 $= \sum \left(\|F_0\| - \|F_c\| \right) / \sum \|F_0\|$ and   wR2 $= \left\{ \sum \left[w \left(F_0^2 - F_c^2 \right)^2 \right] \Big/ \sum \left[w \left(F_0^2 \right)^2 \right] \right\}^{1/2}$ where
$w = 1 \Big/ \left[\sigma^2 \left(F_0^2 \right) + \left(a \cdot P \right)^2 + b \cdot P \right]$ and $P = \left[\left(\text{Max}; 0, F_0^2 \right) + 2 \cdot F_c^2 \right] \Big/ 3$.

5.3.3 DFT calculations

To gain insight into the electronic structures of **1a** and **2**, we carried out the density functional theory (DFT) calculations (at the B3LYP/6-31G* level) on the model molecules **1a**' and **2**',[13] where all the methoxy groups are omitted. The optimized structures were in good agreement with the X-ray structures. As shown in Figure S1, the frontier MOs comprised of HOMO and (HO-1)MO were virtually triply-degenerate for **1a**' (and quasi-triply-degenerate for **2**'). Moreover, those frontier MOs for **1a**' and **2**' were found to be distributed mainly over the three *meta*-phenylenediamine linkers, and therefore, the present double- and triple-decker molecules can be viewed as three oligo(*meta*-aniline) moieties are linked via 1,3,5-benzentriyl decks (Figure 2).
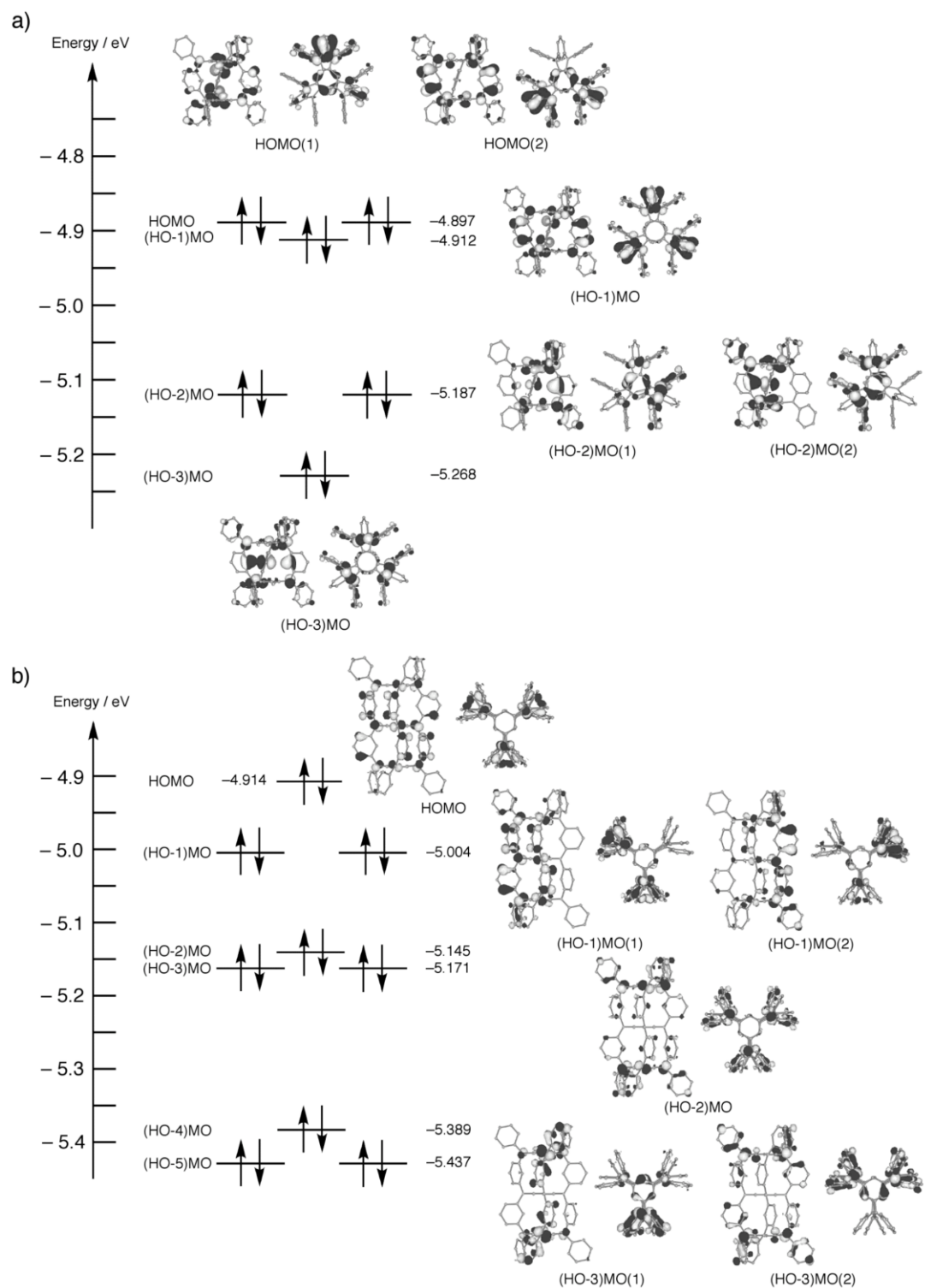
Figure 2. Kohn-Sham MOs and their orbital energy diagrams for a) 1**a**' and b) **2**' (B3LYP/6-31G*).

5.3.4 Electrochemistry

The redox behavior of **1a** and **2** were measured by cyclic voltammetry (CV) in CH_2Cl_2 (0.1M tetra-*n*-butylammonium tetrafluoroborate (nBu$_4$NBF$_4$)) at room temperature. Upon multi-sweep oxidation, both of the peak current and the peak potential increased with repetitive potential cycling for **1a** and **2** (Figure 3). This clearly indicates the electrochemical polymerization on the electrode surface owing to the instability of the oxidized species, though the detailed mechanism remains unclear. After 10 cycles, two discrete oxidation waves were observed at approximately 0.35 and 0.67 V vs. $Fc^{0/+}$ for the triple-decker **2**, while single oxidation wave observed at 0.67 V vs. $Fc^{0/+}$ for double-decker **1a**. In contrast, the introduction of dianisylaminophenyl groups at all the *N*-positions of **1a** resulted in the recovery of reversible multi-redox behavior, probably due to the existence of six *para*-phenylene diamine (PD) moieties as redox centers. As shown in Figure 4, the redox behavior of **1b** can be roughly estimated to be comprised of first two-electron, second four-electron, and third six-electron transfer processes, which means double-decker **1b** is oxidizable up to dodecacation. From the simulation of the observed differential pulse voltammogram (DPV),[14] the first and second oxidation processes of **1b** correspond to the generation of dication (quasi-two-electron transfer: −0.12 (1e) and −0.06 (1e)) and hexacation (quasi-four-electron transfer: +0.03 (4e)), respectively, and the third oxidation process can be judged to be quasi-six-electron transfer (+0.44 (1e), +0.49 (1e), +0.51 (1e), +0.56 (1e), +0.60 (1e), and +0.61 (1e)). Hence, these findings suggest that di(radical cation) and hexa(radical cation) of **1b** can be generated by using appropriate oxidizing agents.

136
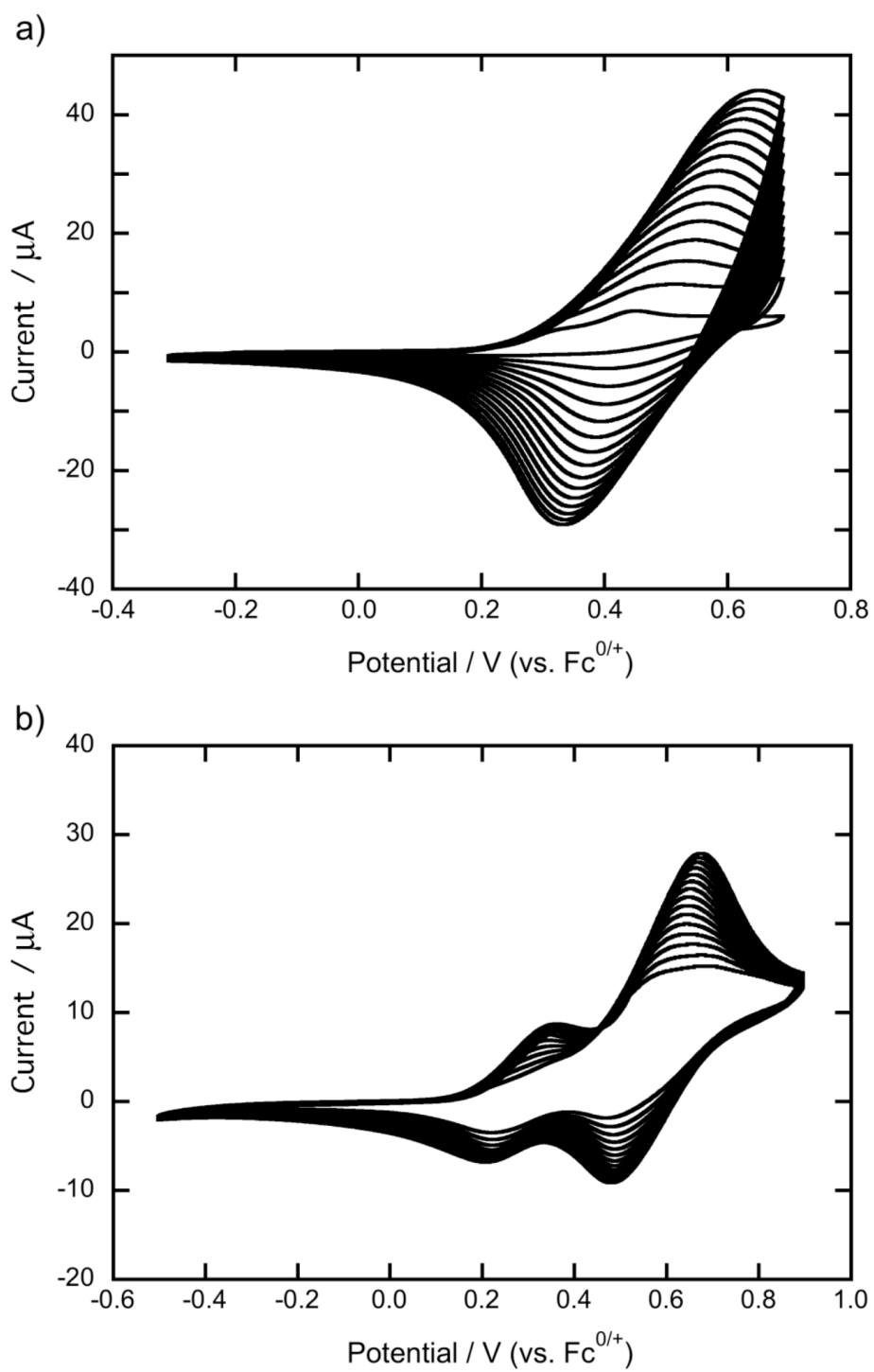
Figure 3. Multi-sweep CV of a) **1a** and b) **2** in 0.1 M CH_2Cl_2/TBABF$_4$ at 298 K (scan rate 100 mV s^{-1}).
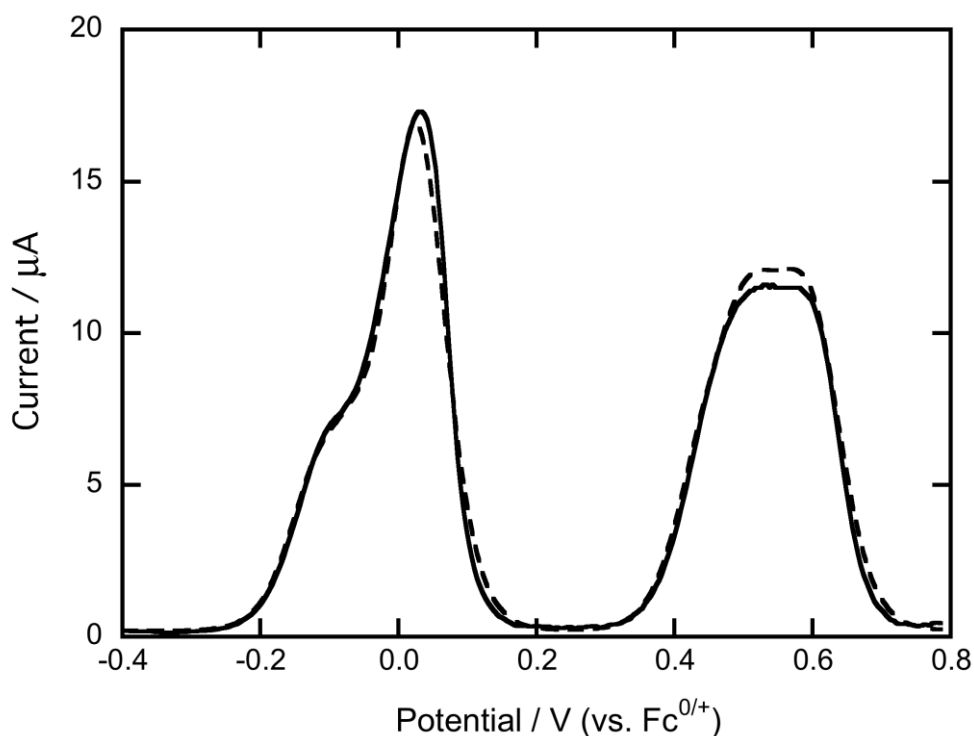
Figure 4. Differential pulse voltammogram (DPV) of **1b** in CH_2Cl_2 (0.1M nBu_4NBF_4) measured with a Pt electrode (surface area: 2 mm^2) at a sweep rate of 0.02 V s^{-1} at 298 K. The broken line indicates the simulated DPV (see text).

5.3.5 Spectroelectrochemistry

In conjunction with the fact that the same dianisylaminophenyl groups are substituted at all the *N*-positions, the optical absorption spectral changes of **1b** in CH_2Cl_2 during the course of the oxidation process were similar with those of the previously studied tetraaza[1_4]metacyclophane[19] (Figure 5). As shown in Figure 5a, a π–π* band with the λ_{max} of 333 nm in the neutral **1b** was changed into three new bands corresponding to the oxidized species from **1b**$^+$ to **1b**$^{2+}$ (λ_{max} = 415, ~600, ~1000 nm) with an isosbestic point at 366 nm. The observed lowest energy band (λ_{max} = ~1000 nm) can be considered as the charge resonance (CR) intervalence band (IV) band due to the the semi-quinone radical cation of *para*-phenylenediamine (PD) moiety,[15] and slightly shifted

138

hypsochromically with increasing oxidation number, whereas the next lowest energy band (λ_{max} = ~600 nm) exhibited a slight bathochromic shift. Further oxidation of $1b^{2+}$ showed continuous increase in absorbance for the CR IV band, with a slight hypsochromic shift (λ_{max} = 920 nm), and the intensity reached up to thrice that of $1b^{2+}$, strongly indicating that $1b^{6+}$ was formed by oxidation of all the PD moieties of $1b$ (Figure 5b). Note that the fact that the decrease in intensity observed in lower energy region of the CR IV band with an isosbestic point at 1113 nm (see inset of Figure 5b), on going from $1b^{2+}$ to $1b^{6+}$, demonstrated the existence of the charge transfer between the neutral and oxidized PD moieties via the *meta*-phenylene and 1,3,5-benzenetriyl linkers, as have been often observed in the mixed valence compounds with *meta*-phenylene and/or 1,3,5-benzenetriyl coupling units.[22c,23] Finally, the intense CR IV band decreased rapidly, when $1b^{6+}$ is further oxidized, and two new bands with the λ_{max} of 524 and 723 nm grew with some isosbestic points (345, 450, and 796 nm), corresponding to a conversion from the semi-quinoidal PD to the quinoidal PD (Figure 5c).

a)
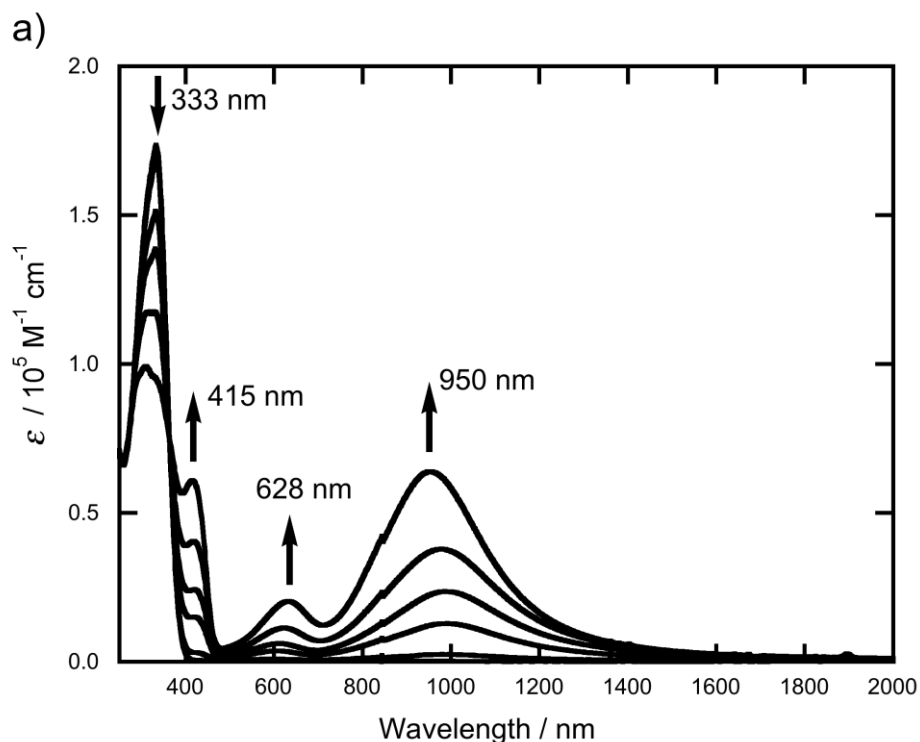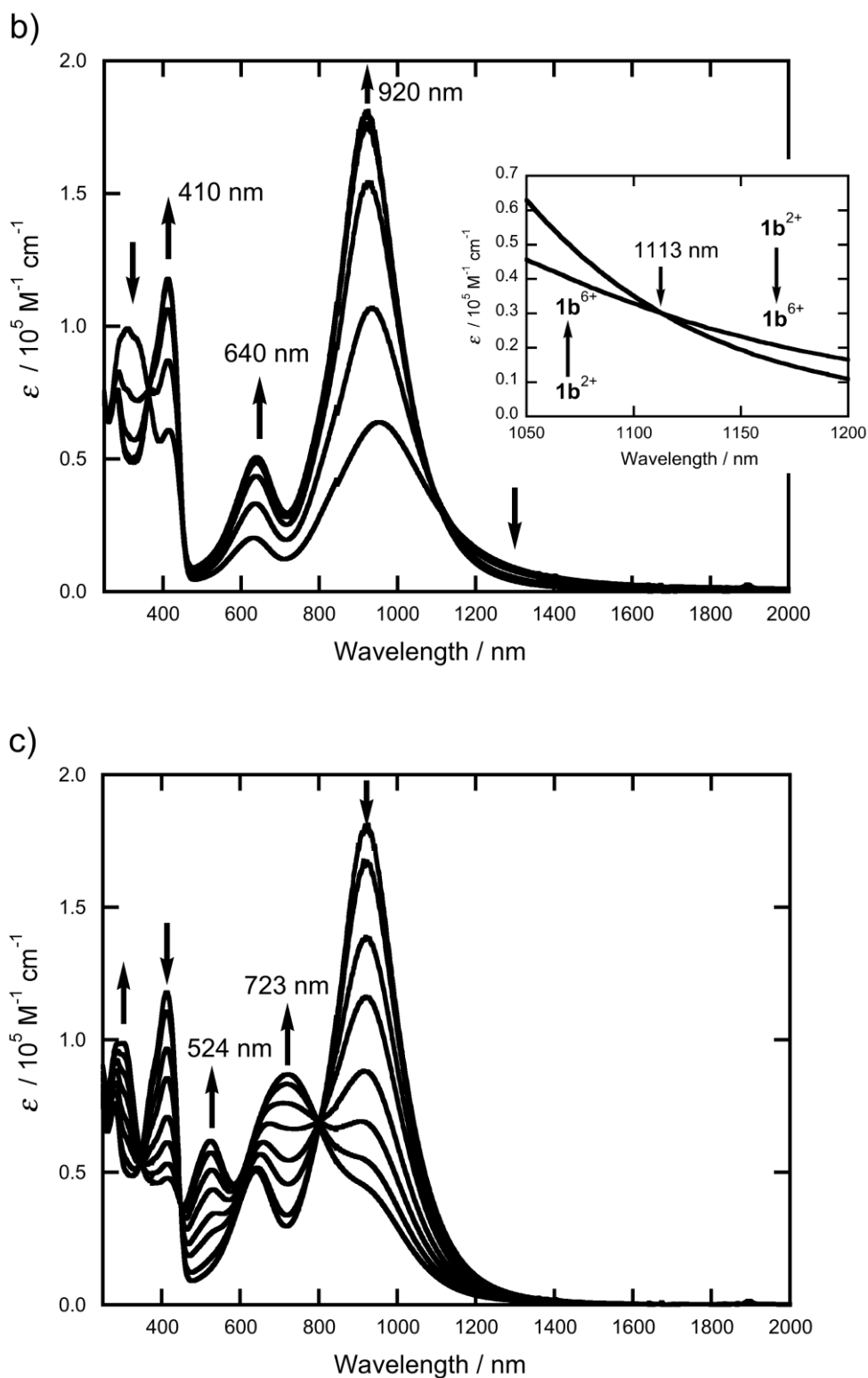
**Figure 5.** UV-vis-NIR absorption spectra of the stepwise electrochemical oxidation of **1b** in CH$_2$Cl$_2$ (0.1 M /nBu$_4$NBF$_4$) at 298 K: a) **1b** to **1b^{2+}**; b) **1b^{2+}** to **1b^{6+}**; c) further oxidation process from **1b^{6+}**.

5.3.6 ESR Spectroscopy

The reversibility of the multi-stage oxidation processes prompted us to determine the spin multiplicity of the polycationic species of **1b**. We have measured the electron spin transient nutation (ESTN) spectra based on the pulsed ESR spectroscopy[24] for the oxidized samples in a rigid glass of CH_2Cl_2 at 5K. The stepwise chemical oxidation were carried out by adding 2 and 6 molar equivalents of tris(4-bromophenyl)aminium hexachloroantimonate (Magic Blue)[25] at 195 K. As shown in Figure 6a and Table 2, the nutation frequency of 24.4 MHz observed after addition of 2 molar equiv. of oxidant can be assigned to the spin-triplet state of $1b^{2+}$, judging from the nutation frequency due to the spin-doublet impurity. This result is in good accordance with the DFT results that two electrons are removed from the degenerate HOMOs (Figure 2). On the other hand, after oxidation of **1b** with 6 molar equiv. of oxidant, two kinds of new signals at 19.5 and 22.6 MHz were detected in addition to those for the impurities with the spin-doublet (11.0 MHz) and spin-triplet (16.6 MHz) multiplicities (Figure 6b), and consequently, these nutation signals were assignable to the spin-allowed transition for the spin-quartet state from the frequency ratio. Hence, this result suggests that **1b** treated with 6 equiv. of oxidant is in spin-quartet state. However, the electronic structure of this high-spin state remains obscure at the present stage, and further examination is needed for elucidation of electronic structure for hexacation of **1b**.
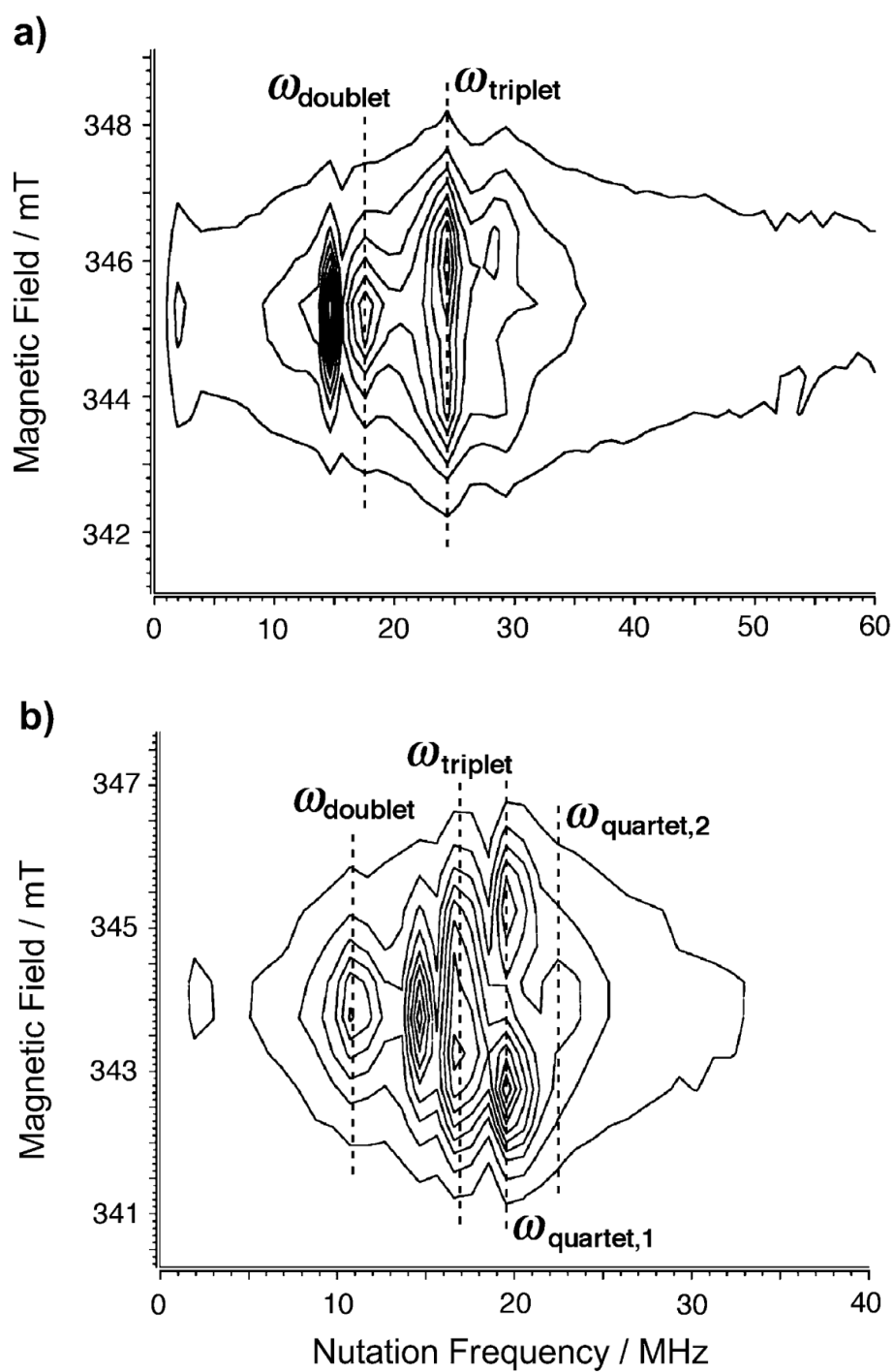
Figure 6. 2D ESTN spectra of **1a** in CH_2Cl_2 at 5K after the addition of a) 2 equiv. and b) 6 equiv. of oxidant.

Table 2: Spectral data of the ESTN spectroscopy for $\mathbf{1b}^{2+}$ and $\mathbf{1b}^{6+}$.

Species	Observed nutation frequency [MHz][a]	Transition assignment
$\mathbf{1b}^{2+}$	24.4 ($\omega_t = \sqrt{2}\omega_d$)	$\lvert 1, \pm 1\rangle \Leftrightarrow \lvert 1, 0\rangle$
(doublet impurity)	17.8 (ω_d)	$\lvert 1/2, +1/2\rangle \Leftrightarrow \lvert 1/2, -1/2\rangle)$
$\mathbf{1b}^{6+}$	19.5 ($\omega_{q,1} = \sqrt{3}\omega_d$)	$\lvert 3/2, \pm 3/2\rangle \Leftrightarrow \lvert 3/2, \pm 1/2\rangle$
	22.6 ($\omega_{q,2} = 2\omega_d$)	$\lvert 3/2, +1/2\rangle \Leftrightarrow \lvert 3/2, -1/2\rangle$
(triplet impurity)	16.6 ($\omega_t = \sqrt{2}\omega_d$)	$\lvert 1, \pm 1\rangle \Leftrightarrow \lvert 1, 0\rangle$
(doublet impurity)	11.0 (ω_d)	$\lvert 1/2, +1/2\rangle \Leftrightarrow \lvert 1/2, -1/2\rangle$

[a] d = doublet, t = triplet, q = quartet.

5.4 Conclusion

In summary, we have succeeded in preparation and characterization of the 1,3,5-benzenetriamine double- and triple-decker, which are the first examples of layered oligoarylamines stacked cofacially through multiple arene linkers. Furthermore, *N*-dianisylaminophenyl-group-substituted double-decker **1b** revealed reversible multi-redox activity, and consequently, the polycationic species, which are generated by treatment of 2 and 6 equiv. of oxidant, were found to be in high-spin state, as is reflected in the highly degenerate frontier MOs. Understanding of the electronic structures of the polycationic species of the present compounds and the further attempts to create the related derivatives, which leads to the robuster high-spin polycationic species, currently being pursued in the context of exploitation of spin-polarized molecular wires.

References and Notes

[1] a) Y. Shirota, *J. Mater. Chem.* **2000**, *10*, 1; b) M. Thelakkat, *Macromol. Mater. Eng.* **2002**, *287*, 442; c) Y. Shirota, H. Kageyama, *Chem. Rev.* **2007**, *107*, 953.

[2] a) B. C. Lin, C. P. Cheng, Z. P. M. Lao, *J. Phys. Chem. A* **2003**, *107*, 5241; b) A. Heckmann, C. Lambert, *Angew. Chem. Int. Ed.* **2012**, *51*, 326.

[3] a) J. P. Wolfe, S. Wagaw, J. F. Marcoux, S. L. Buchwald, *Acc. Chem. Res.* **1998**, *31*, 805; b) J. F. Hartwig, *Acc. Chem. Res.* **1998**, *31*, 852; c) J. F. Hartwig, *Angew. Chem. Int.*

Ed. **1998**, *37*, 2046; d) A. R. Muci, S. L. Buchwald, *Top. Curr. Chem*. **2002**, *219*, 133.

[4] X. Z. Yan, J. Pawlas, T. Goodson, III, J. F. Hartwig, *J. Am. Chem. Soc*. **2005**, *127*, 9105.

[5] a) A. Ito, Y. Yamagishi, K. Fukui, S. Inoue, Y. Hirao, K. Furukawa, T. Kato, K. Tanaka, *Chem. Commun*. **2008**, 6573; b) A. Ito, K. Tanaka, *Pure. Appl. Chem*. **2010**, *82*, 979.

[6] K. Yoshizawa, R. Hoffmann, *Chem. Eur. J*. **1995**, *1*, 403.

[7] a) K. Yoshizawa, K. Tanaka, T. Yamabe, *Chem. Lett*. **1990**, 1331; b) A. Ito, K. Ota, K. Tanaka, T. Yamabe, K. Yoshizawa, Macromolecules 1995, 28, 5618; c) I. Kulszewicz-Bajer, J. Gosk, M. Pawłowski, S. Gambarelli, D. Djurado , A. Twardowski, *J. Phys. Chem. B* **2007**, *111*, 9421; d) A. Ito, D. Sakamaki, H. Ino, A. Taniguchi, Y. Hirao, K. Tanaka, K. Kanemoto, T. Kato, *Eur. J. Org. Chem*. **2009**, 4441.

[8] D. Sakamaki, A. Ito, K. Furukawa, T. Kato, K. Tanaka, *Chem. Commun*. **2009**, 4524.

[9] S. Misumi, T. Otsubo, *Acc. Chem. Res*. **1978**, 11, 251.

[10] a) A. Rajca, *Chem. Rev*. **1994**, *94*, 871; b) A. Rajca, *Chem. Eur. J*. **2002**, *8*, 4835.

[11] Although two aromatic amines are tethered by alkyl linkers, there exists a few reports on the related compounds: a) J. J. Wolff, A. Zietsch, H. Irngartinger, T. Oeser, *Angew. Chem. Int. Ed*. **1997**, *36*, 621; b) J. J. Wolff, U. Seibold, T. Oeser, *Chem. Commun*. **2000**, 89.

[12] M. C. Burla, R. Caliandro, M. Camalli, B. Carrozzini, G. L. Cascarano, L. De Caro, C. Giacovazzo, G. Polidori, R. Spagna, *J. Appl. Cryst*. **2005**, *38*, 381.

[13] The DIRDIF-99 Program System, Technical Report of the Crystallography Laboratory, P. T. Beurskens, G. Admiraal, G. Beurskens, W. P. Bosman, R. de Gelder, R. Israel, J. M. M. Smits, University of Nijmegen (The Netherlands), **1999**.

[14] Program for Crystal Structure Solution and Refinement, G. M. Sheldrick, Universität Göttingen, **1997**.

[15] CrystalStructure 3.8, Crystal Structure Analysis Package, Rigaku and Rigaku

Americas (2000–2007). 9009 New Trails Dr. The Woodlands TX 77381 USA.

[16] J.-M. Fauth, A. Schweiger, L. Braunschweiger, J. Forrer, R. R. Ernst, *J. Magn. Res.* **1986**, *66*, 74.

[17] C. Gemperle, G. Aebli, A. Schweiger, R. R. Ernst, *J. Magn. Res.* **1990**, *88*, 241.

[18] W. B. Mims, *Phys. Rev. B* **1972**, *5*, 2409.

[19] A. Ito, S. Inoue, Y. Hirao, K. Furukawa, T. Kato, K. Tanaka, *Chem. Commun.* **2008**, 3242.

[20] The full geometry optimizations of **1a**' and **2**' in C_3 symmetry were carried out by using Gaussian 09 progaram package: Gaussian 09 (Revision C.01), M. J. Frisch et al.

[21] W. Huang, T. L. E. Henderson, A. M. Bond, K. B. Oldham, *Anal. Chim. Acta* **1995**, *304*, 1.

[22] a) A. Ishitani, S. Nagakura, *Mol. Phys.* **1967**, *12*,1; b) B. Badger, B. Brocklehurst, R. D. Russell, *Chem. Phys. Lett.* **1967**, *1*, 122; c) A. V. Szeghalmi, M. Erdmann, V. Engel, M. Schmitt, S. Amthor, V. Kriegisch, G. Nöll, R. Stahl, C. Lambert, D. Leusser, D. Stalke, M. Zabel, J. Popp, *J. Am. Chem. Soc.* **2004**, *126*, 7834; d) Y. Hirao, A. Ito, K. Tanaka, *J. Phys. Chem. A* **2007**, *111*, 2951; e) A. Ito, D. Sakamaki, Y. Ichikawa, K. Tanaka, *Chem. Mater.* **2011**, *23*, 841.

[23] J. Bonvoisin, J.-P. Launay, W. Verbouwe, M. van der Auweraer, F. C. de Schryver, *J. Phys. Chem.* **1996**, *100*, 17079; b) M. M. Wienk, R. A. J. Janssen, *J. Am. Chem. Soc.* **1997**, *119*, 4492.

[24] a) J. Isoya, H. Kanda, J. R. Norris, J. Tang, M. K. Brown, *Phys. Rev. B*. **1990**, *41*, 3905; b) A. V. Astashkin, A. Schweiger, *Chem. Phys. Lett.* **1990**, *174*, 595.

[25] N. G. Connelly, W. E. Geiger, *Chem. Rev.* **1996**, *96*, 877.

Chapter 6

A Triphenylamine Double-Decker: From Delocalized Radical Cation to Di(radical cation) with Excited Triplet State

6.1 Introduction

Triphenylaminium radical cations are well-known for their remarkable stability and, in addition, the oxidation potential is adjustable by the introduction of a series of substituents, in particular, at the *para*-positions. Thus, they are widely used not only as one-electron oxidative reagents but also as catalysts in organic chemistry.[1] Besides such an application to versatile chemical reagents, the ambient stable radical cations generated from triphenylamine (TPA) derivatives could be utilized as spin sources in molecule-based magnetic materials. In fact, a considerable number of TPA-based molecular multi-spin systems have appeared in the literature. However, from the viewpoint of assemblage of the spin sources into the architecture of the reported molecular systems, the spin-spin exchange coupling pathway has been confined to one- and two-dimensionalities,[2] and accordingly, the TPA-based multi-spin systems with

147

three-dimensional (3D) connectivity are rare.

In 1985, Neugebauer and coworkers reported the first synthesis of a TPA double-decker **1** (Scheme 1),[3] in which two TPA moieties are directly connected by threefold *o,o'-* linkage, in association with an interest in intramolecular interaction between two nitrogen lone pairs.[4] In spite of its sensitivity to oxidation and the formation of persistent radical cation, no detailed information was available concerning the electronic structure. Such a cage-like oligo(triphenylamine) can be regarded as a potent building block to afford the opportunity furnishing new TPA-based macromolecular systems with genuine 3D connectivity. Although neither the parent **1** nor its derivatives have appeared in the literature,[5] an analog **2**, in which two TPA moieties are connected at *para*-positions of all phenyl groups by three *meta*-phenylene-diamine pillars, was prepared in our laboratory. In this chapter, the synthesis and the electronic properties of this new TPA derivative **2** will be reported in detail.
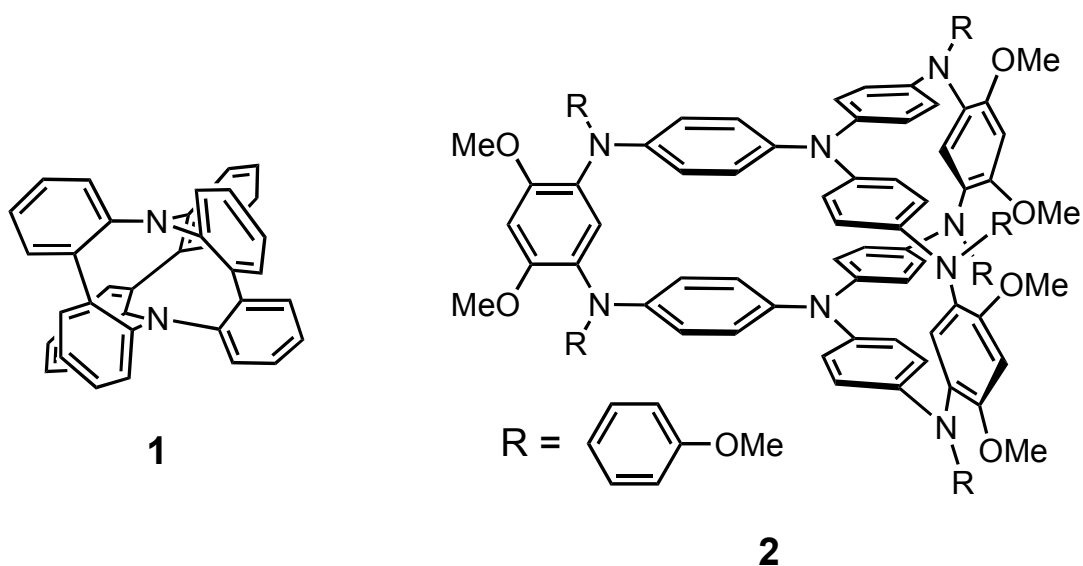
Scheme 1. First reported TPA double-decker **1**[3] and *meta*-phenylenediamine-bridged TPA double-decker **2**.

6.2 Experimental Section

General Methods: Commercial grade regents were used without further purification. Solvents were purified, dried, and degassed following standard procedures. Elemental analyses were performed by Center for Organic Elemental Microanalysis, Kyoto University. ^{1}H and ^{13}C NMR spectra were measured by a JEOL JNM-EX400 FT-NMR spectrometer. Chemical shifts of NMR spectra are determined relative to tetramethylsilane (TMS) internal standard.

X-ray Crystallography for 2. Data collections were performed on a Rigaku VariMax RAPID imaging plate area detector with Cu-Kα radiation at 25˚C. The data were corrected for Lorentz and polarization effects. The structure was solved by using direct methods (SIR-2002[6], expanded by using Fourier techniques (DIRDIF-99[7]), and refined by full-matrix least-squares of F^2 on the basis of 19674 observed reflections and 1141 variable parameters (SHELXL-97[8]). The non-hydrogen atoms were refined anisotropically. Hydrogen atoms were refined by using the riding model. The crystal contains dichloromethane, one of the components of the mixed solvents. The observed NMR spectrum showed that one dichrolomethane molecule per four triphenylamine double-decker molecules was contained in the crystal. Thus, we assumed that the ratio of the solvent occupancy is 0.25. Although the density was calculated to be 0.989 on this assumption, we infer that some parts of the solvent molecules have been lost in air. All the calculations were performed by using CrystalStructure crystallographic software package,[9] except for refinement, which was performed by using SHELXL-97. CCDC-879827 contains the supplementary crystallographic data for this analysis. The data can be obtained free of charge from the Cambridge Crystallographic Data Centre via www.ccdc.cam.ac.uk/data_request/cif.

Electrochemical Measurements. Cyclic voltammograms were recorded using an ALS/chi Electrochemical Analyzer Model 612A with a three-electrode cell using a Pt disk (2 mm^2) as the working electrode, a Pt wire as the counter electrode, and an

Ag/0.01 M AgNO$_3$ (MeCN) as the reference electrode calibrated against ferrocene/ferrocenium (Fc/Fc$^+$) redox couple in a solution of 0.1 M tetrabutylammonium tetrafluoroborate as a supporting electrolyte (298 K, scan rate 100 mVs^{-1}).

ESR Measurements. The cw-ESR spectra were measured using a JEOL JES-SRE2X or a JEOL JES-TE200 X-band spectrometer in which temperatures were controlled by a JEOL ES-DVT2 variable-temperature unit or a JEOL ES-DVT3 variable-temperature unit, respectively. The UV-Vis-NIR spectra were measured with a Perkin Elmer Lambda 19 spectrometer.

Spectroelectrochemical Measurements. Spectroelectrochemical measurements were performed using an optically transparent thin-layer electrode quartz cell (light path length = 1 mm). The working and the counter electrodes were a Pt mesh and a Pt coil, respectively. The reference electrode was an Ag wire. The potential was applied with an ALS/chi Electrochemical Analyzer Model 612A.

Synthetic Details. *N,N'*–dianisyl–4,6–dimethoxy–1,3–phenylenediamine: 1,3–dibromo–4,6–dimethoxy–benzene (1.486 g, 5.020 mmol), *p*–anisidine (1.844 g, 14.98 mmol), NaO*t*Bu (1.530 g, 15.92 mmol), Pd(OAc)$_2$ (113.0 mg, 0.503 mmol), and 1,1'–bis(diphenylphosphanyl)ferrocene (DPPF) (555.3 mg, 1.001 mmol) were dissolved in toluene (12.5 ml) under an argon atmosphere. The resulting solution was refluxed for 3.5 h with stirring. The reaction mixture was washed with saturated aqueous NaCl, and the organic layer was dried (Na$_2$SO$_4$), filtered, and concentrated. The residue was purified on silica gel (1:9 ethyl acetate–toluene), and then recrystallized from ethyl acetate to afford 1.61 g (84.2%) of **2** as red needles: ^{1}H NMR (400 MHz, C$_6$D$_6$) δ 7.436 (s, 1H), 6.932 (d, *J* = 8.8 Hz, 4H), 6.663 (d, *J* = 8.8 Hz, 4H), 6.468 (s, 1H), 5.765 (s, 2H), 3.422 (s, 6H), 3.269 (s, 6H); ^{13}C NMR (100 MHz, acetone–*d$_6$*) δ 154.66, 143.79, 138.66, 128.26, 120.01, 115.12, 106.61, 100.05, 56.88, 55.63, Anal. Calcd for C$_{22}$H$_{24}$N$_2$O$_4$: C, 69.46; H, 6.36; N, 7.36; O, 16.82. Found: C, 69.52; H, 6.30; N, 7.33; O,

17.07.

Triphenylamine double-decker (2): A mixture of Pd(dba)$_2$ (0.432 g, 0.750 mmol) and tri-*tert*-butylphosphine (0.061, 0.60 mmol) in toluene (160 ml) was stirred under an argon atmosphere at room temperature for 5 min. The resulting solution containing palladium catalyst was added via a syringe to a mixture of **2** (1.140 g, 2.99 mmol), tris(4–bromophenyl)amine (0.965 g, 2.00 mmol), and NaO*t*Bu (0.961 g, 10.0 mmol) in a reaction flask under an argon atmosphere, and the reaction mixture was stirred at room temperature for 50 h. The reaction mixture was washed with saturated aqueous NaCl, and the organic layer was dried (Na$_2$SO$_4$), filtered, and concentrated. The residue was purified on silica gel (47:3 toluene–ethyl acetate), and then recrystallized from ethyl acetate to afford 0.131 g (8.1%) of **1** as a pale yellow solid: ^{1}H NMR (400 MHz, C$_4$D$_8$O) δ 7.12 (m, 3+24H), 6.78 (d, J = 8.0 Hz, 12H), 6.60 (s+d, J = 8.0 Hz, 3+12H), 3.72 (s, 18H), 3.52 (s, 18H), Anal. Calcd for C$_{102}$H$_{90}$N$_8$O$_{12}$: C, 75.63; H, 5.60; N, 6.92; O, 11.85. Found: C, 75.68; H, 5.74; N, 6.69; O, 11.76; FAB HRMS (*m*–nitrobenzyl alcohol) *m/z* (relative intensity %) calcd for C$_{102}$H$_{90}$N$_8$O$_{12}$ (M$^+$) 1618.6678, obsd 1618.6626 (88.8).

6.3 Results and Discussion

6.3.1 Synthesis

TPA double-decker **2** was prepared by using Buchwald-Hartwig cross-coupling reaction[10] between tris(4-bromophenyl)amine as a deck and meta-phenylenediamine as a pillar in a ratio of 2:3 (Scheme 2).
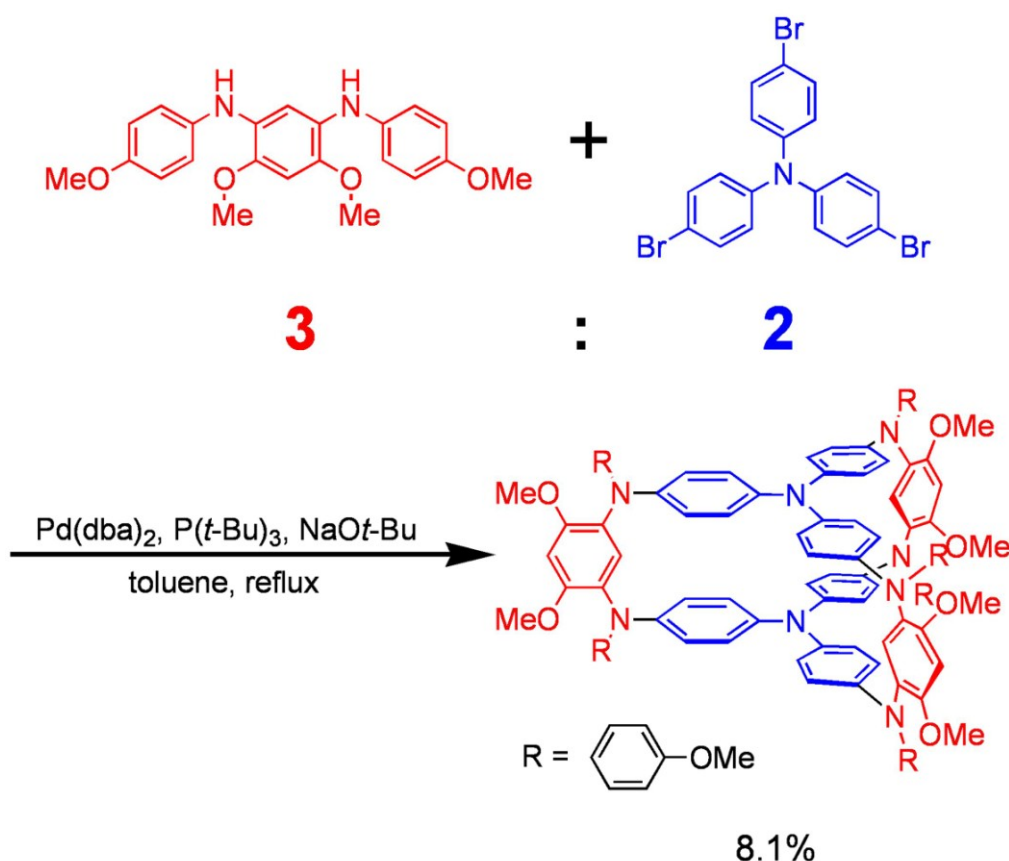

Scheme 2. Synthesis of triphenylamine double-decker.

6.3.2 X-ray Structural Analysis

Slow evaporation of a dilute mixed solution (CH_3OH and CH_2Cl_2) of a pale yellow product **2** gave yellow block crystals suitable for X-ray structure analysis (CCDC 879827). The crystal belongs to the space group $P2_1$ containing two molecules of **2** per unit cell, in which there exist three sites for CH_2Cl_2 molecules so as to fill spaces

between the double-deckers (Table 1).

The X-ray structure of **2** has almost C_{3h} symmetrical trichetria-like[11] shape, when all the methoxy substituents are ignored, and the upper and lower TPA decks adopt almost planar propeller-like conformation (the tilted angles of phenyl rings range from 42˚ to 53˚), and moreover, are totally eclipsed (Figure 1). Three *meta*-phenylenediamine planes are perpendicular to the TPA planes, and therefore, the distance between two TPA decks are estimated to be about 4.9 Å at the peripheral three nitrogen pairs and 5.8 Å at the central nitrogen pair, indicating the direct transannular π-π interaction between two TPA decks is virtually ignorable. The sp^2 planes of the nitrogen atoms are found to be at angles of about 60˚ to the adjacent *meta*-phenylene planes.

top view   side view
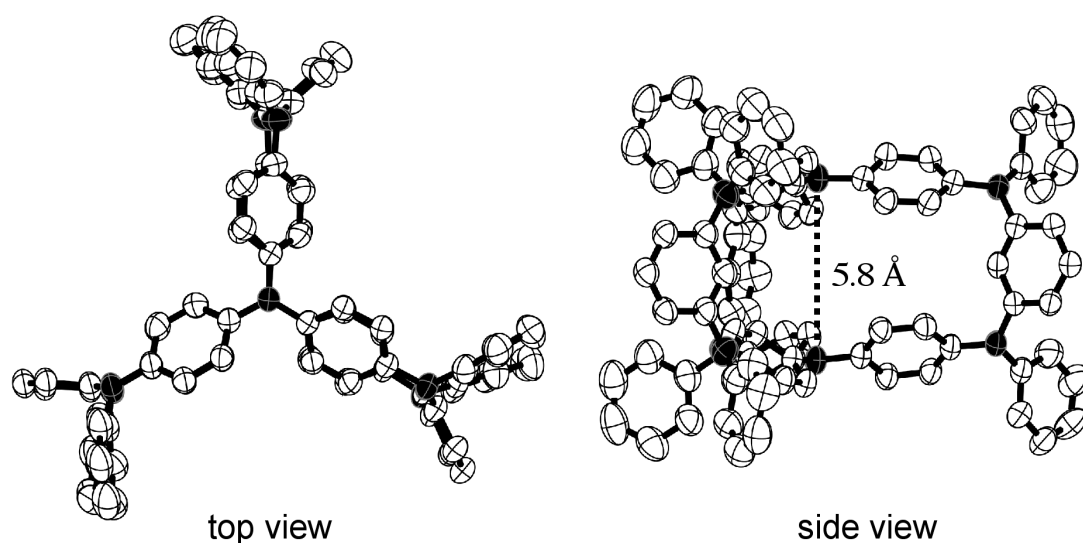
Figure 1. Thermal ellipsoid (50%) plots of **2**. Crystallization solvent molecule, methoxy groups, and hydrogen atoms are omitted for clarity. Nitrogen atoms are colored in black.

153

Table 1: X-ray crystallographic data for **2**.

empirical formula	$C_{102.25}H_{90.50}Cl_{0.50}N_8O_{12}$
	[**2**•$(CH_2Cl_2)_{0.25}$]
formula weight	1641.11
$T\,[°C]$	25±1
$\lambda\,[\text{Å}]$	1.54187
crystal system	monoclinic
space group	$P2_1$ (#4)
Z	2
$a\,[\text{Å}]$	17.3547(6)
$b\,[\text{Å}]$	20.2751(7)
$c\,[\text{Å}]$	17.6429(7)
$\beta\,[°]$	117.4215(14)
$V\,[\text{Å}^3]$	5510.5 (4)
$\rho_{calcd}\,[\text{g cm}^{-3}]$	0.989
$\mu\,[\text{cm}^{-1}]$	6.325
collected data	65009
unique data / R_{int}	19674/0.036
no. of parameters	1141
goodness-of-fit[a]	1.125
$R1$ ($I > 2\sigma$), $wR2$ (all reflections)[b]	0.0683, 0.2076
residual density [e Å^{-3}]	0.57/-0.38

[a] GOF = $\left\{\left[\sum\left[w\left(F_0^2 - F_c^2\right)^2\right]\right]/(n-p)\right\}^{1/2}$, where n and p denote the number of data and parameters.

[b] R1 = $\sum\left(\|F_0\| - \|F_c\|\right)/\sum\|F_0\|$ and wR2 = $\left\{\left[\sum\left[w\left(F_0^2 - F_c^2\right)^2\right]\right]/\sum\left[w\left(F_0^2\right)^2\right]\right\}^{1/2}$ where

$w = 1/\left[\sigma^2\left(F_0^2\right) + \left(a \cdot P\right)^2 + b \cdot P\right]$ and $P = \left[\left(\text{Max}; 0, F_0^2\right) + 2 \cdot F_c^2\right]/3$.

6.3.3 DFT calculations

In accordance with the X-ray structure, DFT calculations (the B3LYP/6-31G* level of theory) also demonstrated that the C_{3h}-symmetric structure was adopted for a model compound **2'**, in which all the methoxy groups are replaced by hydrogen atoms. As is apparent from the HOMO (Figure 2a), the spin density distribution in **2'⁺** revealed delocalization over the entire molecule (Figure 2b). Although the C_{3h} symmetric structure is retained on going from **2'** to **2'⁴⁺**, the quinoid-type deformation in TPA decks was predicted to be remarkable with increase in the degree of oxidation (Table 2).

Table 2: Optimized bond lengths (in Å) at the (U)B3LYP/6-31G* level of theory for **2'**, **2'⁺**, **2'²⁺**, and **2'⁴⁺**.

	2'	**2'⁺**	**2'²⁺**	**2'⁴⁺**
d_1	1.423	1.418	1.414	1.407
d_2	1.404	1.407	1.410	1.416
d_3	1.390	1.386	1.382	1.377
d_4	1.404	1.409	1.415	1.423
d_5	1.405	1.409	1.415	1.423
d_6	1.391	1.388	1.384	1.379
d_7	1.405	1.407	1.410	1.416
d_8	1.421	1.409	1.395	1.382

155

a)

HOMO

top view   side view

(HO-1)MO

top view   side view

b)

top view   side view
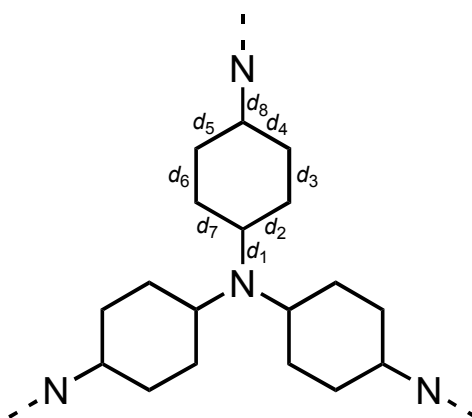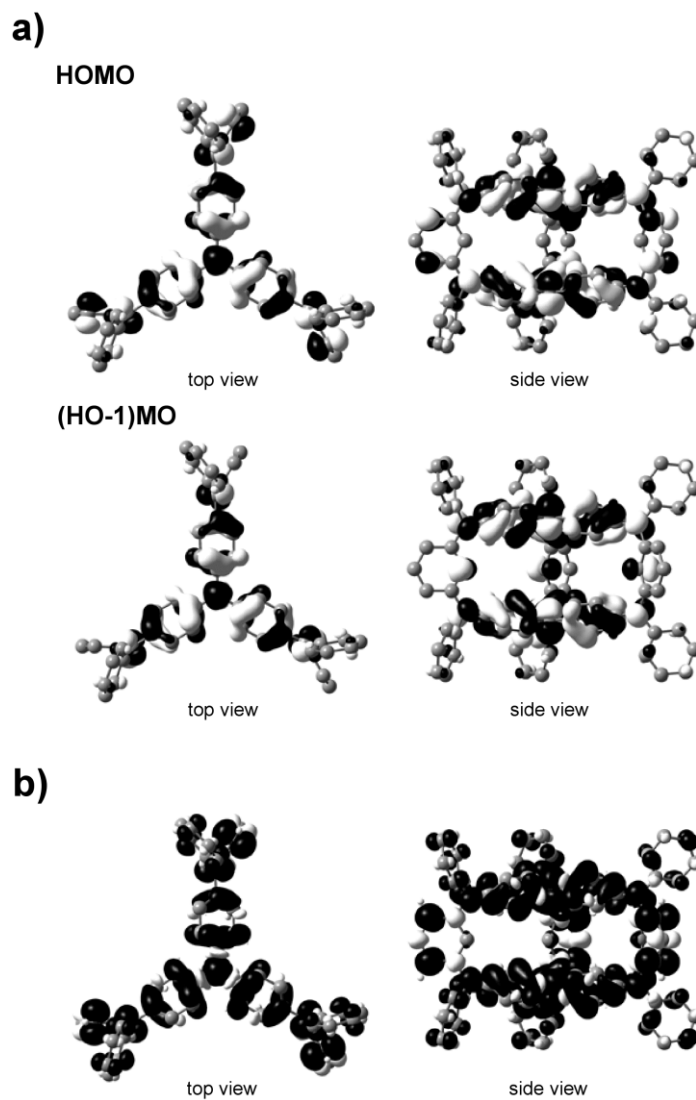
Figure 2. a) HOMO and (HO-1)MO (B3LYP/6-31G*) of **2'** and b) the spin density distribution (black: positive spin, white: negative spin; spin isosurface value = 0.0003 electron au^{-3}) of **2'$^{+}$**.

6.3.4 Electrochemistry

Double-decker **2** exhibited multi-redox behavior due to contribution from the eight TPA redox centers. The observed five oxidation waves are chemically reversible, and the oxidation potentials [E_{ox}^{n} vs. Fc$^{0/+}$ (ne)] are determined to be E_{ox}^{1} = –0.33 V (1e), E_{ox}^{2} =

–0.16 V (1e), $E_{ox}^3 = +0.09$ V (2e), $E_{ox}^4 = +0.46$ V (1e), and $E_{ox}^5 = +0.61$ V (1e), on the basis of cyclic voltammetry (CV) and differential pulse voltammetry (DPV) (Figure 3). It should be noted that, although *meta*-phenylene-linkage is included in connectivity of **2**, the first oxidation potential of $E_{ox}^1 = -0.33$ V is more negative than that of the related all-*para*-phenylene-linked TPA oligomers: hexaaza[1_6]paracyclophane ($E_{ox}^1 = -0.28$ V)[12] and the second generation of dendritic triphenylamines ($E_{ox}^1 = -0.30$ V).[13] More interestingly, the splitting of redox potentials ($E_{ox}^2 - E_{ox}^1 = 170$ mV) indicates a relatively strong electronic coupling between two TPA decks, irrespective of *meta*-phenylene-linkage, and therefore, the intervalence state between the two redox-active TPA decks is expected to appear in radical cation of **2**, as has been elaborately been investigated for TPA-based organic mixed-valence compounds.[14] This is also supported by comparison with the first oxidation potential ($E_{ox}^1 = -0.16$ V (1e)) for the related compound **3**[13] corresponding to a single TPA deck. In addition, two charged radical centers generated via the second oxidation process of **2** are located separately on the upper and lower TPA decks to alleviate the energetically unfavorable Coulombic repulsion, and as a consequence, magnetic interaction takes place between the two-spin system.
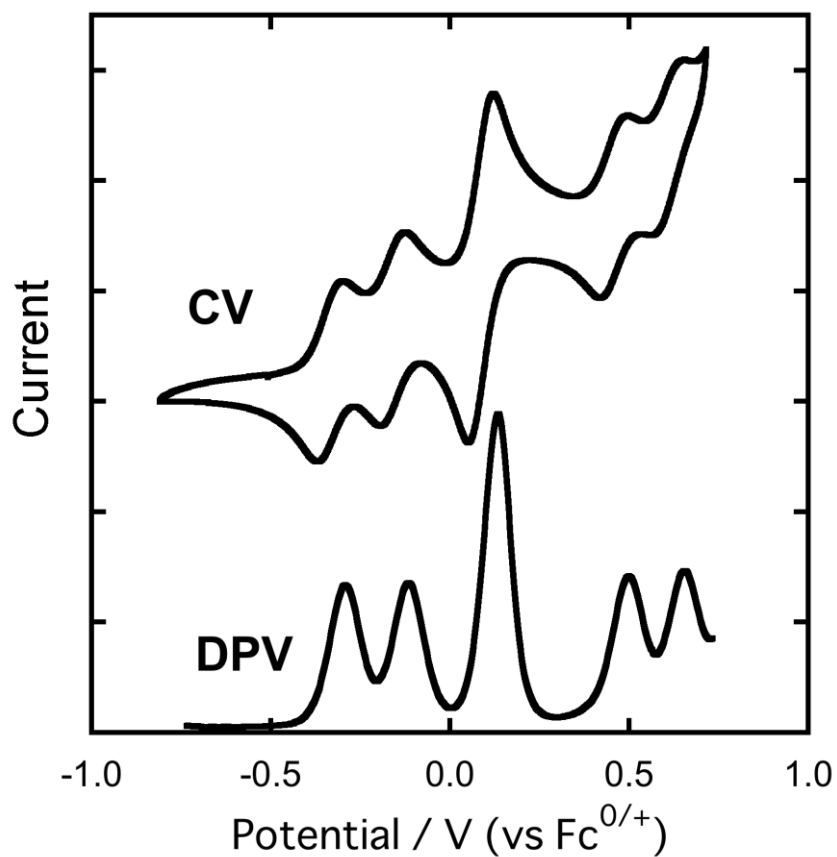
Figure 3. Cyclic voltammogram (CV) and differential pulse voltammogram (DPV) of **2**, measured in CH_2Cl_2 containing 0.1 M nBu$_4$NBF$_4$ at 298 K (scan rate 100 mV^{-1}).

**Scheme 3.** Related compound **3**.

3
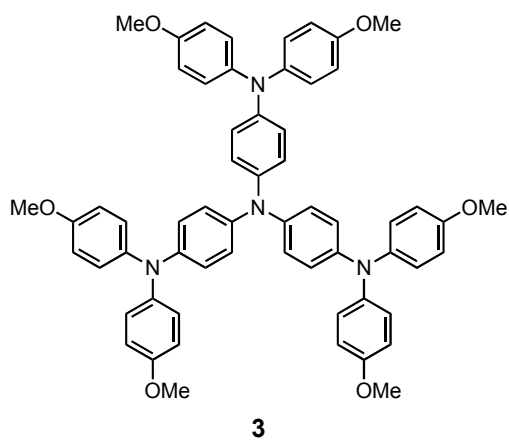
6.3.5 Spectroelectrochemistry

On the basis of the electrochemical studies, we measured the optical absorption spectral change of double-decker **2** in CH_2Cl_2 during the course of the oxidation going from neutral to tetracation $\mathbf{2}^{4+}$ by using optically transparent thin-layer electrochemical cell (Figure 4). To gain insights into the charge distribution of the oxidized double-decker, let us here concentrate on the spectral change in the lowest energy transitions of $\mathbf{2}^{+}$ to $\mathbf{2}^{4+}$ (Figure 5). The lowest energy band at 1332 nm (0.93 eV) observed for $\mathbf{2}^{+}$ is blue-shifted to 1190 nm (1.04 eV), when oxidized into $\mathbf{2}^{2+}$, and the shifted band becomes twice as intense as that for $\mathbf{2}^{+}$. Further oxidation to $\mathbf{2}^{4+}$ resulted in a far more intense band with a further blue-shift (1053 nm (1.18 eV)).[15] For comparison, the spectroelectrochemical measurements were also performed for the reference compound **3** (Figure 6).[13] As a consequent, the observed spectrum for $\mathbf{3}^{+}$ was found to be in good accordance with that for $\mathbf{2}^{2+}$. This result strongly suggests that two charged radical centers in $\mathbf{2}^{2+}$ are located separately on the upper and lower TPA decks. In addition, both spectra observed for $\mathbf{2}^{4+}$ and $\mathbf{3}^{2+}$ were obviously similar although the maximum wavelength for the lowest energy band for $\mathbf{2}^{2+}$ remained unchanged (1190 nm (1.04 eV)). Excitation energies for the oxidized species, $\mathbf{2'}^{+}$, $\mathbf{2'}^{2+}$, and $\mathbf{2'}^{4+}$, were estimated by the time-dependent DFT (TD-DFT) calculations[16] (Figure 7 and Table 3). As shown in Figure 4, the characteristics of the observed spectral change are reasonably reproduced by the theoretical results for the model compound **2'**. Recently, Kaupp and co-workers pointed out the fact that the frequently used B3LYP hybrid functional may lead to erroneous results in organic mixed-valence compounds.[17] Hence, in addition to the B3LYP calculations, we have also performed the DFT optimizations and TD-DFT calculations for $\mathbf{2'}^{+}$, $\mathbf{2'}^{2+}$, and $\mathbf{2'}^{4+}$ by using the B1LYP hybrid functional with 35% exact exchange and the SVP basis sets,[18] as has been recommended by Kaupp and co-workers.[17] In addition, solvents effects have been included by the CPCM polarizable conductor calculation model for CH_2Cl_2 ($\varepsilon = 8.93$).[19] These calculations

resulted in the same trend as B3LYP ones, although the transition energies showed small blue-shifts (Figure 5, Table 4). Therefore, the present TD-DFT calculations strongly suggest that the charged species of 2^+ to 2^{4+} are in delocalized intervalence states. In particular, the lowest energy band for 2^+ is assignable to a transition from doubly degenerate β ((HO-1)MOs) to β (LUMO), which corresponds to the charge resonance between the *meta*-phenylenediamine moieties as pillars and the core TPA decks. Moreover, the intervalence band observed for 2^+ exhibited no noticeable solvatochromism in CH_2Cl_2 (ε = 8.93) and benzonitrile (ε = 25.59), supporting a charge-delocalized character for 2^+ (Figure 8).
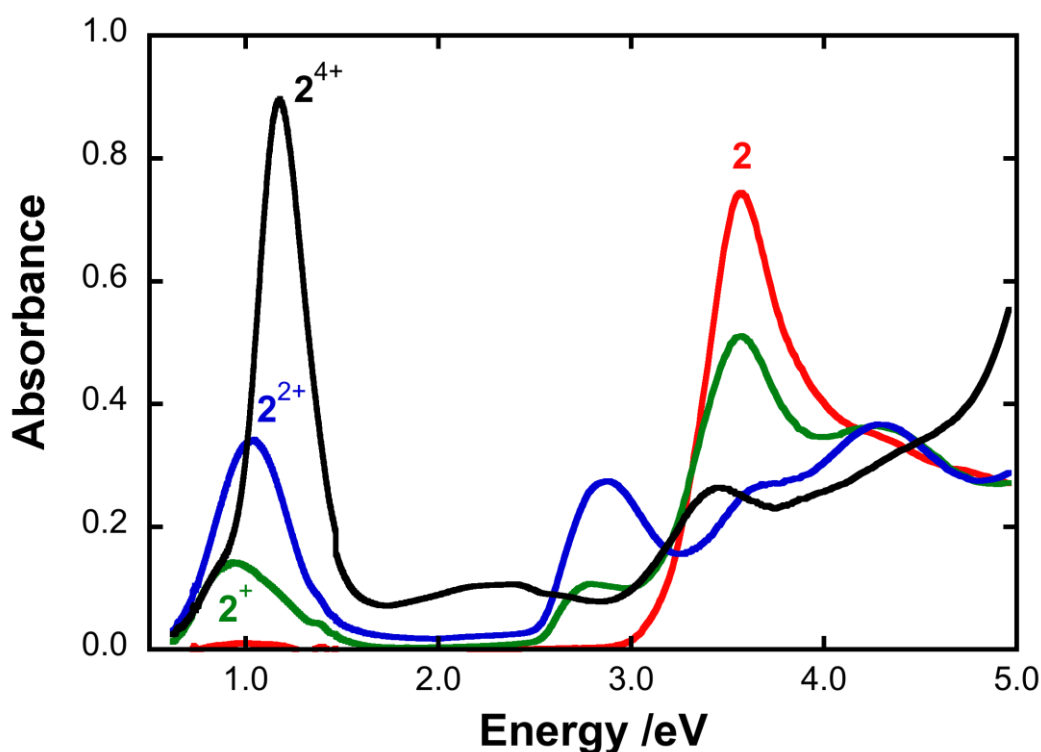
**Figure 4.** UV-Vis-NIR absorption spectra in the stepwise electrochemical oxidation of **2** in 0.1 M CH_2Cl_2/nBu$_4$NBF$_4$ at 298 K.
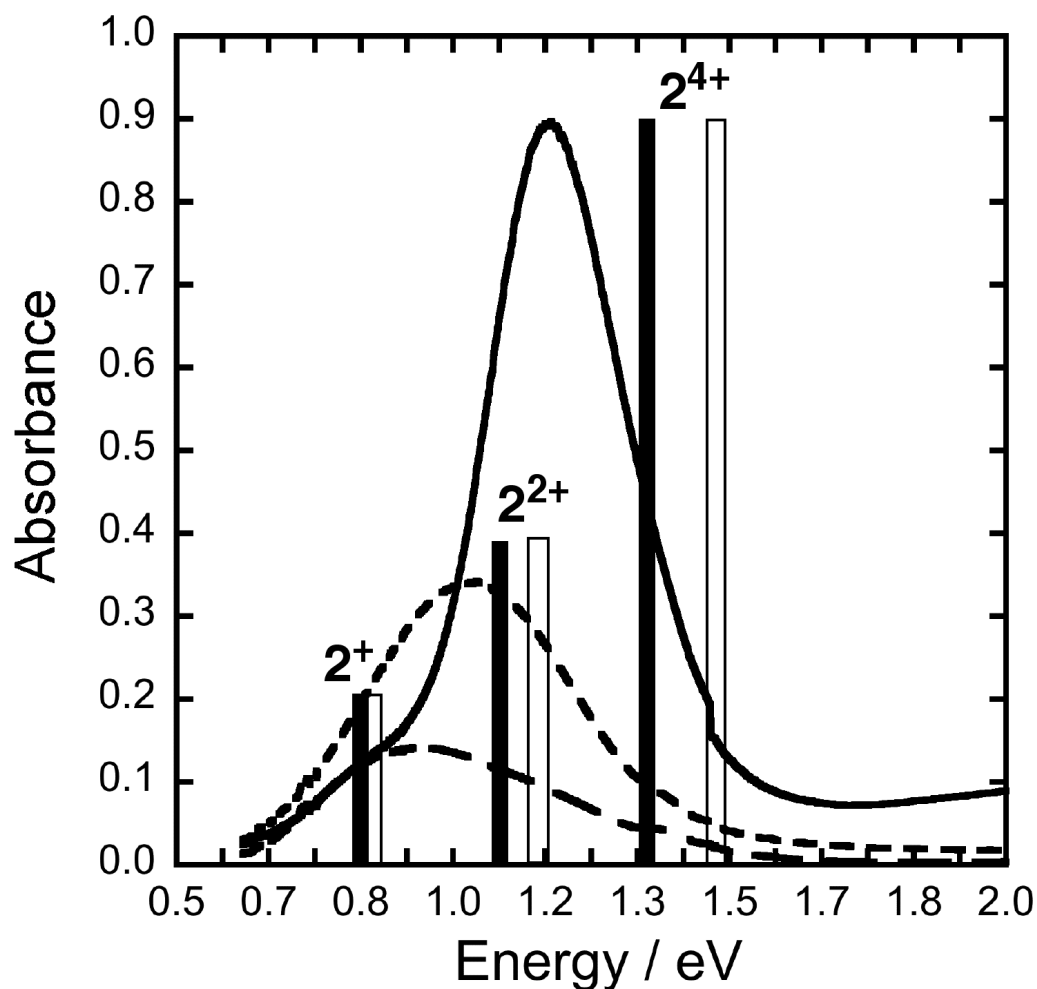
Figure 5. Vis–NIR absorption spectra of the stepwise electrochemical oxidation of **2** to tetracation **2⁴⁺** in CH$_2$Cl$_2$/0.1 M nBu$_4$NBF$_4$ at 298 K: **2⁺** (broken line), **2²⁺** (dotted line), and **2⁴⁺** (solid line). The black and white sticks designate the TD-DFT-calculated lowest energy transition energies and their relative oscillator strengths for **2'⁺**, **2'²⁺**, and **2'⁴⁺** at B3LYP/6-31G* and B1LYP(a = 0.35)/SVP with CPCM solvent model for CH$_2$Cl$_2$, respectively.
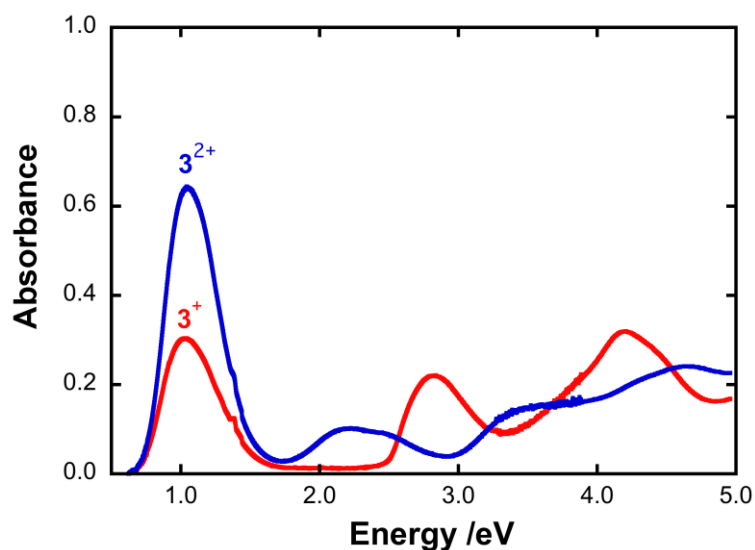
Figure 6. UV-Vis-NIR absorption spectra in the stepwise electrochemical oxidation of **3** in 0.1 M CH_2Cl_2/nBu$_4$NBF$_4$ at 298 K.
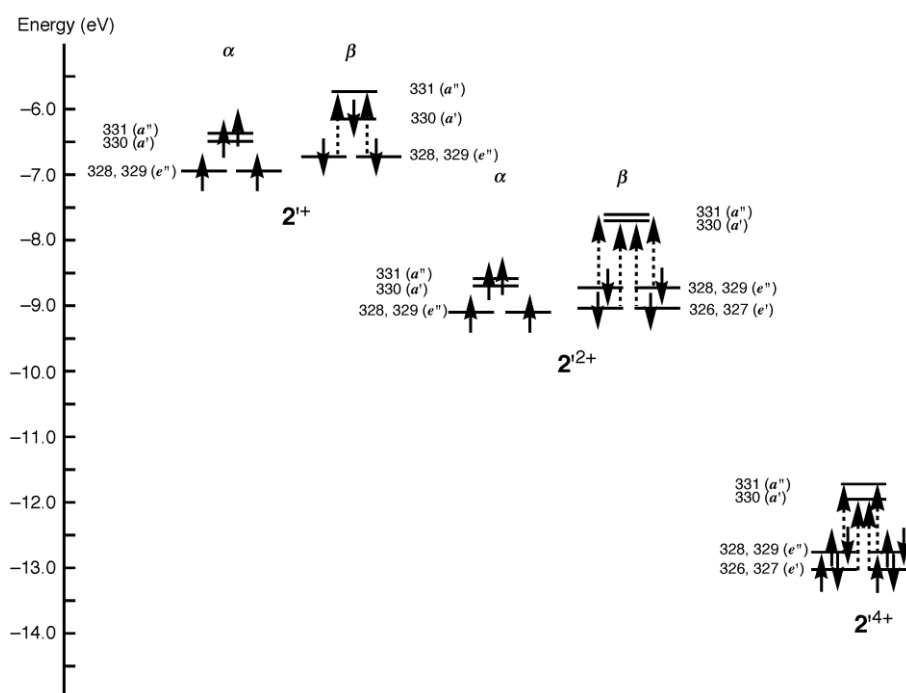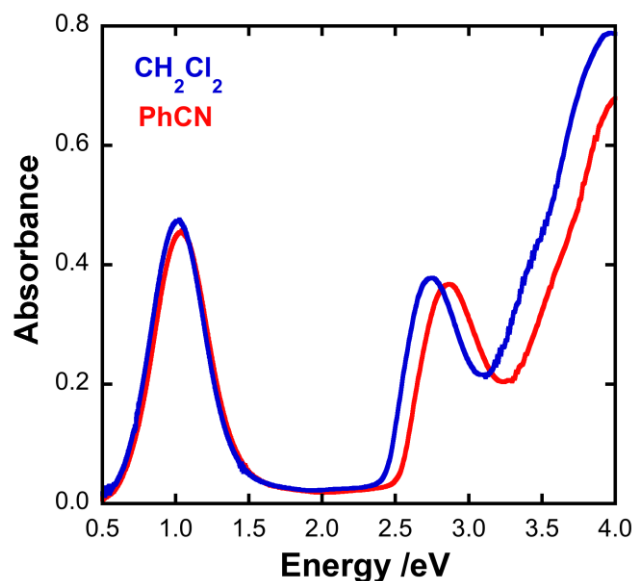

Figure 7. Relative Kohn-Sham MO energy levels for **2'$^+$**, **2'$^{2+}$**, and **2'$^{4+}$** based on the (U)B3LYP/6-31G* level of theory. The arrows with broken lines represent the major contributions to the lowest energy transitions on the basis of TD-DFT calculations ((U)B3LYP/6-31G*).

162

Table 3: TD-DFT ((U)B3LYP/6-31G*) calculations of the low-energy excitation energies for $\mathbf{2}^{\text{·}+}$, $\mathbf{2}^{\text{·}2+}$, and $\mathbf{2}^{\text{·}4+}$.

Species	$h\nu$ (eV) (f)	Assignment
$\mathbf{2}^{\text{·}+}$	0.80 (0.56)	328β, 329β ((HO-1)MOs) → 331β (LUMO) [~100%]
$\mathbf{2}^{\text{·}2+}$	1.11 (1.09)	326β, 327β ((HO-1)MOs) → 330β (LUMO) [72%]
		328β, 329β (HOMOs) → 331β ((LU+1)MO) [18%]
$\mathbf{2}^{\text{·}4+}$	1.31 (2.52)	326β, 327β ((HO-1)MOs) → 330β (LUMO) [32%]
		328β, 329β (HOMOs) → 331β ((LU+1)MO) [20%]

Table 4: TD-DFT ((U)B1LYP(a = 0.35)/SVP with CPCM solvent model for CH_2Cl_2) calculations of the low-energy excitation energies for $\mathbf{2}^{\text{·}+}$, $\mathbf{2}^{\text{·}2+}$, and $\mathbf{2}^{\text{·}4+}$.

| Species	$h\nu$ (eV) (f)	Assignment
$\mathbf{2}^{\text{·}+}$	0.83 (0.80)	328β, 329β ((HO-1)MOs) → 331β (LUMO) [~100%]
$\mathbf{2}^{\text{·}2+}$	1.19 (1.52)	326β, 327β ((HO-1)MOs) → 330β (LUMO) [77%]
		328β, 329β (HOMOs) → 331β ((LU+1)MO) [20%]
$\mathbf{2}^{\text{·}4+}$	1.47 (3.39)	326β, 327β ((HO-1)MOs) → 330β (LUMO) [37%]
		328β, 329β (HOMOs) → 331β ((LU+1)MO) [14%]

Figure 8. UV-Vis-NIR absorption spectra for 2^+ in CH_2Cl_2 ($\varepsilon = 8.93$) and in PhCN ($\varepsilon = 25.59$) at 298 K. 2^+ was generated by adding 1 equiv of tris(4-bromophenyl)ammonium hexachloroantimonate (Magic Blue).

6.3.6 Formation of Charge-Transfer Complex of 2 with TCNQ

Taking this into the low first oxidation potential, **2** is considered to be a good electron-donor. We have checked the possibility of formation of charge-transfer (CT) complexes with acceptor molecules. Combining solutions of **2** and 7,7,8,8-tetracyano-p-quinodimethane (TCNQ) as a typical acceptor molecule in CH_2Cl_2 exhibited a superposition of the absorptions of $2^{\bullet+}$ (0.92 eV) and $TCNQ^{\bullet-}$ ($\sim$1.5 eV [20]), as shown in Figure 9. In addition, the IR spectrum of the isolated powder sample displayed a characteristic decrease in the wavenumber ν_{CN} corresponding to the CN bond stretching vibration of TCNQ [observed $\nu_{CN} = 2179$ cm^{-1}; 2223 cm^{-1} for neutral TCNQ and 2183 cm^{-1} for $TCNQ^{\bullet-}$], as is often utilized as a measure of charge transfer in the CT complex with TCNQ.[21] Thus, this indicates a complete charge transfer occur from **2** to TCNQ.
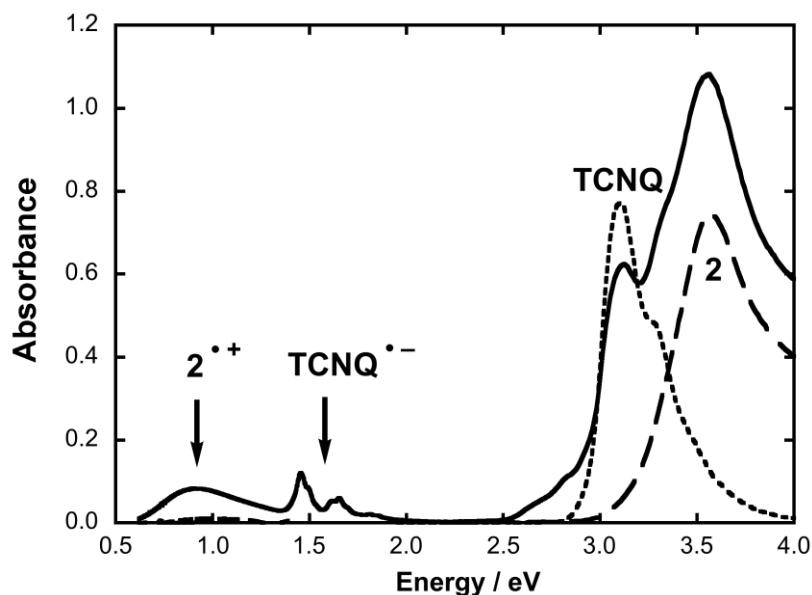
Figure 9. UV-Vis-NIR absorption spectrum of the combined solution of **2** and TCNQ in CH$_2$Cl$_2$ at 298 K.

6.3.7 ESR Spectroscopy

Treatment of **2** with 1 equiv. of tris(4-bromophenyl)aminium hexachloroantimonate (Magic Blue)[1c] in CH$_2$Cl$_2$ at 195 K gave a green solution for **2**$^+$. However, the solution ESR spectrum showed a single broad line with no hyperfine structures (g = 2.0024; ΔH_{pp} (peak-to-peak linewidth) = 1.05 mT), thus affording no information on the spin distribution over the molecular skeleton (Figure 10). On the other hand, the evidence of di(cation radical) for the oxidized species with treated by two equiv. of the Magic Blue was confirmed by the fine-structured ESR spectrum characteristic for spin triplet species in the $g \approx 2$ region, as well as by the weak signal corresponding to the forbidden transition in the $g \approx 4$ region (Figure 11). From the zero-field splitting parameters; D = 4.9 mT and E = 0 mT, the average distance between the radical centers[22] was estimated to be 8.3 Å. The deviation from the face-to-face distance between the two TPA decks (5.8 Å) determined by X-ray analysis strongly suggests that spin-density distributions on each TPA decks are to some extent delocalized over *meta*-phenylenediamine pillars.

165

Figure 12 displays the temperature dependence of the ESR signal intensity for 2^{2+}, and the ground state of 2^{2+} turned out to be in spin singlet state, apparently from decrease in intensity with decreasing temperature. The energy gap between the singlet and triplet states (ΔE_{S-T}) was estimated to be −0.18 kcal mol^{-1}, as a result of curve-fitting with the Bleaney-Bowers singlet-triplet model equation (Eq. (1)).[23]

$$I = \frac{C}{T} \frac{1}{3 + \exp\left(-\dfrac{\Delta E_{S-T}}{k_B T}\right)} \tag{1}$$

On the other hand, as shown in Figure 2a, the HOMO and (HO-1)MO of 2' were found to be of nondisjoint (or coextensive) non-bonding type (NBMOs),[24] which is reflected in the orbital patterns over *meta*-phenylenediamine moieties, and moreover, the quasi-degeneracy and non-disjoint character suggested the high-spin preference for $2'^{2+}$ (ΔE_{S-T} = 5.3 kcal mol^{-1}). The discrepancy between the DFT-calculated energy gap and the experimental result can be ascribed to the fact that the static correlation, in particular, for the singlet state of 2^{2+} is inadequately taken into consideration in the present DFT calculations, and therefore, the present calculations failed to attest the significant effect that large dihedral angle (60˚ to 90˚) between *meta*-phenylene π-plane and the spin-bearing groups results in singlet spin preference in diradicals.[26] In contrast, tetracation 2^{4+}, generated by treatment of 2 with four equiv. of the Magic Blue, was ESR silent, in good accordance with the theoretical consideration.
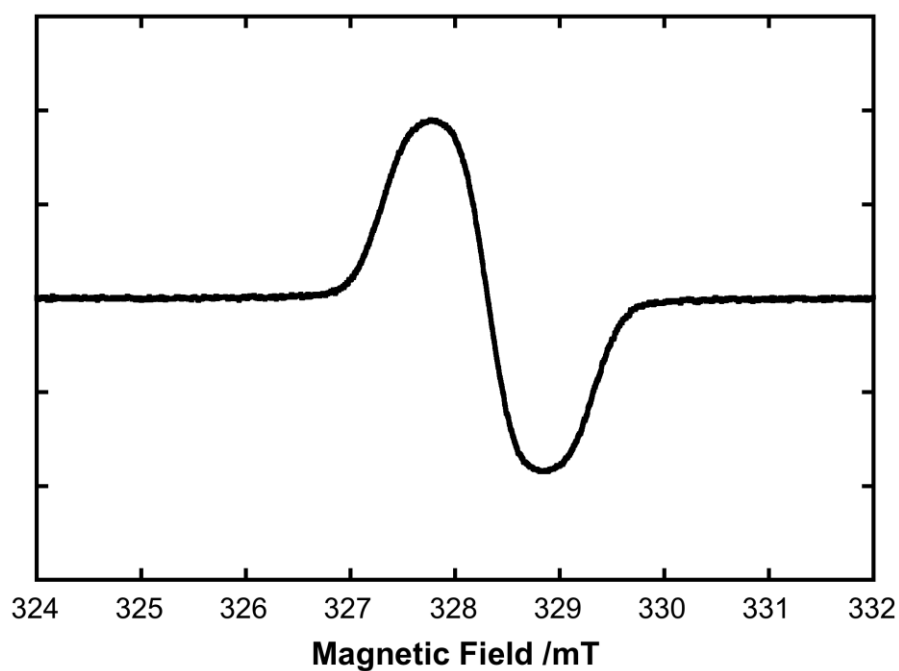
Figure 10. ESR spectrum of 2^+ in CH_2Cl_2 at 293 K.
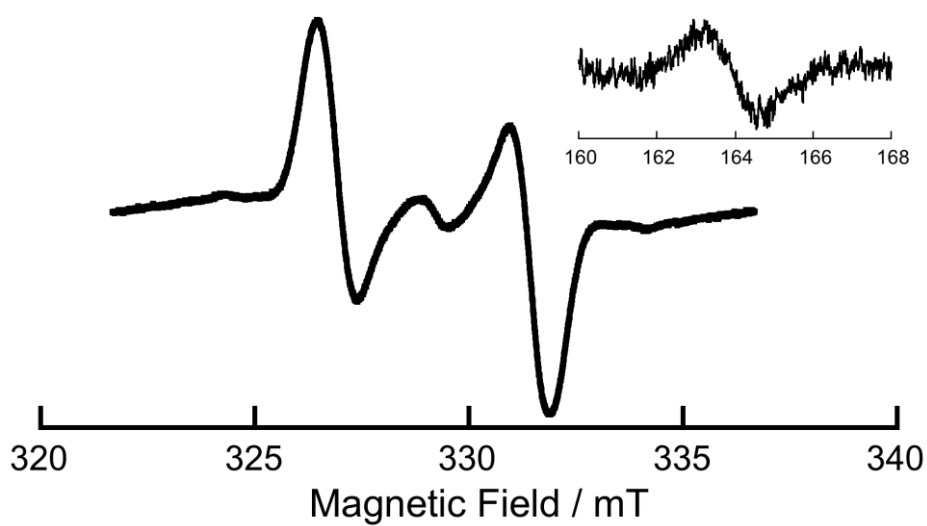
Figure 11. ESR spectrum of 2^{2+} in CH_2Cl_2/n-butyronitrile (3:1) at 123 K (inset: the forbidden resonance observed at 123 K).
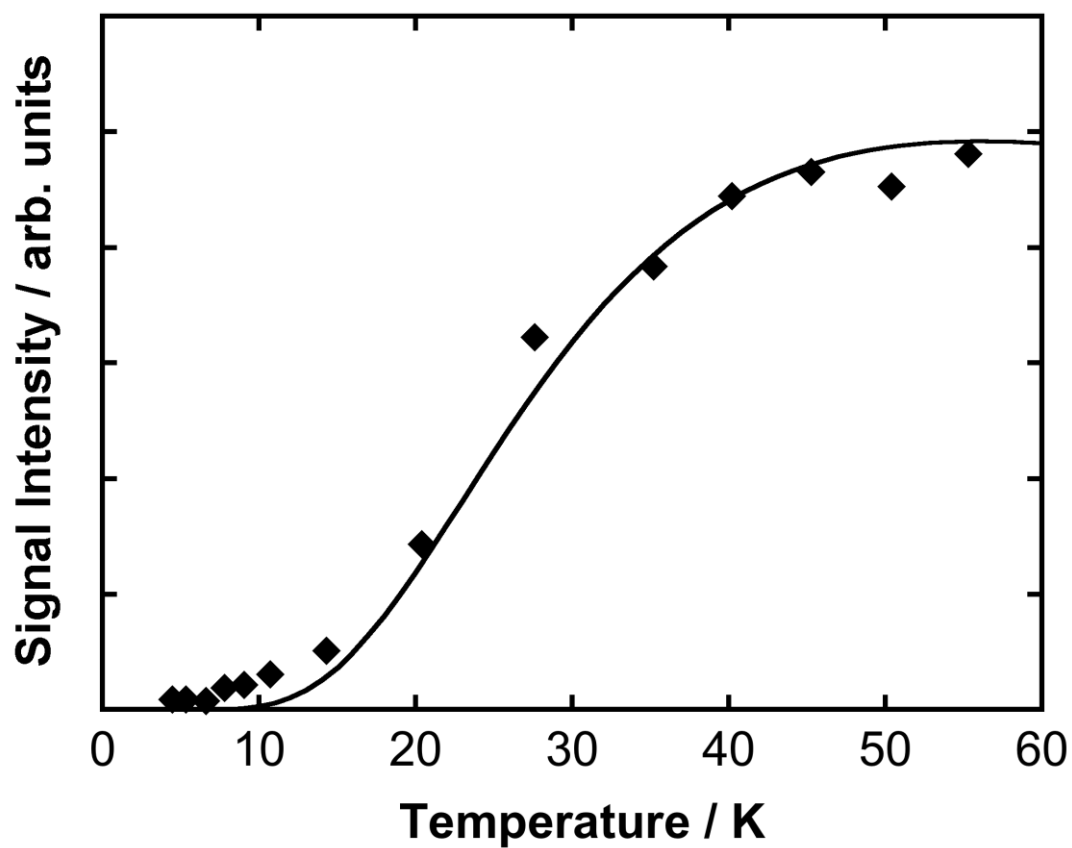
Figure 12. Temperature dependence of the ESR signal intensity of $\mathbf{2}^{2+}$ and the curve-fitting (solid line) with the Bleaney-Bowers singlet-triplet model equation (see text).
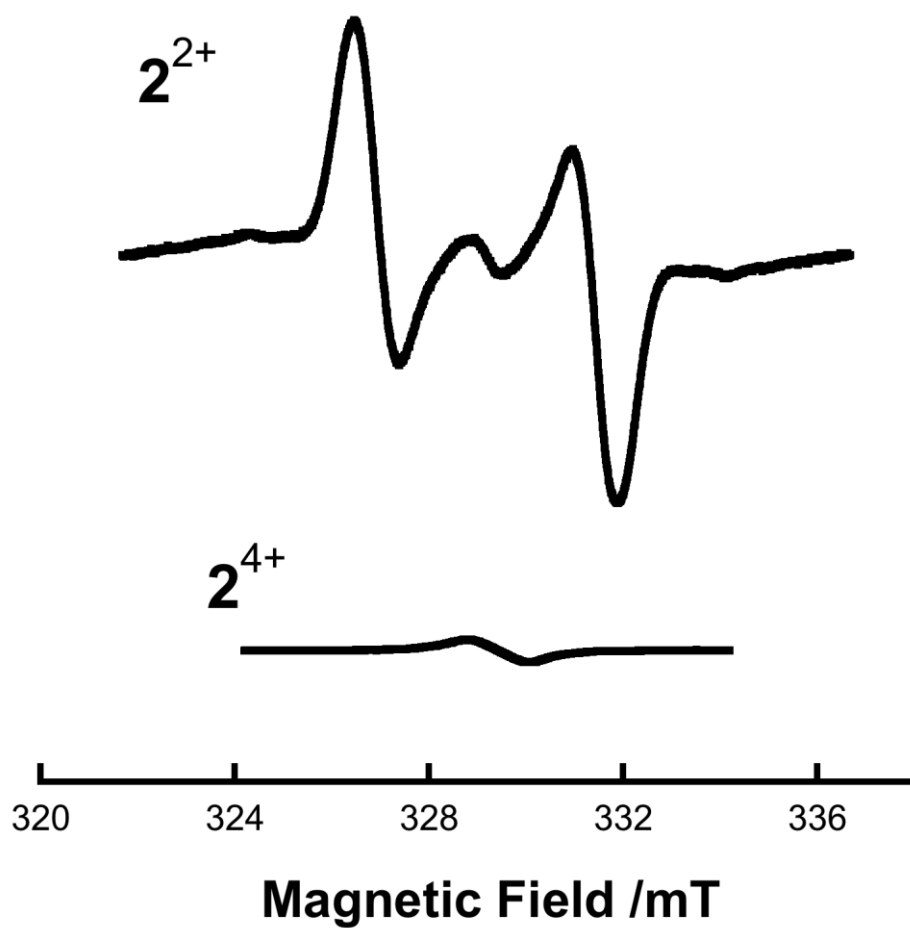
Figure 13. Comparison between the observed ESR spectra for **2**$^{2+}$ and **2**$^{4+}$ in CH$_2$Cl$_2$/*n*-butyronitrile (3:1) at 123 K.

6.4 Conclusion

In this chapter, we have described the electronic structures for the polycationic states of a double-layered TPA linked by three *meta*-phenylenediamine pillars, that is, TPA double-decker. As exemplified by the X-ray analysis, no direct through-space interaction between two nitrogen lone pairs on both TPA decks can be inferred. However, it was clarified that the generated spin in 2^+ is delocalized over the whole molecular skeleton, probably due to through-bond interaction through three-dimensional connectivity in **2**. Furthermore, although the dication of **2** revealed the diradical character originating from the nondisjoint quasi-doubly-degenerate NBMOs due to three *meta*-phenylenediamine pillars, its spin preference was contrary to the simple B3LYP prediction. The outcome of the present study demonstrates that it is not straightforward to endow three-dimensionally-connected TPA-based macromolecular systems with desired electronic properties. To put it the other way around, however, intriguing electronic features can be emerged from this class of molecular systems. The extension to multiple-deckers and the construction of the other related TPA-based architectures with complicated connectivity are currently underway in our laboratory.

References and Notes

[1] a) F. A. Bell, A. Ledwith, D. C. Sherrington, *J. Chem. Soc*. **1969**, 2719; b) S. Dapperheld, E. Steckhan, K.-H. Grosse Brinkhaus, T. Esch, *Chem. Ber*. **1991**, *124*, 2557; c) N. G. Connelly, W. E. Geiger, *Chem. Rev*. **1996**, *96*, 877.

[2] For example, see: a) X. Z. Yan, J. Pawlas, T. Goodson, III, J. F. Hartwig, *J. Am. Chem. Soc*. **2005**, *127*, 9105; b) A. Ito, Y. Yamagishi, K.Fukui, S. Inoue, Y. Hirao, K. Furukawa, T. Kato, K. Tanaka, *Chem. Commun*. **2008**, 6573.

[3] F. A. Neugebauer, S. Kuhnhäuser, *Angew. Chem. Int. Ed.* **1985**, *24*, 596.

[4] R. W. Alder, S. P. East, *Chem. Rev*. **1996**, *96*, 2097.

[5] Closely related caged compounds: a) D. O'Krongly, S. R. Denmeade, M. Y. Chiang, R. Breslow, *J. Am. Chem. Soc*. **1985**, *107*, 5544; b) B. P. Friedrichsen, H. W. Whitlock, *J. Am. Chem. Soc*. **1989**, *111*, 9132; c) B. P. Friedrichsen, D. R. Powell, H. W. Whitlock, *J. Am. Chem. Soc*. **1990**, *112*, 8931; d) R. Berscheid, M. Nieger, F. Vögtle, *Chem. Ber*. **1992**, *125*, 1687; f) F. Vögtle, J. Winkel, *Tetrahedron Lett*. **1979**, *20*, 1561; g) H. Schrage, J. Franke, F. Vögtle, E. Steckhan, *Angew. Chem. Int. Ed. Engl*. **1986**, *25*, 336; h) F. Vögtle, G. Hohner, *Top. Curr. Chem*. **1978**, *74*, 1.

[6] M. C. Burla, M. Camalli, B. Carrozzini, G. L. Cascarano, C. Giacovazzo, G. Polidori, R. Spagna, *J. Appl. Cryst*. **2003**, 36, 1103.

[7] The DIRDIF-99 Program System, Technical Report of the Crystallography Laboratory, P. T. Beurskens, G. Admiraal, G. Beurskens, W. P. Bosman, R. de Gelder, R. Israel, J. M. M. Smits, University of Nijmegen (The Netherlands), **1999**.

[8] Program for Crystal Structure Solution and Refinement, G. M. Sheldrick, Universität Göttingen, **1997**.

[9] CrystalStructure 3.8, Crystal Structure Analysis Package, Rigaku and Rigaku Americas (2000–2007). 9009 New Trails Dr. The Woodlands TX 77381 USA.

[10] a) J. P. Wolfe, S. Wagaw, J. F. Marcoux, S. L. Buchwald, *Acc. Chem. Res*. **1998**, *31*, 805; b) J. F. Hartwig, *Acc. Chem. Res*. **1998**, *31*, 852; c) J. F. Hartwig, *Angew. Chem. Int. Ed*. **1998**, *37*, 2046; d) A. R. Muci, S. L. Buchwald, *Top. Curr. Chem*. **2002**, *219*, 133.

[11] P. A. Ashton, N. S. Isaacs, F. H. Kohnke, G. S. D'Alcontres, J. F. Stoddart, *Angew. Chem. Int. Ed*. **1989**, *28*, 1261.

[12] A. Ito, Y. Yokoyama, R. Aihara, K. Fukui, S. Eguchi, K. Shizu, T. Sato, K. Tanaka, *Angew. Chem. Int. Ed*. **2010**, *49*, 8205.

[13] A. Ito, D. Sakamaki, Y. Ichikawa, K. Tanaka, *Chem. Mater*. **2010**, *23*, 841.

[14] a) J. Hankache, O. S. Wenger, *Chem. Rev*. **2012**, *111*, 5138; b) A. Heckman, C. Lambert, *Angew. Chem. Int. Ed*. **2012**, *51*, 326, and references therein.

[15] Oxidation states higher than 2^{4+} and 3^{2+} were found to be unstable under the

experimental conditions in the present spectroelectrochemical study.

[16] a) R. Bauernschmitt, R. Ahlrichs, *Chem. Phys. Lett*. **1996**, *256*, 454; b) M. E. Casida, C. Jamorski, K. C. Casida, D. R. Salahub, *J. Chem. Phys*. **1998**, *108*, 4439; c) R. E. Stratmann, G. E. Scuseria, M. J. Frisch, *J. Chem. Phys*. **1998**, *109*, 8218.

[17] M. Renz, K. Theilacker, C. Lambert, M. Kaupp, *J. Am. Chem. Soc*. **2009**, *131*, 16292.

[18] A. Schäfer, H. Horn, R. Ahlrichs, *J. Chem. Phys*. **1992**, *97*, 2571.

[19] V. Barone, M. Cossi, *J. Phys. Chem. A* **1998**, *102*, 1995.

[20] Y. Iida, *Bull. Chem. Soc. Jpn*. **1969**, *42*, 71.

[21] J. S. Chappell, A. N. Bloch, W. A. Bryden, M. Maxfield, T. O. Poehler, D. O. Cowan, *J. Am. Chem. Soc*. **1981**, *103*, 2442.

[22] W. B. Gleason, R. E. Barnett, *J. Am. Chem. Soc*. **1976**, *98*, 2701.

[23] B. Bleaney, K. D. Bowers, *Proc. R. Soc. London Ser. A* **1952**, *214*, 451.

[24] a) D. A. Dougherty, *Acc. Chem. Res*. **1991**, *24*, 88; b) J. A. Crayston, J. N. Devine, J. C. Walton, *Tetrahedron* **2000**, *56*, 7829.

[25] a) F. Kanno, K. Inoue, K. Noboru, H. Iwamura, *J. Am. Chem. Soc*. **1993**, *115*, 847; b) S. Fang, M.-S. Lee, D. A. Hrovat, W. T. Borden, *J. Am. Chem. Soc*. **1995**, *117*, 6727.

Chapter 7

The First Synthesis of an *o,p,o,p*-Tetraazacyclophane: The Effect of the *ortho*-Phenylene Linkers on the Structural and Electronic Properties

7.1 Introduction

There have been great interest in the closely stacked π systems, as represented by [2,2]paracyclophanes[1,2] because of their unique structures and, moreover, the possible electronic interactions among the π systems. In the past, various kinds of conjugated units have been used as building blocks of such stacked oligomers. The *para*-phenylenediamine (PD), which is well known redox active compound,[3] is considered as the interesting building unit of the stacked systems because of the predicted intramolecular charge transfer and the spin-spin interaction in the cationic states of the stacked PD molecules. So far, there have been some studies on such cyclophanes composed of two PD units, and their structures and electronic properties have been reported.[4-6] However, in all these studies, the linker units connecting two PD units were confined to alkyl chains such as propyl or pentyl groups, and hence the

electronic interaction between two PD moieties through the covalent bonds of the linker units were considered to be negligibly small, and the direct through-space interaction between two aromatic units were mainly discussed. Therefore, we attempted to replace the alkyl chains in such PD cyclophanes with aromatic linkers so as to increase the through-bond interaction. We adopted the *ortho*-phenylene unit as a linker because this unit will connect two PD groups in close proximity. In this chapter, we will report the details of the structural and electronic properties of the PD cyclophane composed of *ortho*-phenylene linkers **1** (Figure 1). This molecule is regarded as the first example of an *o,p,o,p*-tetraazacyclophane. Therefore, we will clarify the effects of the shortened distance between two PD moieties on the structural and electronic properties by comparing with a *m,p,m,p*-tetraazacyclophane **2**, which has already been studied.[7, 8]
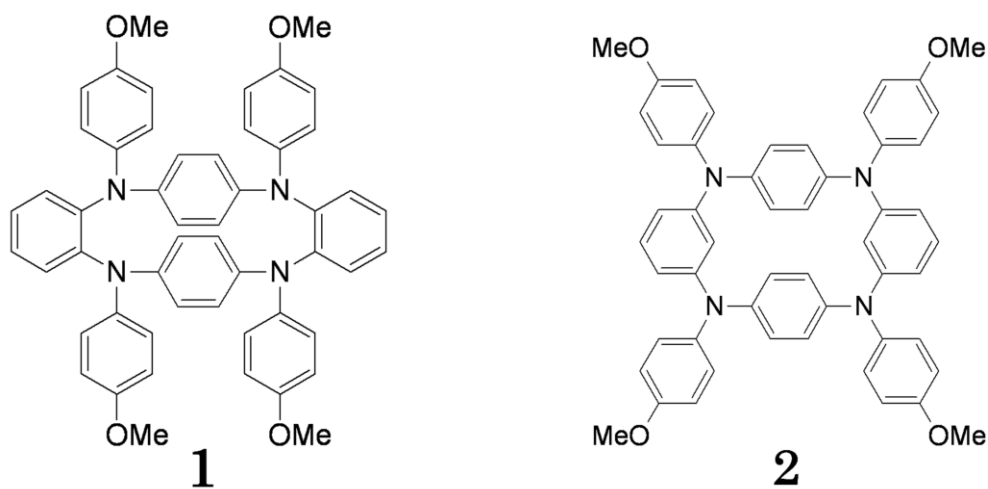
Figure 1. *o,p,o,p*-tetraazacyclophane **1** and *m,p,m,p*-tetraazacyclophane **2**.

7.2 Experimental Section

General Methods: All the purchased reagents were of standard quality, and used without further purification. All the purchased solvents were purified, dried, and degassed by standard procedures. Column chromatography was performed with silica gel (Kanto Chemical Co., Inc., silica gel 60N, spherical neutral). Elemental analyses

were performed by Center for Organic Elemental Microanalysis, Kyoto University. 1H and ^{13}C NMR spectra were measured by a JEOL JNM-AL400 FT-NMR spectrometer. Chemical shifts of NMR spectra are determined relative to internal tetramethylsilane (TMS) standard (δ), and are given in parts per million (ppm). The variable-temperature 1H NMR spectra were measured by a JEO JNM-AL300 FT-NMR spectrometer. Low resolution (LR) fast-atom-bombardment (FAB) mass spectra (MS) were recorded on a JEOL JMS-HX110A mass spectrometer with *m*-nitrobenzyl alcohol as a matrix. UV-Vis-NIR absorption spectra were obtained with a Perkin-Elmer Lambda 950 spectrometer. High resolution electrospray ionization (ESI) mass spectrum was acquired using a mass spectrometer (Thermo Fisher EXACTIVE). Emission spectra were recorded on an absolute PL quantum yield measurement system (HAMAMATSU Quantaurus-QY).

Synthetic Details. *N,N'*–**dianisyl–1,2–phenylenediamine (3):** A mixture of 1,2-dibromobenzene (2.36 g, 10.0 mmol), 4-anisidine (3.64 g, 29.6 mmol), Pd(OAc)$_2$ (0.11 g, 0.5 mmol), P(*t*-Bu)$_3$ (1.0 mmol) and NaO*t*-Bu (2.89 g, 30.0 mmol) in toluene (35 ml) was refluxed under an argon atmosphere for 17 h. The reaction mixture was cooled down to room temperature, and quickly quenched with an aqueous NH$_4$Cl. The organic layer was extracted with ethyl acetate, and dried over NaSO$_4$. After evaporation of the solvent, the crude product was chromatographed on silica gel (hexane/ethyl acetate = 4/1 as eluent) to afford **2** (2.60 g, 81.2%) as a brown solid: ^{1}H NMR (400MHz, acetone-d_6); δ = 3.737 (s, 6H), 6.356 (s, 2H), 6.811-6.841 (m, 6H), 6.950 (d, J = 9.03 Hz, 4H), 7.080-7.104 (m, 4H); ^{13}C NMR (100 MHz, tetrahydrofuran-d_8); δ = 55.80, 115.40, 119.19, 120.54, 122.33, 136.82, 138.75, 155.21; FAB LRMS (dithranol): *m/z* calcd for C$_{20}$H$_{20}$N$_2$O$_2$: 320.39 [M]$^+$; found 320.

o,p,o,p-**Tetraazacyclophane (1):** A mixture of **3** (0.325 g, 1.02 mmol), 1,4-dibromobenzene (0.249 g, 1.06 mmol), Pd(dba)$_2$ (0.058 g, 0.10 mmol), P(*t*-Bu)$_3$ (0.20 mmol) and NaO*t*-Bu (0.290 g, 3.02 mmol) in toluene (200 ml) was stirred under

an argon atmosphere at room temperature for 21 h. After 4 h, the reaction mixture was heated to 110 $^{\circ}$C, and stirred for 12 h. The reaction solution was cooled down to room temperature, and filtered through Celite. The reaction mixture was washed with Brine and the organic layer was separated and dried over Na_2SO_4. After evaporation of the solvent, the crude product was roughly purified by chromatography on silica gel (toluene/ethyl acetate = 19/1 as eluent), and further purified by HPLC to afford **1** (0.018 g, 4.5%) as a white solid: ^1H NMR (400MHz, acetone-d_6); δ = 3.746 (s, 12H), 5.972-6.021 (m, 4H), 6.512-6.605 (m, 4H), 6.811-6.840 (m, 8H), 7.024-7.114 (m, 8H), 7.213-7.429 (m, 8H), 6.817 (s, 8H); ^{13}C NMR (100 MHz, acetone-d_6); δ = 55.81, 115.44, 123.52, 123.84, 123.89, 124.21, 125.24, 125.82, 127.83, 128.43, 128.45, 129.84, 133.23, 133.67, 133.69, 141.09, 141.55, 143.62, 143.68, 145.86, 156.08; ESI HRMS: *m/z* calcd for $C_{52}H_{44}N_4O_4$: 788.3357 $[M]^+$; found 788.3347.

X-ray Crystallography for 1. Data collections were performed on a Rigaku RAXIS-RAPID diffractometer equipped with Rigaku VariMax RAPID imaging plate area detector with Cu-Kα radiation at -180˚C. The data were corrected for Lorentz and polarization effects. The structure was solved by using direct methods (SIR-2004[9]), and expanded by using Fourier techniques (DIRDIF-99[10]), and refined by full-matrix least-squares of F^2 on the basis of 10024 observed reflections and 846 variable parameters (SHELXL-97[11]). The non-hydrogen atoms were refined anisotropically, except for several disordered non-hydrogen atoms, which were refined isotropically. Hydrogen atoms were included in the refinement but restrained to ride on the atom to which they are bonded. The crystal contains acetone molecules, which were used on crystallization. Two acetone molecules per one azacyclophane **1** were contained in the crystal. All the calculations were performed by using CrystalStructure crystallographic software package,[12] except for refinement, which was performed by using SHELXL-97.

DFT Calculations of 1' and 1'$^{+}$. Quantum chemical calculations were performed

with using a hybrid Hartree–Fock/density functional theory (HF/DFT) method ((U)B3LYP).[13] Full geometrical optimization of **1**' and **1**'$^+$ were carried out and their local minimum structures were confirmed by performing subsequent frequency analyses. All the computations employed the 6-31G* basis set.[14] All these computational approaches are implemented in Gaussian 09 package of ab initio MO calculation.[15]

Electrochemical Measurements.   The redox properties were evaluated by cyclic voltammetry (CV) and differential pulse voltammetry (DPV) in CH_2Cl_2 solution at 298 K with 0.1 M tetra-*n*-butylammonium tetrafluoroborate (TBABF$_4$) as supporting electrolyte (scan rate 100 mV s^{-1}) using an ALS/chi Electrochemical Analyzer model 612A. A three-electrode assembly was used, which was equipped with platinum disk (2 mm^2), a platinum wire, and Ag/0.01 M AgNO$_3$ (acetonitrile) as the working electrode, the counter electrode, and the reference electrode, respectively. The redox potential were referenced against a ferrocene/ferrocenium (Fc$^{0/+}$) redox potential measured in the same electrolytic solution.

Spectroelectrochemical Measurements.   Spectroelectrochemical measurements were carried out with a custom-made optically transparent thin-layer electrochemical (OTTLE) cell (light pass length = 1 mm) equipped with a platinum mesh, a platinum coil, and a silver wire as the working electrode, the counter electrode, and the pseudo-reference electrode, respectively. The potential was applied with an ALS/chi Electrochemical Analyzer model 612A.

ESR Measurements.   ESR spectra were recorded on a JEOL JES-TE200 X-band ESR spectrometer, in which temperature was controlled by a JEOL ES-DVT3 variable-temperature unit in the range of 120-300 K. A Mn^{2+}/MnO solid solution was used as a reference for the determination of *g*-values and hyperfine coupling constants.

7.3 Results and Discussion

### 7.3.1 Synthesis and NMR measurements

The target molecule **1** was successfully prepared from *N,N,N',N'*-tetraanisyl-*ortho*-phenylenediamine **3**[16] and *p*-dibromobenzene by using the Buchwald-Hartwig cross-coupling amination reaction[17] (Scheme 1). The simple molecular modeling of **1** expects that the macrocyclic structure is considerably rigid, and actually, the sign of rigidity of the molecular structure appears in the ^{1}H and ^{13}C NMR spectra. Assuming the free rotation of the *ortho*-phenylene linkers at room temperature, only the five aromatic ^{1}H NMR signals are expected. However, 12 couples of aromatic signals were observed in acetone-d_6 at 298 K (Figure 2). This spectrum is compatibly explained by assuming the existence of two conformational isomers: the chair form and the boat form (Figure 3). Judging from the splitting patterns, the conformer corresponding to the signals with the larger intensity is the boat conformer and the smaller signals is the chair conformer.[18] The integration of these peaks gave the relative populations of these two conformers boat : chair = 69 : 31 at 298 K. The energy difference was estimated to be 0.48 kcal mol^{-1} assuming that the relative populations obey the Boltzmann distribution. In addition, the ^{13}C NMR spectrum of **1** also exhibits not 9-line but 20-line signals in the aromatic region, and this could be also explained by the existence of the two conformers. In contrast, the *m,p,m,p*-tetraazacyclophane **2** showed a simple aromatic ^{1}H NMR spectrum indicating the fast flipping of *meta*-phenylene rings connecting two *para*-phenylenediamines. Therefore, these results suggest the further rigidness of the macrocyclic structure of **1**.
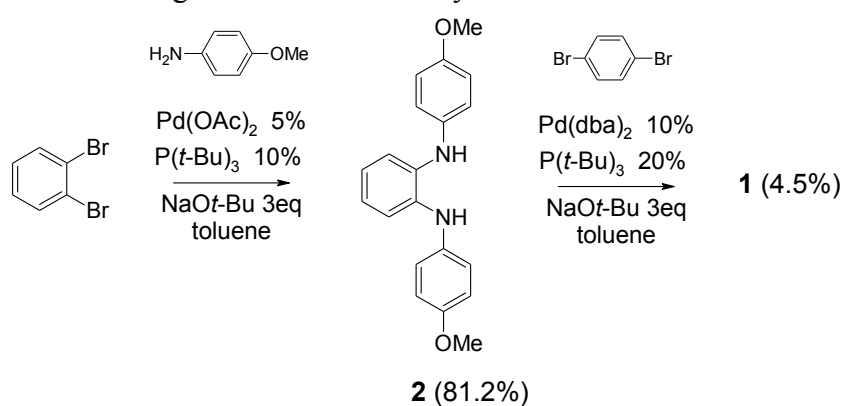

Scheme 1. Synthesis of **1**.
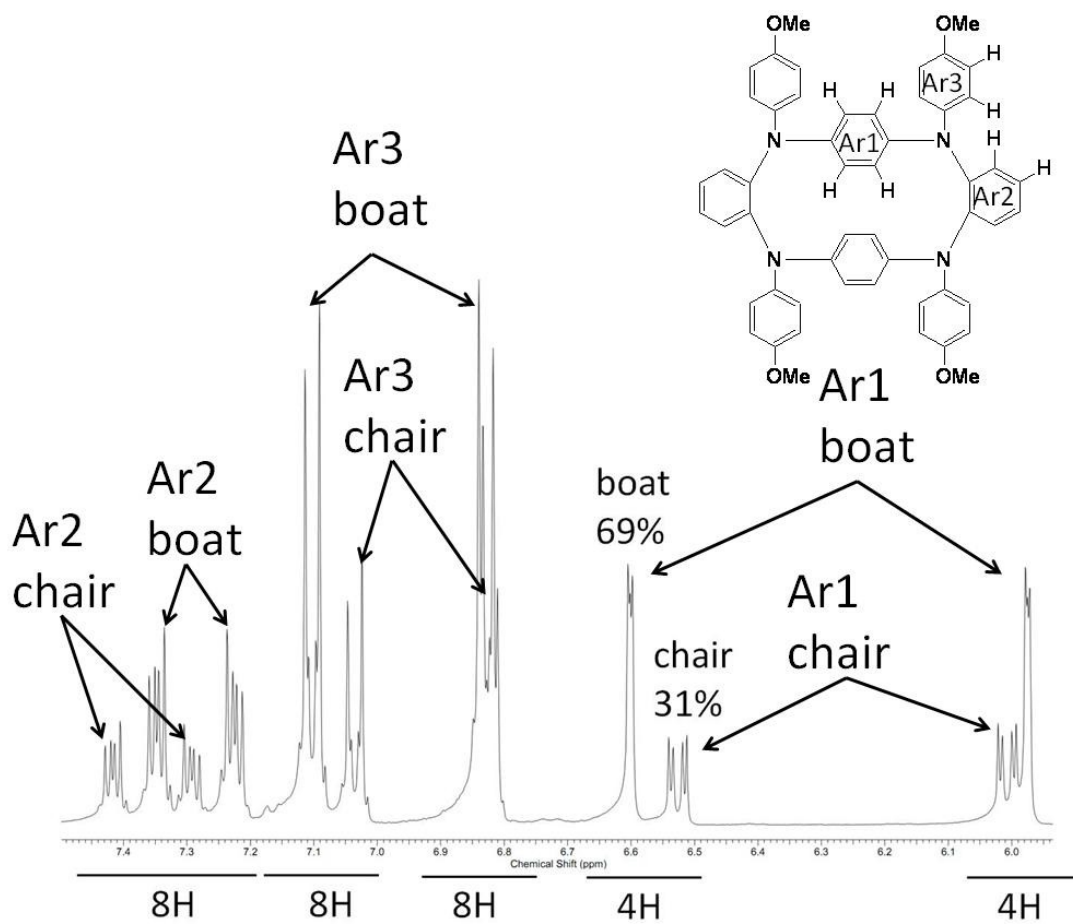
Figure 2. The aromatic region of ^{1}H NMR spectrum of **1** in acetone-*d*6 at 25°C.
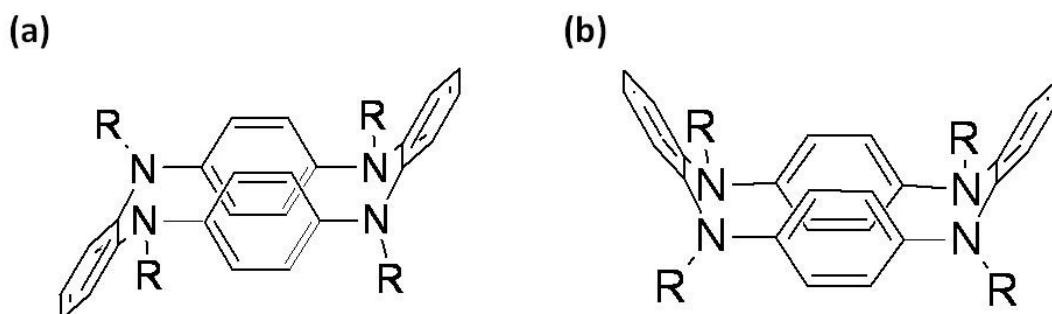
Figure 3. Two conformational isomers of **1**: a) the chair form; b) the boat form.

179

7.3.2 X-ray Structural Analysis

Block crystals of **1** suitable for X-ray structure analysis was obtained by slow

evaporation of a dilute mixed solution (acetone and CH_3OH). The space group of the

crystal was $P1$ and two molecules of **1** are contained per unit cell (Table 1). In the

crystal, all the molecules of **1** adopt the chair conformation with C_i symmetry (Figure 4).

Two benzene rings of PD moieties are almost flat, and cofacially stacked to each other.

The distance between these two benzene rings are about 3.1 Å, and this close distance

may allow the through-space charge or energy transfer as is the case of the $[2_n]$ and $[3_n]$

cyclophanes. The two C-N bond lengths in one PD moiety differ substantially (1.3991

and 1.4452 Å, Table 2).
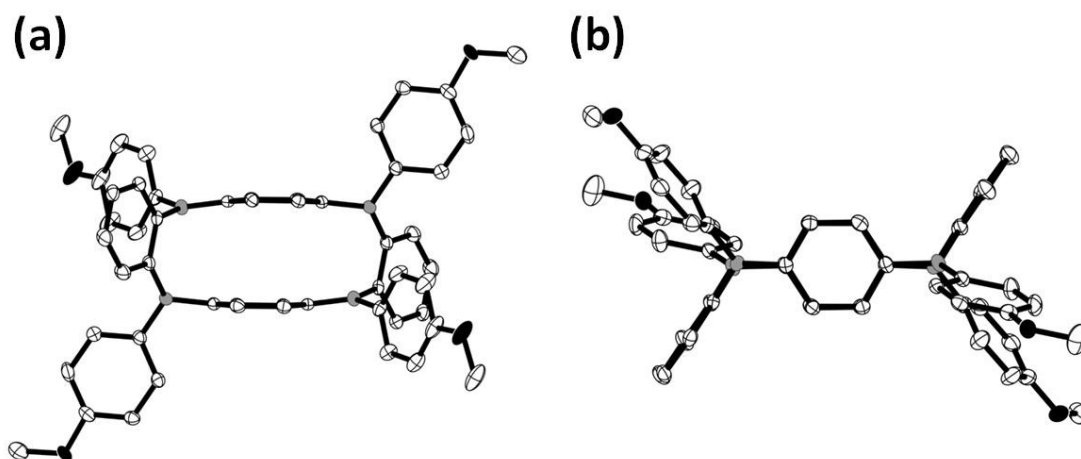
Figure 4. ORTEP representation of **1**.

Table 1: X-ray crystallographic data for **1**.

empirical formula	$C_{58}H_{56}N_4O_6$
	[**1** · (acetone)$_2$]
formula weight	905.10
T [˚C]	-180 ± 1
λ [Å]	1.54187
crystal system	triclinic
space group	$P\bar{1}$ (#2)
Z	2
a [Å]	11.879(5)
b [Å]	13.771(5)
c [Å]	15.511(6)
α [˚]	99.018(5)
β [˚]	108.092(5)
γ [˚]	90.316(3)
V [Å^3]	2378.1(16)
ρ_{calcd} [g cm^{-3}]	1.264
μ (MoKα)[cm^{-1}]	0.82
collected data	31747
unique data / R_{int}	10928/0.0383
no. of parameters	642
goodness-of-fit[a]	1.085
$R1$ ($I > 2\sigma$), $wR2$ (all reflections)[b]	0.0873, 0.2240
residual density [e Å^{-3}]	0.53/-0.62

[a] GOF = $\left\{ \sum \left[w\left(F_0^2 - F_c^2\right)^2 \right] \Big/ (n-p) \right\}^{1/2}$, where n and p denote the number of data and parameters.

[b] $R1 = \sum \left(\|F_0\| - \|F_c\| \right) / \sum \|F_0\|$ and $wR2 = \left\{ \sum \left[w\left(F_0^2 - F_c^2\right)^2 \right] \Big/ \sum \left[w\left(F_0^2\right)^2 \right] \right\}^{1/2}$ where

$w = 1 \Big/ \left[\sigma^2 \left(F_0^2\right) + (a \cdot P)^2 + b \cdot P \right]$ and $P = \left[\left(Max; 0, F_0^2\right) + 2 \cdot F_c^2 \right] \Big/ 3$.

Table 2: Crystallographic bond length for **1**.

	Bond length (Å)
N1–C1	1.4452
N2–C4	1.3991
C1–C2	1.3878
C2–C3	1.3874
C3–C4	1.4054
C4–C5	1.4068
C4–C5	1.3904
C5–C6	1.3929
N2–C7	1.4330
N3–C12	1.4229
C7–C8	1.3979
C8–C9	1.3874
C9–C10	1.3881
C10–C11	1.3877
C11–C12	1.4025
C12–C7	1.4069
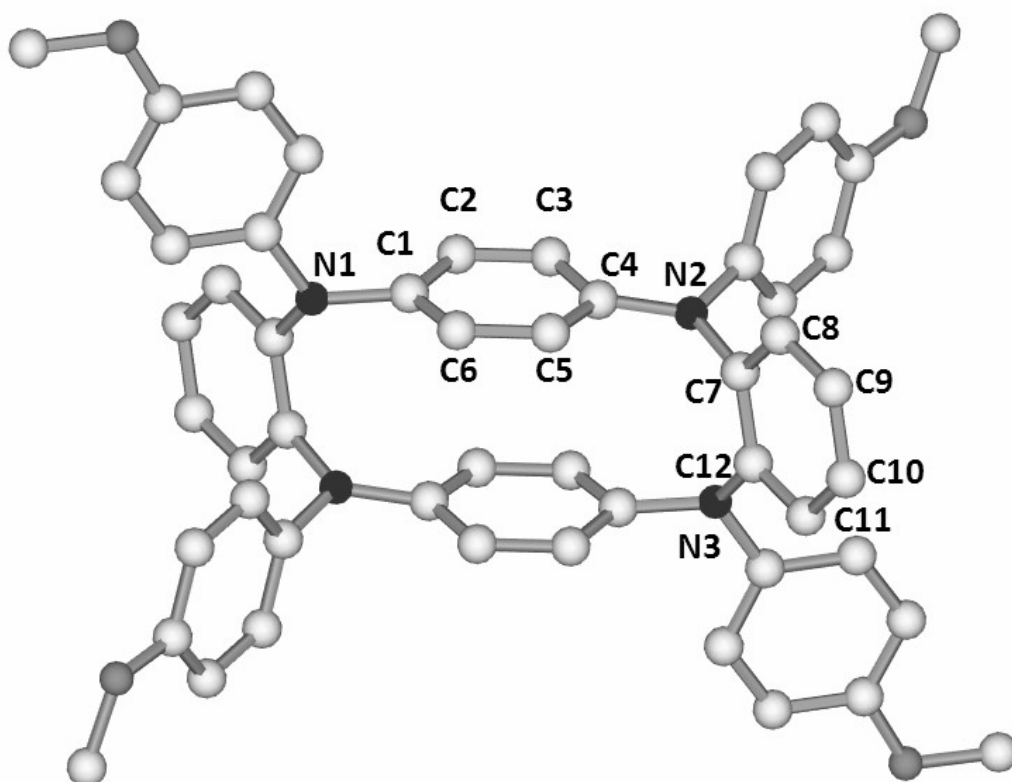
7.3.3 Variable Temperature NMR Experiments

To investigate the conformational change between the two conformers, we carried out the variable temperature ^{1}H NMR measurement in DMSO-d_6 in the temperature range from 298 K to 423 K (Figure 5). The shapes of the spectra basically unchanged in the temperature range from 298 K to 363 K. However, the signals began to broaden at 383 K. The ^{1}H signals except for that of the PD moieties of these two isomers coalesced at 423 K, and the number of the aromatic ^{1}H signals was reduced to 6 from 12. If the rate of the conformational change is significantly faster than the NMR time-scale, the protons of the *para*-phenylene moieties in the macrocycle will show one signal[18] and we will observe the five different aromatic ^{1}H signals, and hence this result indicates the considerable rigidness of the *o,p,o,p*-tetraazacyclophane skeleton. The activation energy of the chair-boat inversion was estimated as *ca*. 22 kcal mol^{-1}.[19] When the spectrum was measured just after cooling from 423 K to 298 K again, the spectral shape completely recovered.
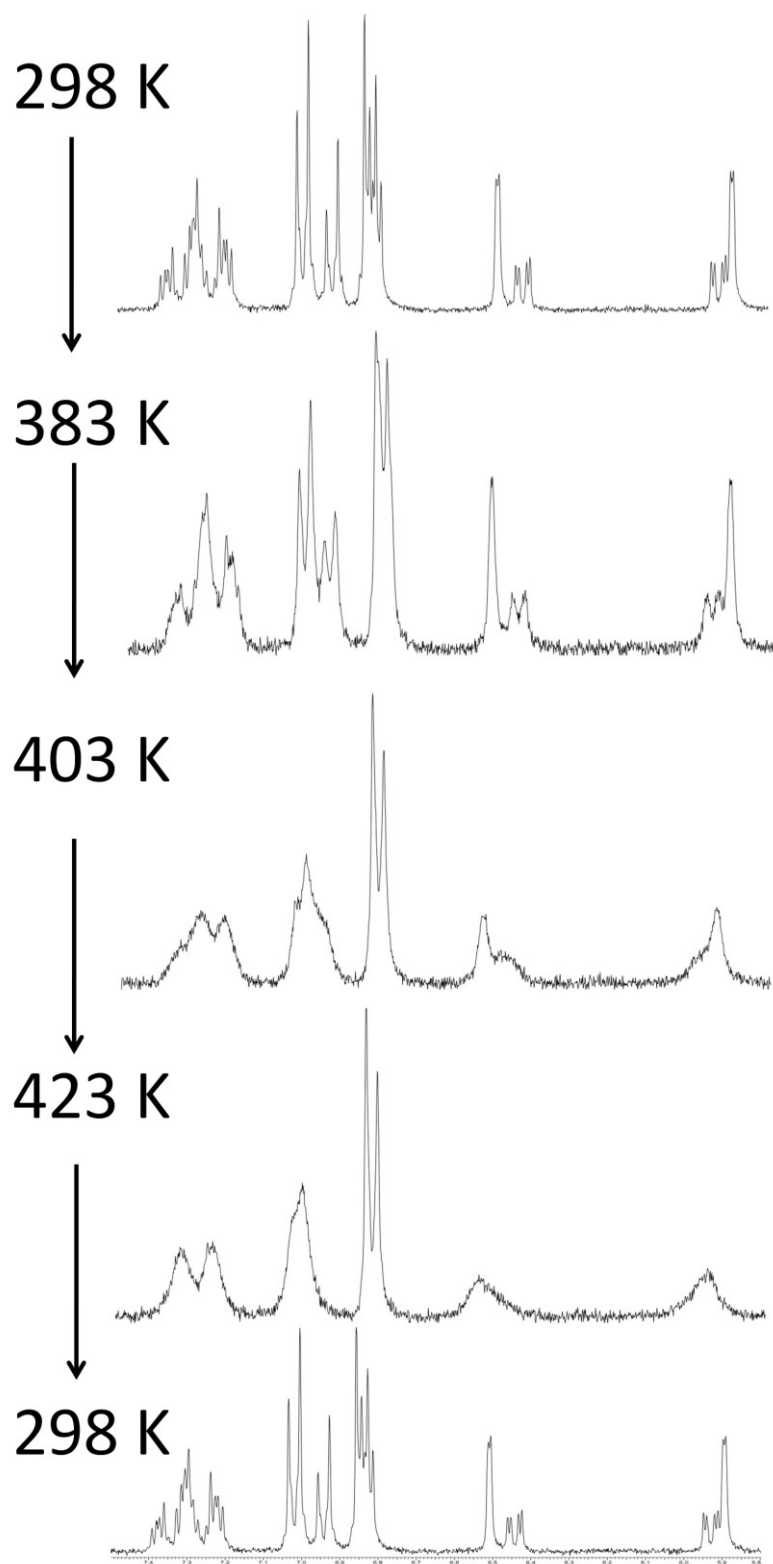
**Figure 5.** VT ^{1}H NMR spectra of **1** in DMSO-d_6.

184

7.3.4 DFT Calculations

As mentioned above, an *o,p,o,p*-tetraazacyclophane has two conformational isomers, the boat form and the chair form. We carried out the geometry optimization by the DFT method on for these two conformers of a model compound of **1'**, in which the methoxy groups are replaced by hydrogen atoms so as to found the stable conformations. As the results of the geometry optimization and the frequency analyses, the stable structures of the boat form with C_i symmetry and the chair form with C_1 symmetry were found (Figure 6). The boat form was calculated to be slightly stable by 0.264 kcal mol^{-1} than the chair form, and this result accorded with the ^{1}H NMR measurement. The calculated structure of the chair conformer which was found in the crystals was in good agreement with the crystal structure.
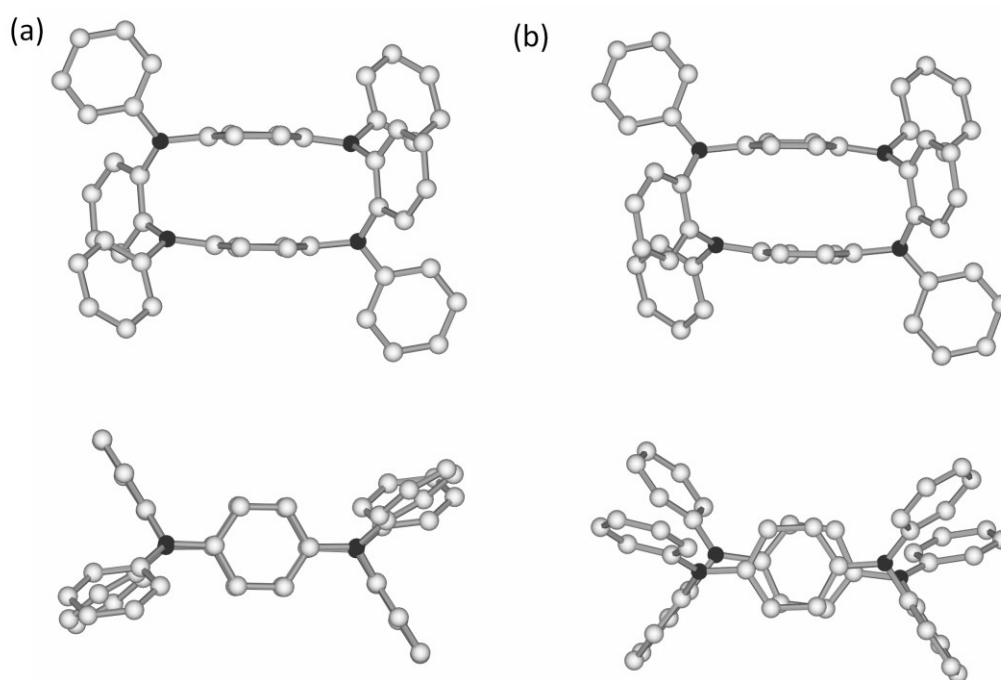
Figure 6. DFT-optimized structures of **1'**: a) the chair form; b) the boat form.

The orbital energy diagrams of these conformers are shown in Figure 7 and 8. In both conformers, the HOMO and (HO-1)MO are quasi-degenerate and (HO-2)MO and (HO-3)MO are also quasi-degenerate. The MO coefficients are fully delocalized over the two *para*-phenylenediamine moieties and also the two *ortho*-phenylene moieties.

HO-1MO (a$_g$) -4.7892 eV   HOMO (a$_u$) -4.7593 eV

HO-3MO (a$_u$) -5.4464 eV   HO-2MO (a$_g$) -5.4428 eV
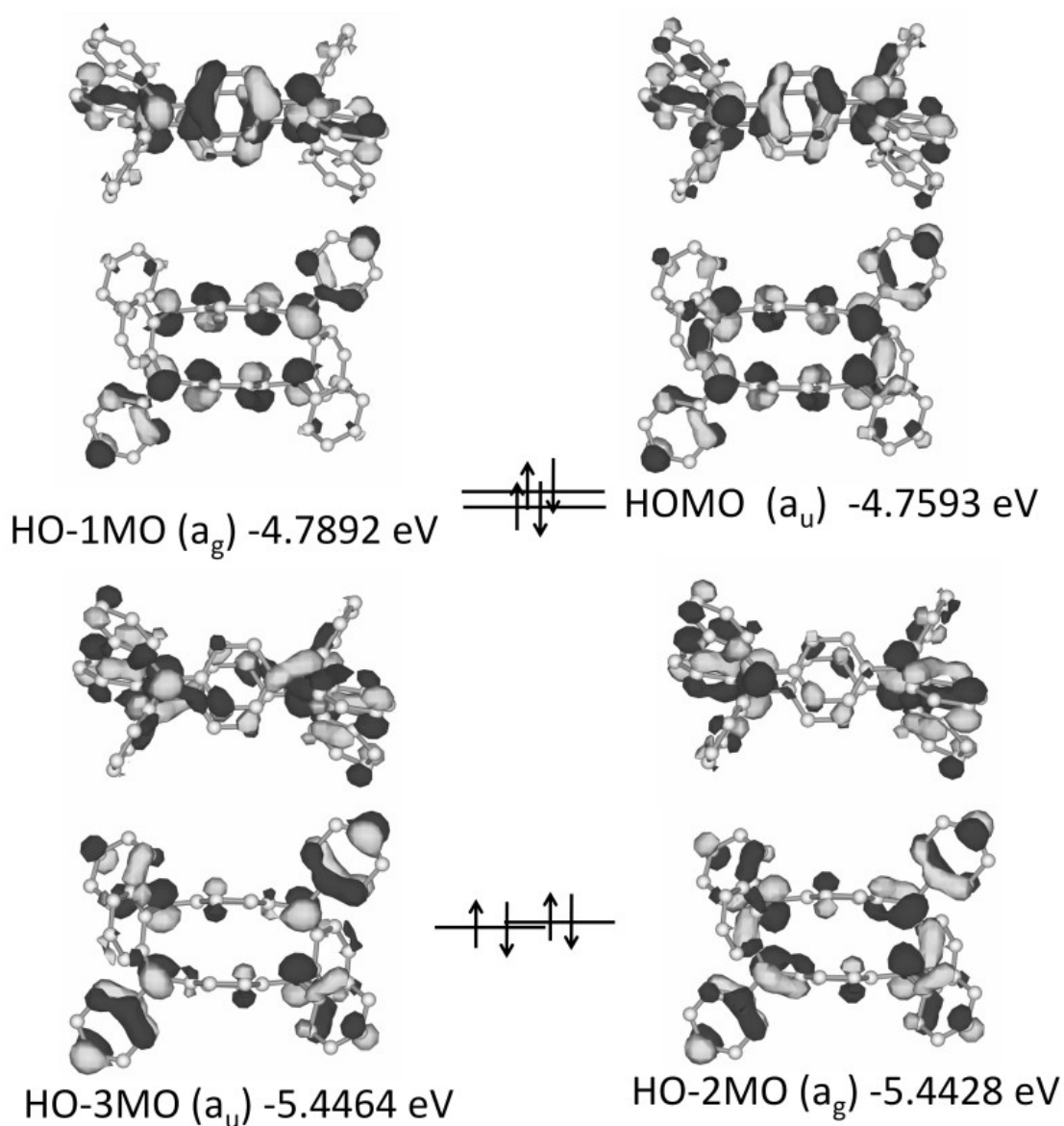
Figure 7. Frontier MOs of **1**' with the chair conformation (B3LYP/6-31G* level).
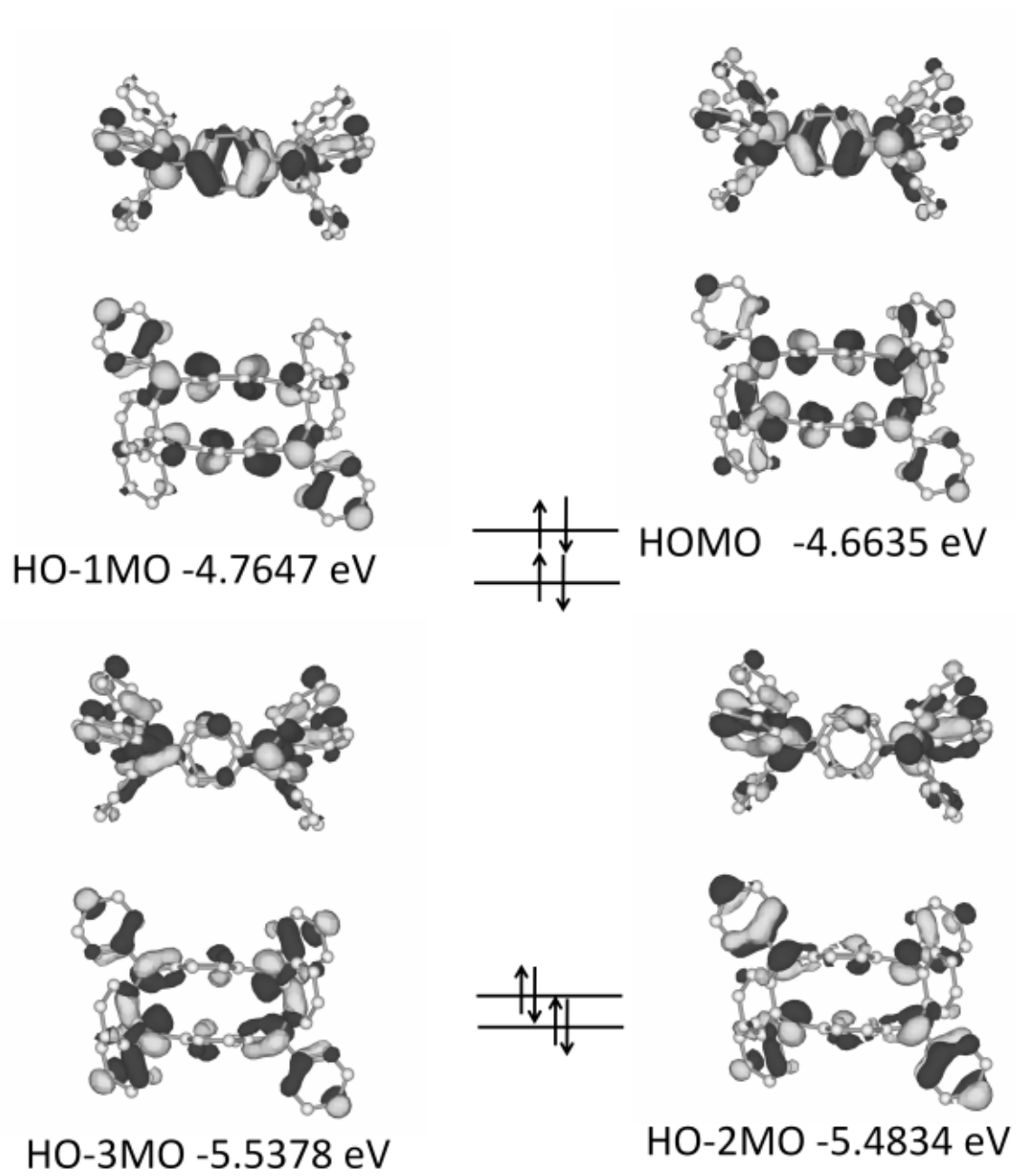
Figure 8. Frontier MOs of **1**' with the boat conformation (B3LYP/6-31G* level).

The DFT calculations of monocationic states of two conformers were also carried out (Figure 9 and 10). For both conformers, two local minimum structures with the different charge distributions: the structure with the localized spin (or the positive charge) on one PD moiety, and the structure with the delocalized spin over the two PD moieties. For the chair conformation, the spin-localized structure was calculated to be stable than the spin-delocalized one by 1.05 kcal mol^{-1}. In the spin-localized structure, the C-N bond lengths of the PD unit with a spin (1.3752 Å) are significantly shortened compared to those of the other PD unit (1.4315), and as a result, the PD bearing the radical spin have a bended structure. On the other hand, the structure with the delocalized spin had an almost C_i symmetric shape, and the C-N bond length alternation occurred in both PD moieties, in a similar way to the crystal structure of neutral **1**.
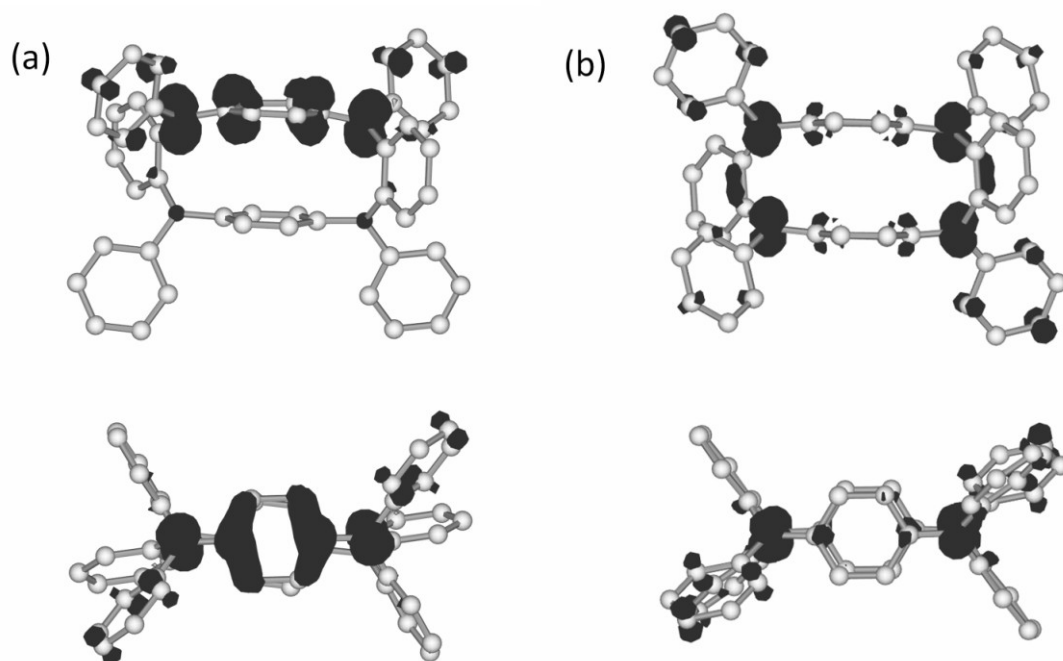
Figure 9. Spin density distributions of **1**$^{'+}$ of the chair conformer: a) the spin-localized structure; b) the spin-delocalized structure (UB3LYP/6-31G*; black: positive spin, white: negative spin; spin isosurface value = 0.003 electron au^{-3}).

For the boat conformers, the delocalized structure was calculated to be slightly stable. In this case, however, the energy difference between the two structures was very small (0.02 kcal mol^{-1}). These two structures also showed similar C-N bond length alternation to the corresponding structures of the chair conformer. In the spin-localized structure of the boat conformer, the C-N bonds in the positively charged PD unit (1.3718 and 1.3851 Å) were also shorter than those in the other PD unit (1.4277 and 1.4306 Å), and in the spin-delocalized one, each PD units had a long and short C-N bond. For both conformers, the energy difference between the spin-localized and delocalized structures was considerably small, and moreover, the interconversion between the two structures can be occurred without the flipping of the *ortho*-phenylene units requiring a high activation energy. These results suggest that the generated radial spin can easily move all over the macrocycle in both conformers.
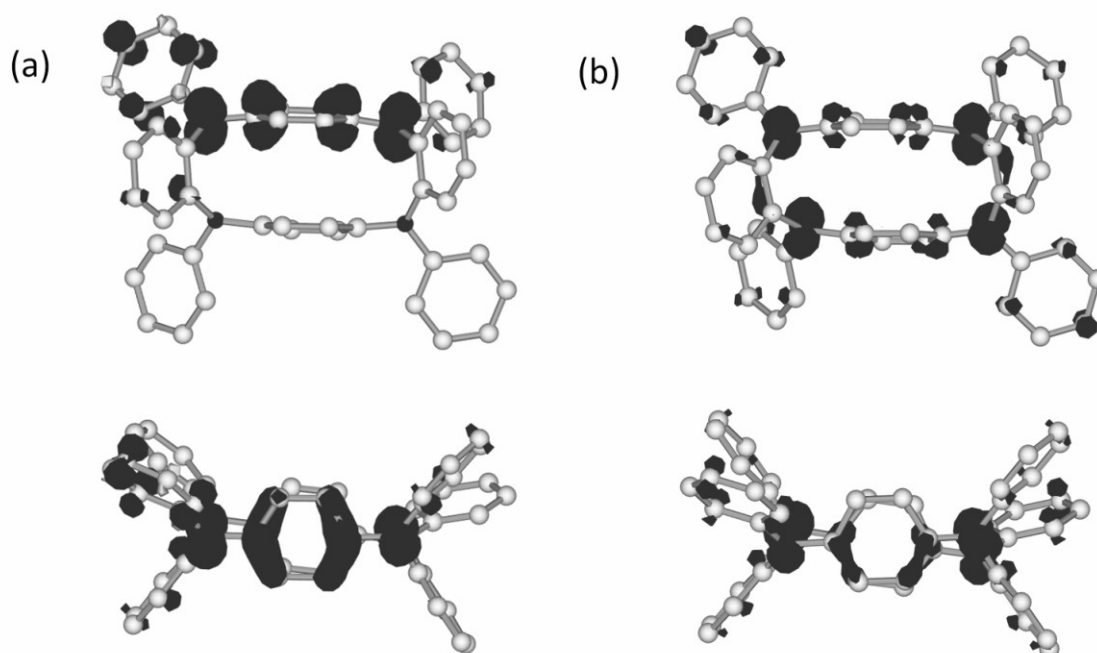
Figure 10. Spin density distributions of **1**$^{\prime+}$ of the boat conformer: a) the spin-localized structure; b) the spin-delocalized structure (UB3LYP/6-31G*; black: positive spin, white: negative spin; spin isosurface value = 0.003 electron au^{-3}).
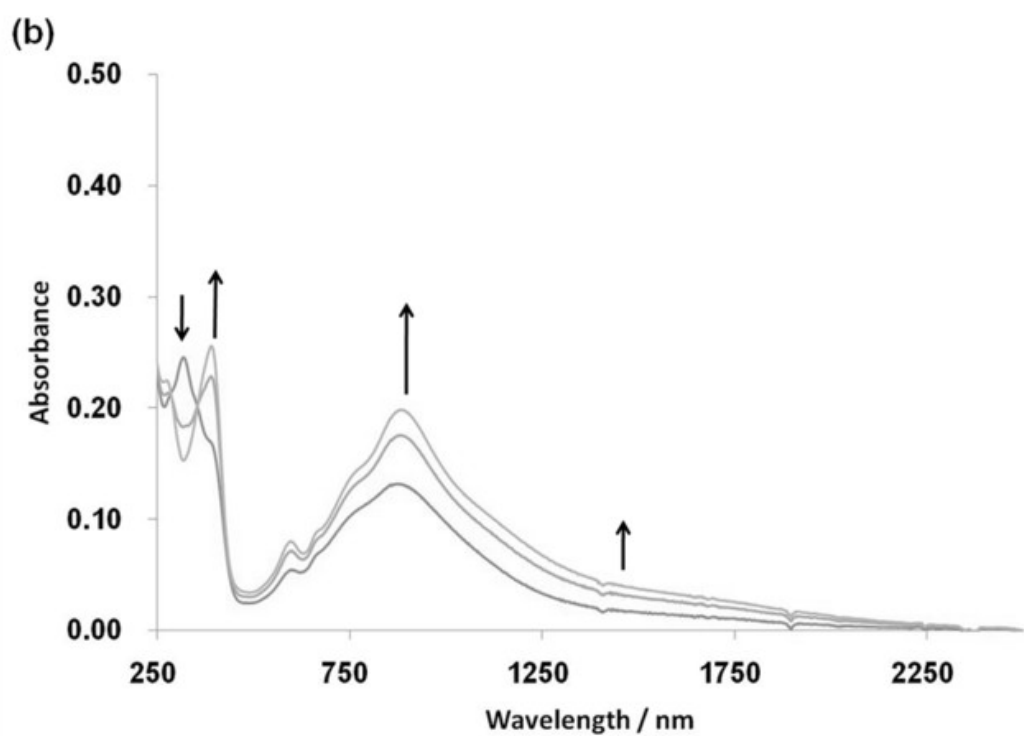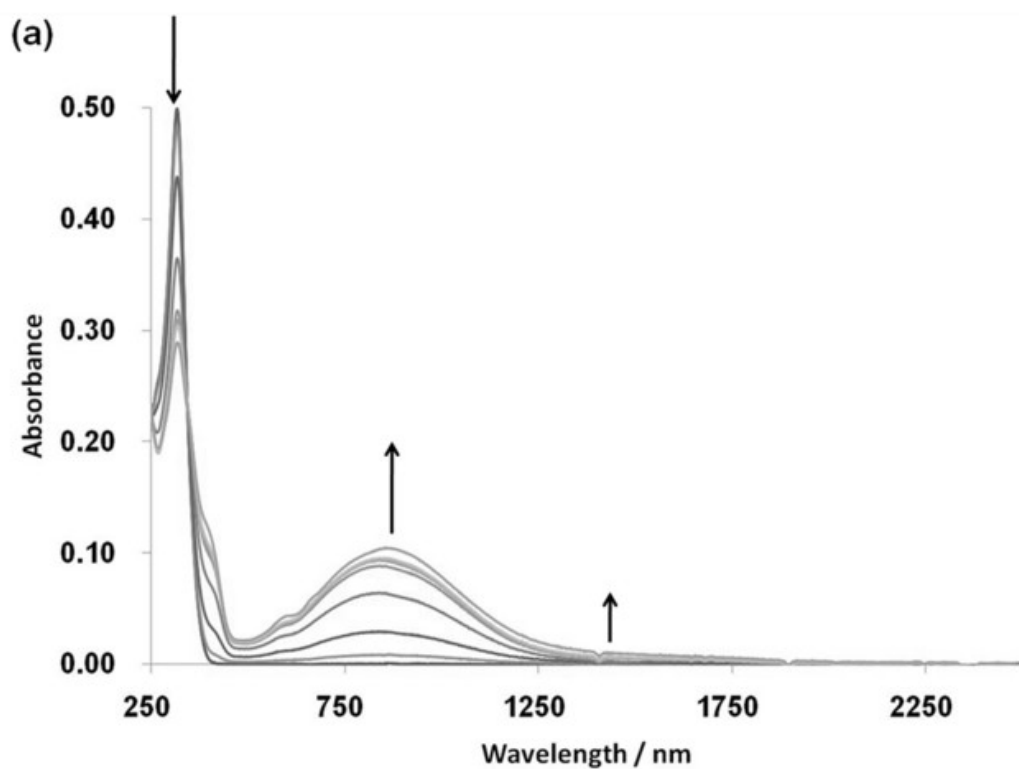
7.3.5 Electrochemistry

The redox behaviour of **1** was measured by cyclic voltammetry and differential pulse voltammetry in CH_2Cl_2 (0.1 M tetra-*n*-butylammonium tetrafluoroborate, 100 mVs^{-1}) at room temperature. As shown in Figure 11, **1** showed three one-electron redox couples, and the shape of the voltammogram was unchanged after repeated potential cycling. The large potential splitting between the first and second oxidation (E_{ox}^1 = -0.087 V, E_{ox}^2 = 0.255 V, ΔE = 342 mV) indicates the existence of a strong electron coupling among the nitrogen atoms via the *ortho*-phenylene linkers, in contrast to the values of the alkyl-chained PD dimers which showed the quasi-two-electron removal at the first oxidation step ($\Delta E \simeq 0$ mV)[5,6], and that of the *pseudogem*-5,8,14,17-tetrakis(dimethylamino)[3,3]paracyclophane (ΔE = 140 mV).[4] Furthermore, the ΔE value of **1** is larger than that of the *m,p,m,p*-tetraazacyclophane **2** (ΔE = 230 mV)[7c], suggesting that the replacement of the *meta*-phenylene linkers with the *ortho*-linkers strengthens the electronic communication in **1**. Although **1** has four nitrogen atoms, the oxidation wave corresponds to the removal of the forth electron could not be observed, and this is probably because the strong coulombic repulsions within the crowded structure of **1** prohibits the generation of the tetracationic state.
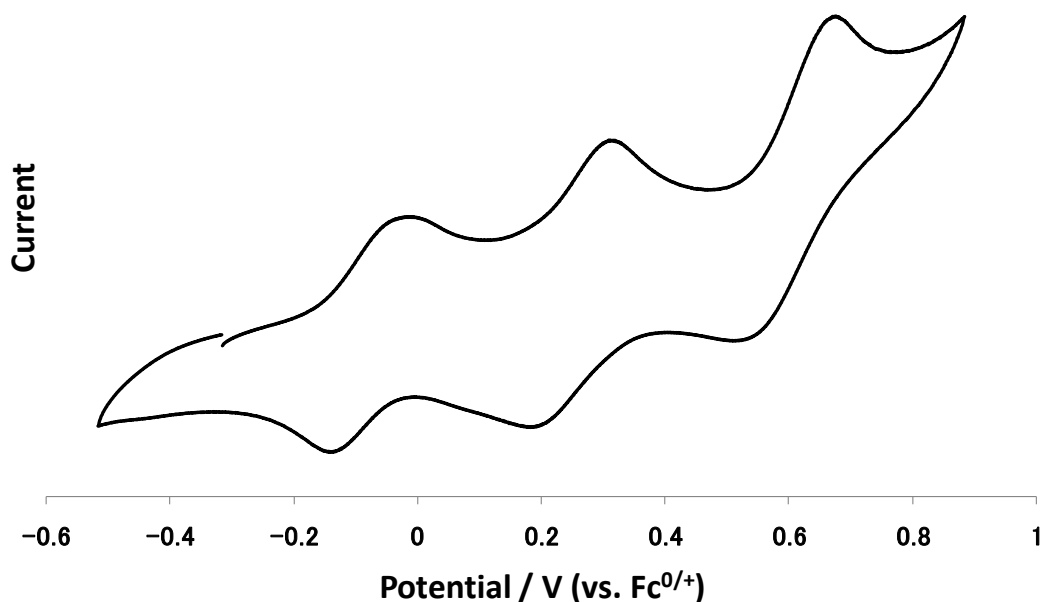
Figure 11. Cyclic voltammogram (CV) of **1**, measured in CH_2Cl_2 containing 0.1 M nBu$_4$NBF$_4$ at 298 K (scan rate 100 mV s^{-1}).

7.3.6 UV-Vis-NIR Spectroscopy

In order to clarify the electronic properties of the cationic states of **1**, the absorption spectral changes upon electrochemical oxidation were measured by the spectral electronic method. Figure 12a shows the spectral changes during the oxidation processes from neutral **1** to **1**$^+$. In this oxidation process, a new absorption band at 1.43 eV (λ_{max} = 865 nm) appeared. During the further oxidation to **1**$^{2+}$, the absorption band at 865 nm continued to grow up with a slight red-shift to 897 nm and reached up to about twice that of **1**$^+$. In addition, the weak absorption band in the lower energy region around 1500 nm was continuously increased in the course of the oxidation from **1** to **1**$^{2+}$. Although the detail of this absorption is unclear in this stage, this band may correspond to the charge transfer between the two PD moieties through the *ortho*-phenylene linkers.[20]

191

Figure 12. UV-vis-NIR spectra of the electrochemical oxidation of (a) **1** to **1**$^+$, (b) **1**$^+$ to **1**$^{2+}$ in CH$_2$Cl$_2$ / 0.1 M n–Bu$_4$NBF$_4$ at room temperature.

7.3.7 Fluorescence Spectroscopy

The emission properties of **1** in THF solution were measured. To investigate the effect of the closely stacked aromatic rings in **1** on the fluorescence emission, the emission properties of the *m,p,m,p*-tetraazacyclophane **2** and *N,N,N',N'*-tetraanisyl-*para*-phenylenediamine **4**, which is a partial structure of these molecules were also measured as the reference compounds of **1**. The results were shown in Figure 13 and Table 3. These three compounds have similar absorption maxima around 310 nm, so we used a fixed excitation wavelength of 310 nm for these three molecules. Although **2** and **4** have similar emission maxima, the emission maximum of the *o,p,o,p*-tetraazacyclophane **1** (442 nm) is red-shifted by about 200 and 170 meV relative to those of **2** and **4**, respectively. These results suggest the presence of excimer-like state in **1**, which was observed in the case of the stacked oligo(phenylene ethynylene) dimers.[21]
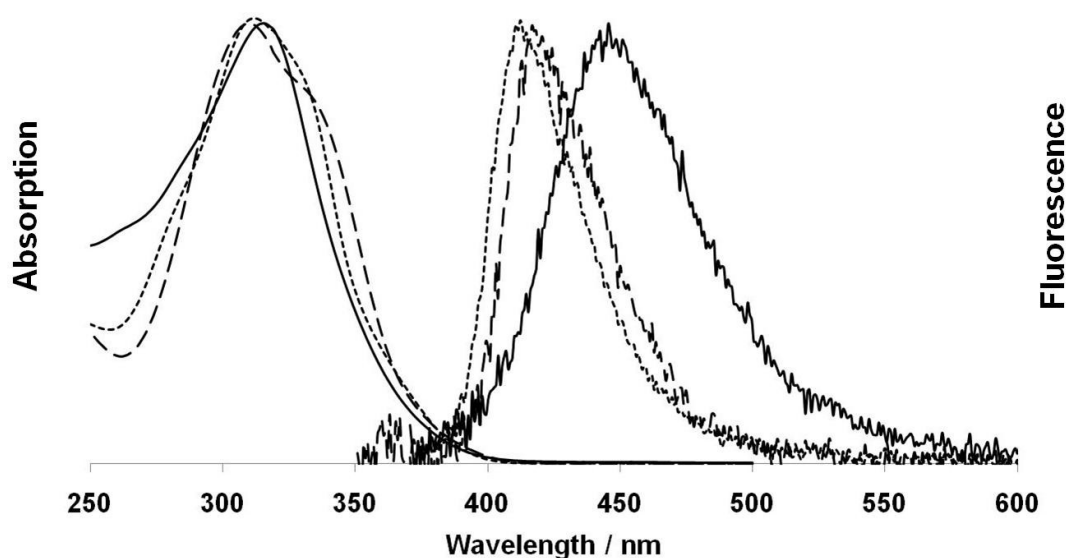

Figure 13. Absorption and emission spectra of **1** (solid line) **2** (dotted line), and **4** (dashed line) in THF. Both absorption and emission peaks are nomarized.

Table 3: Properties of the absorption and emission spectra.

Species	Absorption maxima [nm (eV)]	Emission maxima [nm (eV)]	Quantum yield
1	315 (3.94)	442 (2.81)	0.035
2	312 (3.97)	412 (3.01)	0.029
4	310 (4.00)	416 (2.98)	0.032

7.3.8 Solution ESR measurements

The ESR sprctrum of $\mathbf{1}^+$ generated by chemical oxidation of **1** by 0.5 equivalent of tris(4-bromophenyl)aminium hexachloroantimonate in dichloromethane was measured. As shown in Figure 14, the spectrum with nine lines was observed at 293 K. This spectrum pattern was successfully simulated in terms of the hyperfine interactions with four ^{14}N nuclei (a_N(4N) = 0.300 mT), 24 ^{1}H nuclei (a_H(24H) = 0.045 mT) belonging to two *para*-phenylene moieties in the macrocycle (8H) and the benzene rings of four anisyl groups (16H). For the cofacially linked PD molecules with trimethylene- and pentamethylene-linkers, the ESR measurements of the monocationic states showed the spectra with hyperfine interactions from two ^{14}N nuclei, because the generated spin was basically confined to one PD moiety.[6c] On the other hand, in this case, the radical spin was considered to be moving between two PD moieties through the *ortho*-phenylene linkers on a time scale faster than ESR experiment at 295 K. These results clearly indicate that the electron communication between two PD moieties is fairly enhanced by replacing the alkyl linkers with the *ortho*-phenylene linkers. The hyperfine structures basically did not change in the temperature range from 293 K to 213 K, and hence, this clearly demonstrates that the efficient electron transfer can occur between two PD moieties at low temperature.
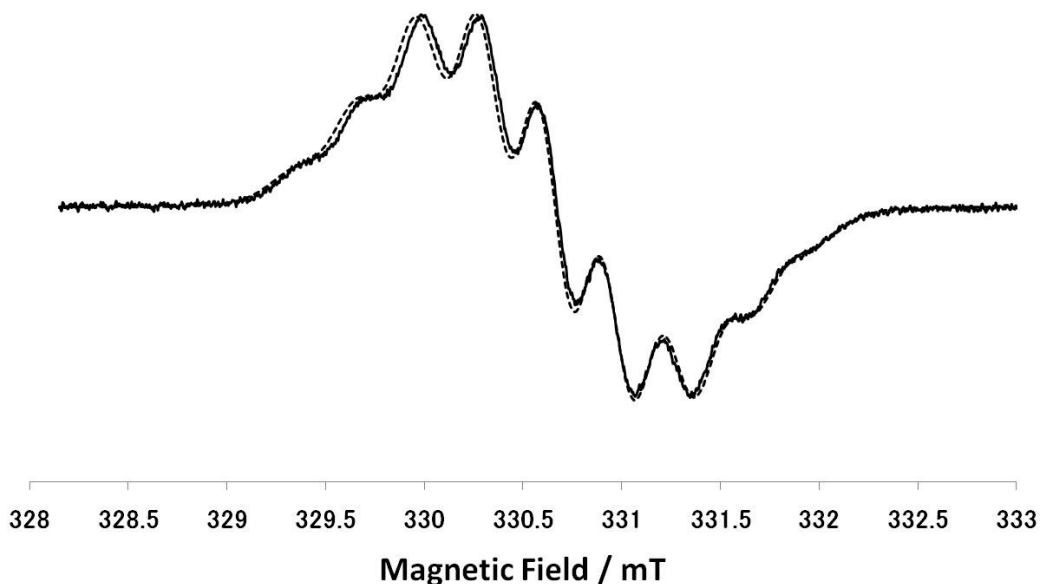
Figure 14. ESR spectrum of **1**$^{•+}$ in CH$_2$Cl$_2$ at 293 K (solid line) and simulated spectrum (dotted line).

7.4 Conclusion

In summary, we have succeeded to prepare an *o,p,o,p*-tetraazacyclophane **1** for the first time. The X-ray single crystal analysis of **1** revealed its structure of which the two PD units were cofacially stacked at a distance of 3.1 Å. The variable-temperature ^{1}H NMR measurements suggested the rigidness of this molecule having the high energy barrier to conformational isomerization. The electrochemical spectroscopy observed the lower energy absorption band which suggested the existence of the intramolecular electron transfer between two PD moieties. The emission maximum of **1** in THF solution was red-shifted compared to that of the *m,p,m,p*-tetraazacyclophane **2**, suggesting the presence of the excimer-like excited state of **1**. The solution ESR spectra of **1**$^+$ with nine lines demonstrated that the radical spin was equally distributed on the four nitrogen atoms in the time scale of the ESR measurement. The results of this chapter represented the availability of the *ortho*-phenylene units as a linker unit for connecting

195

the π-systems so as to construct optical and electronic functional materials.

References and Notes

[1] D. J. Cram, H. Steinberg, *J. Am. Chem. Soc*. **1951**, *73*, 5691.

[2] F. Vögtle, Cyclophan-Chemie; B.G. Teubner: Stuttgart, Germany, **1990**.

[3] a) S. F. Nelsen, H. Q. Tran, M. A. Nagy, *J. Am. Chem. Soc*. **1998**, *120*, 298; b) S. F. Nelsen, R. F. Ismagilov, D. R. Powell, *J. Am. Chem. Soc*. **1998**, *120*, 1924; c) S. F. Nelsen, R. F. Ismagilov, Y. Teki, *J. Am. Chem. Soc*. **1998**, *120*, 2200; d) S . E. Bailey, J. I. Zink, S. F. Nelsen, *J. Am. Chem. Soc*. **2003**, *125*, 5939; e) J. V. Lockard, J. .I Zink, A. E. Konradsson, M. N. Weaver, S. F. Nelsen, *J. Am. Chem. Soc*. **2003**, *125*, 13471.

[4] H. A. Staab, G. Gabel, C. Krieger, *Chem. Ber.* **1987**, *120*, 269.

[5] H. Takemura, K. Takehara, M. Ata, *Eur. J. Org. Chem*. **2004**, 4936.

[6] a) S. F. Nelsen, G. Li, K. P. Schultz, H. Q. Tran, I. A. Guzei, *J. Am. Chem. Soc*. **2008**, *130*, 11620; b) A. S. Jalilov, G. Li, S. F. Nelsen, I. A. Guzei, Q. Wu, *J. Am. Chem. Soc*. **2010**, *132*, 6176; c) A. Rosspeintner, M. Griesser, I. Matsumoto, Y. Teki, G. Li, S. F. Nelsen, G. Gescheidt, *J. Phys. Chem. A* **2010**, *114*, 6487; d) A. S. Jalilov, S. F. Nelsen, I. A. Guzei, Q. Wu, *Angew. Chem. Int. Ed*. **2011**, *50*, 6860.

[7] a) A. Ito, Y. Ono and K. Tanaka, *Angew. Chem. Int. Ed*. **2000**, *39*, 1072; b) A. Ito, S. Inoue, Y. Hirao, K. Furukawa, T. Kato and K. Tanaka, *Chem. Commun*. **2008**, 3242; c) A. Ito, Y. Yamagishi, K. Fukui, S. Inoue, Y. Hirao, K. Furukawa, T. Kato and K. Tanaka, *Chem. Commun*. **2008**, 6573.

[8] a) T. D. Selby and S. C. Blackstock, *Org. Lett*. **1999**, *1*, 2053; b) S. I. Hauck, K. V. Lakshmi and J. F. Hartwig, *Org. Lett*. **1999**, *1*, 2057; c) I. Kulszewicz-Bajer, V. Maurel, S. Gambarelli, I. Wielgus and D. Djurado, *Phys. Chem. Chem. Phys*. **2009**, *11*, 1362.

[9] M. C. Burla, R. Caliandro, M. Camalli, B. Carrozzini, G. L. Cascarano, L. De Caro, C. Giacovazzo, G. Polidori, R. Spagna, *J. Appl. Cryst*. **2005**, *38*, 381.

[10] The DIRDIF-99 Program System, Technical Report of the Crystallography Laboratory, P. T. Beurskens, G. Admiraal, G. Beurskens, W. P. Bosman, R. de Gelder, R. Israel, J. M. M. Smits, University of Nijmegen (The Netherlands), **1999**.

[11] Program for Crystal Structure Solution and Refinement, G. M. Sheldrick, Universität Göttingen, **1997**.

[12] CrystalStructure 3.8, Crystal Structure Analysis Package, Rigaku and Rigaku Americas (2000–2007). 9009 New Trails Dr. The Woodlands TX 77381 USA.

[13] K. Ragavachari, *Theor. Chim. Acc*. **2000**, *103*, 361 and references cited therein.

[14] W. J. Hehre, L. Radom, P.v. R. Schleyer, J. A. Pople, *Ab Initio Molecular Orbital Theory*, Wiley, New York, **1986**.

[15] M. J. Frisch, *et al*., Gaussian 09 (Revision C.01), Gaussian, Inc., Wallingford CT, **2009**.

[16] T. Wenderski, K. M. Light, D. Ogrin, S. Bott, C. J. Harlan, *Tetrahedron Letters* **2004**, *45*, 6851.

[17] a) J. P. Wolfe, S. Wagaw, J. F. Marcoux, S. L. Buchwald, *Acc. Chem. Res*. **1998**, *31*, 805; b) J. F. Hartwig, *Acc. Chem. Res*. **1998**, *31*, 852; c) J. F. Hartwig, *Angew. Chem. Int. Ed*. **1998**, *37*, 2046; d) A. R. Muci, S. L. Buchwald, *Top. Curr. Chem*. **2002**, *219*, 133.

[18] K. Sako, T. Meno, H. Takemura, T. Shinmyozu, T. Inazu, *Chem. Ber.* **1990**, *123*, 639.

[19] M. V. Baker, M. J. Bosnich, D. H. Brown, L. T. Byrne, V. J. Hesler, B. W. Skelton, A. H. White, C. C. Williams, *J. Org. Chem*. **2004**, *69*, 7640.

[20] G. Nöll, M. Avola, *J. Phys. Org. Chem.* **2006**, *19*, 238.

[21] a) S. P. Jagtap, S. Mukhopadhyay, V. Coropceanu, G. L. Brizius, J. L. Brédas, D. M. Collard, *J. Am. Chem. Soc.* **2012**, *134*, 7176; b) S. Mukhopadhyay, S. P. Jagtap, V. Coropceanu, J. L. Brédas, D. M. Collard, *Angew. Chem. Int. Ed*. **2012**, *51*, 11629.

General Conclusion

In this thesis, the author has studied the electronic and magnetic properties of the aromatic amines with characteristic structures from the both experimental and theoretical points of view. The new findings in this thesis are summarized as follows.

In Chapter 1, the author studied the charge and spin distributions of the two extended *para*-phenylenediamine derivatives with dendritic structures: the C_2-symmetric molecule having six nitrogen atoms and the C_3-symmetric molecule having ten nitrogen atoms. The redox properties were measured by cyclic voltammetry, and it was demonstrated that the former molecule was stably oxidized up to tetracation, and the latter hexacation. The potential differences between the first and the second oxidation potentials of these compounds were smaller than that of the *N,N,N',N'*–tetraanisyl–1,4–benzenediamine, which both of the two molecules had as their central unit, suggesting that the Coulombic repulsion between the two positive charges could be alleviated by the extended PD moieties. From the measurement of the absorption spectra during the electrochemical oxidations and the ESR measurement of these cations, the charge (or spin) distribution of the cationic states gradually changed so as to reduce the Coulombic repulsion between the generated positive charges.

In Chapter 2, the author prepared two octaazacyclophanes as simple extensions of tetraaza[1$_4$] *m,p,m,p*-cyclophane. From the DFT calculations on the model compounds, it was suggested that these two cyclophanes were categorized into non-disjoint or coextensive molecules, which serve as promising candidates for high-spin molecules. The electrochemical measurements revealed that the both two molecules exhibited multi-redox activity, and they were oxidized up to the octacation. The UV-vis-NIR spectroelectrochemical measurements demonstrated that the generated charges were mainly confined into *para*-phenylenediamine (PD) moieties in octaaza[1$_8$]*m,p,m,p,m,p,m,p*-cyclophane, whereas the generated charges were delocalized over the extended PD moieties in octaaza[1$_8$]*m,p,p,p,m,p,p,p*-cyclophane. The pulsed ESR measurement revealed that almost pure spin-triplet state was realized for the dicationic state of octaaza[1$_8$]*m,p,p,p,m,p,p,p*-cyclophane, whereas in the di- and tetracation of octaaza[1$_8$]*m,p,m,p,m,p,m,p*-cyclophane, the high and the lower spin states coexist even at low temperatures, probably due to fragility of spin coupling pathway by facile conformational changes.

In Chapter 3, to prepare the aromatic amine system which has a higher spin multiplicity in the oxidized states, the author adopted the method of connecting two macrocyclic aromatic amines which have the triplet ground state in the dicationic state by the ferromagnetic coupling unit. Based on this strategy, the author succeeded to synthesize the novel handcuffs-shaped aromatic amine composed of two tetraaza[1$_4$]*m,p,m,p*-azacyclophane moieties linked by the linear ferromagnetic coupling unit. The electrochemical measurements revealed that this molecule can be stably oxidized up to dodecacationic state. From the continuous wave ESR measurements of the di-, tri-, and tetracation of this compound showed the spectra with no definitive fine-structure and we could not observe the forbidden resonances. However, the ESTN measurements based on the pulsed ESR method clearly showed the spectra indicating existence of the high-spin species in the higher oxidized states and showed that the

hexacation has the spin septet state. These results demonstrated that the high-spin alignment among the two macrocyclic moieties and the linker units were successfully accomplished.

In Chapter 4, the author synthesized the huge macrocyclic aromatic amine composed of the two tetraaza[1$_4$]m,p,m,p-azacyclophane moieties as an example of the cylindrical multi-spin system. This molecule was classified as a pseudobeltane according to Vögtle's nomenclature. This compound was prepared in a one-pot manner by using the Buchwald-Hartwig cross-coupling amination reaction between the 1,3,5-benzenetriamine derivative and 1,3-dibromobenzene. We could obtain the single crystals of this molecule, and the molecular structure was clarified by the X-ray crystal analysis. This molecule had the cavity (ca. 5Å×8Å) formed between the two tetraazacyclophane macrocycles, and the two tetraazacyclophane moieties are sideslipped by 3 Å in parallel with each other in association with an inclination (56˚) of the two PD bridges. Electrochemical analysis revealed the multi-electron redox activity originating from six PD units, and it was demonstrated that this macrocycle could be oxidized up to the dodecacationic state. The solution ESR spectrum of the monocationic state generated by chemical oxidation exhibited the multiplet hyperfine structure resulting from the twelve nitrogen nuclei, indicating that the generated spin is delocalized over the whole of the molecular framework. In addition, the solution ESR spectral shapes changed with decreasing temperature, and this tendency was explained by considering the thermally activated interconversion between two sideslipped structures. The barrier to this thermal interconversion was estimated to be 5.0 kcal mol^{-1}. The ESTN measurement revealed that the tetracation of this molecule has the ground quintet state.

In Chapter 5, the author intended to extend macrocyclic aromatic amines which have a two-dimensional topology to the three-dimensional topology, and as the first examples of such molecules, the author prepared the novel cage-like aromatic amines consisting

of double- and triple-layered 1,3,5-benzenetriamines connected by three *meta*-phenylene linkers. The peculiar structures of these double- and triple-layered aromatic amines were clearly demonstrated by the X-ray crystal analyses. The electrochemical studies revealed that the cationic states of the molecules without PD moieties were unstable and caused the electrochemical polymerization, whereas the derivative with the six PD branches showed the stable multi-electron oxidation properties. The pulsed ESR spectroscopy of the cationic states of the 1,3,5-benzenetriamine double-decker with the PD branches indicated the existence of the high-spin species up to the spin quartet state.

In Chapter 6, as another example of the three-dimensionally extended aromatic amine, we synthesized the molecule in which two triphenylamines were connected at *para*-positions of all phenyl groups by three *meta*-phenylenediamine pillars. The molecular structure was successfully determined by the single crystal X-ray analysis, and the distance between the two central nitrogen atoms of both triphenylamine decks were revealed to be 5.8 Å. From the DFT calculations, the radical spin in the monocation was predicted to be delocalized over the entire molecule. The electrochemical studies showed the quite low first oxidation potential of this molecule suggesting that the high electron-donating property, and we actually succeeded to prepare the charge-transfer complexes with 7,7,8,8-tetracyano-*p*-quinodimethane. The di(cation radical) of this molecule showed the fine-structured ESR spectrum characteristic for spin triplet species at 123 K, and from the zero-field splitting parameters, the average distance between the two radical centers was calculated to be 8.3 Å. The intensity of the triplet signal decreased with decreasing temperature, suggesting the singlet ground state of the dication. As a matter of fact, the energy gap between the singlet and triplet states (ΔE_{S-T}) was estimated to be -0.18 kcal mol^{-1}, from the curve-fitting with the Bleaney-Bowers singlet-triplet model equation.

In Chapter 7, the author aimed to realize the stacked aromatic amine system with a much shorter separation distance and synthesized the novel cyclophane in which two PD moieties were connected by two *ortho*-phenylene linkers. This molecule was the first example of an *o,p,o,p*-tetraazacyclophane. The ^{1}H nuclear magnetic resonance (NMR) spectrum of this cyclophane suggested the existence of the two conformational isomers: the boat conformer and the chair one. The X-ray single crystal analysis revealed that all the molecules were in their chair form in the crystals. On the variable-temperature ^{1}H NMR experiments, the spectral shapes were unchanged from 298 K to 363 K, and the aromatic ^{1}H signals did not completely coalesced even at 423 K, suggesting the remarkable rigidness of the macrocyclic skeleton. The electrochemical measurements revealed that the large splitting between the first and the second oxidations, ΔE = 342 mV, and this indicated the strong electronic coupling between the two PD moieties through the *ortho*-phenylene linkers. The solution ESR of the monocation of this molecule showed nine-lined spectra resulting from the hyperfine interaction with the four equivalent nitrogen nuclei, and this indicated that the generated radical spin were completely delocalized over the whole of the macrocyclic structure in the time-scale of the ESR measurements. The emission wavelength of the *o,p,o,p*-tetraazacyclophane was red-shifted by about 0.2 eV compared with that of the *m,p,m,p*-tetraazacyclophane and *N,N,N′,N′*-tetraanisyl-*para*-phenylenediamine, suggesting the presence of the excimer-like state in the *o,p,o,p*-tetraazacyclophane with the closely stacked PD moieties.

In this thesis, we investigated the electronic properties of various aromatic amines with the characteristic structures mainly from the points of view of the intramolecular electron transfer and the spin-spin interaction toward obtaining further knowledge of the relationships between the molecular structure and properties. Through these studies, we have demonstrated that we can create organic materials with various different electronic properties by properly designing the molecular structures even from a few kinds of

typical elements. The author hopes that the present thesis will contribute to further development of the materials science and also hopes that the concept presented in this thesis will make possible solution to the expected depletion of rare-earth elements.

List of Publications

Chapter 1

(1) Spin–Delocalization in Charged States of *Para*–Phenylene–Linked Dendritic Oligoarylamines

A. Ito, D. Sakamaki, Y. Ichikawa, K. Tanaka, *Chem. Mater*. **2011**, *23*, 841-850.

Chapter 2

(2) *Meta–Para*–Linked Octaaza[1_8]cyclophanes and Their Polycationic States

D. Sakamaki, A. Ito, K. Furukawa, T. Kato, K. Tanaka, submitted.

Chapter 3

(3) High-Spin Polycationic States of an Alternate *Meta-Para*-Linked Oligoarylamine Incorporating Two Macrocycles

D. Sakamaki, A. Ito, K. Furukawa, T. Kato, K. Tanaka, *Chem. Commun*. **2009**, *30*, 4524-4526.

Chapter 4

(4) A Polymacrocyclic Oligoarylamine with Pseudobeltane Motif: Towards a Cylindrical Multi-Spin System

D. Sakamaki, A. Ito, K. Furukawa, T. Kato, M. Shiro, K. Tanaka, *Angew. Chem. Int. Ed.* **2012**, *51*, 12776-12781

Chapter 5

(5) 1,3,5–Benzenetriamine Double- and Triple–Decker

D. Sakamaki, A. Ito, K. Tanaka, K. Furukawa, T. Kato, M. Shiro, *Angew. Chem. Int. Ed.* **2012**, *51*, 8281-8285.

Chapter 6

(6) A Triphenylamine Double-Decker: From a Delocalized Radical Cation to a Diradical Dication with an Excited Triplet State

Y. Yokoyama, D. Sakamaki, A. Ito, K. Tanaka, M. Shiro, *Angew. Chem. Int. Ed*. **2012**, *51*, 9403-9406.

Chapter 7

(7) The First Synthesis of an *o,p,o,p*-Tetraazacyclophane: The Effect of the *ortho*-Phenylene Linkers on the Structural and Electronic Properties

D. Sakamaki, A. Ito, K. Tanaka, to be submitted.

The following papers are not included in this thesis:

(8) Polycationic States of Oligoanilines Based on Wurster's Blue

A. Ito, D. Sakamaki, H. Ino, A. Taniguchi, Y. Hirao, K. Tanaka, K. Kanemoto, T. Kato, *Eur. J.Org. Chem*. **2009**, *26*, 4441-4450.

(9) Fusion of Phosphole and 1,1'-Biacenaphthene: Phosphorus(V)-Containing Extended π-Systems with High Electron Affinity and Electron Mobility

Y. Matano, A. Saito, T. Fukushima, Y. Tokudome, F. Suzuki, D. Sakamaki, H. Kaji, A. Ito, K. Tanaka, H. Imahori, *Angew. Chem. Int. Ed*. **2011**, *50*, 8016-8020.

(10) Effects of Carbon−Metal−Carbon Linkages on the Optical, Photophysical, and Electrochemical Properties of Phosphametallacycle-Linked Coplanar Porphyrin Dimers

Y. Matano, K. Matsumoto, H. Hayashi, Y. Nakao, T. Kumpulainen, V. Chukharev, N. V. Tkachenko, H. Lemmetyinen, S. Shimizu, N. Kobayashi, D. Sakamaki, A. Ito, K. Tanaka, H. Imahori, *J. Am. Chem. Soc*. **2012**, *134*, 1825-1839.